OBSERVATIONAL AND THEORETICAL ESTIMATION OF THE CONTRIBUTION OF ANTHROPOGENIC AND NATURAL AEROSOLS TO RADIATIVE FORCING OF THE ATMOSPHERE

Sanat Kumar Das

Ph. D. Thesis
October 2008

PHYSICAL RESEARCH LABORATORY,
AHMEDABAD - 380 009, INDIA

OBSERVATIONAL AND THEORETICAL ESTIMATION OF THE CONTRIBUTION OF ANTHROPOGENIC AND NATURAL AEROSOLS TO RADIATIVE FORCING OF THE ATMOSPHERE

A thesis submitted to

Gujarat University

for the degree of

Doctor of Philosophy in Physics

by

Sanat Kumar Das

October 2008

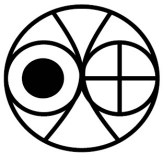

Space and Atmospheric Sciences Division
PHYSICAL RESEARCH LABORATORY,
AHMEDABAD - 380 009, INDIA

CERTIFICATE

I hereby declare that the work presented in this thesis is original and done by me. It has not formed the basis for the award of any degree or diploma by any University or Institution, except where due acknowledgment has been made in the text.

Sanat Kumar Das
(Author)

Certified by :

Prof. A. Jayaraman
(Thesis Supervisor)
Space and Atmospheric Sciences Division,
Physical Research Laboratory,
Navrangpura, Ahmedabad, India

Dedicated to

Maa & Baba

Acknowledgements

It is a great pleasure to express my heartfelt gratitude to all those, whose advices and encouragement helped me a lot and who always stood beside me during the course of my thesis work.

I would like to thank my supervisor, Prof. A. Jayaraman, for his guidance during my research work at PRL. He is the first person who introduced me to the world of scientific research. With his constant help, inspiration and support I could successfully complete my thesis. He was always accessible and willing to help during all these years. As a result, my doctoral research tenure at PRL was smooth and rewarding.

I am grateful to Prof. Shyam Lal and Prof. M.M. Sarin for their encouragement and all the support during my thesis work. My special thanks to Profs. H. Chandra and S. Ramachandran for their valuable suggestions and the scientific discussions. I also thank Rajesh, Venkatramani, Modh Bhai and Sunil for their help during all my experiments.

My sincere thanks to Dr. H. Gadhavi (Harish Bhai) who was always present in need. I learnt a lot working with him. My special thanks to Lokesh (lokusir), Neeraj, Dilip, Amit, Ranga, Sudheer, Ashwini, Kirpa, Sumita for the various scientific discussions.

I acknowledge Land Processes Distributed Active Archive Center (LPDAAC) of EOS, NASA for proving the land surface reflectance data used in the study. Acknowledgements are due to Air Resources Laboratory, NOAA, USA for providing the HYSPLIT model and the wind data used in the air back-trajectory analysis and NOAACIRES Climate Diagnostic Center, USA for providing NCEP reanalysis data over various study regions.

I would like to thank Som Kumar Sharma (Sharma-ji), Drs. Dibyendu Chakrabarty (Dipu-da), Varun Sheel, Anirban Das (Anirban-da) for their valuable advices, encouragement and for always making the environment lively.

I wish to thank my dear friends Subimal, Shreyas, Satya and Subhasis who made my life enjoyable and refreshing. I am also grateful to all the PRL football, volleyball, cricket team members and TT co-players for providing great fun and entertainment.

My sincere acknowledgements to my colleagues at PRL: Ravi, Jyoti, Anil, Sasi, Sumanta, Parimal, Tarak-da, Prasanta-da, Sarika, Jayendra-da, Lokesh (Loku-sir), Santosh Bhai, Rajneesh, Charan, Asoka, Subhranshu-da, Nagar, Moortikai, Murali, Koushik-da, Arpita-di, Rudra, RP, Antra, Vandana, Utpal-da, Suranjana, Ramakrishna, Kushwaha, Ritesh, Salman, Akhilesh, Santosh, Bindu, Gyan, Lokesh , Sumanta, Shuchita, Bhatt, Alok, Naveen, Rahaman, and all other members of PRL.

I am grateful to the PRL library for providing valuable books, journals, scientific papers. Thanks to PRL transport officers and drivers for their help and cooperation during my scientific field works.

Thanks are due to all my colleagues at Mt. Abu: Rajesh-bhai, Mathur-ji, Purohit-ji, Jain-ji, Kothari-ji, Pitamber-ji, Naran Singh and Padam Singh for their support during my observations at Gurushikhar. I would like to thank Profs. P. Venkatakrishnan, A. Ambastha, Drs. Nandita Srivastava, Shibu K. Mathew, Brajesh Kumar and Sanjay Gosain for their warm welcome and logistic support during my campaign at Udaipur and my colleagues Sanjeev, Rohan, Ram and Anand who made a homely atmosphere during my stay. I thank Dr. R. Baskaran and his IGCAR-RSD coworkers whose cooperation and logistic support during my campaign at

Kalpakkam helped me in producing fruitful results that became an important part of my thesis. I am also thankful to all scientists of NARL, Gadanki, especially Drs. Nirvikar, Alok, Ratnam and Sridharan for providing me a friendly atmosphere during my stay at Tirupati.

I am indebted to my M. Sc. friends Biswajit, Raj and Kadir for providing a stimulating and fun environment in which I learnt and grew.

Words are not sufficient to express my thanks to my loving wife, friend and colleague Uma for her constant unconditional support and helping me to successfully finish my thesis and being always beside me during my Ph.D work. I am the proud father of my little son, Adi whose smiles were perineal source of energy after long hours of daily research work.

I wish to thank my dear sisters, Suchitra and Moutusi and and my younger brother-in-law, Prosun. I deeply express my thanks to my (Late) grandmother who left all of us with her sweet memories. I am thankful to my parents-in-law for providing conducive family atmosphere and my cute sister-in-law, Kousi for her cheerfulness.

I would not be sitting in front of my computer typing these acknowledgements without Maa and Baba. I am indebted to them for their love, support, and their paramount confidence in me. My parents have always put education as a first priority in my life, and raised me to set high goals and work hard to achieve them. They taught me to value honesty, courage, and humility above all other virtues in life. They have always been with me as an unwavering support. I dedicate my thesis to them.

Sanat

Contents

List of Tables

List of Figures

Abstract

The objective of this thesis is to quantify the influences of anthropogenic and natural aerosols on aerosol radiative forcing from the observation of the optical and physical properties of aerosol. The emphasis is placed on the investigation of seasonal variation of aerosols over an urban region, Ahmedabad and a relatively pristine region, Mt. Abu in the western part of India and to estimate the seasonal variation in the anthropogenic and natural aerosol radiative forcing over these regions.

Chapter 1 gives a brief introduction of atmospheric aerosols, their production, size distribution and removal processes. It is followed by a short description about the major atmospheric processes which maintain the radiation balance of Earth-atmospheric system. There after, the perturbation of this radiative balance due to aerosols by the interaction of the incoming shortwave solar radiation and outgoing longwave radiation is described. Due to the short residence time aerosol perturbation is more significant in the regional scale than on the global scale. The importance of the present work in the above context is discussed.

Chapter 2 presents briefly the description of the instruments that were used during the study period. The physical and optical properties of aerosols were

measured by Sunphotometer, Microtops, Quartz Crystal Microbalance Cascade Inpactor, Aethalometer, Nephelometer and Aerosol Size Spectrometer.

In *Chapter 3* the observed aerosol properties are discussed in detail. Firstly, the seasonal variation of various aerosol properties obtained from the observations from January 2006 to December 2007 at Ahmedabad and Mt. Abu are described. According to meteorological conditions, the observation period is divided into four seasons viz, winter (December-February), premonsoon (March-May), monsoon (June-August) and postmonsoon (September-November). At Ahmedabad columnar AOD (at 0.5μm) was found to be minimum (0.27$\pm$0.06) during monsoon and maximum (0.41$\pm$0.14) during postmonsoon. During winter and pre-monsoon AOD values were 0.35$\pm$0.02 and 0.30$\pm$0.03, respectively. The surface aerosol mass concentration also showed a seasonal variation but is not similar for all modes. The nucleation aerosols mass concentration was maximum during winter whereas the accumulation aerosols was maximum during monsoon and coarser aerosols like dust aerosols were abundant during premonsoon. Consequently, the number concentration also showed a similar seasonal variation. BC mass concentration was maximum at 4.8$\pm$1.6 μg.m^{-3} during winter and minimum at 1.1$\pm$0.1 μg.m^{-3} during monsoon, which is very similar to the variation of nucleation aerosols. However, during November BC concentration anomalously increased due to large amount of biomass burning. At Ahmedabad the diurnal variation of BC mass concentration showed two peaks, one during morning and the other during late evening hours. A seasonal variation was also observed in the BC peak concentration. In the hill-top region, Mt. Abu, AOD was a factor of three times less than that over Ahmedabad. At Mt. Abu AOD (at 0.5μm) was minimum (0.09$\pm$0.03) during winter and maximum (0.18$\pm$0.05) during post-monsoon. During premonsoon and monsoon AOD was 0.16$\pm$0.08 and 0.10$\pm$0.02, respectively. The surface aerosol mass concentration showed a different seasonal variation when compared to that at Ahmedabad. Nucleation and accumulation aerosols were maximum during postmonsoon whereas coarse aerosols showed a maximum during premonsoon. The number concentration also varied similarly. BC mass concentration was

maximum during premonsoon and minimum during monsoon at Mt. Abu. Sharp diurnal peaks like those at Ahmedabad were not observed over Mt. Abu. However, BC mass concentration was enhanced during day time as the BC produced at the foothill area reaches the hilltop due to strong thermal convection. During winter the observatory comes into the free-tropospheric region and therefore AOD and aerosol mass concentration are minimum. During premonsoon there is a large enhancement of anthropogenic aerosols like BC due to increase in the local tourism. The hill-top region is also influenced by two major natural aerosol types that are transported from surrounding region. One is seasalt that is transported from Arabian sea during monsoon and the other is dust aerosols transported from the 'Thar' desert during premonsoon.

Chapter 4 presents results from special campaigns and projects to study the major changes of aerosols properties over different environments. Indo-Gangetic basin is one of the most densely populated and highly polluted regions of the globe and is a source region for anthropogenic aerosols like BC due to large amount of biomass and fossil fuel burning and major industries. As a result, during winter fog is often produced in this region which has a large influence on aerosols and on the radiative balance of Earth-Atmosphere system. As a part of the Indian Space Research Organization Geosphere Biosphere Programme (ISRO-GBP) a land campaign was conducted during December 2004, and aerosol optical properties were studied at Hissar, situated in the Indo-Gangetic basin. Interesting results on aerosol properties prior to, during and after foggy days were obtained. AOD was found to be 0.34 ± 0.1 prior to foggy days which however increased to 0.66 ± 0.3 during foggy days and after foggy days it came down to 0.46 ± 0.1. During foggy days the hourly AOD variation was also found to be very high caused due to rapid changes in the relative humidity. Angstrom exponent, calculated from spectral analysis of AOD, reveals that prior to foggy days, bigger particle concentration was dominant than compared to clear days. Aerosol mass concentration was found to be 95 μg.m^{-3} before foggy days, 231μg.m^{-3} during foggy days and 103 μg.m^{-3} after foggy days. The fog event was also found to alter the aerosol size distribution.

An increase in the number concentration of the nucleation mode (radius <0.1 μm) particles along with a decrease in the mode radius showed the formation of freshly nucleated aerosols. In the case of accumulation mode (0.1 μm$<$radius$<$1.0 μm) an increase in the mode radius was observed showing the hygroscopic and coagulation growth of particles. To study aerosol properties in a coastal environment a campaign was carried out at Kalpakkam, an eastern coastal station of India during March 2006, as part of the Integrated Campaign for Aerosols, gases, and Radiation Budget (ICARB). Being a coastal station, Kalpakkam experiences land and sea breezes and hence large variations in the aerosol properties were observed during different breeze conditions. Land breeze carries large amount of BC aerosol to the measurement site and contributes to the enhancement of aerosol absorption. The observed SSA therefore decreased to $\sim$0.80 during land breeze and was 0.92 during sea breeze period. However, during a cyclonic event in the Bay of Bengal (BoB) this decrease in the SSA was small due to seasalt loading into the atmosphere. During measurement period all the aerosol parameters exhibited minimum during sea breeze and maintained a background level. However, these background aerosol properties also enhanced when the wind was coming from Indo-Gangetic Basin via BoB instead of central BoB or the Arabian sea via North Indian Ocean. The background BC mass concentration increased by a factor of 1.6. In the western part of India frequently occurring dust storms produce major changes in aerosol properties. The dust aerosols are produced by dust storms in the nearby desert areas and enhance the aerosol optical depth, number concentration in the hill-top region. Due to these dust storms the background single scattering albedo (SSA) also changed. During premonsoon these dust storms increase the dust loading in the atmosphere over western region of India. During a campaign in Udaipur aerosol properties were observed and compared with those at Ahmedabad and Mt. Abu during April 2007. The main findings are as follows. Maximum AOD was found at Ahmedabad followed by Udaipur and Mt. Abu. The nucleation aerosols mainly containing anthropogenic aerosols were four times more at Ahmedabad and two times more at Udaipur when compared to Mt. Abu whereas as coarse aerosols

mainly containing natural dust aerosols were maximum at Udaipur followed by Ahmedabad and Mt. Abu. Two peaks were observed in the diurnal BC variation at Ahmedabad whereas only one significant peak during morning hours was observed at Udaipur. The BC mass concentration was maximum during morning at both Ahmedabad and Udaipur whereas during afternoon it went down to the background level and was equal to the BC mass concentration at Mt. Abu.

In *Chapter 5*, the method to compute aerosol radiative forcing is described briefly and the seasonal variations of aerosol radiative forcing over Ahmedabad and Mt. Abu are presented. In addition, aerosol radiative forcing during different meteorological conditions at different location of India are also discussed. At Ahmedabad there is a large seasonal variation of aerosol properties and therefore, SSA showed large variation with maximum at 0.86 ± 0.04 during monsoon and minimum at 0.80 ± 0.09 during postmonsoon. The atmospheric forcing showed a large variation in the range of 27.5 ± 14.7 to 49.1 ± 4.3 Wm^{-2}. Due to the variation of boundary layer height the aerosol properties showed a large variation at Mt. Abu and hence the radiative forcing. SSA was minimum at 0.83 ± 0.01 during premonsoon and maximum at 0.90 during winter, and consequently the atmosphere forcing varied from 6.1 ± 1.8 to 23.6 ± 5.5 Wm^{-2}. Due to the background condition the radiative forcing is less by factor of two to four at Mt. Abu than that at Ahmedabad. During dust storm at Mt. Abu the radiative forcing increased significantly. During premonsoon the shortwave radiative forcing is maximum at the urban region, Ahmedabad due to maximum amount of BC mass concentration, followed by semi-arid region, Udaipur and minumun at Mt. Abu whereas the net forcings are similar at Ahmedabad and Udaipur due to equivalent amount of dust aerosol in the atmosphere. At eastern coastal region large transportation of BC mass concentration from Indo-Gangetic Basin via BoB causes large aerosol radiative forcing. The aerosol radiative forcing at Hissar, a station in Indo-Gangetic Basin, shows maximum during foggy period than during other days during December 2004. During foggy days the large variation of relative humidity caused a huge change in the aerosol properties which changed the total scenario of diurnal

variation of aerosol radiative forcing during foggy days and even at TOA forcing becomes negative to positive due to increase in the radiative forcing.

In *Chapter 6* the contribution of anthropogenic and natural radiative forcing to the total forcing at Ahmedabad and Mt. Abu and their seasonal variation is discussed. At Ahmedabad, anthropogenic aerosol radiative forcing is dominating during all seasons whereas natural forcing is dominating only during monsoon. During monsoon there is transportation of seasalt as well as locally produced dust particles due to high surface winds which increases the natural forcing. At Mt. Abu natural forcing is dominating during premonsoon and monsoon due to the enhancement of natural dust and seasalt aerosols during these seasons, respectively. However, during postmonsoon and winter natural and anthropogenic forcings are less and contributing equally to total forcing. This is due to the decrease in transported seasalt aerosol during postmonsoon and during winter, the observation site becomes a free-tropospheric station. In addition, the diurnal BC variation also has a large influence on the radiative forcing at Ahmedabad and Udaipur and is larger at the former station. The minimum BC concentrations at all the three stations are equivalent however, the background forcing are not similar. The difference between the Ahmedabad background forcing and that of Mt. Abu forcing is more than a factor of two greater than the difference between those at Udaipur and Mt. Abu. In the coastal region, Kalpakkam, the daily short range transportation of BC aerosols from Chennai and its surroundings causes large forcing during land breeze than during sea breeze. The long range transportation of BC from Indo-Gangetic Basin via Bay of Bengal enhances the background forcing in the coastal region.

Finally, the results obtained from the present study are summarized and the scope for future work is also discussed briefly.

CHAPTER 1

Introduction

1.1 Aerosols and their Properties

Aerosols, the tiny solid and/or liquid particles suspended in the air, are the most crucial component of the earth's atmosphere that have a large impact on the climate change. Aerosols are of both natural and anthropogenic origin. The major natural aerosol components are sea-salt, soil dust, natural sulfates, volcanic aerosols and those generated by natural forest fires whereas the major anthropogenic aerosols are sulfate, soot and organics. By scattering and absorbing of the incoming solar radiation and outgoing terrestrial radiation these aerosols perturb the radiative balance of the atmosphere. Natural aerosols are particularly important because they provide the base level aerosol impact and there is no effective control on them unlike their anthropogenic counterparts. On the global scale the abundance of natural aerosols is several times higher than the anthropogenic aerosols. The latter are however being given greater importance as the atmospheric loading of these aerosols, especially those containing sulfur and carbon, has substantially increased since the preindustrial times (*IPCC*, 2007). Because

of their relatively short lifetimes, the concentrations of anthropogenic aerosols are highest over those regions with high industrial activities and/or biomass burning, and their climatic impacts are believed to be most pronounced there (*Charlson et al.*, 1992; *Kiehl and Briegleb*, 1993; *Ramanathan et al.*, 2001a,b; *Takemura et al.*, 2005, etc.). In those regions, the increase in aerosols also leads to an increase in the cloud droplet concentration and a decrease in cloud droplet size which tends to lower the precipitation efficiency. Increasing amount of anthropogenic aerosols and consequent modification of the atmospheric temperature structure may also induce perturbation in convection and monsoonal circulations which can alter the hydrological cycle (*Boucher et al.*, 1998; *Ramanathan et al.*, 2001b; *Graf*, 2004; *Liepert et al.*, 2004).

Major natural aerosols are seasalt and dust. Seasalt aerosols are highly abundant, can constitute up to 75% by mass of all natural aerosols (*Blanchard and Woodcock*, 1980) and are produced by bursting of bubbles over oceanic surface. Dust aerosols are formed by winds mostly in the arid regions of the world. The long range transport of dust aerosols by the combined action of convection currents and general circulation systems make these aerosols a significant constituent even at locations far from their sources (*Prospero et al.*, 1981; *Tegen and Fung*, 1994; *Arimoto*, 2001; *Tegen*, 2003; *Zender et al.*, 2003; *Ginoux et al.*, 2004, etc.). The major anthropogenic aerosols, sulfate, soot or Black Carbon (BC) and organics are mainly produced by biomass, fossil fuel burning, burning of garbages, industrial outlets, etc. As the sources and the production mechanisms are different, the aerosols have a wide size distribution, which can be different in different parts of the globe. Mostly, the aerosol size distribution for a particular location depends on the production and removal mechanisms of the aerosols. According to size, aerosols are classified into nucleation mode (radius$<0.1\mu$m), accumulation mode ($0.1<$ radius<1.0) and coarse mode (radius$>1.0\mu$m). Depending on whether aerosols are formed chemically or physically, they are found in nucleation or accumulation mode. Nucleation mode aerosols are mainly formed by gas-to-particle conversion whereas accumulation mode aerosols are formed by the coagulation processes or

heterogeneous condensation of gas vapor onto aerosols. Nucleation aerosols contribute very little to the total aerosol mass but are the most predominant in number. Major aerosol amount exists in accumulation mode. Accumulation aerosols are most important aerosols as they not only have relatively longer life times, but also have high scattering coefficient at visible wavelengths and hence directly affect the radiation budget. Anthropogenic aerosols mainly belong to the accumulation mode, and can have the largest impact on climate (*Jones and Slingo*, 1996). Accumulation mode aerosols also have a major impact on cloud properties and can change the cloud condensation nuclei (CCN) properties which indirectly effects the radiation budget (*Lohmann and Lesins*, 2002).

Aerosols are transported over short or long distances depending on their size and altitude at which they are present, before they are removed from the atmosphere. Dry and wet depositions are the two major removal processes of aerosols. Dry deposition mainly happens when the aerosols are settled by the gravitational force or due to their impacts on the surface owing to their inertia or atmospheric turbulence. Wet deposition is the process by which aerosols are flushed out by rain or swept out by the gravitational force after they become a large particle by condensation growth. These processes such as transportation and depositions control the residence time of the aerosols. Nucleation mode aerosols have higher rate of condensation growth and coagulation processes. As a result, they can be quickly transferred to the accumulation mode. Therefore, these aerosols have smaller residence time in the atmosphere. However, aerosol residence time is longer when they are transferred from troposphere to stratosphere. This occurs mainly due to less water vapor present in the stratosphere which does not favour wet deposition. In general, in the lower troposphere the residence time of aerosols is about a week and in upper troposphere, it increases up to a month whereas in stratosphere it can be maximum of about 3 years (*Jayaraman et al.*, 1995).

1.2 Role of Aerosols in Climate

The climate system is a complex, interactive system consisting of the atmosphere, land surface, ice, water bodies like ocean and living things. The ultimate energy source of all the governing processes in the climate system is sun. The amount of solar energy received at the top of the earths atmosphere in a unit area at any instant of time is about 1,370 Wm^{-2}, and the amount of energy per square meter averaged over the entire planet is one-quarter of this energy. About 30% of this received energy is reflected back to the space. Two third of this reflected energy is due to the cloud and aerosols in the atmosphere. The rest one third energy is reflected back by the earth's surface. The remaining part of the energy that is not reflected is absorbed by the earth's surface and atmosphere. Due to the sphericity of the Earth, more energy is received by the tropics than the high latitudes where sunlight strikes at a lower angle. The energy is transferred from equatorial regions to higher latitudes via atmospheric and oceanic circulations. The atmospheric circulation is mainly driven by the latent heat released when the water vapor condenses into clouds. Therefore, atmospheric and oceanic circulations help to attain the climate equilibrium. On the other hand, to balance the incoming energy, the Earth radiates the same amount of energy in the long wavelength into the space. At the top of atmosphere (TOA), the absorbed shortwave solar energy is balanced by the outgoing longwave terrestrial radiation. Any process which disturbs this radiative balance, can cause climate change and is known as radiative forcing. The changes in concentration of atmospheric constituents like greenhouse gases and aerosols can produce large perturbations in the radiative balance and hence induce climate change. Greenhouse gases absorb longwave radiation and cause warming effect in the atmosphere whereas aerosols affect the incoming shortwave solar radiation by scattering and/or absorbing and can cause cooling or heating of the atmosphere depending on their physical, optical and chemical properties. Aerosols also have a large impact on the outgoing longwave terrestrial radiation by absorbing, emission and scattering. During the post-industrial era, the effect of

aerosols in the global climate change has become significant as the concentration of atmospheric aerosols of anthropogenic origin is steadily increasing (*Houghton et al.*, 1996). However, the production of these aerosol is spatially inhomogeneous, and has resulted in hot spots of high aerosol concentration in various parts of the world. The radiative forcing in these regions therefore has become much more important on the regional scale.

Natural aerosols provide a base level of aerosol impact on radiation budget and there is no effective control on the production of natural aerosols. Besides, on the global scale, the percentage contribution of natural aerosols is more than that of the anthropogenic aerosols (*Andreae*, 1995). Among the natural aerosols, dust has an important role to play in the radiative forcing as it directly affects the earth's radiation budget. In the last 20 years, major efforts have been made by numerical studies (e.g., *Liu and Westphal*, 2001), ground and satellite based studies (e.g., *Torres et al.*, 1998; *Sun et al.*, 2001; *Prospero et al.*, 2002; *Christopher et al.*, 2003; *Christopher and Wang*, 2004) in different parts of the world to understand the temporal and spatial characteristics of airborne dust aerosols in the source regions and its impact on climate change. However, aerosol radiative forcing is one of the largest sources of uncertainty in estimating climate change because of the increasing amount of anthropogenic aerosols (*Charlson et al.*, 1992; *Houghton et al.*, 1995). Recent modelling and field studies indicate that one of the major contributing aerosol to the climate change is black carbon (BC), which is a result of incomplete combustion of coal, diesel, petrol, biofuels and biomass burning (*Lindberg*, 1993). Due to the short life-time of BC in the atmosphere, its concentration is highest in those regions with high industrial activity and/or biomass burning and the strong radiative forcing occurs over those regions (*Kiehl and Briegleb*, 1993; *Ramanathan et al.*, 2001b, etc.). The importance of BC is due to its high absorbtion of the visible and infrared radiation which contributes to global warming (*Jacobson*, 2001). Its long range transport can also be used as an anthropogenic tracer in the submicron size regime (*Parungo et al.*, 1994). During winter an anthropogenic haze is produced largely from South East Asia due to high pollutant emissions in those areas (*Lelieveld et al.*, 2001) and

spreads over Bay of Bengal as well as North Indian Ocean. Observations during Indian Ocean Experiment (INDOEX) found a haze which is a mixture of several inorganic and carbonaceous species including absorbing black carbon and dust, over North Indian ocean. The in-situ experiments reported that anthropogenic aerosols contributed as much as 80% to the aerosol loading and the optical depth over open ocean due to the presence of this haze (*Ramanathan et al.*, 2001b). This haze, carrying 10-15% BC (by mass), causes the regional radiative fluxes to change by an order of magnitude larger than the global mean forcing by greenhouse gases (*Krishnan and Ramanathan*, 2002; *See et al.*, 2006). It also contributes to a major impact on hydrological cycle (*Satheesh and Ramanathan*, 2000) and near surface heat budget over nearby continental regions (*Wang*, 2004).

1.3 Scope of the Present Study

In recent years, there is a growing interest to investigate the influence of aerosols on the climate change through direct and indirect radiative effects. Our present knowledge on the regional scale variation of aerosol properties is however not sufficient to fully incorporate the effects of aerosols in climate change studies. In order to fill-in the knowledge gap, there have been a large number of field campaigns conducted around the globe, such as Aerosol Characterization Experiment (ACE) (*Bates et al.*, 2002), Tropospheric Aerosol Radiative Forcing Observational Experiment (TARFOX) (*Russel et al.*, 1999), Smoke, Clouds, and Radiation- Brazil (SCAR-B) (e.g., *Nobre et al.*, 1998; *Christopher et al.*, 2000), Indian Ocean Experiment (INDOEX) (*Ramanathan et al.*, 2001b), etc. Among these experiments, ACE was designed to increase our understanding of atmospheric aerosols affecting the Earth's climate system. ACE-1 focused mainly on the natural aerosols over southern hemispheric mid-latitudes and the goal of the study was to understand the properties and controlling factors of the remote marine aerosols which are relevant to radiation balance and climate (*Bates*, 1999; *Hainsworth et al.*, 1998; *Griffiths et al.*, 1999). ACE-2 was conducted to study the atmospheric radiative effects on

the North Atlantic Ocean where large anthropogenic aerosols and dust are transported from Europe and Africa, respectively (*Russell and Heintzenberg*, 2000). While ACE-1 and ACE-2 were concentrated on the natural and anthropogenic aerosols, respectively, ACE-Asia was coordinated for the complex mix of natural and anthropogenic aerosols over Asia (*Huebert et al.*, 2003; *Seinfeld et al.*, 2004). There have been consistent efforts over the Indian region to characterize the spatial and temporal variations of aerosols through campaigns realized under the Indian Middle Atmosphere Program (IMAP) during the mid eighties and early nineties (e.g., *Jayaraman and Subbaraya*, 1993) and lately under the Indian Space Research Organisations Geosphere Biosphere Program (ISRO-GBP) (e.g., *Subbaraya et al.*, 2000; *Jayaraman et al.*, 2006). The recent experiments like INDOEX suggested that South and Southeast Asia are major source regions of anthropogenic aerosols and these aerosols have large influences over oceanic regions adjacent to Indian subcontinent (e.g., *Jayaraman et al.*, 1998; *Lelieveld et al.*, 2001; *Ramanathan et al.*, 2001b; *Satheesh and Srinivasan*, 2002). Within the Indian region, the Indo-Gangetic Basin (IGB), located in the northern part of India, is of particular importance as it is a highly aerosol loaded region and has the largest aerosol optical depth during both summer and winter seasons (*Jethva et al.*, 2005). In this region the domestic energy consumption largely depends on biofuels (such as cow-dung cake, wood, straw and other agriculture wastes) in rural areas and mainly fossil fuels in urban areas. During winter, industrial urban locations like Kanpur and Delhi show high amounts of BC loading which has a large radiative forcing impact on climate (*Tripathi et al.*, 2005; *Ganguly et al.*, 2006b). In the Indo-Gangetic Basin (IGB), occurrence of fog is a common feature during winter. At high relative humidity conditions aerosols act as condensation nuclei, which help to produce the fog, which, in turn, can alter the properties of the aerosols (*Pandis and Seinfield*, 1990). Fog, in general, starts occurring late at night and can continue up to next day noon. In the present study, the aerosol properties and their changes during fog conditions in the IGB through a month long field campaign conducted at Hissar in December 2004 as part of the ISRO-GBP Land Campaign-II are addressed. The fog induced aerosol properties

are discussed and diurnal variation of aerosol radiative forcing during the fog period and compared with that during clear sky conditions. During January-May, the haze, a mixture of anthropogenic BC, sulfates, nitrates which are abundant over Indo-Gangetic Basin, and the natural aerosols such as sea salt and mineral dust, spread over the Bay of Bengal and contribute to the large reduction in the surface radiation over oceanic surface as well as coastal areas. In order to investigate the reduction in solar radiation at the surface due to the transportation of this haze to the east coast region of India, aerosol properties have been studied at Kalpakkam as a part of the Integrated Campaign for Aerosols, gases, and Radiation Budget (ICARB) programme during March 2006. Being a costal region Kalpakkam has an experience of land and sea breezes and hence there is a large change of aerosols properties and is discussed.

A major part of the present research work is devoted to understand the seasonal variation of aerosols properties and its radiative effect over Ahmedabad, an urban region in the western part of India and Mt. Abu, a high altitude station in the same region with a pristine environment. Several interesting features like seasonal and inter-annual variations in aerosol properties are observed and discussed in *Chapter 3*. These variations are largely due to changes in meteorological conditions. The background aerosol physical and radiatively active properties are influenced by the dust aerosols coming from the 'Thar' desert during premonsoon and also seasalt aerosols transported from Arabian sea during monsoon. Besides these long term observation a small campaign was carried out for the study of aerosols properties in semi-arid environment at Udaipur. The objective of this campaign is the comparative investigation of aerosol properties in the various parts of western India during dust prone season.

All the present long term and campaign mode observations of aerosol properties are used to estimate the radiative forcing over different study regions and are discussed in *Chapter 5*. The radiative forcing is also estimated during different meteorological conditions. Finally the anthropogenic and natural aerosol radiative forcing is delineated and their seasonal variation is also discussed in *Chapter 6*.

CHAPTER 2

Measurement Techniques

The instruments, operated for measuring the various physical and optical properties of aerosols are Sunphotometer, Microtops, Quartz Crystal Microbalance Cascade Inpactor, Aethalometer, Nephelometer and Aerosol Size Spectrometer for the present study at different locations. The working principle, methodology and the measurement uncertainties are briefly discussed in this chapter.

2.1 Sunphotometer

Aerosol Optical Depth (AOD) was measured by hand-held Sunphotometer by measuring the direct solar radiation intensity at the ground. This instrument is built in-house at the Physical Research Laboratory, Ahmedabad. The Sunphotometer consists of an interference filter, photodiode and necessary electronics (*Acharya and Jayaraman*, 1995) . Direct solar intensity was measured at seven wavelength bands using optical interference filters, centered around 0.400, 0.500, 0.670, 0.750, 0.875 and 1.050 μm. The total field of view of the sunphotometer is 8° and was achieved using a baffle attached in front of the photometer. The measurement was

taken only on cloud-free days form 0830 to 1630 local hours. Beer-Lambert law is used to calculate AOD and shown below :

$$I(\lambda) = I_0(\lambda)\left(\frac{r_0}{r}\right)^{-2}\exp\left[-m\tau\right] \tag{2.1}$$

where $I(\lambda)$ and $I_0(\lambda)$ are the instantaneous intensity of the monocromatic solar radiation at wavelength λ, at the ground and top of the atmosphere (TOA), respectively, m is relative air mass (ratio of actual path to the vertical path), τ is the total optical depth and r is the Sun Earth instantaneous distance and r_0 is the Sun Earth mean distance. The solar intensity I at the ground was measured by the Sunphotometer in volt. I_0 is derived from the Langley plot technique in which the logarithm of I is plotted against the relative airmass and I_0 is the value of I, extrapolated to relative airmass of zero. The relative airmass can be derived from the relation (*Young*, 1994),

$$m = \frac{1.002432\cos^2\chi + 0.148386\cos\chi + 0.0086467}{\cos^3\chi + 0.149864\cos^2\chi + 0.0102963\cos\chi + 0.000303978} \tag{2.2}$$

where χ is the solar zenith angle which can be derived form the relation,

$$\cos\chi = \cos\delta\cos\phi\cos h + \sin\delta\sin\phi \tag{2.3}$$

where δ is the sun's declination, ϕ is the longitude of the location and h is the local hour angle. Eq. 2.2 provides a better accuracy for Earth's curvature and the atmospheric refraction of the solar radiation and for smaller solar zenith angles ($<60^\circ$) Eq. 2.2 becomes $m = \sec\chi$. The atmospheric molecules and aerosols contribute to the total optical depth $\tau(\lambda) = \tau_a(\lambda) + \tau_{ray}(\lambda) + \tau_{ma}(\lambda)$, where τ_a is the aerosol optical depth, τ_{ray} is the Rayleigh scattering by the air molecule and τ_{ma} is the molecular absorption. The direct solar radiation received at the Earth's surface depends on the composition of the atmosphere and amount of each species. To calculate the AOD, the transmittance (T_i) of the different components in the atmosphere in the optical band from 0.300 μm to 1.200 μm was obtained from the

Santa Barbara DISORT Atmospheric Radiative Transfer (SBDART) Model (*Ricchiazzi et al.*, 1998). The optical depth of a particular atmospheric component (c) was obtained using the relation,

$$\delta_c(\lambda) = \frac{\int_{\lambda_1}^{\lambda_2} T_c(\lambda) FT(\lambda) d\lambda}{\int_{\lambda_1}^{\lambda_2} FT(\lambda) d\lambda} \tag{2.4}$$

where $FT(\lambda)$ is the filter transmission for the wavelength from λ_1 to λ_2. The filter transmission was observed in the laboratory with the help of a double-beam spectrometer. The Rayleigh Optical Depth (ROD) was obtained by calculating the effective Rayleigh scattering crosssection (σ_{eff}) by the relation,

$$\sigma_{eff}(\lambda) = \frac{\int_{\lambda_1}^{\lambda_2} \sigma_{ray}(\lambda) FT(\lambda) d\lambda}{\int_{\lambda_1}^{\lambda_2} FT(\lambda) d\lambda} \tag{2.5}$$

where $\sigma_{ray}(\lambda)$ is the Rayleigh scattering crosssection using Nicolet's equation (*Nicolet*, 1984). ROD was calculated by using the column integrated air number density ($N = 2.16E + 25cm^{-2}$) for the tropical model atmosphere, multiplied by the average Rayleigh scattering cross section in the optical band from λ_1 to λ_2. For the AOD calculation the maximum error is less than $\pm 15\%$ due to instrumental error (due to bias and precision). Ignoring the contribution from "forward" scattering to the measured solar radiation intensity (*Jayaraman et al.*, 1998) also contributes to the error.

2.2 Microtops

Aerosol Optical Depth (AOD) was measured using a hand-held Microtops II (Solar Light Co., Inc., USA) (*Morys et al.*, 2001; *Ichoku et al.*, 2002) on cloud-free days. This instrument can measure AOD at five different wavelengths centered at 0.380, 0.440, 0.500, 0.675, 0.870 μm simultaneously. To measure the AOD at 1.020 μm wavelength associated with ozone and columnar water vapor another Mictotops II was used. Both the Microtops were regularly calibrated once in a month and all

the calibrated constants were obtained from Langley's plot analysis carried out at Mount Abu (26.6°N, 72.7°E, 1.7 km asl), less affected by anthropogenic activity. To obtain the calibration constant observations have been made on cloud-free days.

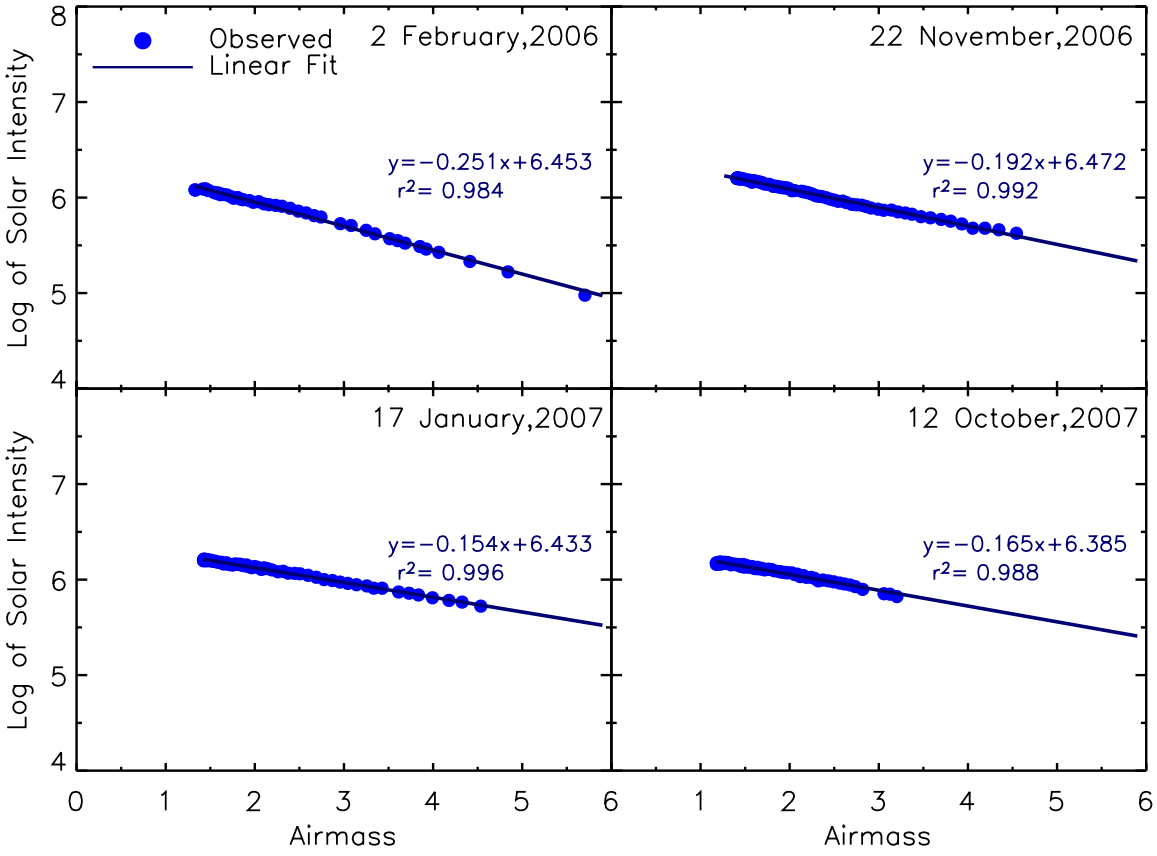

Figure 2.1: *Langley plots are shown for 0.5 µm wavelengths for four months. The blues circles and magenta triangles represent the forenoon and afternoon observed solar radiance at the surface. The best fitted linear lines, obtained from the Beer-Lambert's relation are drawn for forenoon and afternoon separately and the intercept of the y-axis gives the solar radiance at the top of atmosphere ($I_0(\lambda)$) and the difference slope is due to slightly change of AOD during forenoon and afternoon observation*

In Fig. 2.1 Langley plots have been shown for four months at 0.5 μm wavelength. The best fitted linear line, obtained from the Beer-Lambert's relation (Eq. 2.1) during the observational period gives the solar radiance $I_0(\lambda)$ at the top of atmosphere. $I_0(\lambda)$ values are given in Table 2.1 for 6 different channels of Microtops during the period 2006-2007. During the observations three consecutive measurements ware taken at a time to reduce the manual error. The absolute uncertainty

Table 2.1: *The Calibration Constants ($I_0(\lambda)$) for six different channels of Microtps readings during Feb'06 to Dec'07 at Mt. Abu. These constants are obtained from Langley Plot method.*

Month and Year	Calibration Constants $I_0(\lambda)$					
	0.380 μm	0.440 μm	0.500 μm	0.675 μm	0.870 μm	1.020μm
Feb 2006	6.87	6.20	6.42	7.14	6.57	6.89
Mar 2006	6.86	6.22	6.42	7.14	6.58	6.85
May 2006	6.85	6.20	6.40	7.12	6.55	6.78
Jun 2006	6.80	6.16	6.36	7.08	6.50	6.88
Sep 2006	6.78	6.14	6.36	7.08	6.57	6.83
Oct 2006	6.89	6.22	6.41	7.18	6.59	6.83
Nov 2006	6.99	6.32	6.49	7.20	6.61	6.85
Dec 2006	6.98	6.33	6.51	7.20	6.61	6.82
Jan 2007	6.92	6.27	6.43	7.19	6.65	6.81
Feb 2007	6.89	6.25	6.43	7.16	6.61	6.80
Mar 2007	6.86	6.22	6.40	7.14	6.59	6.81
Apr 2007	6.85	6.21	6.40	7.14	6.56	6.87
May 2007	6.86	6.23	6.44	7.17	6.59	6.85
Jun 2007	6.46	6.25	6.43	7.16	6.61	6.84
Oct 2007	6.84	6.20	6.44	7.11	6.55	6.84
Dec 2007	6.84	6.22	6.40	7.15	6.63	6.80

of measured AOD is not more than 0.03 at every wavelength (*Morys et al.*, 2001; *Ichoku et al.*, 2002).

2.3 Quartz Crystal Microbalance Cascade Impactor

Aerosol mass concentration was measured using a 10-stage Quartz Crystal Microbalance (QCM) cascade impactor (model PC-2, California Measurements Inc., USA) and the aerosol size distribution at the ground level was determined. The aerosols were collected in 10 stages of the impactor with 50% efficiency cut-off radii at 12.5, 6.25, 3.2, 1.6, 0.8, 0.4, 0.2, 0.1, 0.05 and 0.025 μm from stage 1 to 10, respectively. The air flow rate through the impactor was kept at 240 ml/min. The typical sampling period was 300 *sec* for each measurement. The QCM observations were made at every hour throughout the day. The air inlet was installed vertically to minimize the loss of aerosol particles within the inlet tube. Each stage of the impactor has two identical piezoelectric crystal sensors, as shown in Fig. 2.2 and

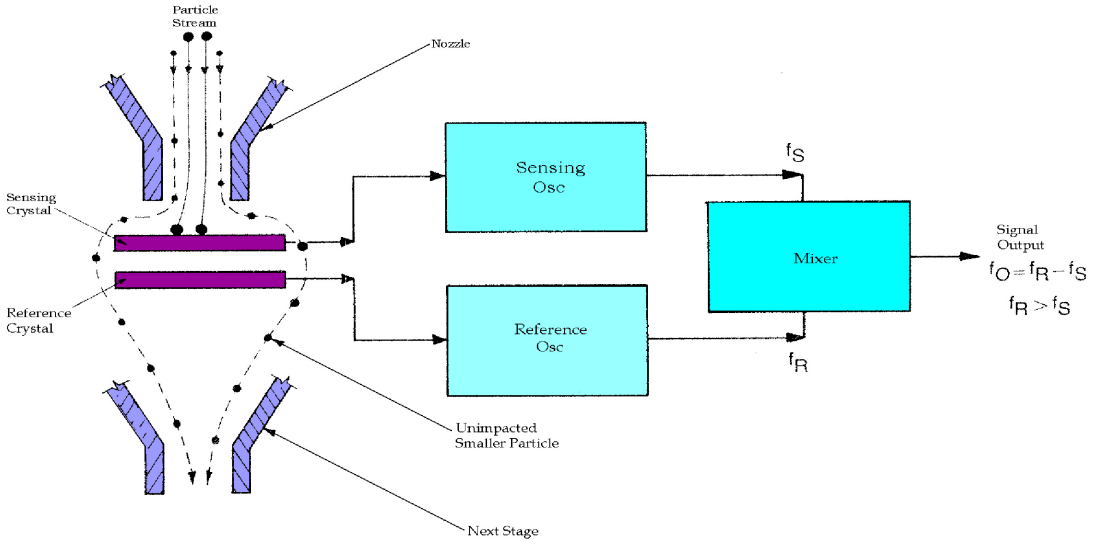

Figure 2.2: *Schematic of one of the stages of a Quartz Crystal Microbalance Cascade Impactor*

the ambient air passes through each of these sages. The aerosol stream accelerates through a nozzle with a small high-speed jet and impinges on the closer quartz crystal plate, known as sensing crystal. The heavier particles collide with the crystal plate due to their inertia and lighter particles are carried out by the air flow and continue to travel forward. A thin coating of grease on the crystal ensures the capture of the particles impinged and the frequency of the crystal changes instantaneously. The other identical crystal is immediately behind the sensing crystal and is known as reference crystal. As it is behind the sensing crystal, there is no particle impaction and hence its frequency is unchanged. Once the sampling is over, the difference between the sensing and reference crystal frequencies (Δf) gives the corresponding aerosol mass concentration, $\Delta m = -(1.4 \times 10^{-9})\Delta f$. The main uncertainty comes into the aerosol mass concentration due to the bouncing of aerosols and their sliding from the crystal plate. A thin grease coating on the crystal reduces these effects. Another cause which contributes to the uncertainty, is the reduction of crystal frequency due to aging effect. The relative temperature change of the crystals during each sampling period of 5 minute is very small and uncertainty due to change of temperature can be neglected. The maximum uncertainty due to

all the above mentioned factors in the measured aerosol mass concentration of all the ten stages is within 25% (*Jayaraman et al.*, 1998). The other major uncertainty which arises due to the swelling of aerosol during higher relative humidity (RH) conditions. This effect is also included in the aerosol mass calculation according to necessity (*Ramachandran and Jayaraman*, 2002; *Ramachandran et al.*, 2006).

2.4 Aethalometer

Black Carbon (BC) mass concentration is derived from the measured real-time light attenuation using a multichannel Aethalometer (AE-47 of Magee Scientific, Berkeley, USA). Aethalometer is a time based light attenuation instrument which has seven wavelength narrow bandwidth light sources ranging from the near ultraviolet to the near infrared region with a reference and a broadband sensing detectors. This is a filter based technique used to measure the light attenuation due to the particle deposition onto a quartz fiber filter (*Hansen et al.*, 1982, 1984). In the present study, BC concentration is determined by measuring the attenuation of a beam of light, at seven wavelengths, *viz*, 0.380, 0.470, 0.520, 0.590, 0.660, 0.880 and 0.950 μm, transmitted through the sample collected on the filter. With the help of a pump and inlet tube ambient air is sucked at a rate of 3 $l.min^{-1}$ and measurements are taken round the clock, and the data are averaged for every five minutes and stored.

The absorption coefficient (β_{abs}) is defined by Beer-Lambert's law $I = I_0 e^{\beta_{abs} \cdot l}$, where I_0 is the intensity of the incident light and I is the intensity of the transmitted light passing through a medium of thickness l. Aethalometer measures light attenuation ($ATN = 100 ln \frac{I}{I_0}$) through an aerosol embedded quartz filter, where I and I_0 are the intensities of light transmitted through the sampled and a blank spot (unsampled) filter, respectively. The attenuation absorbtion coefficient (β_{ATN}) for a sampled time duration $\triangle t$, is $\beta_{ATN} = \frac{A}{100Q} \frac{ATN}{\triangle t}$ where A is the area of the spot of

sample over the filter and Q is the volumetric sampling flow rate. BC concentration (μg.m^{-3}) is calculated by the following relation

$$BC = \frac{\beta_{abs}}{\sigma_{abs}} = \frac{\beta_{ATN}}{\sigma_{ATN} R(ATN)} \tag{2.6}$$

where σ_{abs} and σ_{ATN} are the mass specific absorption and attenuation cross-sections (in unit $m^2.g^{-1}$), respectively and σ_{ATN} is derived using the simple relation $\sigma_{ATN} \equiv \sigma_{abs} C$. It is well known that attenuation absorbtion coefficient, β_{ATN} may differ from the actual aerosol absorption coefficient, β_{abs} of the deposited aerosol particles (*Petzold et al.*, 1997; *Weingartner et al.*, 2003; *Schmid et al.*, 2006, etc.). This significant difference occurs due to enhancement of the optical path length by the multiple scattering of light beam at the filter fiber and also due to "shadowing effect". For these reasons the calibration constants C and R(ATN) are introduced to correct for the attenuation absorption coefficient. C is the calibration constant due to the multiple scattering of the light at the filter fibers in the unloaded filter and is greater than unity. This multiple scattering of light leads to an enhancement of optical path (*Liousse et al.*, 1993). C generally depends on the nature of the filter. Other calibration constant, R(ATN) is introduced due to "shadowing effect". This effect occurs due to the increase in filter loading which reduces the optical path length and hence decreases the absorption coefficient. R(ATN) varies with the amount of aerosol particles deposited on the filter and also on the optical properties of the deposited particle. For the unloaded filter R should be unity *i.e.*, R(ATN = 0) =1. R also depends on the single scattering albedo (ω) of the sampled aerosol associated with the deepness of the aerosol embedded into the filter matrix which depends on the particle size, particle morphology and the flow rate. For Aethalometer (AE-47) the highest particle loading on the filter is appreciable for maximum change in ATN up to 0.78, 0.55 and 0.30 for 0.380, 0.520 and 0.880 μm, respectively, and beyond which the filter tape is automatically forwarded to expose a new pristine filter spot (ATN$\sim$0). In the Fig. 2.3 time series of three absorbance, ATN(380), ATN(520), ATN(880) are shown, represented by blue circles, green triangles and red squares, respectively.

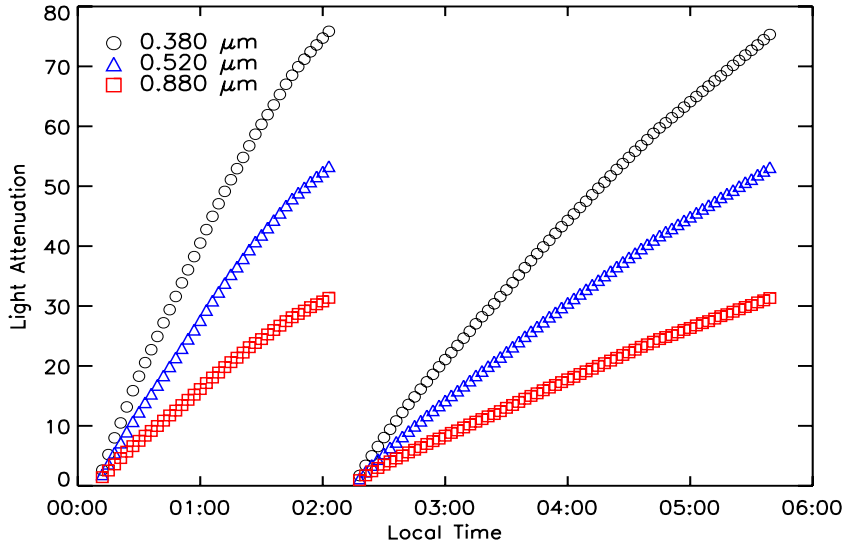

Figure 2.3: *A typical time series of light attenuation (ATN) of Aethalometer for 0.380, 0.520 and 0.880 μm at Ahmedabad during winter season*

The main uncertainty in the measurements comes from the variability in σ_{ATN} in Eq. 2.6. The exact knowledge of σ_{ATN} is necessary for the calculation of BC concentration from Aethalometer. σ_{ATN} strongly depends on the aerosol type and age (*Liousse et al.*, 1993; *Petzold and Niessner*, 1995). The observed value of σ_{ATN} (measured with the incandescent lamp instrument) varies from 5 m^2g^{-1} (remote area) to 14 m^2g^{-1} (urban region). At the remote continental site σ_{ATN} is taken as 9.3 m^2g^{-1} (*Lavanchy et al.*, 1999) whereas for the most polluted site; near the street it is 20 m^2g^{-1} (*Liousse et al.*, 1993). In the present study σ_{ATN} is taken as 16.6 m^2g^{-1} corresponding to 0.880 μm for the AE-47 Aethalometer. This value is comparable with that of the urban region but for the other regions this is either comparable or higher than the actual value. As a result the reported BC concentration represents the minimum values. The other uncertainties in the measured BC concentration come from the measurement of flow rate of ambient air, sampled spot area and the detector response. The flow rate was checked periodically with a bubble flow meter. Considering the combined effect of all these factors, the maximum uncertainty

in the measured BC concentration is about 10% (*Ramachandran and Rajesh*, 2007).

2.5 Nephelometer

Scattering coefficient of aerosol is obtained with the help of an Integrated Nephelometer (Model M903), manufactured by Radiance Research, California, USA. Nephelometer is used to measure the scattering coefficient of the aerosol in the ambient air which comes through a temperature controlled inlet and passes out from the measurement volume (Fig. 2.4). The measurement volume is illuminated by a flash lamp and the scattered light is measured at 0.530 μm by a photomultiplier tube kept perpendicular to air flow. The instrument is regularly calibrated in laboratory by the procedure as described by *Charlson et al.* (1968). The offset of the instrument is corrected by passing particle-free air and span calibration is done by passing gases of high scattering coefficient such as CO_2. In Fig. 2.4 the optical design of a typical Integrated Nephelometer is shown. The main body consists of a thin-walled aluminum tube. Optical receiver is kept at one end of the tube and a light trap at the other end to provide a dark background against which to view the light scattered by the aerosols and/or gases. Illumination is provided by a quartz-halogen lamp with a built-in elliptical reflector. The reflector focuses the light onto one end of of the optical pipe, which serves to thermally isolate the lamp from the sensing volume. The output end of the optical pipe is an opal glass diffuser that provides a nearly Lambertian light source. A broadband-coated 400 mm focal length lens is used to collimate the diverging light defined by apertures in the body of the instrument. From the lens, the scattered light enters into the photomultiplier tube (PMT) passing through a 40 nm bandpass filter, centered at 0.530 μm, into a photomultiplier (Green channel). The reference chopper, which rotates at 23Hz, consists of three separate areas - signal, dark and calibrate - as shown in the inset.The signal section simply allows all light to pass through unaltered. The dark section blocks all light to provide a measurement of PMT background noise. The calibration section scattered by internal surfaces and gas portion of the aerosol.

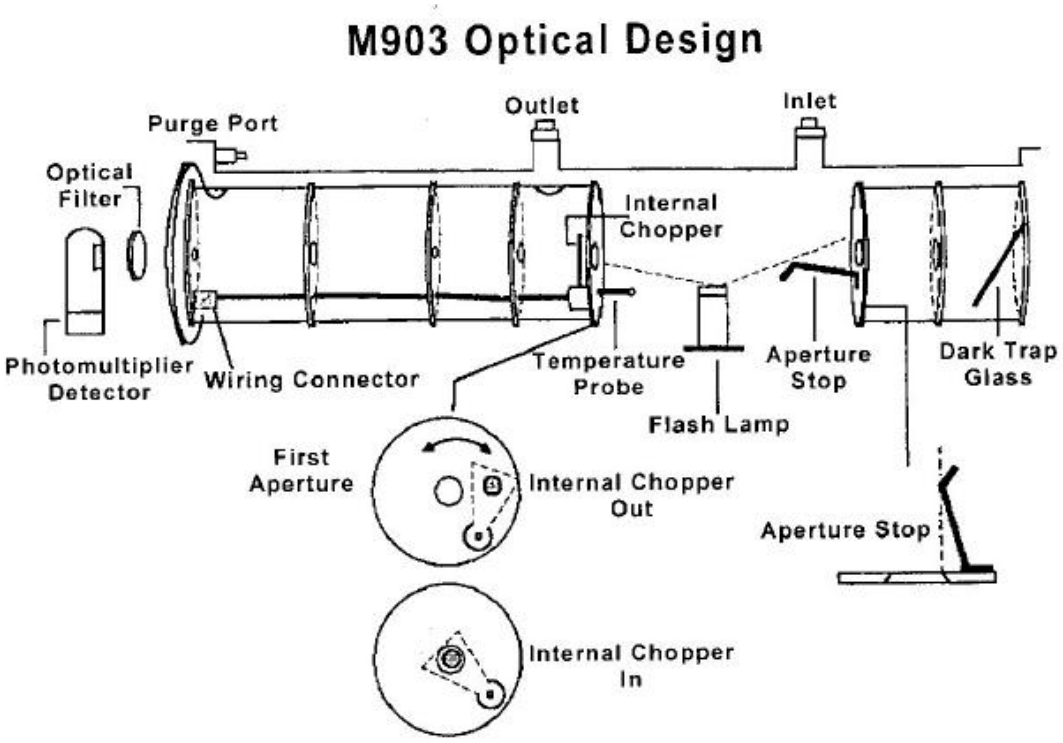

Figure 2.4: *Optical design of atypical single wavelength Integrated Nephelometer*

Correction for changes in gas density is accomplished continuously by means of pressure and temperature sensors. In addition, the relative humidity (RH) of the sample volume is monitored and a second temperature sensor at the outlet keeps track of sample heating.

The major uncertainties in the scattering coefficient measurements arise during the calibration procedures, different environment conditions, photon counts etc. During the calibration procedure the uncertainties are introduced by changes in temperature (T) and pressure (P) of the standard gas and presence of water vapor. During the calibration period these sources of errors can be eliminated by using dry air (bottled standard air or dry ambient air) (*Anderson et al.*, 1996). The total uncertainties in scattering coefficient are about 0.42% for air and 0.95% for CO_2 (*Anderson et al.*, 1996). Other uncertainties come from photon counting and wavelength dependency. During measurement photon counts for three forms, i.e. raw, scale and normalized. Raw and scaled count rates (in Hz) are defined for three portions of the rotating shutter, *i.e.*, calibrate, signal and dark. The normalized photon

count represents the combination of the three scaled count to derive a signal that is corrected for dark counts and changes in lamp brightness. So the uncertainties of this normalized photon counts should be included into the total uncertainties of Nephelometer measurements. There is also a small correction for photomultiplier dead time but does not affect the uncertainties because it only comes into play at high photon count rates. For an ideal Nephelometer, the light source should be Lambertian point source, and scattered by volume elements that act as point sources of scattered light. Other uncertainties are related to the source of light and different particle sizes. The error in the Nephelometer measurement is less than 10% for accumulation-mode or smaller particles (*Anderson et al.*, 1996).

2.6 Aerosol Size Spectrometer

Surface aerosol number concentrations were measured using Grimm Aerosol Technik (Ainring, Germany) Aerosol Spectrometers (model 1.108). The instrument is field portable, weighing 2.4 kg, with maximum operational period of up to 7 hours using an integral internal battery (or indefinite with an external 110/220V power supply). The ambient air is sucked by a small pump at air flow rate 1.2 $l.min^{-1}$. The air passes though a detector cell which consists of a semiconductor laser source and a receptor diode. When particles are passing through the detector cell the laser light interacts with the particles and generates a scattered light signal proportional to the size of the aerosol particles. A receptor diode collects scattered light at 90° and the signal is processed in a multichannel size classifier. The optics are protected against contamination using a sheath air flow. According to the size the signal is counted in 15 different size bins of 0.3-0.4, 0.4-0.5, 0.5-0.65, 0.65-0.8, 0.8-1.0, 1.0-1.6, 1.6-2.0, 2.0-3.0, 3.0-4.0, 4.0-5.0, 5.0-7.5, 7.5-10.0, 10.0-15.0, 15.0-20.0, $>$20 μm diameter. This instrument is operated round the clock and data were collected continuously as 1 min averages, stored on a removable data card, and downloaded and processed using Grimm 1.174 software. Ambient temperature and humidity were measured continuously using a Grimm (Model 1.154)

accessory sensor probe, with data also stored as 1 minute averages. All particles are collected on an outlet filter for further chemical or other gravimetric analysis. This instrument is placed just beside the QCM instrument and it is made sure that both instruments are drawing the same air sample. The number distribution observed by Grimm is comparable with the number distribution calculated from aerosol mass concentration observed by QCM (*Jayaraman et al.*, 2006).

CHAPTER 3

Results on Aerosol Characteristics

Measurement of the physical and optical properties of aerosols is very important to estimate the aerosol radiative forcing, which is an important parameter in quantifying the climate change. The radiatively important properties of atmospheric aerosols are determined at the most fundamental level by the aerosol composition and size distribution. Various closure studies have been successfully conducted which lend added credibility to the measurements of the individual quantities (*McMurry et al.*, 1996; *Clarke et al.*, 1996; *Hegg et al.*, 1997; *Quinn and Coffman*, 1998; *Wenny et al.*, 1998; *Raes et al.*, 2000; *Gupta et al.*, 2006, etc). Aerosol optical depth is the most important parameter which is used to estimate the aerosol radiative forcing. The study of the aerosol size distribution is also very important to understand the climate change. For example, the aerosols in accumulation mode (0.1μm$\leq$radius$\leq$1.0 μm) have large scattering efficiency, longer life time and most importantly the major anthropogenic aerosols which can easily perturb the climate change fall in this size range and hence have to be understood separately. The aerosol radiative forcing is also very sensitive to the single scattering albedo. A small change in this aerosol parameter can change the sign of radiative forcing

from negative to positive. This can be possible due to the enhancement of large absorbtion of solar light by the aerosols present in the atmosphere. Black carbon is one of these absorbing aerosols which contribute more to the reduction of solar radiation at the surface. The concentration of the various aerosol components and hence the aerosol radiative forcing is not uniform around the globe. Therefore, regional study of aerosol radiative forcing is very important to understand the global climate change more precisely.

3.1 Urban Aerosols

Recent increase in number of automobiles and industrialization in the urban regions lead to large production of anthropogenic aerosols and other gaseous pollutants. These urban aerosols are a mixture of anthropogenic aerosols, natural aerosols and also aerosols formed by gas-to-particle conversion (*Hess et al.*, 1998; *Seinfeld and Pandis*, 1998). They are highly concentrated over the urban regions and appear as hot islands in the global aerosol maps and contribute maximum perturbation to the global radiative balance demanding a regular investigation.

3.1.1 Site Location and Meteorological Parameters

The measurement site for the present study is in the campus of the Physical Research Laboratory (23.03°N, 72.55°E, 80m asl), Ahmedabad. Ahmedabad is one of the highly industrialized cities in the western part of India. The city has approximately six million population and has several small and large scale industries and a coal based thermal plant (capacity 350 MW/day) situated about 10 km far from the observational site. Rapid increase in the number of automobiles in the city is contributing significantly to the amount of anthropogenic aerosols. In addition, the city is located about 500 km south-east of the Thar Desert and therefore, Ahmedabad becomes a semiarid region. Thus, the measurement site is a suitable place for the study of both anthropogenically enriched aerosols and the natural soil dust

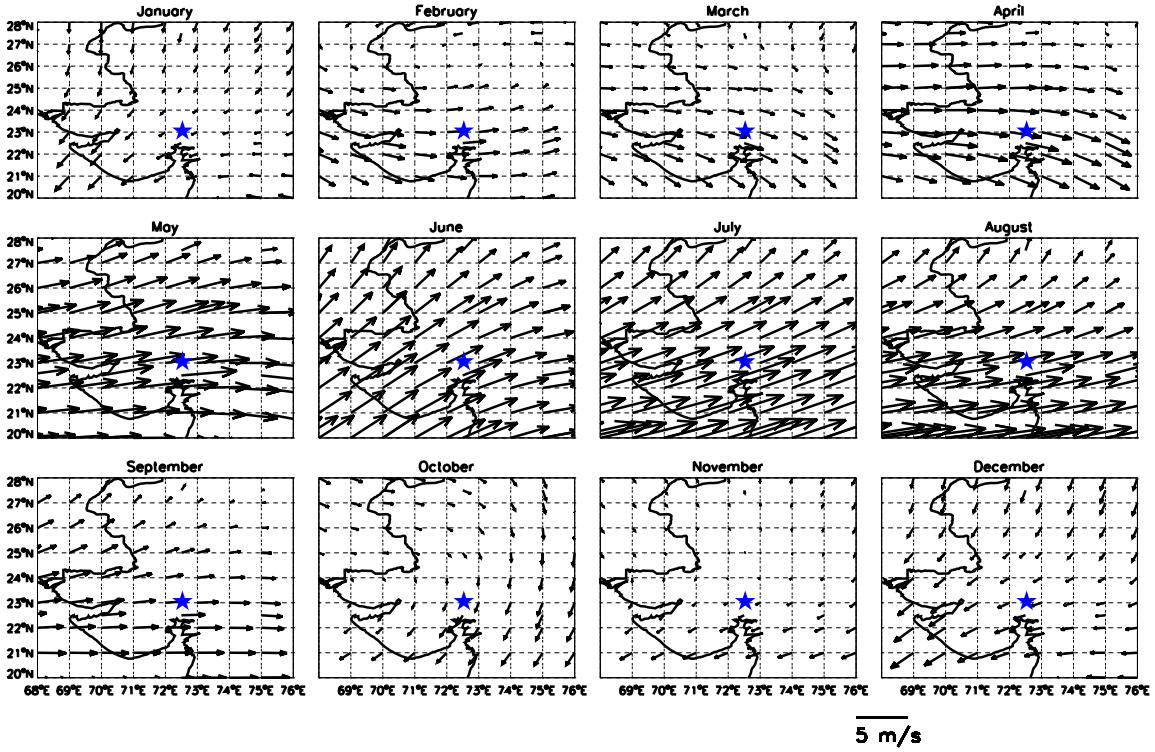

Figure 3.1: *Monthly mean wind parameters over Ahmedabad at 950 hpa altitude during 2007. Star symbol denotes the location of Ahmedabad.*

aerosols.

At Ahmedabad the major seasons are winter (Dec-May), premonsoon (Apr-May), monsoon (Jun-Aug) and postmonsoon (Sep-Nov). Fig. 3.1 shows the wind pattern over western part of India at 950 hpa level obtained from NCEP/NCAR reanalysis data. A large seasonal variation was observed in the wind direction and wind speed over Ahmedabad (blue star). During December–January, wind was mainly coming form north-east and as the month passed the wind speed slowly increased and changed direction. During premonsoon, wind was westerly and stronger. During monsoon, strong wind came from Arabian sea and during post-monsoon, wind was calm. The other meteorological parameters, viz., temperature, pressure and relative humidity (RH) show a variation that is similar during both years 2006 and 2007. Fig. 3.2 shows the diurnal variation of these parameters. During premonsoon, temperature was maximum and was higher than 40°C in the middle of day. During winter, there was a large diurnal variation in temperature

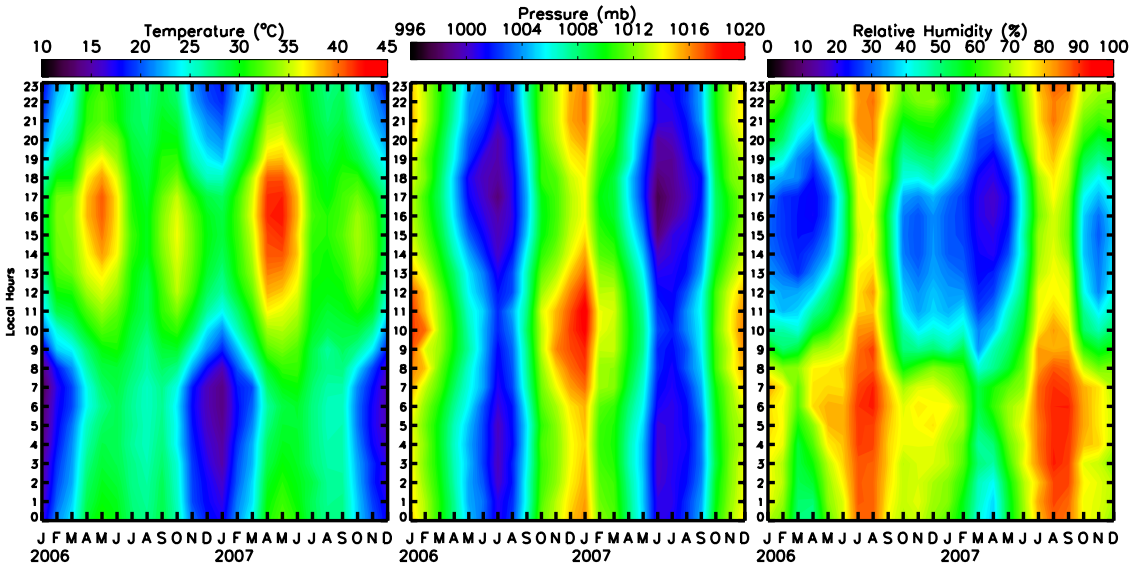

Figure 3.2: *Meteorological parameters at Ahmedabad during 2006-2007.*

with day time values greater than 30°C and the night time values lower than 15°C. During winter pressure was maximum and especially during morning it was the highest. During monsoon, pressure was minimum and during the rest of the year the pressure showed a little variation. RH also showed a seasonal variation. During monsoon, RH was more than 75% and during the other seasons RH was less than or equal to 50%.

Rainfall is another important meteorological parameter which strongly influences the aerosol loading in the atmosphere. Also, aerosol quantity and quality affect the cloud condensation nuclei and therefore the lifetime and precipitation pattern are modified. On the other hand, amount of rainfall determines the aerosol removal processes from the atmosphere. Though the investigation of aerosol and rainfall relation is beyond the main aim of the present work, study of rainfall variation is useful to draw conclusion about the amount of aerosol and its residence time over a site. Fig. 3.3 shows the monthly rainfall over Ahmedabad since January 2006 to December 2007. At Ahmedabad rainfall mainly occurs during summer monsoon. The climatorological mean rainfall over Ahmedabad is about 700 mm. In both the years the total rainfall is above this mean. Ahmedabad received relatively higher rainfall during 2006 than 2007.

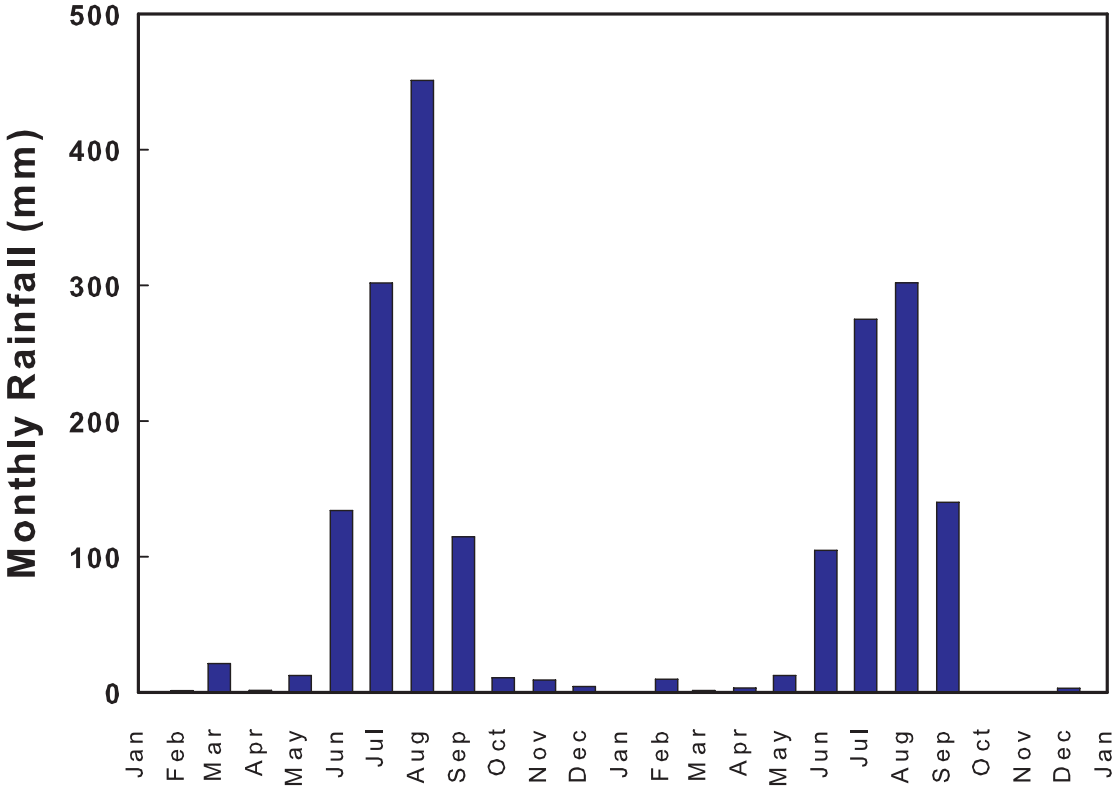

Figure 3.3: *Monthly rainfall over Ahmedabad from January 2006 to December 2007.*

3.1.2 Aerosol Optical Depth over Ahmedabad

The monthly Aerosol Optical Depth (AOD) spectra, measured during cloud free days are shown in Fig. 3.4. The magenta and black colors represent the AOD during 2006 and 2007, respectively. The vertical bar represents $\pm 1\sigma$ variation about the monthly mean values. AOD values during both years are comparable. An annual pattern is observed in higher wavelength ($\geq 0.5\mu$m) and also in lower wavelength ($\leq 0.5\mu$m) AOD values. The lower wavelength AOD values are mainly governed by the fine aerosols whereas higher wavelength AOD values by coarser aerosols (*Reid et al.*, 1999). The lower wavelength AOD values gradually decreased and higher wavelength AOD values increased from winter to premonsoon (Fig. 3.5). The main reasons are as follows. During winter thermal convection is weak and boundary layer is shallow due to low surface temperature. Hence, fine aerosols,

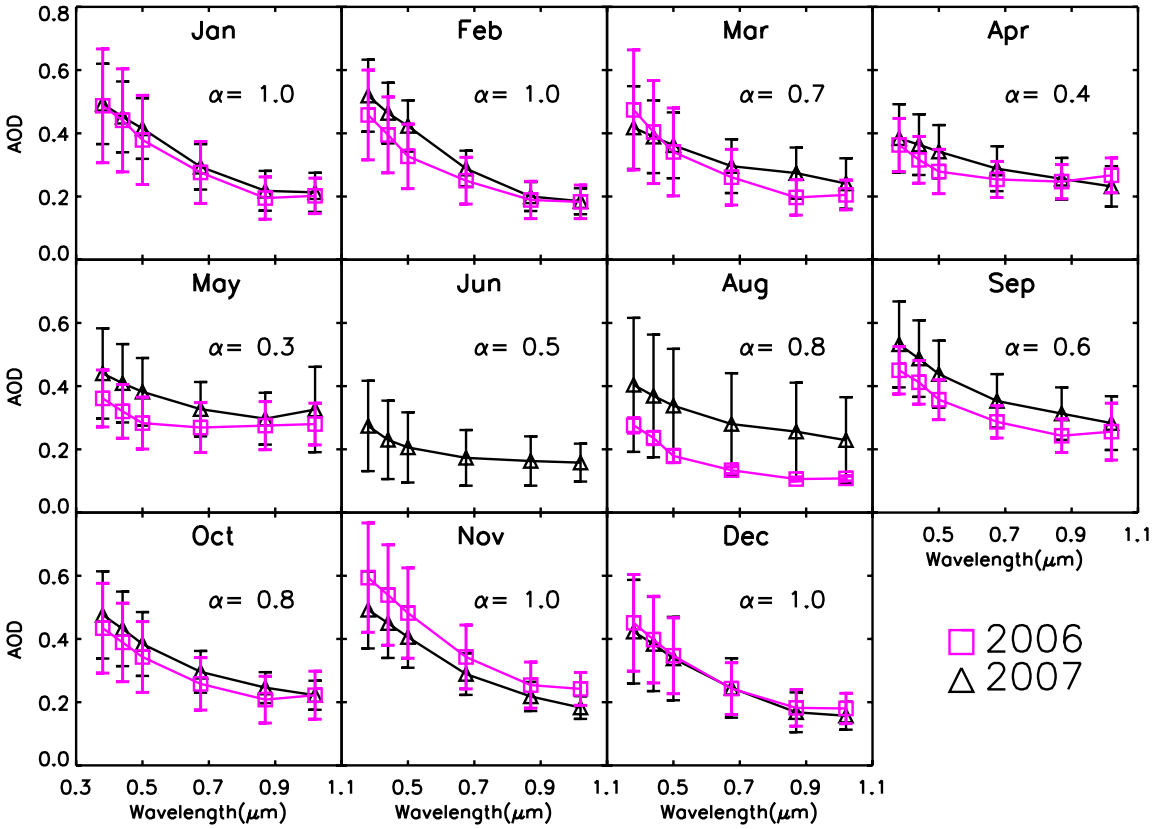

Figure 3.4: *Monthly variation of AOD spectra using Microtops obtained over Ahmedabad.*

mainly produced by gas-to-particle conversion enhanced and influenced the lower wavelength AOD. As winter passed, temperature increased (Fig. 3.2) and the thermal convection became stronger along with an increase in boundary layer height. As a result, the fine aerosols got more room to dilute and in addition, stronger wind also helped to move them away from the measurement site. Hence due to low abundance of fine aerosols lower wavelength AOD values decreased. However, during premonsoon, large amount of soil derived aerosols were lifted into the atmosphere by the strong wind thereby increasing the coarser aerosol concentration. Thus the longer wavelength AOD increased. During monsoon, mainly in August, AOD increased and this could be due to the presence of a thick layer of aerosol observed in 0.5-2.0 km altitude over Ahmedabad (*Ganguly et al.*, 2006a).

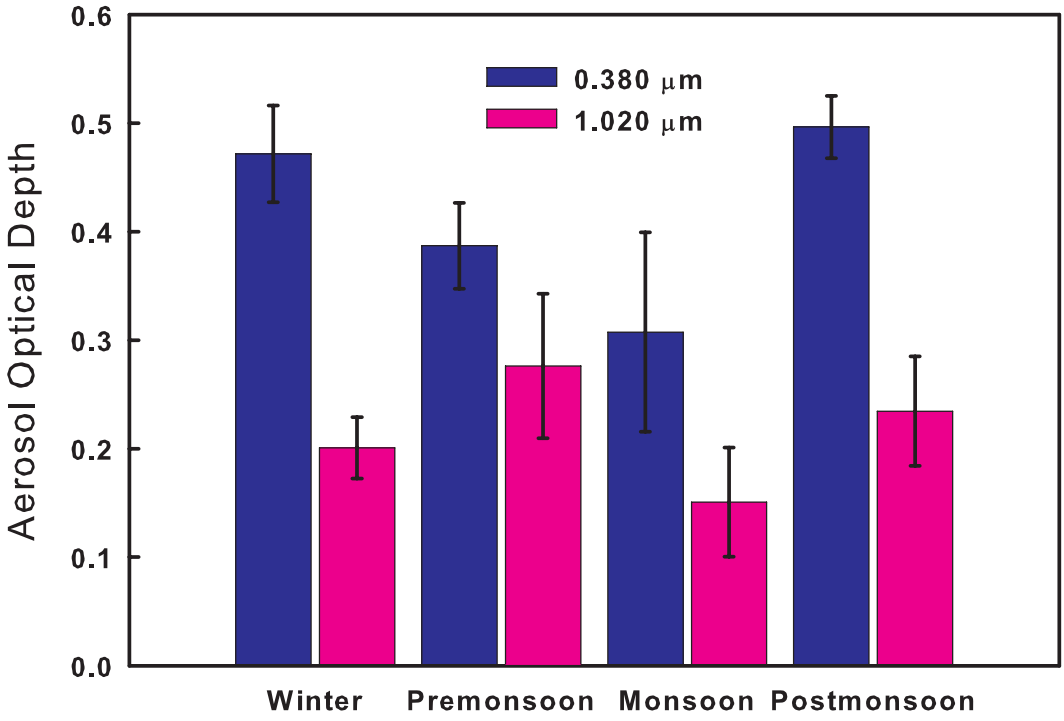

Figure 3.5: *Seasonal AOD variation over Ahmedabad during study period.*

However, August 2006 AOD values were low as the measurements were taken immediately after rain. During postmonsoon, the lower wavelength AOD increased once again and reached a maximum. During this season thermal convection and wind speed were weak due to low temperature. A combination of these two effects resulted in accumulation of fine aerosols at measurement site and therefore, lower wavelength AOD values were high.

The Angstrom exponent (α), defined as the slope of the logarithm of AOD versus the logarithm of wavelength (in μm), is an important parameter that provides the basic information about columnar particle size distribution (*Eck et al.*, 1999; *Reid et al.*, 1999; *Cachorro et al.*, 2001, etc.). α is higher for relatively higher concentration of fine particles and as the number of coarser particles increase, α decreases. The

Angstrom parameter showed a decreasing trend with seasons from winter to premonsoon. This also indicates that fine aerosols are dominating during winter and coarser aerosols are dominating during premonsoon.

3.1.3 Aerosol Mass Concentration

Aerosol mass concentration measured separately in ten different sizes by Quartz Crystal Microbalance (QCM) cascade impactor has been classified into three different categories, viz., nucleation (radius$<$0.1 μm), accumulation (0.1μm$\leq$radius$\leq$1.0 μm) and coarse (radius$>$1.0 μm) mode particles . Nucleation mode aerosols represent total aerosols collected in stages 9-10 , accumulation mode aerosols are the total aerosols of stages 5-8 and coarse mode aerosols are the total aerosols collected in stages 2-4. Aerosols collected in stage 1 are not considered in the calculation because all the aerosols whose radius is greater than 12.5 μm are collected in this stage. Thus, there is no definite aerosol radius represented by this stage.

In Fig. 3.6 shows the seasonal variation of aerosol mass concentration near surface at Ahmedabad for three size modes, averaged for the years 2006 and 2007. The contribution of nucleation mode aerosols to the total mass was minimum at 4.5$\pm$0.2μg.m^{-3} during premonsoon and maximum at 18.6$\pm$11.8 μg.m^{-3} during winter followed by postmonsoon (mean, 16.9$\pm$4.3 μg.m^{-3}) and monsoon (mean, 14.9$\pm$1.8 μg.m^{-3}). In general, the nucleation mode consists of gas-to-particle converted aerosols that are produced anthropogenically (like, fossil fuel and biomass burning) (*Hess et al.*, 1998). October to December is festival season at Ahmedabad and during this period enormous number of crackers are burnt. In addition to this, burning of garbages, solid wastes and fallen leaves in different parts of the city also contribute to the large production of nucleation aerosols. Hence during postmonsoon nucleation mode aerosol mass concentration was high and was maximum during winter. This is due to shallow boundary layer which enhanced the nucleation mass concentration during winter. During premonsoon, the boundary layer

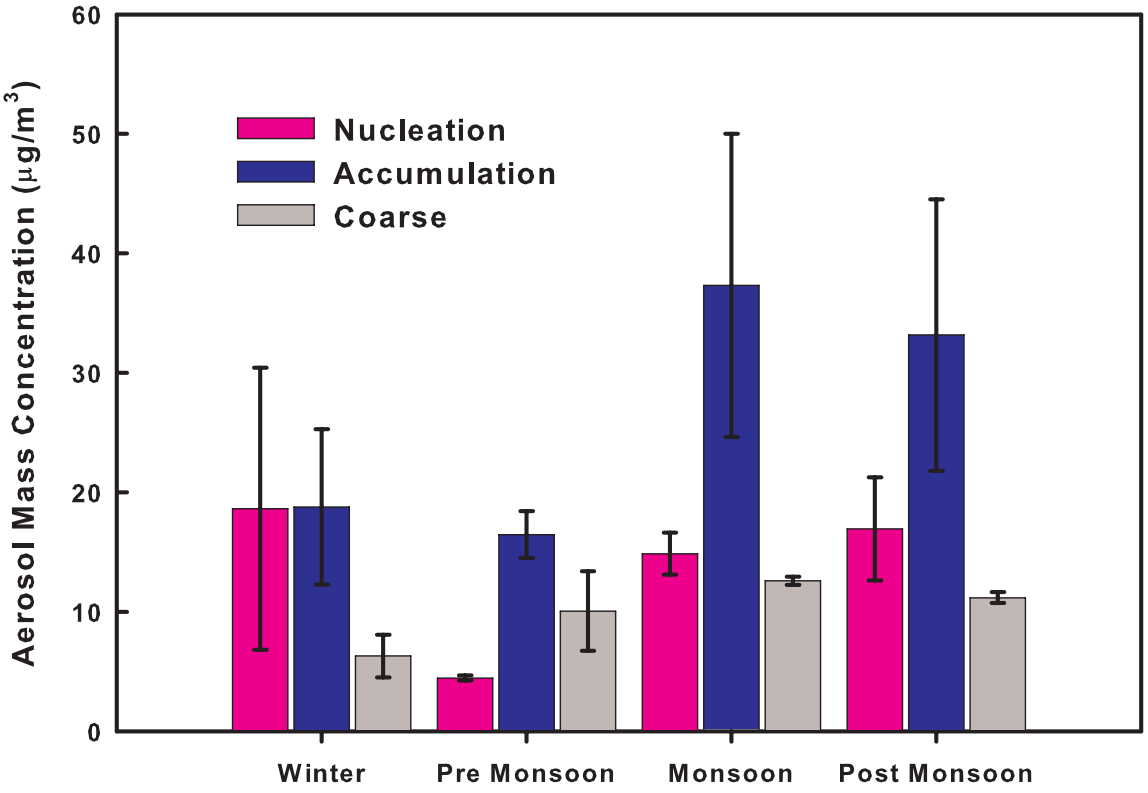

Figure 3.6: *Seasonal variation of near surface aerosol mass concentration classified into three categories, namely, coarse mode, accumulation mode and nucleation mode particles, averaged for two years of data available from 2006 to 2007 over Ahmedabad.*

height increased due to higher temperature. This caused stronger thermal convection which reduced the nucleation mass concentration and in addition strong advection diluted concentration.

The accumulation mode aerosols mainly consist of water soluble aerosols and are produced by the coagulation of nucleation particles and condensational growth of the aerosols. At Ahmedabad accumulation aerosol mass concentration was maximum at 37.3 μg.m^{-3} during monsoon and minimum at 16.5 μg.m^{-3} during premonsoon. During monsoon, high RH favored the condensation growth by absorbing moisture and/or an aqueous solution of any soluble constituents and the aerosols coagulate and therefore the accumulation aerosol mass was maximum. But during premonsoon low RH did not favor these processes and high wind moved away the aerosols from the measurement site and minimized the accumulation aerosols.

The coarse mode aerosols mainly consist of either soil born dust aerosols or the aerosols formed by condensation growth and coagulation processes. During premonsoon soil born dust aerosols in the coarse mode increased at Ahmedabad. The predominant coarse mode aerosols are iron rich aerosols, aluminium oxides and calcium carbonate (*Rastogi and Sarin*, 2005a) which indicates that they mainly come from the Earths crust due to strong wind during this season. During monsoon and postmonsoon coarser aerosols were less abundant in soil born dust aerosols as the large surface area is covered by vegetation. Generally, during these seasons the accumulation mode aerosols swell by condensation and coagulation processes at high RH condition and become coarse mode aerosols, thus increasing their mass concentration.

3.1.4 Aerosol Number Concentration

Aerosol number concentration is obtained from the measured aerosol mass concentration from QCM observations at Ahmedabad using appropriate mass density, which is valid for urban environment and the prevailing relative humidity conditions (*d'Almeida et al.*, 1991; *Hess et al.*, 1998). Size distribution of aerosol at any location is primarily governed by relative strengths of the different production and removal mechanisms (*Jaenicke*, 1993). Aerosol size distribution is mainly a combination of many log-normal distributions where different modes carry the information of different kinds of aerosol (*Porter and Clarke*, 1997; *Bates et al.*, 1998; *Koponen et al.*, 2003; *Ramachandran and Jayaraman*, 2002; *Ganguly et al.*, 2006b, etc.). Fig. 3.7 shows the aerosol size distributions during the four seasons at Ahmedabad. The vertical bar represents $\pm 1\sigma$ variation about the monthly mean number concentration of different sizes of aerosols. It is observed that the size distribution is tri-modal distribution and each mode can be fitted using the log-normal distribution, given below:

$$\frac{dn(r)}{d\log r} = \frac{N}{\sqrt{2\pi}\log\sigma}\exp\left[-\frac{\log^2\left(\frac{r}{r_m}\right)}{2(\log\sigma)^2}\right] \tag{3.1}$$

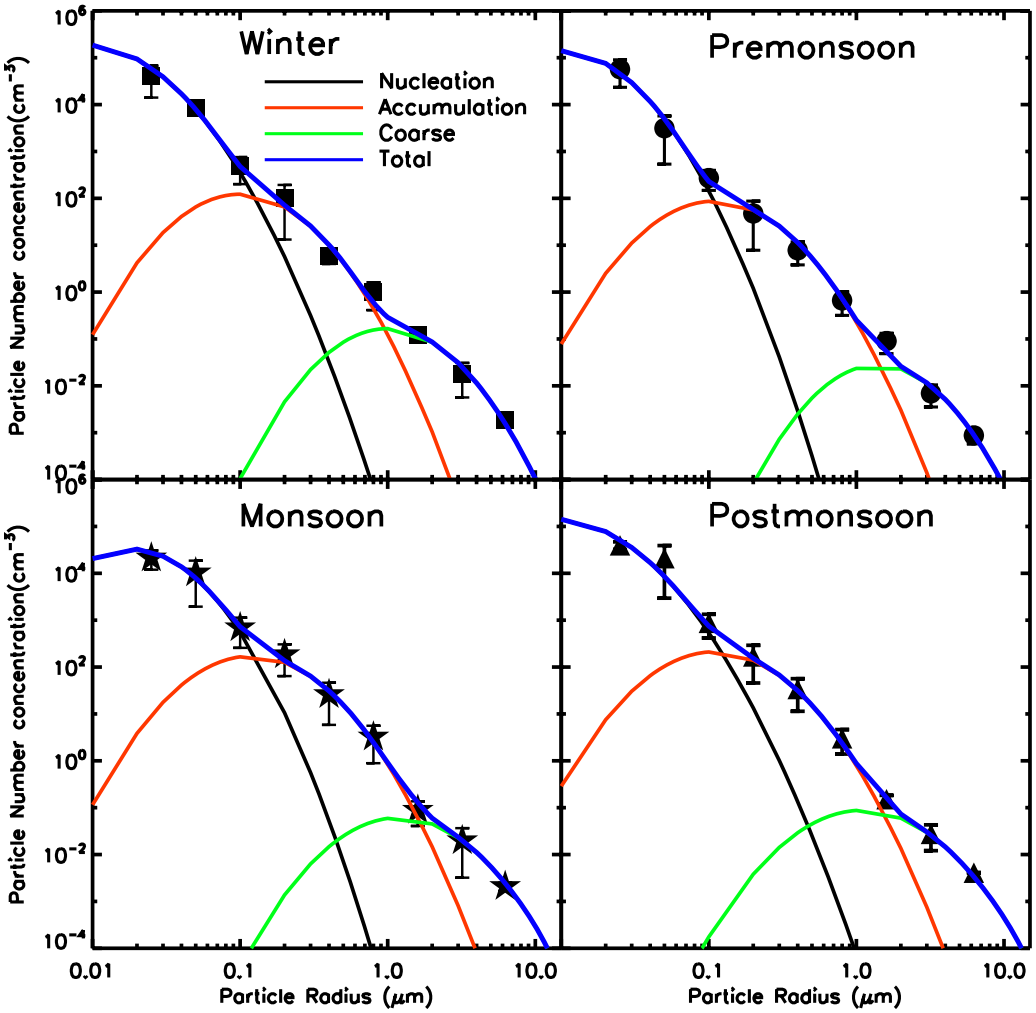

Figure 3.7: *The seasonal variation of aerosol number size distribution over Ahmedabad.*

where N is the peak number concentration (cm^{-3}), σ is the width of log-normal distribution and r_m is the mode radius for a particular mode. The aerosol number distribution is highly influenced by the aerosol production mechanism and removal processes. It is observed that the three modes exist in all four seasons but their parameters are different in different seasons. This indicates that at Ahmedabad the amount of aerosols as well as their sources are different in different seasons. The three modal parameters for all the four seasons are given in Table 3.1. The mode radius (r_m) for nucleation mode was in the range of 0.009-0.018 μm and the number concentration (N) was found to be minimum at 50000 cm^{-3} during monsoon and maximum at 320000 cm^{-3} during winter. Similarly mode radii of

accumulation and coarse modes were in the range of 0.10-0.12 μm and 1.0-1.4 μm, respectively. Comparing with these modal parameters with various kinds of aerosols, classified by earlier workers (e.g., *d'Almeida et al.*, 1991; *Hess et al.*,

Table 3.1: *Average Values of Size Distribution Parameters Obtained by Fitting Lognormal Curves to the Measured Aerosol Number Size Distribution Over Ahmedabad*

Seasons	Nucleation			Accumulation			Coarse		
	N cm^{-3}	r_m μm	σ μm	N cm^{-3}	r_m μm	σ μm	N cm^{-3}	r_m μm	σ μm
Winter	320000	0.009	1.97	190	0.10	1.86	0.25	1.0	1.82
Premonsoon	220000	0.010	1.86	140	0.11	1.90	0.04	1.4	1.77
Monsoon	50000	0.018	1.82	280	0.12	1.91	0.10	1.2	1.91
Postmonsoon	260000	0.009	2.00	350	0.11	1.93	0.15	1.1	1.97

1998), it is found that water soluble aerosols (mainly sulphate and nitrate) and seasalt aerosols mainly belong to the accumulation mode. These sulphate aerosols are produced in the atmosphere by the chemical reactions of gaseous precursors which is mainly coming into the atmosphere by the sulphur dioxide (SO_2) emitted from different anthropogenic sources (*Charlson et al.*, 1992; *Birmili and Wiedensohler*, 2000). In general, accumulation mode aerosols are hygroscopic in nature. During monsoon, mode radius of accumulation mode increases by condensation and coagulation growth. But the observed number concentration did not reach maximum due to high wind speed. However, during postmonsoon, it was maximum at 350 cm^{-3} due to low wind speed and low boundary layer height. Therefore, the anthropogenically produced aerosols could not move away from the measurement site.

Mode radius of coarse aerosols was maximum at 1.4 μm during premonsoon and minimum at 1.0 μm during winter. During premonsoon low RH condition makes the Earth's surface loose and high wind carries large amount of soil born aerosols into the atmosphere. So the coarser aerosols were dominating during this season. However, during monsoon and postmonsoon, soil born aerosols were less abundant, due to rain wash out during monsoon (*Rastogi and Sarin*, 2005b).

However, the number concentrations of coarse mode during these seasons was relatively high because accumulation aerosols swelled at high RH condition and become coarse aerosols. Therefore, dominance of coarse aerosols increased with smaller mode radius than that during premonsoon.

3.1.5 Monthly Variation of Black Carbon Mass Concentration

Black carbon (BC) produced due to incomplete combustion of carbon-based fuels (*Andreae*, 1995; *Novakov et al.*, 2000; *Jacobson*, 2001; *Venkataraman et al.*, 2005, etc) is the most efficient light absorbing aerosol component in the atmosphere. BC has major contribution to alter the radiative balance by absorbing the solar radiation in the visible spectrum. As a result, it cools the surface and warms the atmosphere (*Haywood and Shine*, 1995; *Krishnan and Ramanathan*, 2002). Recent study of BC contribution to radiative forcing by *Jacobson* (2001) shows that BC has a great contribution towards global warming and it is the second most important component of global warming after CO_2 and has a larger impact on direct radiative forcing than that of methane. As a result, in populated countries like India and China, the large production of BC aerosols has a large impact on the hydrological cycle and precipitation pattern (*Ramanathan et al.*, 2001b; *Satheesh and Srinivasan*, 2002; *Menon et al.*, 2002). In India the fraction of BC production from fossil fuel burning, open burning and biofuel combustion to the global emission is significantly large and hence it is necessary to estimate radiative impact of different kinds of BC not only on global scale but also in the regional scale.

Fig. 3.8 shows the diurnal variation of BC mass concentration at Ahmedabad during 2007. During postmonsoon, BC mass concentration was maximum at $5.7 \pm 5.1\ \mu g.m^{-3}$ followed by winter ($3.3 \pm 1.1\ \mu g.m^{-3}$) and premonsoon ($2.5 \pm 0.8\ \mu g.m^{-3}$). During monsoon it was minimum at $1.0 \pm 0.1\ \mu g.m^{-3}$. During November, BC concentration increased anomalously due to maximum contribution by cracker firing during festival nights and the monthly mean BC concentration was at $11.5 \pm 3.2\ \mu g.m^{-3}$. One of the major urban regions in India is Delhi (28.63°N, 77.17°E) where

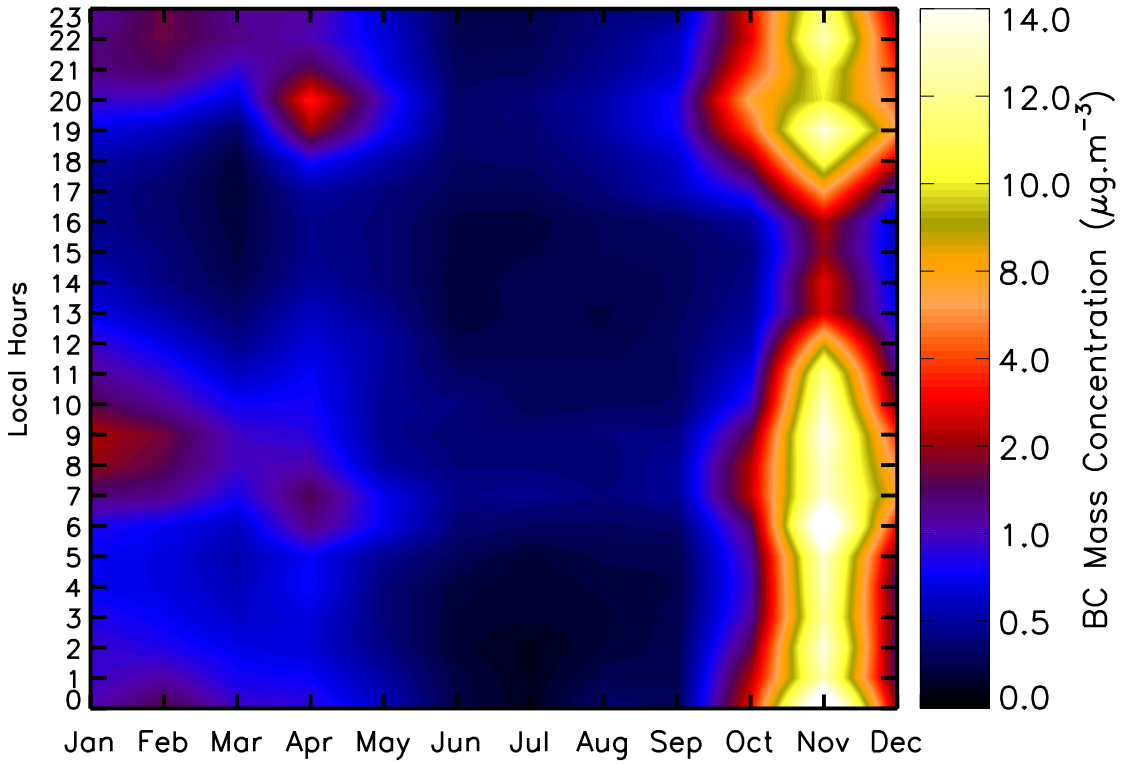

Figure 3.8: *Diurnal variation of BC mass concentration over Ahmedabad. There are two peaks observed in the diurnal BC mass concentration variation and the peak concentration also shows seasonal variations.*

the maximum BC concentration was 29±14 μg.m^{-3} during December 2004 (*Ganguly et al.*, 2006b). Another urban region in the Indo-Gangetic basin is Kanpur (23.43°N, 80.33°E) where high BC has been observed in the range 6-20 μg.m^{-3} (*Tripathi et al.*, 2005). Indo-gangetic basin is a source region of BC in India and there is a large transportation of BC from western to eastern region of Indo-gangetic basin during dry seasons (December-April). As a result at Kharagpur (23.5°N, 87.5°E) an eastern most urban region in the Indo-Gangetic Basin, a large variation of BC concentration was observed from 16μg.m^{-3} to 2μg.m^{-3} during December 2004 to April 2005 (*Nair et al.*, 2007).

There were two peaks in the diurnal BC variation at Ahmedabad similar to other urban regions of India (e.g., *Tripathi et al.*, 2005; *Ganguly et al.*, 2006b). The

first peak occurred during morning at 0700-1000 local hours and another started at nearly 1900 local hours and sustained up to the middle of the night, as shown in Fig. 3.8. The peak intensity also showed a seasonal variation which is influenced by not only the source and removal processes of BC but also the meteorological conditions at the location. During winter, both morning and nocturnal peaks had maximum strength. Gradually, the peak strength reduced due to advection by strong wind during premonsoon. In addition, high temperature resulted in stronger thermal convection and large boundary layer height. Hence, due to large ventilation the peak concentrations reduced. The thermal convection was stronger during afternoon period of premonsoon and therefore, BC mass concentration decreased to less than 0.5 μg.m^{-3}. During monsoon due to high rain BC particles were washed out from the atmosphere and hence amplitude of diurnal variation was small. Again during postmonsoon BC concentration increased due to shallow boundary layer and low wind speed sustained the BC for longer period.

3.2 Background Aerosols

3.2.1 Site Location and Meteorological Parameters

Major aerosol parameters have been monitored during 2006 and 2007 at Physical Research Laboratory's observatory situated at Gurushikhar, Mt. Abu (24.65°N, 72.78°E), the highest peak (1.7 Km asl) of Aravalli range of India. The observatory being a prohibited hilltop area makes the measurement site relatively anthropogenic free and hence is a suitable place for background aerosol measurements in the western part of India. Being very close (∼300 km) to 'Thar Desert' observatory gives an opportunity to study the dust aerosol which is transported from desert in premonsoon season (April-May). The monthly averaged wind pattern of Mt. Abu is shown in the Fig. 3.9. During premonsoon season wind is westerly and carries large amount of dust particles from the desert areas. During monsoon (June-August) wind changed it direction from westerly to south-westerly and becomes

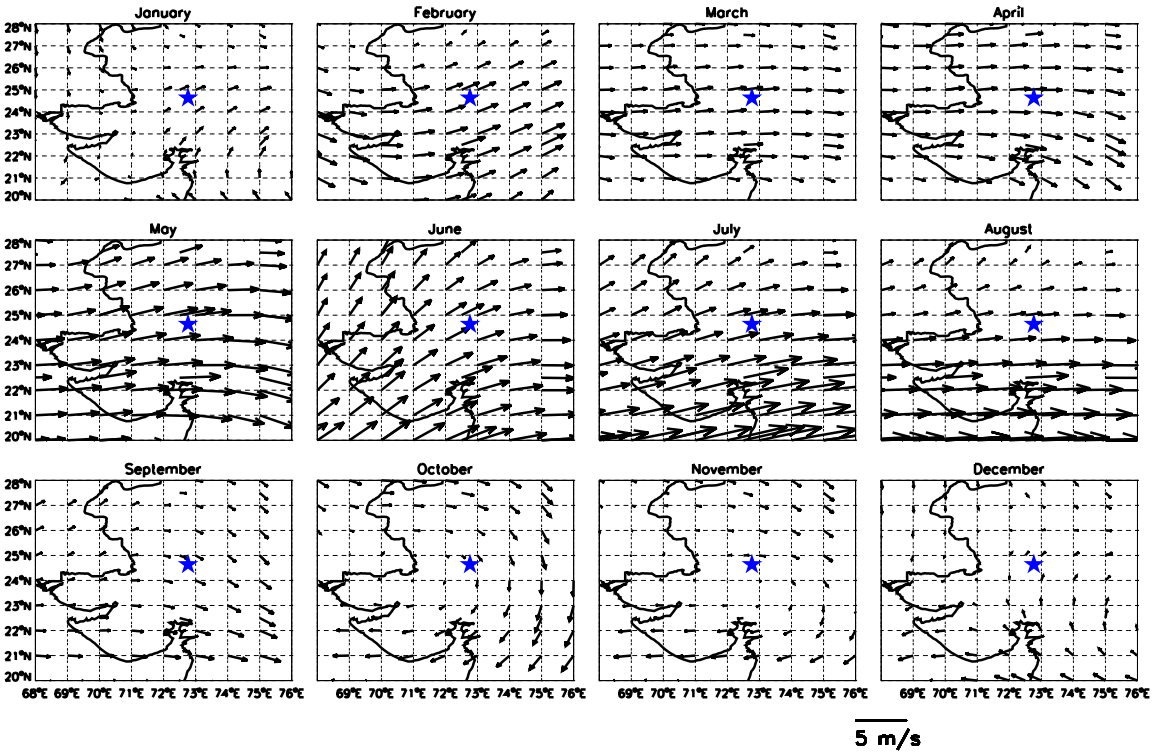

Figure 3.9: *Wind parameters over Mt. Abu during 2007 at 850 hpa.*

stronger. This strong south-westerly wind enhanced the abundances of seasalt in the hill top areas as they are transported from the Arabian sea. During postmonsoon wind direction becomes random and speed is also minimum. During winter also wind is slow but after February wind becomes stronger and westerly. Among the other meteorological parameter durnal variation of temperature and relative humidity (RH) are shown in the Fig. 3.10 for different seasons. During winter the temperature has the minimum at 15.5±3.0°C and maximum at 23.0±3.3°C during premonsoon, followed by monsoon (mean, 19.3±2.0°C) and postmonsoon (mean, 18.3±1.4°C). In case of Rh, the minimum is observed at 24.6±6.4% during premonsoon and maximum is at 88.3±10.5% during monsoon, followed by 54.7±22.8% during postmonsoon and 30.7±8.3% during winter. There is a diurnal variation in hourly averaged temperature in every seasons whereas there is no significant variation present in the diurnal RH at Mt. Abu. During day time the temperature has increased and peak is observed at 1000-1500 local hours during winter and premonsoon. But the peak has shifted in the morning during monsoon

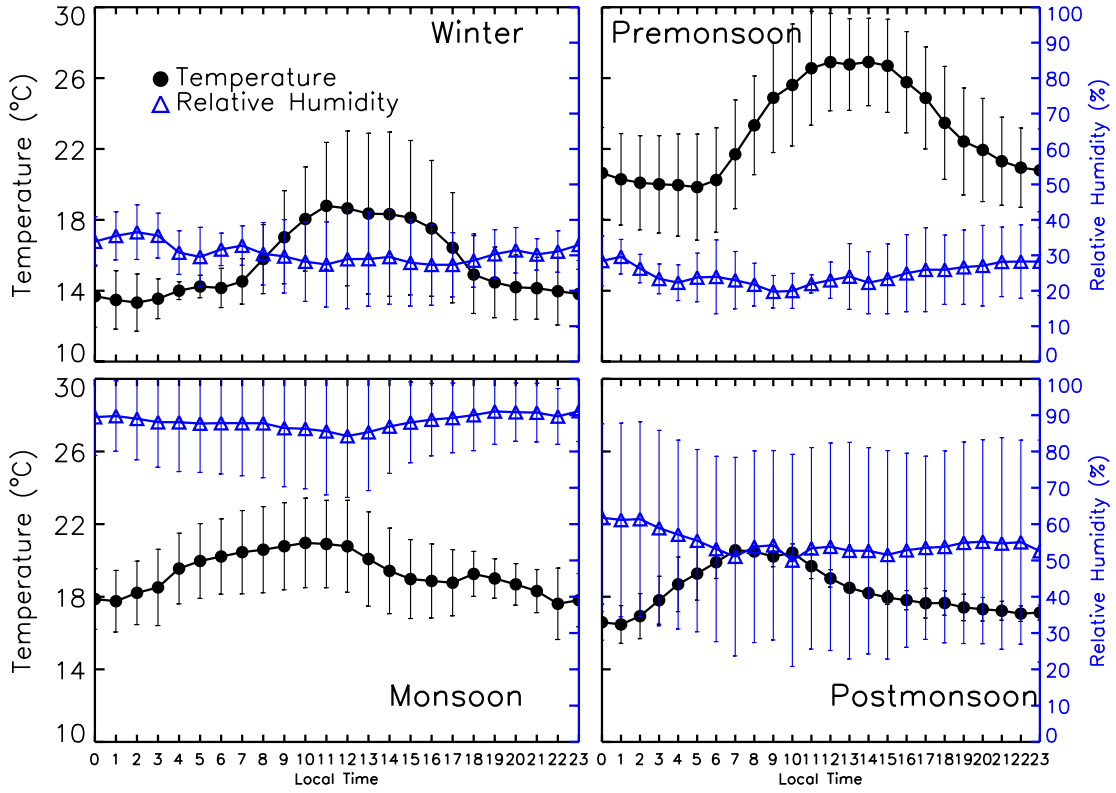

Figure 3.10: *Average diurnal variation of temperature and RH for the observation period of different seasons at Mt. Abu. Vertical bars represent $\pm 1\sigma$ variation about the hourly mean values.*

and postmonsoon. But similar peak is absence in diurnal variation of RH. The vertical bar represent the $\pm 1\sigma$ variation about the hourly mean values of every season. During Monsoon and postmonsoon RH has a large variation about the mean. During monsoon all the measurements of aerosol parameters are carried out only in June (mean RH, 63.9$\pm$12.6%). Aerosol observation could not be possible in July and August due to overcast sky, rain and high RH. Fig. 3.11 shows the monthly variation of rainfall over Mt. Abu from January 2006 to December 2007. Mt. Abu has maximum rainfall during summer monsoon. During 2007 total rainfall is relatively higher than 2006. Mt. Abu also received significant amount of rain during February 2007.

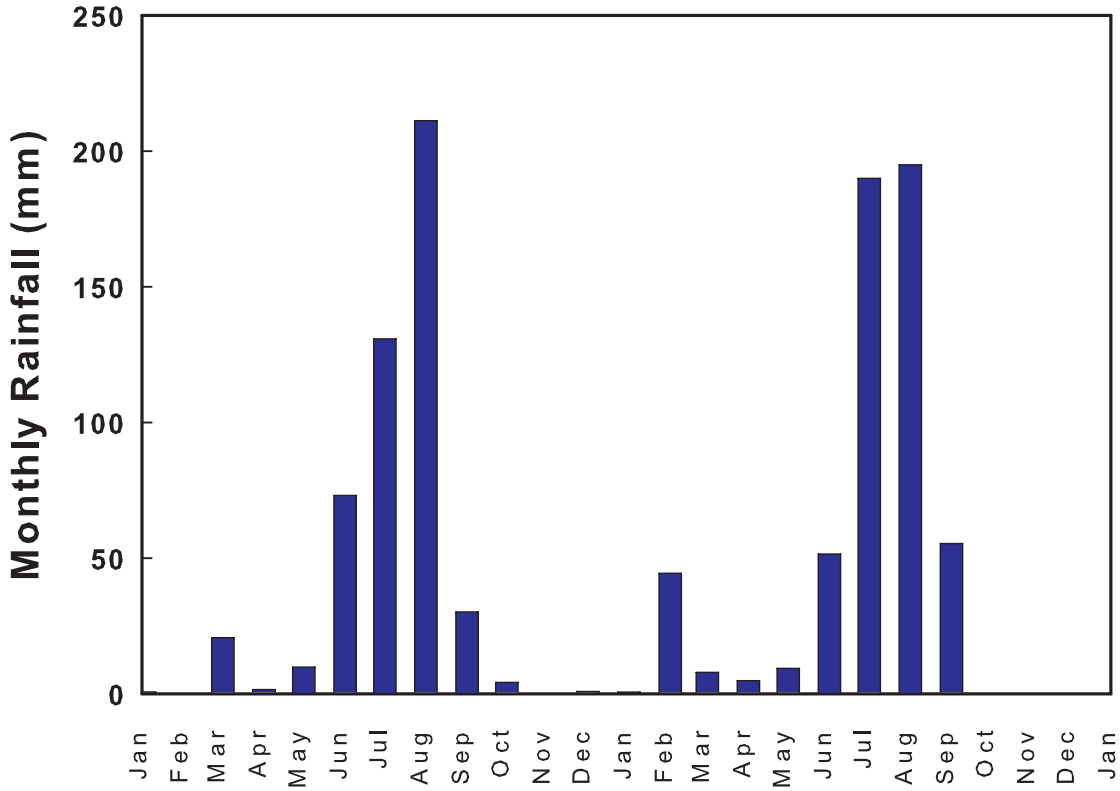

Figure 3.11: *Monthly rainfall over Mt. Abu from January 2006 to December 2007.*

3.2.2 Monthly AOD Variation

The time series of monthly averaged AOD spectrum measured during cloud free days at the hilltop station since January 2006 to December 2007 is shown in Fig. 3.12. Vertical lines represent $\pm\sigma$ variation about the monthly mean AOD. In all wavelength AODs are minimum at 0.1 ± 0.002 at 0.5 μm during winter and as the month progresses AODs gradually increased and reached the maximum value of 0.22 ± 0.02 at 0.5 μm during premonsoon. In the beginning of postmonsoon, AOD observed is relatively high at 0.17 ± 0.01 at 0.5 μm in September. During July and August observations could not be possible due to overcast sky and rain. In the whole year observation at the hilltop area monthly variation is seen in the AOD spectrum mainly due to the following reasons. First, there is a large variation of boundary layer height. In the earlier observation carried out over another tropical Indian station, Gadanki (13.5°N, 79.2°E), *Krishnan and Kunhikrishnan* (2004)

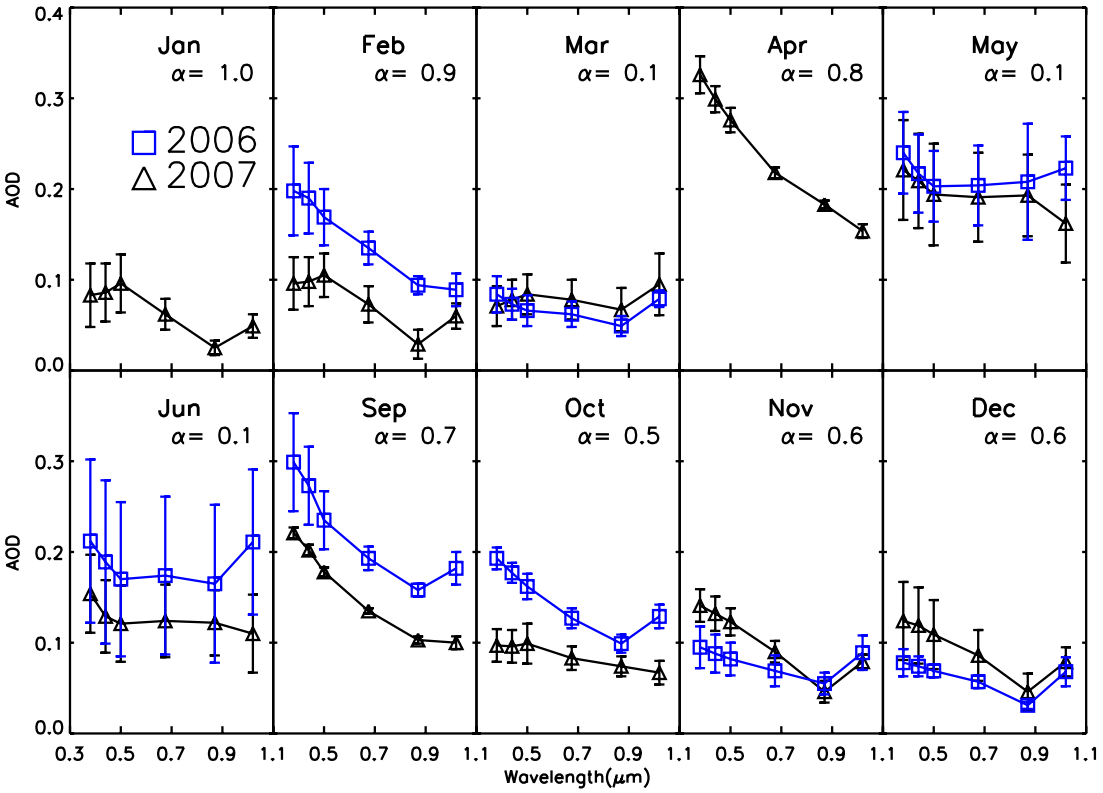

Figure 3.12: *Monthly variation of AOD spectra obtained from Microtops measurements over Mt. Abu.*

studied the yearly boundary layer height variation and observed minimum during winter and maximum during premonsoon. During winter the boundary layer height becomes less than the observation altitude and hence the observation site comes in the free tropospheric region. So in this season AOD becomes minimum. During premonsoon the observation site is within the boundary layer and AOD has increased. But in April at 0.5 μm wavelength AOD has increased to 0.28$\pm$0.01 which is almost three times that during March. The reason is due to an increase of anthropogenic activities in the hilltop area by the tourists. Production of anthropogenic aerosol enhances the lower wavelength AOD. Only in April there is a large abundance of anthropogenic as well as natural dust aerosols which enhanced the whole AOD spectrum. During September AOD has increased again due to huge transportation of seasalt from Arabian sea (*Rastogi and Sarin*, 2005a) and due to the

presence of a very stable aerosol layer of about 1.5 km thickness over the inversion layer during monsoon season in the Western India, reported by *Ganguly et al.* (2006a).

AOD at 1.02 μm also shows the same monthly variation over Mt. Abu. During premonsoon higher wavelength AOD was maximum at 0.19 ± 0.05. The satellite observations show that during this period dust storms occurred over arid and semi-arid part of Western India and loaded huge dust aerosols into the atmosphere. Strong wind transports these dust particles to the hilltop area and increases the higher wavelength AOD during premonsoon.

The spectral dependence of AOD is normally parameterized through angstrom wavelength exponent (α) which is the slope of the logarithm of AOD versus the logarithm of wavelength (in micron) and provides the basic information about the columnar particle size distribution (*Reid et al.*, 1999). α is higher for relatively higher number of smaller particles and as the number of bigger particles increases α decreases. It can even become zero for the relatively large number of coarse-made soil particles (*Tanré et al.*, 1988; *Nakajima et al.*, 1989; *Tomasi et al.*, 1983, etc). In the present study α is obtained from the Sunphotometer measured AOD on the entire wavelength (0.380 - 1.020 μm). In Fig. 3.12 the monthly variation of α is shown. In the present study α varies from 0.1 to 1.0. During premonsoon α becomes minimum. Satellite observations show that premonsoon is a dust storm prone season and very frequently dust storms occur over 'Thar' Desert and strong wind transports the soil born dust to other parts of India (*Dey et al.*, 2004; *Pant et al.*, 2006). Mt. Abu is situated very close to 'Thar' desert and so during this period transported dust enhances the longer wavelength AOD. Only in April the longer wavelength AOD becomes high but α has a higher value than March because the vehicular anthropogenic production of smaller sizes aerosols have increased due to increase in tourists in flow and hence the lower wavelength AOD (0.5 μm) has increased by almost a factor of three than that of March and as a result α increased. During May the higher wavelength AOD is almost same as April whereas the lower wavelength AOD has decreased by a factor of two due to decrease of vehicular

anthropogenic production by reduced number of tourists. For the same reason α has also low value in June, the beginning of monsoon. But in September, beginning of postmonsoon, α increases. During the monsoon season heavy rain washes out aerosols and reduces the soil born dust aerosols at hill top regions. During this period wind is coming form the Arabian sea which enhances seasalt aerosol concentration at the hilltop area by transportation (*Rastogi and Sarin*, 2005a). Enhancement of smaller aerosols (mainly from seasalt aerosols) increases the α. After October seasalt transportation decreases and therefore, it reduces α value. During November and December α again increases due to increase of anthropogenic smaller aerosols by biomass burnings mostly of the fallen leaves of the forest.

3.2.3 Aerosol Mass Concentration at Mt. Abu

Fig. 3.13 shows the seasonal variation of aerosol mass concentration (μg.m^{-3}) for all three modes, viz., nucleation, accumulation and coarse modes at the hill top region, Mt. Abu from January 2006 to December 2007. The total aerosol mass concentration observed was minimum at 16.5$\pm$1.5 μg.m^{-3} during winter and maximum at 25.8$\pm$2.7 μg.m^{-3} during postmonsoon followed by premonsoon (19.9$\pm$5.6 μg.m^{-3}) and monsoon (16.7$\pm$6.0 μg.m^{-3}). This variation is similar to that observed in columnar AOD at Mt. Abu. The accumulation aerosol mass was contributing maximum to the total aerosol mass during all seasons and the coarse mode aerosol mass was also contributing equivalently only during premonsoon. This is due to large transportation of dust aerosol from 'Thar' desert during this season which enhanced the coarse aerosol mass.

In general, nucleation aerosols contribute less to the total aerosol mass concentration. This contribution was maximum during postmonsoon when the wind was almost calm and RH was relatively high. This atmospheric condition helps in gas-to-particle conversion and enhances the nucleation mode aerosols resulting in the maximum mass of 6.4$\pm$1.1 μg.m^{-3} observed during this season. During winter the nucleation mass concentration decreased to 3.2$\pm$0.1 μg.m^{-3} as the boundary

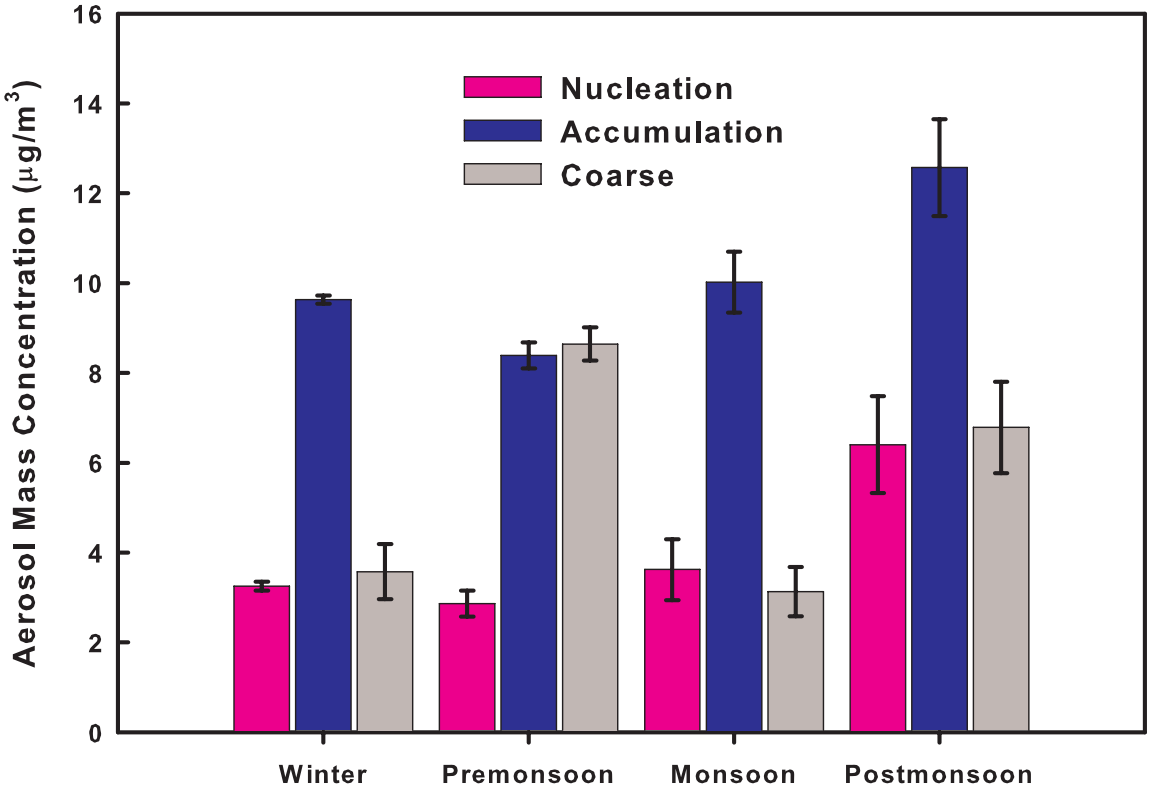

Figure 3.13: *Seasonal variation of near surface aerosol mass concentration over Mt. Abu averaged for 2006 and 2007 and classified into three categories, namely, coarse mode, accumulation mode and nucleation mode particles.*

layer height decreased and the measurement site was in free troposphere. During premonsoon also, the nucleation aerosol mass was comparable (2.9±1.8 μg.m^{-3}) when the boundary layer height was maximum which gives more room for these aerosols to dilute. In addition, strong wind also helped in removing the aerosols from the measurement site during this season.

The seasonal variation observed in the accumulation aerosols is similar to the nucleation aerosols. The accumulation aerosol mass concentration was minimum at 8.4±2.8 μg.m^{-3} during premonsoon and maximum at 12.6±0.6 μg.m^{-3} during postmonsoon followed by monsoon (10.0±1.0 μg.m^{-3}) and winter (9.6±1.6 μg.m^{-3}). Accumulation aerosols are mainly produced by the condensation growth and coagulation of nucleation aerosols. During premonsoon these processes are slowed down due to low RH and hence the low accumulation aerosol mass. During monsoon seasalt aerosols were transported from the Arabian sea and high RH

maintained them in accumulation mode, increasing the mass concentration. During postmonsoon, minimum wind speed resulted in low ventilation causing the observed maximum. During winter accumulation mode aerosol mass concentration reduced as the the measurement location become a free-tropospheric site.

The coarse mode aerosols show a slightly different seasonal behaviour at Mt. Abu. During premonsoon, they mainly consist of dust aerosols transported from 'Thar' desert and the mass concentration is maximum at 8.6 ± 0.4 μg.m^{-3}. It is minimum at 3.1 ± 0.5 μg.m^{-3} during monsoon due to wash out of the dust aerosols by heavy rains. During postmonsoon, the coarse aerosol mass concentration was slightly enhanced to 6.8 ± 1.0 μg.m^{-3} as the accumulation aerosols, which mainly consist of seasalt particles, swelled up by absorbing water vapor at high RH conditions and become coarse mode particles.

3.2.4 Seasonal Variation of Aerosol Number Concentration

Aerosol number concentration is obtained from the observed aerosol mass concentration from QCM observations for the hilltop area using appropriate mass density valid for semi-arid background atmosphere and prevailing relative humidity conditions (*d'Almeida et al.*, 1991; *Hess et al.*, 1998). Figure 3.14 shows the typical aerosol size distributions for the four seasons. The vertical bar represents $\pm\sigma$ variation about the monthly mean number concentration of different sizes of aerosols. In all seasons, the size distribution showed tri-modal distribution and each mode could be fitted using the log-normal distribution (Eq. 3.1). The three modal parameters for all the seasons are given in Table 3.2. At Mt. Abu the number concentration (N) of nucleation and accumulation mode are lower by an order of magnitude than that at Ahmedabad while for coarse mode it is comparable. Since Mt. Abu is far from anthropogenic activity, the anthropogenically influenced modes (nucleation and accumulation) have smaller number concentrations. However, the proximity to 'Thar' desert and similarity of the surface conditions of Mt. Abu and Ahmedabad make the coarse mode number concentrations comparable.

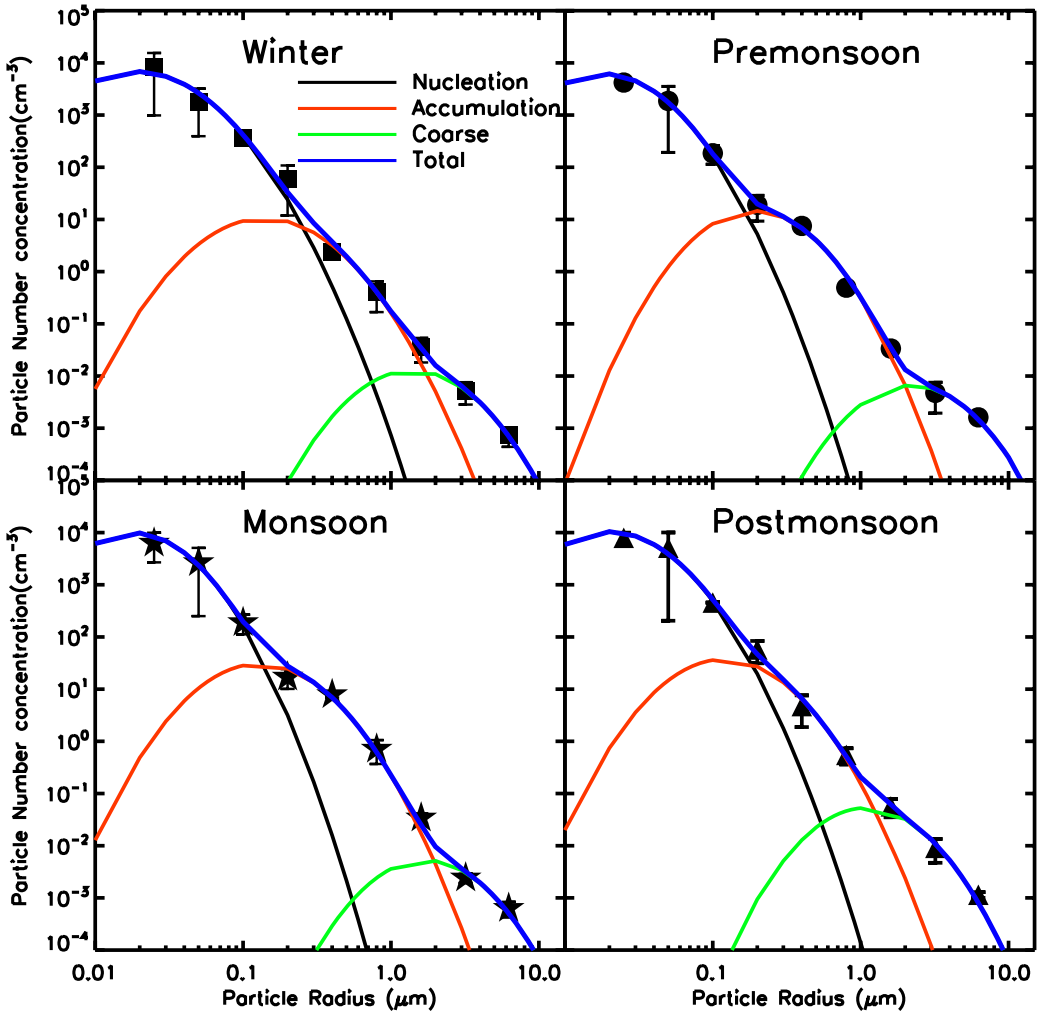

Figure 3.14: *The seasonal variation of aerosol number size distribution obtained over Mt. Abu.*

The radii of nucleation mode lie in the range of 0.018-0.020 μm and number concentration for this mode is found to be maximum during postmonsoon and minimum during premonsoon and monsoon. Similarly the radii for corresponding accumulation and coarse modes lie in the range of 0.12-0.19 μm and 1.1-2.1 μm, respectively.

Accumulation aerosols are mainly produced by the condensation growth and coagulation of nucleation aerosols. During winter accumulation mode aerosols number concentration (N) was minimum at 18 cm^{-3}. During premonsoon, the anthropogenic activities were maximum at Mt. Abu which increased N of accumulation mode to 22 cm^{-3}. During monsoon, it further increased to 50 cm^{-3}. It

Table 3.2: *Average Values of Size Distribution Parameters Obtained by Fitting Lognormal Curves to the Measured Aerosol Number Size Distribution Over Mt. Abu*

Seasons	Nucleation			Accumulation			Coarse		
	N cm^{-3}	r_m μm	σ μm	N cm^{-3}	r_m μm	σ μm	N cm^{-3}	r_m μm	σ μm
Winter	12000	0.019	2.0	18	0.14	2.0	0.02	1.4	1.9
Premonsoon	10000	0.018	1.9	22	0.19	1.8	0.01	2.2	1.8
Monsoon	15000	0.018	1.9	50	0.13	1.9	0.01	1.7	1.8
Postmonsoon	17000	0.020	1.9	60	0.12	1.9	0.08	1.1	1.8

is due to the wind coming from Arabian sea (Fig. 3.9) that carried large amount of sea salt and enriched the sea salt aerosols at the hill top region (*Rastogi and Sarin*, 2005a). During high RH conditions these sea salt aerosols belong to the accumulation mode. Later during postmonsoon, wind was south-easterly and the transported sea salt reduced. However, burning of biomass like garbage and fallen leaves increased and so BC particle concentration was enhanced. Therefore, high production, shallow boundary layer height and low wind speed made the accumulation mode aerosol number concentration reach a maximum at 60 cm^{-3} during this season.

During premonsoon, there is large transportation of mineral dust aerosols from 'Thar' desert which enhanced the abundance of coarse mode aerosols at the hill top area. The coarse mode radius was maximum at 2.2 μm. During monsoon, rain washed out these dust aerosols from the atmosphere while the abundance of coarse aerosols is also high during monsoon and postmonsoon because of the swelling accumulation mode aerosols at high RH condition and as a result mode showed lower value than that of premonsoon.

3.2.5 Diurnal Variation of Black Carbon Mass Concentration

In recent years, global climate has received considerable attention due to increase in the percentage contribution of anthropogenic aerosols on the Earth's radiation

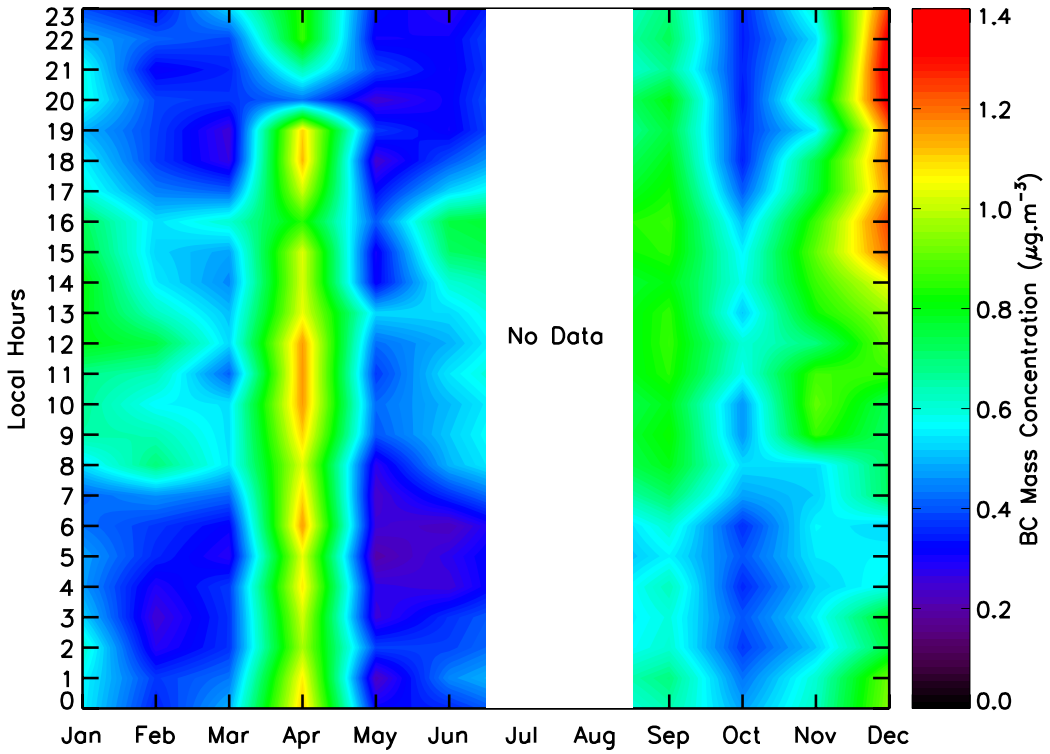

Figure 3.15: *Diurnal and monthly variation of BC mass concentration over Mt.Abu.*

budget (*Haywood and Ramaswamy*, 1998). BC particles exist mainly in the accumulation mode and can transport over long distance (*Chýlek et al.*, 1984) from the source to pristine environment and perturb the climate of pristine environment, like that of Mt. Abu. The diurnal variation of BC mass concentration is shown in Fig. 3.15. Observations were not possible in July and August due to monsoon rain. Minimum BC concentration was observed during June (0.428 ± 0.128 μg.m^{-3}) and maximum was observed during premonsoon (0.665 ± 0.478 μg.m^{-3}) followed by winter (0.608 ± 0.246 μg.m^{-3}) and postmonsoon (0.620 ± 0.158 μg.m^{-3}). At Mt. Abu the BC concentration was an order of magnitude less than that at Ahmedabad in all seasons. During April, the anthropogenic activities were maximum at Mt. Abu due to increase in local tourists and resulted in maximum BC concentration at 1.00 ± 0.170 μg.m^{-3} which is a factor of two higher than the earlier month. The

annual mean BC mass concentration was 0.580±0.104 μg.m^{-3}. In another study, at high altitude station, Nainital (29.4°N, 79.5°E, 1950m asl), in central Himalayas, mean BC was observed to be 1.36±0.99 μg.m^{-}3 during December 2004 (*Pant et al.*, 2006) which shows Mt. Abu is less affected by anthropogenic activities during winter.

The diurnal variation of BC mass concentration does not show any significant morning and nocturnal peaks like Ahmedabad. However, increased BC was observed during the noon hours except during November and December. The reason is for such an increase is that during the day time the thermal convection becomes stronger and so the pollutants at the foothill area rise up to the hilltop region and enhance the BC concentration. During November and December the night time BC concentration was larger by a factor of 2. During these months the nearby villagers burn wood and fallen leaves to keep themselves warm thereby increasing the BC mass concentration. During January to March this nocturnal enhancement was not observed. The reason is that the boundary layer height is less than the station altitude during this period and the night time BC that is produced could not reach the hill top region due to weak thermal convection. During this period hill top region becomes pollutant free region.

CHAPTER 4

Aerosol Studies during Special Campaigns/Projects

Aerosol properties are highly variable and largely depend upon the production mechanism and local meteorological parameters. Relative Humidity (RH) is one of the important parameters which largely influence the aerosol properties. In North India, fog is a common event during winter due to the large variation of RH over the Indo-Gangetic basin. To investigate the influence of fog on aerosol properties, a campaign was organized during December 2004 at Hissar, situated in the Indo-Gangetic basin. This campaign was part of a national land campaign, supported by the Indian Space Research Organization Geosphere Biosphere Programme (ISRO-GBP). The Indo-gangetic basin is also well known for the production of large amount of aerosols. The major part of these aerosols are produced anthropogenically (e.g., *Lelieveld et al.*, 2001; *Ganguly et al.*, 2006b; *Nair et al.*, 2007). However, during January to March, a mixture of aerosol particles mainly produced from south east Asia is transported to North Indian Ocean via Bay of Bengal (*Novakov et al.*, 2000; *Ramanathan et al.*, 2001b; *Satheesh et al.*, 2002, etc.). Therefore, the transported aerosols have large influence on coastal climate by changing the costal aerosols properties. To investigate this effects a campaign was organized during

March 2006 at Kalpakkam, an eastern coastal station in India. This campaign was part of the Integrated Campaign for Aerosols, gases and Radiation Budget (ICARB) sponsored by ISRO. The results of both the aforementioned campaigns have been discussed in this chapter. Also a major part of the chapter is devoted to measurement of the changes in aerosol properties during dust storm at Mt. Abu in May 2006 and over arid region during April 2007.

4.1 Fog Induced Aerosols Properties

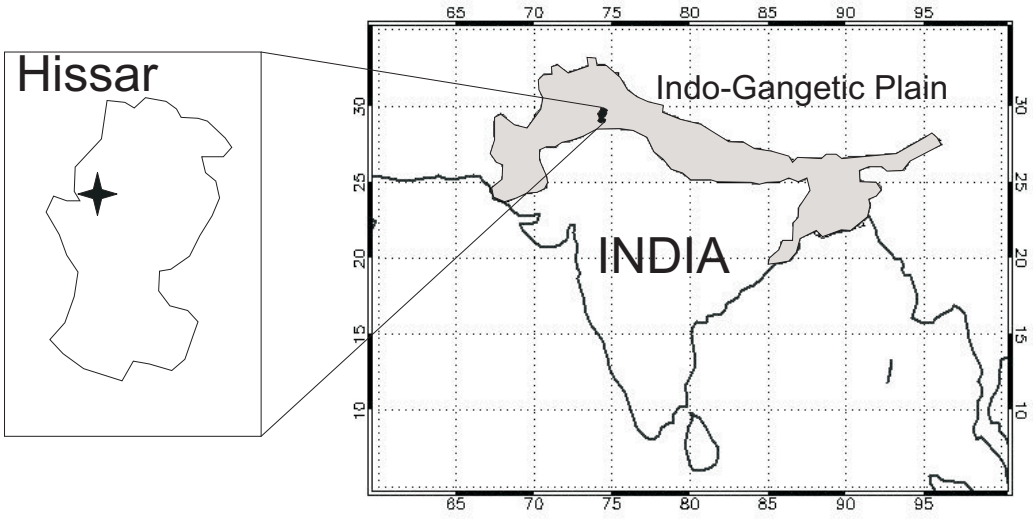

Figure 4.1: *Map showing the Indo-Gangetic Basin (IGB) and the observation site at Hissar (29.13°N, 75.70°E).*

In the Indo-Gangetic Basin (IGB), occurrence of fog during winter season is a common feature. At high relative humidity condition aerosols act as condensation nuclei, which help to produce the fog that in turn can alter the properties of aerosols (*Pandis and Seinfield*, 1990). Fog, in general, starts occurring at late night and continue up to about next day noon hours. In this paper we study the aerosol properties and their changes during fog conditions in the IGB through a month long field campaign conducted at Hissar (29.13°N, 75.70°E) (Fig. 4.1) in December 2004 as a part of the ISRO-GBP Land Campaign-II. We also estimate the aerosol

radiative forcing and its diurnal variation during the fog period and compare with that during clear sky condition.

4.1.1 Meteorological Conditions

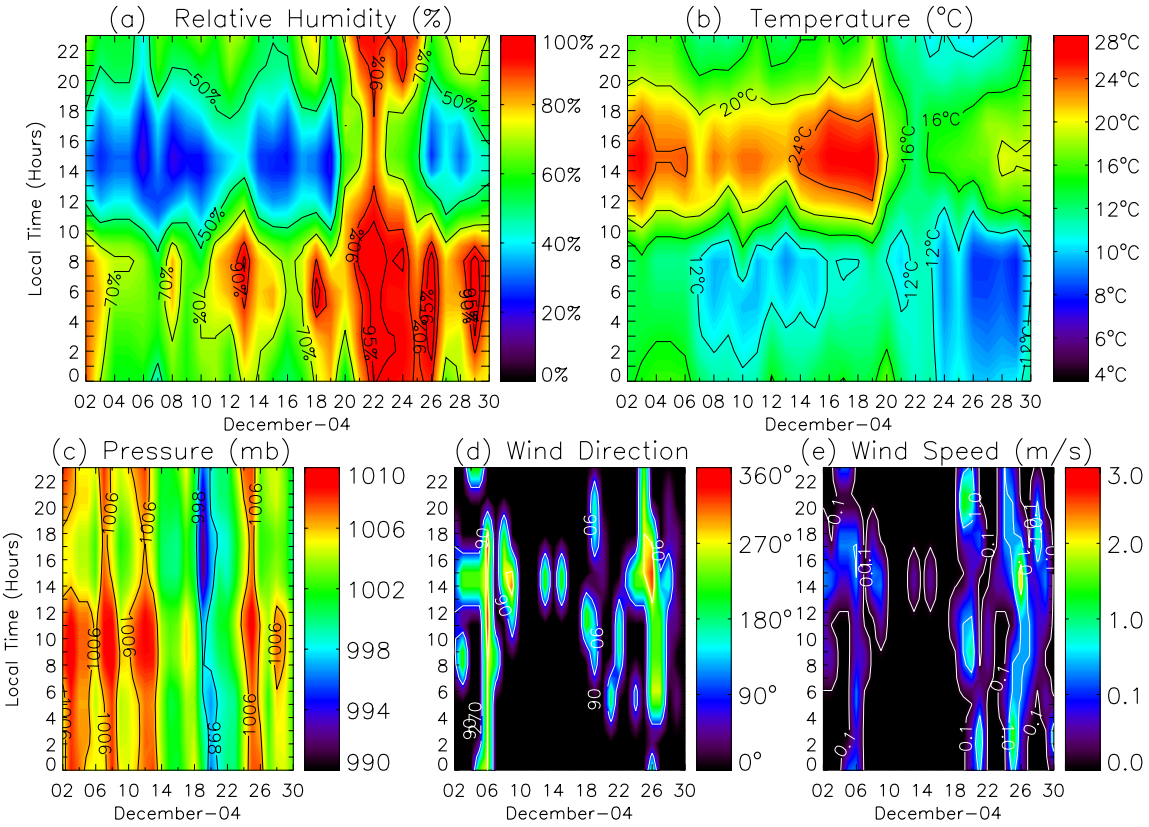

Figure 4.2: *Relative humidity, temperature, pressure, wind direction and speed observed at Hissar during the campaign period. 12, 13, 14, 20th and 22nd are the foggy days.*

Meteorological parameters are the important tools to characterize the fog event. In our present work, we have divided all the data into three groups, namely, 'prior to foggy days' (6th, 8th and 11th Dec), 'during foggy days' (12th, 13th and 14th Dec) and 'after the foggy days' (15th, 17th, 18th and 27th Dec) on the basis of different meteorological conditions. Fig. 4.2a shows the variation of RH during the observation period. Prior to 12th December no strong variation in RH was observed, but

on 12^{th}, 13^{th} and 14^{th}, during morning hours RH was found very high and significant diurnal variation was observed. On 19^{th} and after 21^{st} almost everyday RH showed high value during morning and decreased rapidly and even reached values below 25% during afternoon hours. On 22^{nd} the fog event continued all over the day as the RH remained high throughout the day. On 15^{th}, 17^{th}, 18^{th} and 27^{th} Dec no significant change in RH variation was observed during the whole day and no fog event was observed. These days are considered as 'after the foggy days'. Temperature and pressure values (Fig. 4.2b-c) also showed variations similar to that of RH. During the foggy days both the surface pressure and temperature decreased. Prior to and after foggy days these two parameters showed almost similar variation. The wind in general was observed to come mainly from the NE direction (Fig. 4.2d). During the foggy days wind was in general calm during the forenoon (FN) period (Fig. 4.2e), which helped to retain the fog over a long time. During afternoon (AN) the wind speed was found higher than the FN values, and also during the non-foggy days the wind speed was found higher.

4.1.2 Measurements

During the campaign period, from 1st to 30^{th} December the spectral Aerosol Optical Depth (AOD) and the aerosol mass size distribution were measured at Hissar. The AOD was obtained by measuring the direct solar radiation intensity at the ground by a hand-held Sunphotometer, built in-house at the Physical Research Laboratory, Ahmedabad. The Sunphotometer consists of an interference filter, photodiode and necessary electronics (*Acharya and Jayaraman*, 1995). Direct solar-intensity was measured at seven wavelength bands by using optical interference filters, having maximum transmission centered around 400, 500, 668, 750, 875 and 1050-nm with corresponding full-width at half maximum (FWHM) of 18, 13, 9, 10, 12 and 25-nm respectively. The field of view of the Sunphotometer is kept at 6° by using a front-end baffle. Observations were made during cloud-free conditions, from 0830 to 1630 hrs. local time with typical half an hour interval between the

measurements. Each observation consists of measurements taken successively for all the optical channels by changing the interference filters. While the absolute error in AOD calculation is about 0.03 the relative error can reach up to a maximum of 15% due to instrumental error (due to bias and precision) and ignoring the contribution from "forward" scattering particularly during high aerosol condition and for high zenith angle observation (*Jayaraman et al.*, 1998). Aerosol Mass Concentration was measured using a 10-stage Quartz Crystal Microbalance (QCM) cascade impactor (model PC-2, California Measurements Inc., USA) and the aerosol size distribution at the ground level was determined. The aerosols were collected in 10 stages of the impactor with 50% efficiency cut-off radii at 12.5, 6.25, 3.2, 1.6, 0.8, 0.4, 0.2, 0.1, 0.05 and 0.025 μm from stage 1 to 10 respectively. The air flow rate through the impactor was kept at 240 ml/min. The typical sampling period was 60 sec for each measurement. The maximum uncertainty in the measured mass for all the ten stages of QCM is within 25% (*Jayaraman et al.*, 1998). The QCM was operated from the terrace of the observatory building at a height of about 6m. The air inlet was installed vertically to minimize the loss of aerosol particles within the inlet tube. The relative temperature change of the crystals during each sampling period of 1 minute is too small and can be neglected. The QCM observations were made during the day with an interval of about one hour from 0800 - 1700 hrs. local time except for days when the RH was above 75% as well as during dense fog condition to avoid any damage to the QCM crystals. The QCM data is also compared with the aerosol mass independently obtained using a High Volume Sampler (HVS), which had a maximum cut-off radius of 10 μm.

4.1.3 Aerosol Optical Depth

Fig. 4.3 shows the AOD spectra obtained in the wavelength range from 400 nm to 1050 nm from 6^{th} December to 30^{th} December '04. Only 10 days of observations could be made as other days were either cloudy or influenced by heavy fog condition. Prior to the occurrence of fog over Hissar, daily AOD data are available

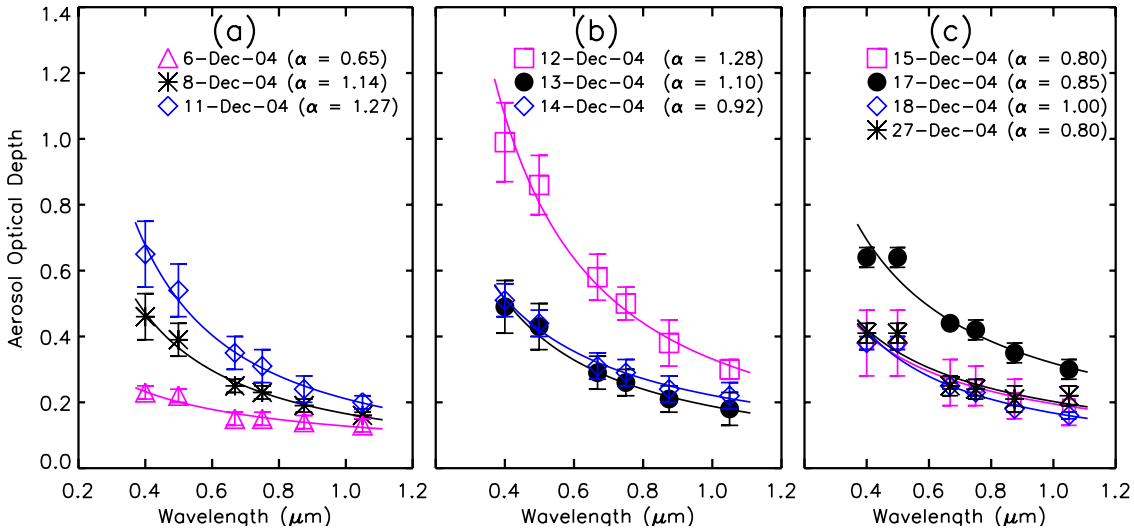

Figure 4.3: *Average aerosol optical depth (AOD) values obtained (a) prior to foggy days (6, 8 and 11th December 2006) (b) during foggy days (12, 13 and 14th December 2006, afternoon hours) and (c) after foggy days (15, 17, 18 and 27th December 2006). Measurements could not be made on other days due to cloudy sky condition. Best fitted lines, drawn by least square method, are also shown in the figure.*

for 3 days. Among the 'prior to foggy days' period, 6th December has the lowest AOD value, which gradually increased on later days. On 11th December, prior to the start of the foggy period, the AOD at 500-nm showed a maximum value of 0.54 (Fig. 4.3a). During foggy days, AOD observations at FN hours were not possible due to poor visibility. After fog has dissipated, AOD observations could be made in the AN hours under clear sky condition. In general higher AOD values were observed during foggy days. On 12th December the highest AOD value of 0.99 has been observed at 500-nm (Fig. 4.3b). The values were however less on 13th and 14th December. 15th December was a cleaner day with comparatively less AOD values (Fig. 4.3c) indicating scavenging of particles during the foggy period. Delhi (28.63°N, 77.17°E), which is 200 km southeast of Hissar, is another most polluted urban region in the IGB. The monthly averaged AOD at 500 nm during December 2004 was reported as 0.91±0.48 (*Ganguly et al.*, 2006b) whereas in Hissar it was 0.46±0.18. At Kanpur (23.43°N, 80.33°E), another major industrial

region in the IGB, situated 350 km further east from Delhi a monthly mean AOD value of 0.77±0.29 was reported for the same period (*Tripathi et al.*, 2005). Prior to the foggy days period, the wavelength exponent of the AOD (angstrom parameter, α) was found higher than compared to that for the foggy days. A decrease in α value indicates the relative increase in the amount of bigger particles, and in the present case the hygroscopic growth of the particles during the foggy days. After the foggy days α value was found increasing, implying a loss of bigger particles due to scavenging during the foggy period. Formation of freshly nucleated submicron particles can also increase the α value and in the present case both the mechanisms were responsible for the observed increase in the value.

4.1.4 Aerosol Mass Concentration

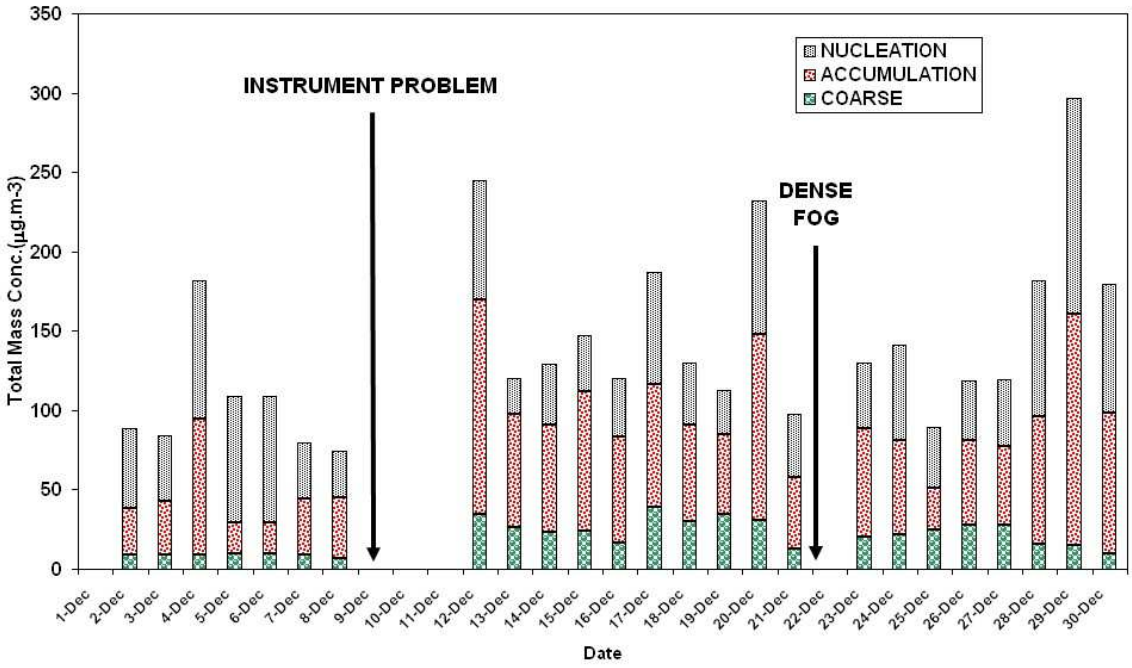

Figure 4.4: *Average aerosol mass concentration obtained during the campaign period. The total mass values are averaged for nucleation (particles radii <0.1 µm), accumulation (0.1-1.0 µm) and coarse (>1.0 µm) modes. Observations were made only for RH <75%. No measurements were made during dense fog condition.*

The role of aerosols in climate change depends apart from their optical and chemical properties also on their size distribution as it controls both the vertical and horizontal dispersal of particles. The aerosol mass concentration at Hissar, prior to foggy days was comparatively low, about 100 μg.m^{-3} (with the exception of 4th Dec) with respect to the foggy and after foggy days (Fig. 4.4). During foggy days mass concentrations were found in general high. At higher RH there is a possibility that the particles get coated with aqueous solution of any soluble constituents (*Lubin et al.*, 2002). After foggy days the aerosol mass concentration reduced but did not reach the value that was obtained prior to the foggy days. The observed reduction in the aerosol mass concentration is mainly attributed to the scavenging of particles during the foggy days.

4.1.5 Aerosol Number Distribution

Table 4.1: *Aerosol mass concentration (M), number concentration (N), mode radius (r_m) and width (σ) of the fitted lognormal distributions for the nucleation mode, accumulation mode, and the coarse mode.*

	Nucleation				Accumulation				Coarse			
Days	M	N	r$_m$	σ	M	N	r$_m$	σ	M	N	r$_m$	σ
Before Fog	9.0	45000	0.030	1.28	37.1	350	0.10	1.31	57.6	0.018	2.8	1.16
Foggy	26.0	72000	0.025	1.35	107.3	800	0.16	1.23	71.2	0.18	1.8	1.23
After Fog	23.4	40000	0.029	1.25	62.6	470	0.13	1.28	48.9	0.15	1.7	1.25

The measured aerosol mass concentration is converted into aerosol number distribution in the size region 0.025-12.5 m for the three periods viz., before foggy days (2-8th Dec), during foggy days (12-14, 20, 29th Dec) and after foggy days (15-19, 21, 23-28 and 30th Dec) by using appropriate densities for the particles, taking into account the measured RH value. The aerosol number distributions for the three periods are shown in Fig. 4.5a-c. The vertical bars correspond to the standard

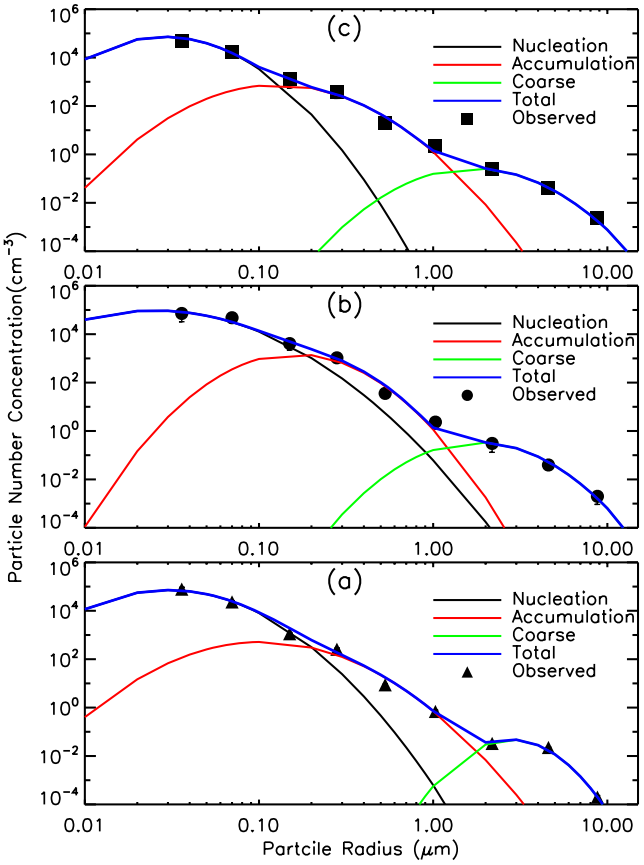

Figure 4.5: *Mean aerosol number distribution (a) prior to foggy days (mean of 2-8 December 2004) (b) during foggy days (mean of 12-14, 20 and 29 December 2004) and (c) after foggy days (mean of 15-19, 21, 23 - 28 and 30 December 2004). The observed values are fitted with log-normal curves individually for the three modes viz, nucleation, accumulation and coarse modes. The sum of the three modes is also shown.*

deviation of the mean value, representing the variation in the number density values within a day. The observed data is best fitted by a sum of three individual log-normal curves for the three modes, viz., nucleation mode (r<0.1 μm), accumulation mode (0.1<r<1.0 μm), and the coarse mode (r>1.0 μm), with varying mode radius (r_m) and standard deviation (σ). Table 4.1 gives the aerosol number concentration N in cm^{-3}, $r_m$and for the three modes. During foggy days an increase in aerosol mass concentration is found in all the three modes while the increase is larger in the nucleation and accumulation modes. The nucleation and accumulation mode particles are mainly water soluble or soot particles. During

foggy periods either the water soluble particles adsorb water and become larger while the soot particles can get coated with either liquid water or an aqueous solution of any soluble constituents (*Lubin et al.*, 2002), resulting in an increase in their mass. Our observation also shows that there was a large increase in the number concentration in the nucleation mode particles. It is interesting to note that, there is a reduction in the mode radius value (which could be determined with an accuracy of about 0.002 or better for all modes) of the nucleation mode particles from 0.03 to 0.025 μm during foggy days, which shows the addition of freshly nucleated particles, while in the accumulation mode the mode radius shifts to larger side, from 0.1 to 0.16 μm showing the growth of the particles. Thus, during foggy days the increase in nucleation mode particles is mainly due to the addition of freshly nucleated particles while in the accumulation mode, the observed increase in mass is mainly due to the hygroscopic and coagulation growth of particles. However, after the foggy days there was a decrease observed both in the mass and number concentration of the particles in all the three modes and the decrease was stronger in the coarse mode indicating the scavenging of particles during the foggy days, which however was more efficient for the coarse particles.

4.2 Aerosol Characteristics over East Coast of India

The Eastern coastal region of India is most important place to investigate the properties of both, local produced and transported aerosols. The adjacent oceanic region Bay of Bengal (BoB), has special importance for its surrounding highly polluted land mass. Large amount of anthropogenic aerosols come to the oceanic environment with the SW monsoon wind and hence it also affects the coastal regions. Now-a-days east coast regions get large attention due to the large transportation of anthropogenic aerosols from the northern India via BoB. During the SE monsoon period the atmosphere of east coast region is populated by this transported anthropogenic aerosol. In the present study, we present the changes of the aerosol properties due to changes in wind direction and hence the changes in the

aerosol radiative forcing over Kalpakkam. The present observation is a part of ongoing Indian Space Research Organisation (ISRO) sponsored multi-platform field campaign named Integrated Campaign for Aerosols, gases and Radiation Budget (ICARB). This campaign carried out field measurements for aerosols and trace gases over 20 stations at different parts of the Indian main land and coastal regions and onboard cruise observations over BoB and Arabian Sea and onboard aircraft observation mainly over coastal region. The continuous variation of aerosol properties was studied at Kalpakkam during 16-31 March 2006. In this section we describe the important features observed at Kalpakkam during the campaign period.

4.2.1 Decription of the Observation Site and Meteorology

Comprehensive observations of aerosol optical and physical properties were carried out at Kalpakkam (12.56°N, 80.12°E) between 16-31 March 2006. Kalpakkam is a small town with population around twenty thousand, situated on eastern seashore of India. It is known for having nuclear power station, except for that there is no major industrial activity around town. Main economic activity of the town is agriculture. The land is covered with paddy fields, other green vegetation and sea backwaters. The major industrial town closest to Kalpakkam is Chennai of population more than eight million, 80 km north of Kalpakkam. The measurement site is remote and far from human activity. The measurement site is enriched by natural aerosols mainly marine aerosols from BoB and anthropogenic aerosols generated locally due to biomass burning of agricultural waste and cooking fuel as well as anthropogenic aerosols transported from Chennai, India's third largest city in terms of population. March is the month when there is no major agriculture waste burning activity take place in this region and hence possibility of contribution from agriculture waste burning during field observation is ruled out. Major anthropogenic aerosols like BC are believed to be transported from interior of peninsular India and BoB depending upon wind condition.

Meteorological conditions over Kalpakkam are typical of coastal station. Wind

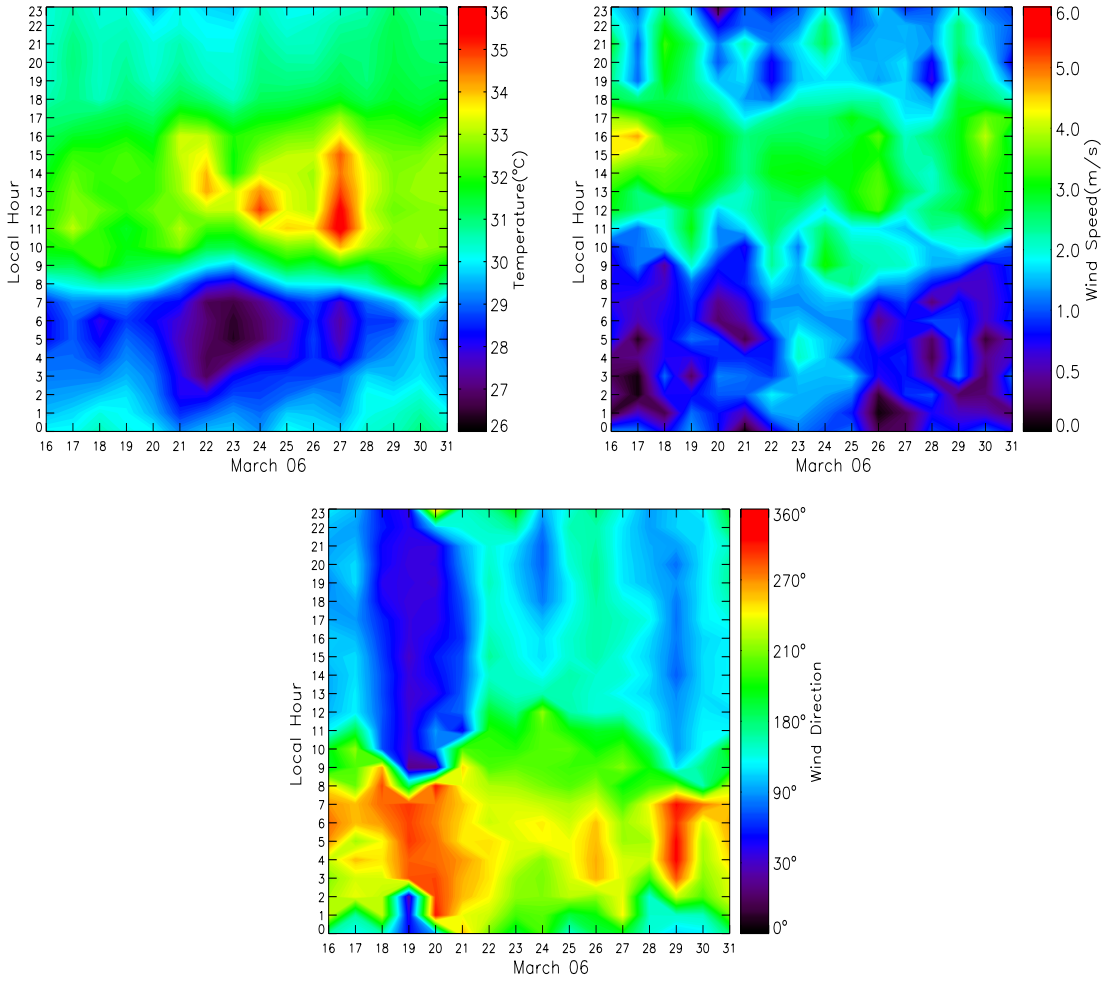

Figure 4.6: *Meteorological parameters at Kalpakkam during the campaign period.*

speed, wind direction and temperature for the campaign period are shown in Fig. 4.6. Wind blows from west to east during early morning hours (land breeze) and from east to west during rest of the time (sea breeze). During campaign period temperature varied between 26 and 36°C with maximum occurring around 2 pm local time and 5 am morning hours. Wind speed varied between 0 and 6 m/s with maximum wind speed occurring during afternoon (during sea breeze).

In addition to making observations of local meteorological conditions, seven days air back trajectories arriving at measurement site at the altitude of 500 m during local noon were calculated for each day using HySPLIT-4 model (Hybrid Single-particle Langrangian Integrated Trajectory version 4)(*Draxler and Hess*, 1998).

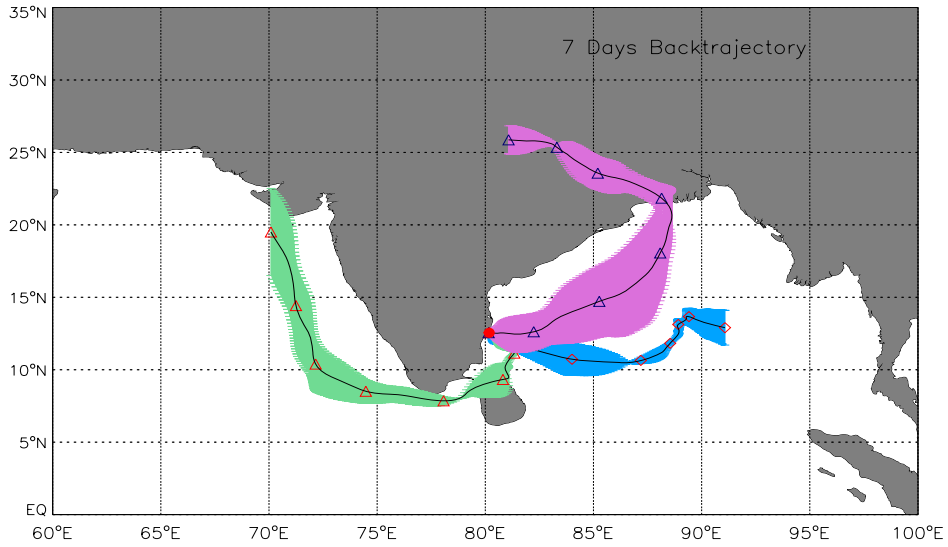

Figure 4.7: *Seven days air back trajectories for the measurement site, Kalpakkam are shown. Back trajectories have been grouped according their origin like 1) Central BoB (Blue shaded), 2) Indo-Gangetic Basin (IGB) (Magenta Shaded) and 3) North Indian Ocean (NIO) (Green shaded).*

It is found that air was coming from central BoB between 16 and 19 March, Indo-Gengetic basin (IGB) between 20 and 29 March and Arabian sea via north Indian ocean (NIO) between 30 and 31 March (Fig. 4.7).

Aerosols observations are discussed for influence of local meteorological condition such as sea breeze and land breeze and observations during sea breeze are further discussed for long range transport.

4.2.2 Aerosol Optical Depth

Aerosol Optical Depth (AOD) was obtained by using Microtops at six different wavelengths viz. 0.380, 0.440, 0.500, 0.675, 0.870, 1.020 μm during the campaign period on cloud-free days. Aerosol Optical Depth (AOD) observations at Kalpakkam were made at every half hour interval between 0900 and 1700 hours Indian standard time (IST) for cloud free sky. Each set of observation consists three observations made in immediate succession and median of three observations is taken as representative AOD for given half hourly interval. Spectral AODs observed for three different origin of air parcel described earlier (Fig. 4.7) namely central bay

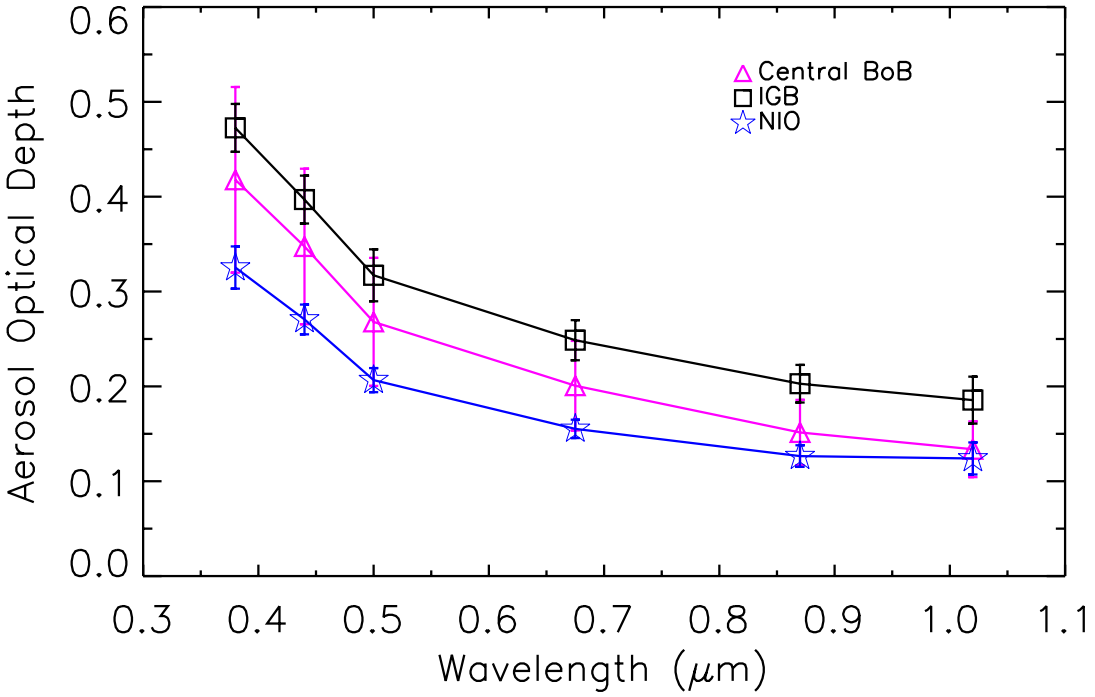

Figure 4.8: *Averaged AOD spectral for three different cases viz, 1)wind coming from Central BoB 2)Wind coming from Indo-Gangetic Besin (IGB) and 3) Wind coming from North Indian Ocean (NIO).*

of Bengal (BoB), Indo-Gangetic Basin (IGB) and Northern Indian Ocean are shown in Fig. 4.8. Vertical bar over data point shows the two sigma variation in AOD for given averaging period. Air parcel originating from NIO has the lowest AOD and air parcel originating from IGB has the highest AOD. Mean AOD at 0.5 μm is 0.27 for Central BoB, 0.32 for IGB and 0.20 for NIO (Fig. 4.8). With change of origin of air parcel spectral characteristics of AOD also changes. Angstrom parameter which is a slope of log of wavelengths vs. log of AODs, have similar values for air parcel originating from BoB and IGB but lower values for NIO. Since wind carried a large amount of BC from the IGB (discussed later) and due to increase in solar radiation absorbtion by these transported absorbing aerosols, coloumnar AOD has increased. When wind blowing from NIO carried less BC, AOD reduced due to less absorbtion of sunlight.

The AODs at lower wavelengths are mainly affected by the anthropogenically produced fine mode aerosols (*Reid et al.*, 1999). At Kalpakkam AOD at 0.5μm

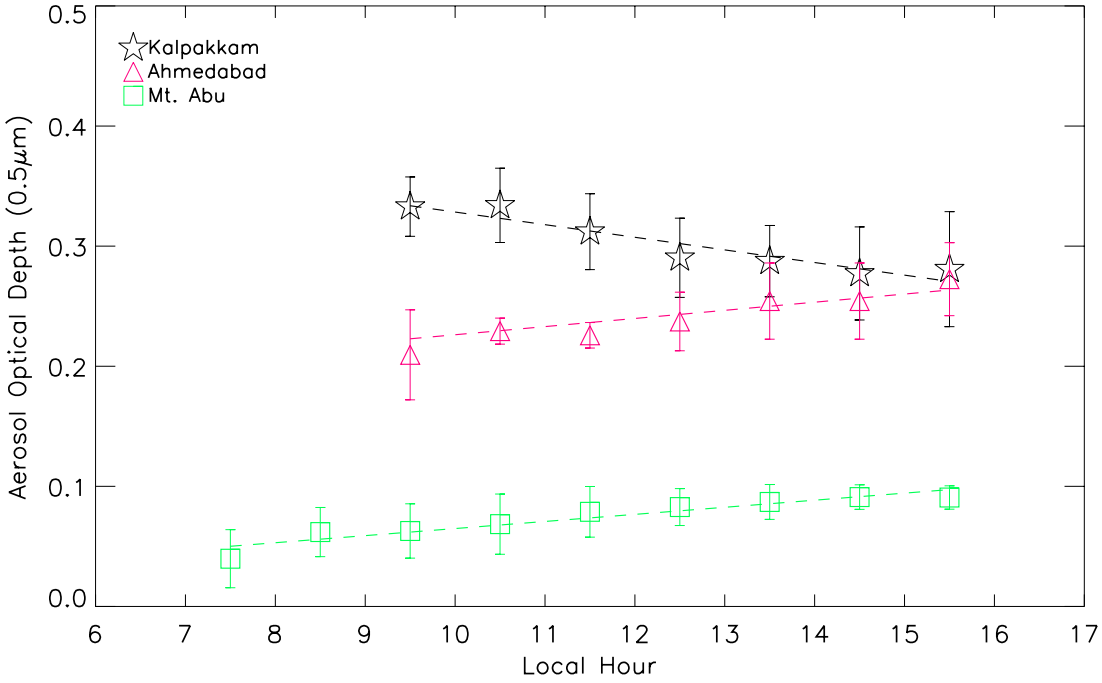

Figure 4.9: *Diurnal variation of AOD (0.5μm) over Kalpakkam (Coastal station), Ahmedabad (Urban Station) and Mt. Abu (Hill Station) during March06. At Ahmedabad and Mt. Abu AODs are increasing as day progresses but at Kalpakkam AOD decreases.*

showed higher values during morning hours and decreased as the day progresses (Fig. 4.9). In general the breeze direction had changed its direction at about 1100 hours, as shown in Fig. 4.6. During land breeze AOD was higher than that during sea breeze. The observed mean AOD had reduced from 0.32±0.03 to 0.28±0.04 as the breeze changes its direction. *Satyanarayana et al.* (1999) studied the characteristics of marine boundary layer over Indian Ocean and reported that there is no large diurnal variation in the marine boundary layer height over relatively homogeneous ocean surface. *Krishnan and Kunhikrishnan* (2004) investigated the boundary layer height over a tropical station, Gadanki (13.5°N, 79.2°E), 200 km far from Kalpakkam, and reported that maximum boundary layer height is in April with sufficient ventilation. Being a coastal tropical station, Kalpakkam experiences minimum boundary layer height variation and sufficient ventilation during the campaign period, were contributing less towards the diurnal variation in AOD. The main reason for the variation was the change in wind direction. During the

land breeze wind carried more BC from Chennai and its surrounding suburban areas, thereby absorbing more solar radiation at the surface and increased the AOD. As the day progressed, wind changed its direction from main land to sea and carried less black carbon and reduced the AOD.

At Chennai, an urban coastal station, the trend was slightly increasing as the day progresses during February, 2001 (*Ramachandran and Jayaraman*, 2003). At Ahmedabad also, an urban semi-arid location in western India, the AOD at 0.5μm showed an increasing trend. By afternoon AOD increased by a factor of 1.3 at Ahmedabad (Fig. 4.9). At Gurushikhar (1.7 km asl), Mt. Abu, the highest observatory in the Aravalli range, AOD showed the same increasing trend during the same period, and the increased by a factor of more than two. During March the temperature at Gurushikhar was 13.0°C during morning and increased to 26.0°C by afternoon. Due to a two fold increment in temperature large convection occurred and the pollutant sub micron aerosols got more room to lift up and in addition as the day progressed increased anthropogenic activities at the hill top enhanced the observed AOD. At Ahmedabad also as the day progressed the temperature increased by maximum 5°C and in addition to increased anthropogenic activities. Being an urban region the AOD at Ahmedabad was always higher than that at Gurushikhar. The increment in AOD at Ahmedabad is very similar to Chennai. However at Kalpakkam, a coastal station, the AOD showed a decreasing trend due to change in wind direction from land breeze to sea breeze.

The Angstrom wavelength exponent α, the slope of the logarithm of AOD versus the logarithm of wavelength (in micron), is one of the important parameter that provides the basic information about the columnar particle size distribution. But α has different values in different wavelength regimes. The α value calculated at the shorter wavelengths best describes the submicron particle distribution and at longer wavelengths describes the micron particle distribution (*Reid et al.*, 1999). In the present study, α is computed in the two regimes, namely 0.38-0.5 μm and 0.5-1.02 μm for the two breezes. During land breeze $\alpha_{0.38-0.5}$, calculated at shorter wavelengths, is 1.42$\pm$0.10 and $\alpha_{0.5-1.02}$, calculated at longer wavelengths,

is 0.18±0.03. During sea breeze the values are 1.19±0.12 and 0.16±0.03, respectively. A significant difference between $\alpha_{0.38-0.5}$ and $\alpha_{0.5-1.02}$ clearly indicates the two dominating modes of particles in the submicron and micron regions. $\alpha_{0.38-0.5}$ is higher than $\alpha_{0.5-1.02}$ during both the breezes which shows that micron particles are dominating throughout. However, $\alpha_{0.38-0.5}$ is high during land breeze than during the sea breeze. It can thus be inferred that smaller particles in the submicron region are enhanced during land breeze. But there is no significant variation in $\alpha_{0.5-1.02}$ for the two breezes which implies that there is no significant variation in the micron size particle distribution.

4.2.3 Black Carbon Mass Concentration

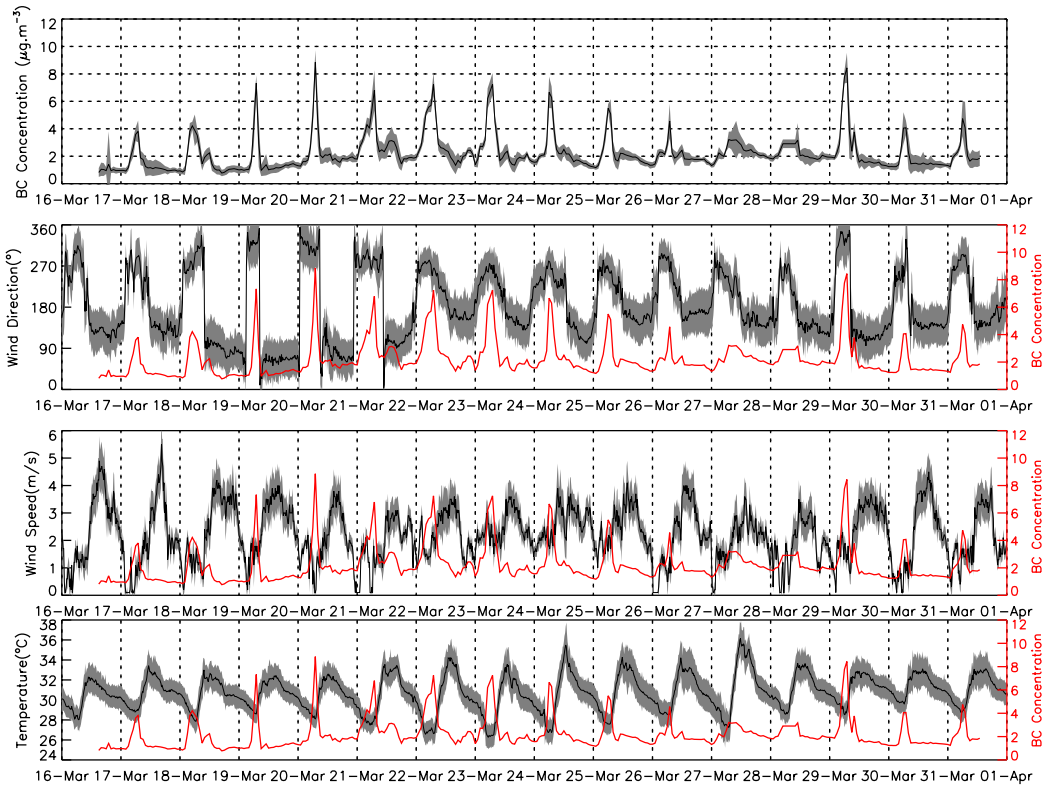

Figure 4.10: *Diurnal variations of black carbon concentration, wind direction, wind speed and temperature obtained over Kalpakkam. The shaded region is the variation of the respective parameter.*

Fig. 4.10 shows the hourly averages of black carbon (BC) concentration during

the campaign period. Hourly averages of wind direction, wind speed and temperature are also given for comparison. The shaded regions represent the two sigma variation of each parameter. On 28 March during 0700-1000 local hours there was no BC data due to a technical problem in the Aethalometer. The diurnal variation of BC concentration at Kalpakkam shows only one peak in the morning whereas previous studies over other stations in the main land of India like Ahmedabad, Delhi, Kanpur (*Ganguly et al.*, 2006a,b; *Tripathi et al.*, 2005) showed two peaks, one in the morning and another in the evening. These stations are mainly urban regions and both peaks had occurred due to the combined effects of increased anthropogenic activities and fumigation effect. The present study shows only a morning peak in the BC concentration during 0400-0900 hours whereas the evening peak is absent (Fig. 4.11). At Kalpakkam wind plays a key role in the diurnal variation of BC. During the morning hours increased anthropogenic activities such as biomass burning and vehicular emissions at Chennai and surrounding suburban areas produced more BC and land breeze carried this BC rich air to the measurement site producing the morning peak at measurement site. The peak BC concentration is four times the background value. Also, the peak occurred where wind speed and temperature were minimum (Fig. 4.10). This meteorological condition resulted in less turbulence and helped to accumulate more BC at the measurement site. As the day progressed, surface temperature gradually increased (Fig. 4.10) due to solar heating and convection became more stronger. So the atmospheric BC got more room to dilute. Simultaneously, the wind changed its direction from land to sea with an increase in speed (Fig. 4.6). As a result the BC concentration gradually decreased and came down to the background level. During the evening as wind was coming from the sea, identified as sea breeze, BC concentration remained in the background level and hence the diurnal variation does not show an evening peak.

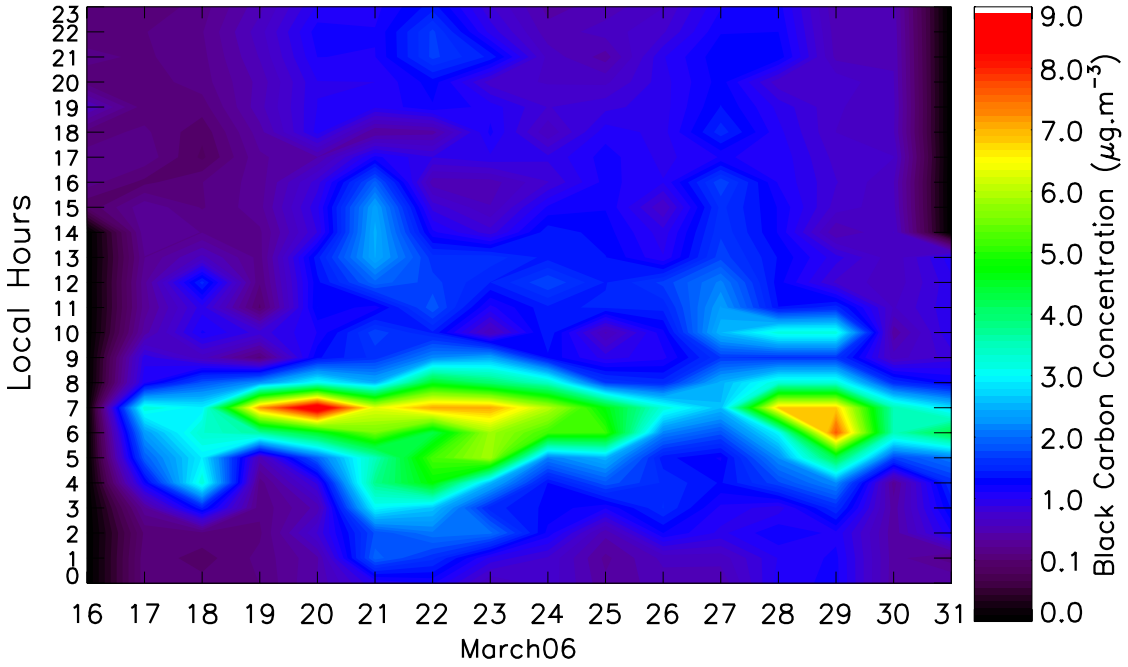

Figure 4.11: *Temporal variation in BC concentration ($\mu g.m^{-3}$) at Kalpakkam during the campaign period. There is only one peak during morning when the wind is coming from the continent.*

As defined by *Hess et al.* (1998), in "continental average" aerosol model BC concentration is 0.5 μgm^{-3}. BC concentration increases by almost a factor of 4 in "continental polluted" aerosol model and becomes 2.1 μgm^{-3} but in the case of "urban" aerosol model BC concentration is 7.8 μgm^{-3}. At Kalpakkam the mean background BC concentration during 16-19 and 30-31st March was 1.2 μgm^{-3}. During these periods of observation BC concentration at Kalpakkam was close to the "continental average" aerosol model. During 20-29 March the mean background BC concentration increased by a factor of 1.6 and became 2.0 μgm^{-3} which is very near to the BC concentration in "continental polluted" aerosol model. The morning peak BC concentration was more then twice the BC concentration of "continental polluted". During 20-29 March most of these peaks even reached more than the BC concentration of "urban" aerosol model due to an increase in the background BC concentration. When the wind is from the Indo-Gangetic basin, the air mass

carried large amount of BC and hence the mean background BC concentration increased by a factor of 1.6 during sea breeze as shown in the Fig. 4.11.

4.2.4 Particle Number Concentration

Grimm particle size spectrometer was used to measure the aerosol number concentration (L^{-1}) continuously during the campaign period. This instrument can measure the number concentration of particles at 14 different sizes simultaneously. The total particle number concentration is divided into two parts, submicron size particle (size $<$1 micron) and micron size particle (size $>$1 micron) number concentration. The variation of submicron and micron size particle number concentration during the campaign period is shown in Fig. 4.12. The variation in submicron particle number concentration was very similar to the variation of BC mass concentration. During land breeze submicron particle concentration increased and later decreased during the day as the wind changed its direction. The peak concentration occurred during 0400-0900 local hours. This clearly indicates that BC particles are dominating in the submicron regime. During sea breeze the submicron particle number concentration decreased and the variation is minimum. However, during 27-28 March there was an increase in the submicron particles by a factor of two during the sea breeze. Satellite observations during this period showed that a cyclone formed in the BoB and due to which more sea salt was produced and increased the submicron as well as the micron particle (*Koepke et al.*, 1997; *Hess et al.*, 1998) number concentration at the measurement site.

The micron particle number concentration is also shown in Fig. 4.12. There is no significant diurnal variation in the micron particle concentration. The variation is very similar to the variation of aerosol scattering coefficient (as discussed later). The micron particles are mainly sea salt particles dominated in the coastal regions. During the cyclonic period (27-28 March) the micron size sea salt also increased and the enhancement was observed at the measurement site.

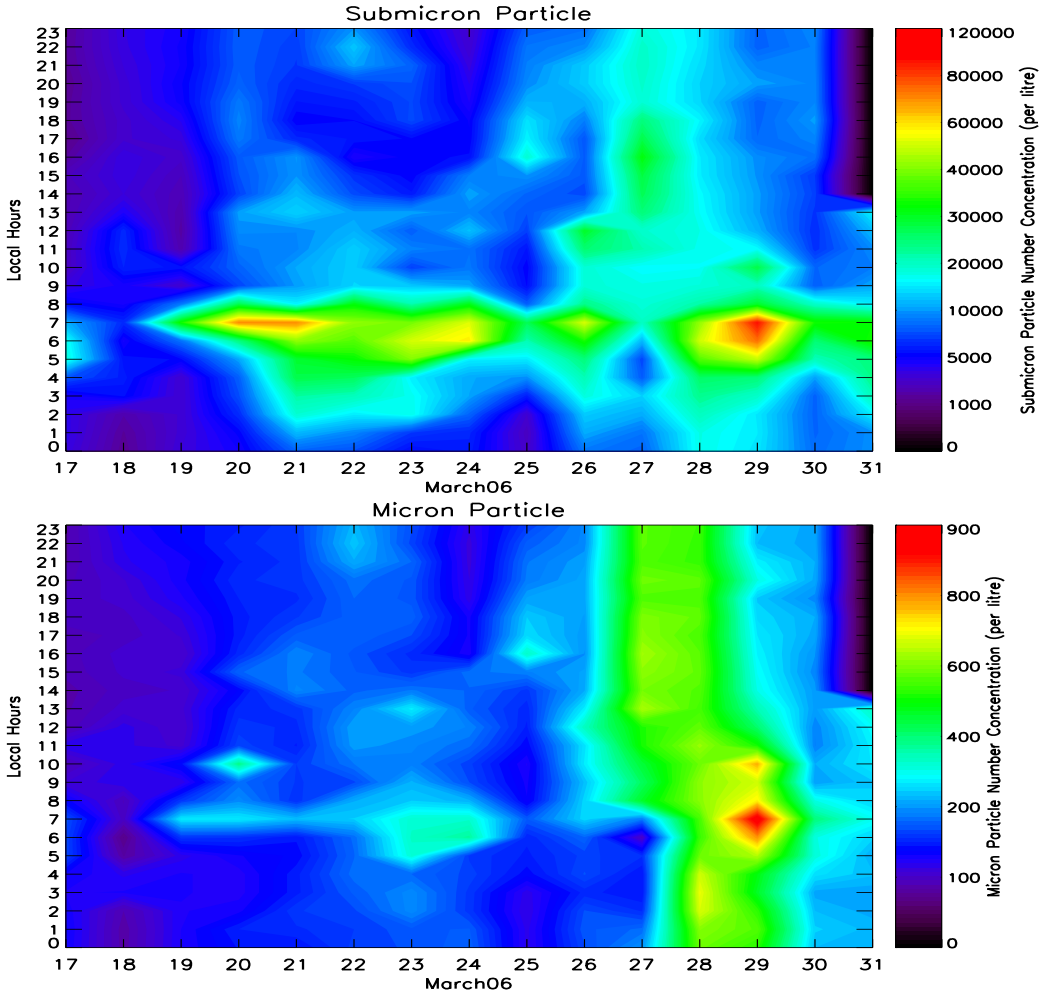

Figure 4.12: *Temporal variation of submicron and micron particles observed over Kalpakkam. The sub micron particles variation is vary similar to the BC variation whereas micron particles variation does not show any strong diurnal variation.*

4.2.5 Aerosol Absorption Coefficient

Aerosol absorption coefficient (β_{abs}) is an important parameter to estimate the aerosol radiative forcing. In the present study, the absorption coefficient is calculated from the Aethalometer raw data at seven wavelengths, viz., 0.37, 0.47, 0.52, 0.59, 0.66, 0.88 and 0.95 μm. Detail procedures are explained in literature (*Hansen et al.*, 1982; *Bodhaine*, 1995; *Weingartner et al.*, 2003) and hence the procedures are not repeated here. The spectral dependency of absorption coefficient follows a power law relationship of the form $\beta_{abs} = K.\lambda^{-\alpha'}$ where K and α' are the absorption

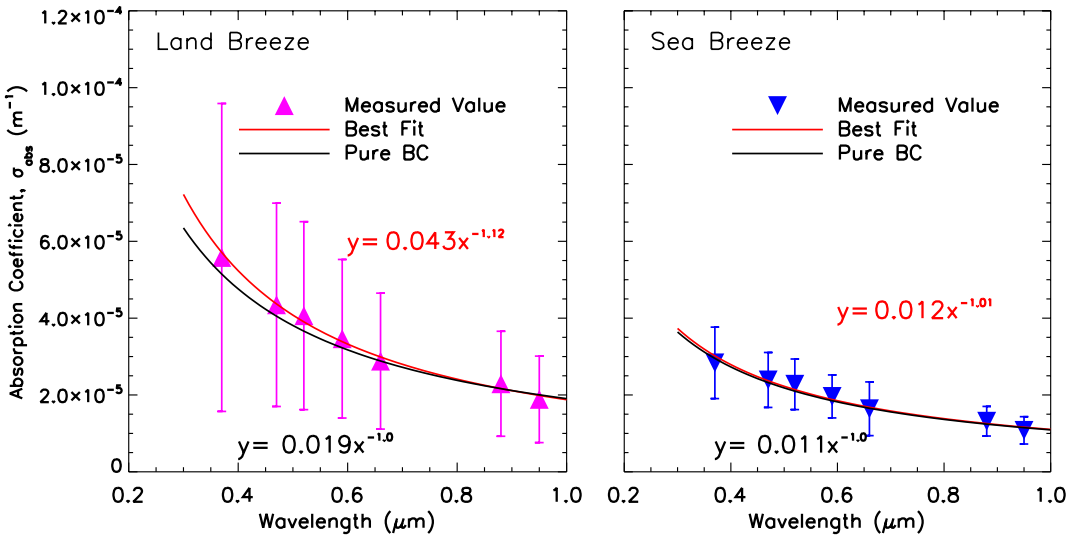

Figure 4.13: *Averaged spectra of aerosol absorbtion coefficient for Land Breeze and Sea Breeze. Best fitted power law curve and compared with the model spectral power law for pure atmospheric absorbing BC.*

angstrom coefficients (*Kirchstetter et al.*, 2004). The absorption angstrom exponent, α' has an important role in characterizing the source production of the absorbing aerosols (*Kirchstetter et al.*, 2004). For pure black carbon α' is equal to unity i.e., the absorption coefficient is inversely proportional to the wavelength. In principle the BC measured at all wavelengths should be equal. However, in practice it shows different values at different wavelengths because the spectral dependence of light absorption is mainly controlled by the size of the graphite cluster (*Bond*, 2001; *Bond and Bergstrom*, 2006) and the size of the graphite cluster strongly depends on the combustion process and the temperature of the combustion. The spectral dependence is stronger ($\alpha' = 2.0$) in case of aerosols produced from biomass burning and the spectral dependence is weaker ($\alpha' = 1.0$) in case of aerosols from fossil fuel burning mainly from the motor vehicular emission (*Kirchstetter et al.*, 2004). A mixture of BC with other aerosols also can exhibit a weak spectral dependence (*Jacobson*, 2000; *Bond*, 2001; *Bergstrom et al.*, 2002). The absorption angstrom exponent is shown in Fig. 4.13 during land and sea breeze at Kalpakkam. During land breeze α' is about 1.12 showing a weaker spectral dependence. As already

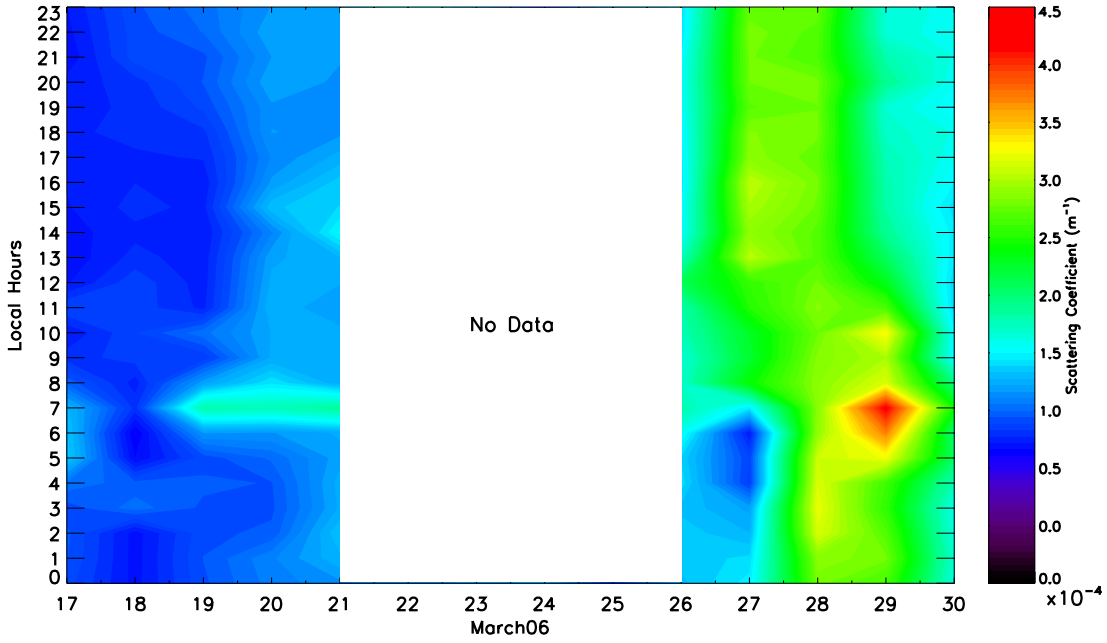

Figure 4.14: *Temporal variation of aerosol scattering coefficient at Kalpakkam.*

discussed above, the BC measured during the land breeze is coming mainly from Chennai and surrounding suburban areas and so it can be stated that the BC is produced more from the fossil fuel burning. During sea breeze also α' is about 1.01 showing a weaker spectral dependence again. However since this BC is being carried from over the sea, the BC could be in a mixing state. Further laboratory experiments in a controlled environment simulating maritime conditions and modelling studies are required to understand the mixing state spectral dependency.

4.2.6 Aerosol Scattering Coefficient

Aerosol scattering coefficient (β_{sca}) was measured by a Nephelometer continuously throughout the campaign period and the daily variation is shown in Fig. 4.14. During 21-27 March data was not stored due to some technical problem in the instrument. Aerosols that contribute maximum to the scattering coefficient are the inorganic water soluble particles like sulphate, nitrate etc which are mainly anthropogenic origin. These aerosols are commonly coming into the atmosphere

by fossil fuel burning, ammonium from fertilizer, biomass combustion (*Charlson et al.*, 1992; *Penner et al.*, 1994). Seasalt is one of the natural aerosols which also contributes to the scattering coefficient. Small coastal wave breaking commonly produces coarser seasalt aerosols (size $>$ 1 micron) and these seasalt aerosols contribute maximum in the visible range scattering coefficient (*Clarke et al.*, 2003). At Kalpakkam no significant diurnal variation in aerosol scattering coefficient was found. This implies that at Kalpakkam mainly the scattering coefficient is governed by the coastal seasalt aerosols. During 18-21 May an increase in scattering coefficient was found at about 0700 local hours. Wind analysis shows that large amount of anthropogenic aerosols including BC were transported from the Chennai and its surroundings which enhanced the scattering coefficient. After 27 March scattering coefficient increased due to huge amount of seasalt produced over ocean by cyclone in the Bay of Bengal during 27-28 March. Transportation of these particles to the coast enhanced the scattering coefficient by a factor of about two.

4.2.7 Single Scattering Albedo

Form the aerosol absorption coefficient (β_{abs}) and scattering coefficient (β_{sca}) the single scattering albedo ω_0 can be calculated using the relation $\omega_0 = \beta_{sca}/(\beta_{sca} + \beta_{abs})$. Single scattering albedo is an important parameter in the radiative forcing estimation. In the "urban" aerosol model ω_0 (at 0.5 μm) is 0.76 due to presence of maximum soot whereas in the "continental clean" model ω_0 is 0.96 due to absence of soot (*Hess et al.*, 1998). So the "urban" aerosol model exhibits more warming effects than compared to "continental clean". In case of "marine clean" and "marine polluted" aerosol model ω_0 are 0.99 and 0.96 respectively. The significant difference between "clean" and "polluted" models depends on the amount of absorbing soot. A region becomes polluted due to enhancement of the anthropogenic soot particles by emission and/or transportation and thus reduces ω_0. In case of marine region enhancement of soot particles does not contribute more in magnitude of the radiative forcing at the Top of the Atmosphere (TOA) (*Podgorny and Ramanathan*,

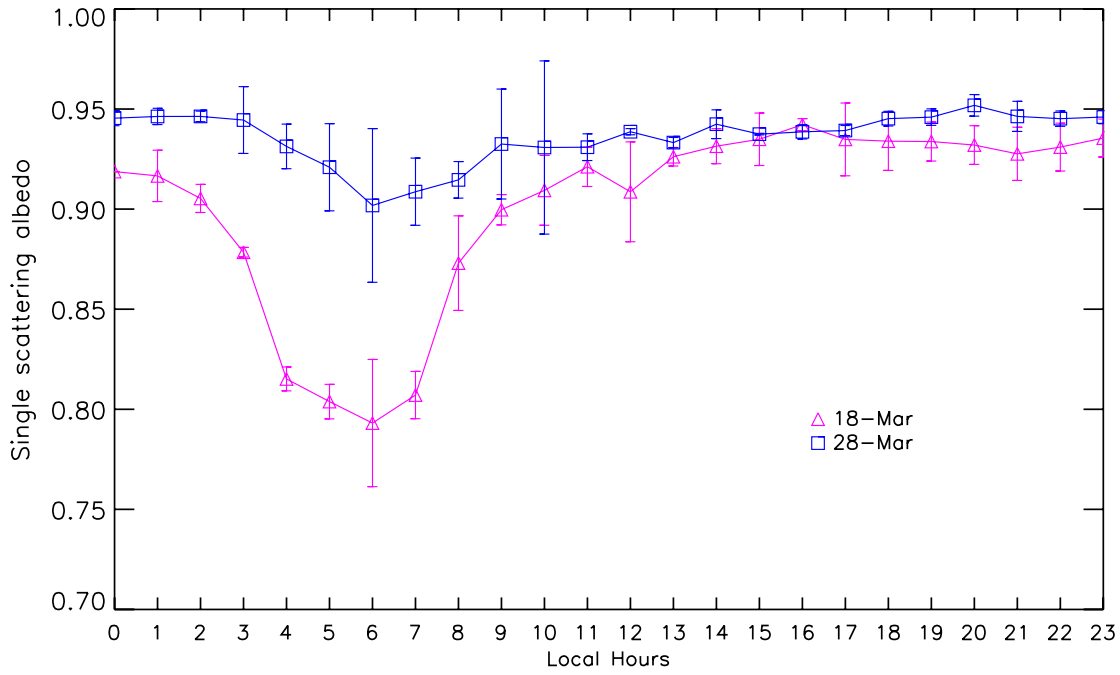

Figure 4.15: *Temporal variation of Single Scattering Albedo at Kalpakkam.*

2001) but it results the positive radiative forcing due to its absorption properties. Soot strongly absorbs reflected radiation in the lower layers of the atmosphere and effects more on ω_0.

Many researchers e.g., *Ramachandran and Jayaraman* (2002); *Satheesh et al.* (2002); *Vinoj et al.* (2004); *Ganguly et al.* (2005) showed that ω_0 is 0.85-0.88 at different locations of BoB during the INDOEX experiment. This value is lower than that of the "marine polluted" model. During the North-East monsoon seasons large BC concentration, coming from South-east Asia, loads into the oceanic atmosphere and surrounding costal areas. In the Eastern coast region the value of ω_0 is lower than that over BoB and the coastal land. *Ramachandran* (2005) reported that at Chennai it is 0.77 which is very close to ω_0 of the "urban" model. In the present study, single scattering albedo is obtained using the scattering coefficient at 0.530 μm from Nephelometer and the absorption coefficient at 0.520 μm from Aethalometer. The diurnal variation of the single scattering albedo at Kalpakkam is shown in Fig. 4.15.In a typical day like 18 March during land breeze ω_0 becomes 0.79 which is

very close for 'Urban' environment whereas during sea breeze ω_0 becomes 0.92 which is very close for 'Marine polluted' environment. During land breeze there is transportation of BC aerosols from Chennai and its surrounding suburban regions which reduces ω_0. During sea breeze this transportation of BC from the continent is blocked which results in enhancement of ω_0 to 0.92. However, there is a long range transportation of BC aerosols from Indo-Gangetic Basin via BoB during 20-29 March. This BC transportation enhanced the background BC values by a factor of 1.6. During 27-28 March there is a cyclonic event in the BoB which results enhancement of natural seasalt aerosols in the marine and costal atmosphere. From Nephelometer observation the scattering coefficient has increased by a factor of two. The Aethelometer observation shows that there is less variation in the BC amount. As the coastal seasalt aerosols are enhanced, the ω_0 is becomes 0.90 during land breeze and 0.94 during sea breeze. After the cyclonic event on 28 March ω_0 shows relatively less diurnal variation.

4.3 Study of Aerosol Properties during Dust Storm Condition at Mt. Abu

In the present work we have studied major aerosol properties during 10 May to 13 May 2006 over a hilltop station, Mt. Abu in the western part of India. During this period two major dust storms were observed and they changed the background aerosol properties and hence the aerosol radiative forcing.

4.3.1 Meteorological Parameters and Aerosol Index

During pre-monsoon season (April-May) the boundary layer is above the observation site. During this season temperature is high enough (above $\sim$25°C) and the thermal convection is strong. The wind pattern over the western region of India is shown in the Fig. 4.16 during the study period. Wind was coming from mainly

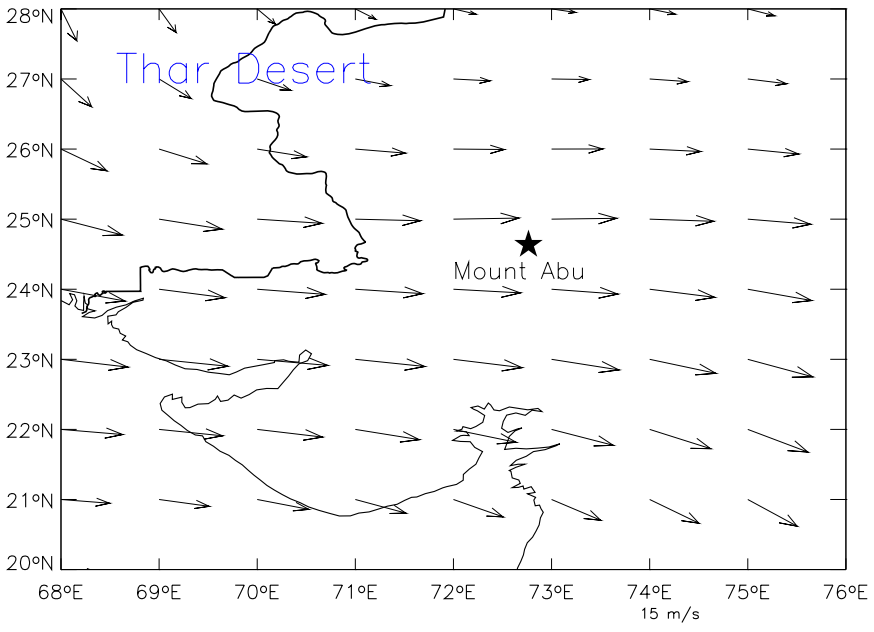

Figure 4.16: *Averaged wind pattern at 850 mb level during the study period (10 to 13 May 2006) over the western part of India.*

westerly with high speed nearly at 10 m/s. The other meteorological parameters like wind speed, temperature and relative humidity (RH) observed in every minute interval using automatic portable weather station installed at the roof of the observatory are shown in Fig. 4.17. On 10 and 11^{th} May three storms were observed consequently . They occurred during 0800-0900, 1300-1600 and 2000-0200 local hours. During the stormy periods wind speed was 12-20 m/s which is relatively high at the hill top region. During a normal day (12^{th} May) mean wind speed was 6.0$\pm$2.0 m/s. At the hilltop, the local temperature had a smooth diurnal variation with maximum of 28°C during noon and minimum of 24°C during late night. Observed mean RH was 30$\pm$7% during the observation period. During observational period the sky was cloud-free and there was no rainfall.

Fig. 4.18 shows the time series of aerosol index (AI) obtained from Total Ozone Mapping Spectrometer (TOMS) satellite during the observation period. This parameter is a measure of the change in the amount of measured backscattered UV radiation by the air and aerosols at 0.360 μm with respect to that computed for a pure molecular atmosphere (*Herman et al.*, 1997; *Hsu et al.*, 2000; *Chiapello et al.*,

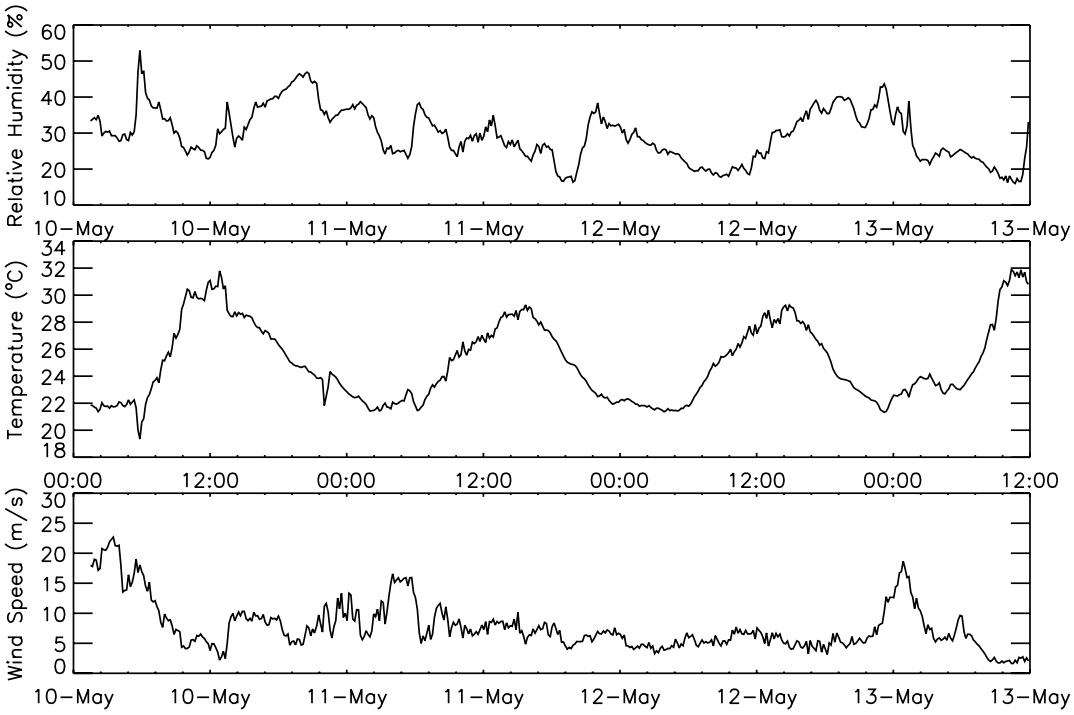

Figure 4.17: *Observed meteorological parameters over Mt. Abu for the study period.*

2000). AI is defined such that positive values generally correspond to the ultraviolet absorbing aerosols and negative values to nonabsorbable aerosols (*Chiapello et al.*, 2000). AOD has a good linear correlation with ground based observations (*Hsu et al.*, 1999) and this has been theoretically verified (*Torres et al.*, 1998). To understand the dust prone regions AI is a very useful parameter (*Sabbah et al.*, 2001). In the present study we use AI to indicate the dust enhanced day in the western part of India. On 10^{th} May one dust storm was observed in the western part of India and AI was nearly 2.0 over the observation site (Fig. 4.18) and on rest of the days AI was $\sim$1.5. It indicates that during the dust storm soil dust particles are lifted up into the atmosphere and increased AI on 10^{th} May. After that strong thermal convection supports the mixing of the fine dust particles with air and as a result a high AI value is maintained over the western part of India.

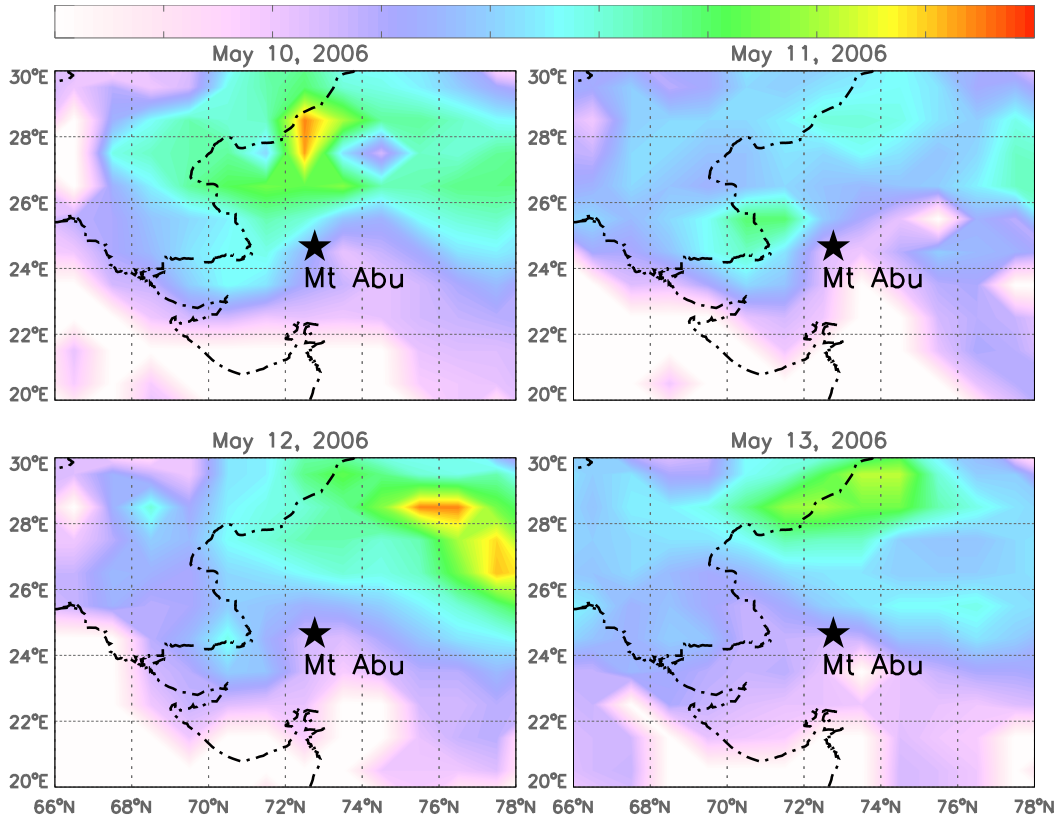

Figure 4.18: *Regional variation of aerosol index obtained from TOMS satellite. The greenish region indicates the origin of dust storm and bluish shaded region represent dust transported regions. Mt. Abu, located by a star in the figure, is in the dust transported region.*

4.3.2 Changes in Aerosol Optical Properties during Dust Storm

At a particular wavelength Aerosol Optical Depth (AOD) represents the total attenuation of solar light at the Earth's surface. AOD has a strong spatial distribution. In arid and semi-arid regions AOD is highly variable due to the uneven distribution of the mineral dust. In the western part of India AOD has a large spatial and temporal distribution due to uneven distribution of mineral dust produced by local dust storm at the desert region and strong wind transported this dust to the other places of western part of India. Mainly mineral dust influences AOD by its scattering properties of solar radiation associated with the strong absorbance in the visible radiation (*Dickerson et al.*, 1997; *Hess et al.*, 1998). So the columnar aerosol optical depth (AOD) is highly influenced by the dust which is transported

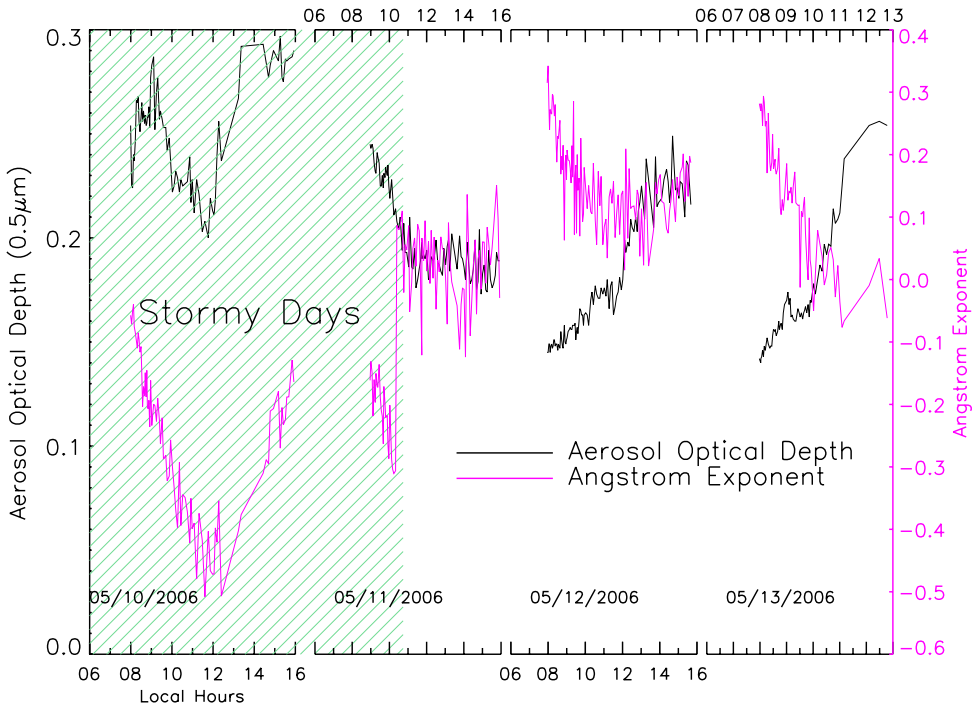

Figure 4.19: *Observed AOD values during dust storm and non-dust storm period over Mt. Abu. The shaded region represents the storm period.*

from the 'Thar' desert during this premonsoon season. The time series of columnar AOD (at 0.5 μm) is shown in Fig. 4.19 for the period 10-13th May at the hill top region, Mt. Abu. During normal days (like 12 and 13 May) minimum AOD of 0.14 during the morning and maximum of 0.25 during afternoon has been observed. This is because of the local dynamics of boundary layer. As the day progresses the thermal convection increases and the upwelling convection brings more aerosols to higher altitudes and hence enhances the columnar AOD. On the first stormy day (10th May) there is a sharp increase of AOD during the stormy periods during 0800-0900 local hours and by about 1000 local hours the columnar AOD reduces and comes to minimum of 0.2 during local noon hours. Later, the columnar AOD again increases and reaches the maximum of 2.9 at 1330 local hours. The Angstrom wavelength exponent (α) is one of the important parameter which is the slope of the logarithm of AOD versus the logarithm of wavelength (in micron) and provides the basic information about the columnar particle size distribution. But α has

different values for different pair of wavelengths (*Reid et al.*, 1999). In the present study the α value calculated in the range 0.380 – 0.870 μm gives the information about the aerosol size distribution. The higher values of α indicate the relatively large number of smaller sizes aerosols and low value of α implies that the bigger sized aerosols are increased in number. The soil borne aerosol particles decreases α value nearly to zero. In the Fig. 4.19 the magenta colored line shows the time series of Angstrom exponent. On first stormy day (10^{th} May) α is decreasing as day progresses. During the stormy period α is very close to zero. Due to strong wind (Fig. 4.17) α remains nearly zero values during afternoon. During the stormy period the dust particles are transported from the desert as well as the strong wind lifted up the local loose soil particles in the hill top area and as a result the columnar AOD has increased and the α decreases to nearly zero. But during the afternoon period the storm enhances AOD values again and makes α nearly equal to zero.

On the normal day (namely 12^{th} May) α remains constant at 0.3. This indicates the aerosol number distribution remains same during the whole day and the upwelling increases all sizes of aerosols.

4.3.3 Aerosol Number Concentration

In the premonsoon season the surface aerosol number distribution is highly influenced by the dust storm over the desert region. Fig. 4.20 shows the time series variation of total number concentration of aerosols in the range of 0.3-20.0 μm and different size revolved aerosols. The variation of total number concentration (Fig. 4.20(a)) is very similar to the variation of wind speed and columnar AOD and the angstrom exponent. In Fig. 4.20, large impact of two major dust storms on the aerosol number concentration can be easily observed. Two of the storms are during day time on 10^{th} May and another during the midnight on 11^{th} May. On 10 and 11^{th} May during the dust storm the total aerosol number concentration has increased by a factor of three to four. This increase has been observed in all sizes

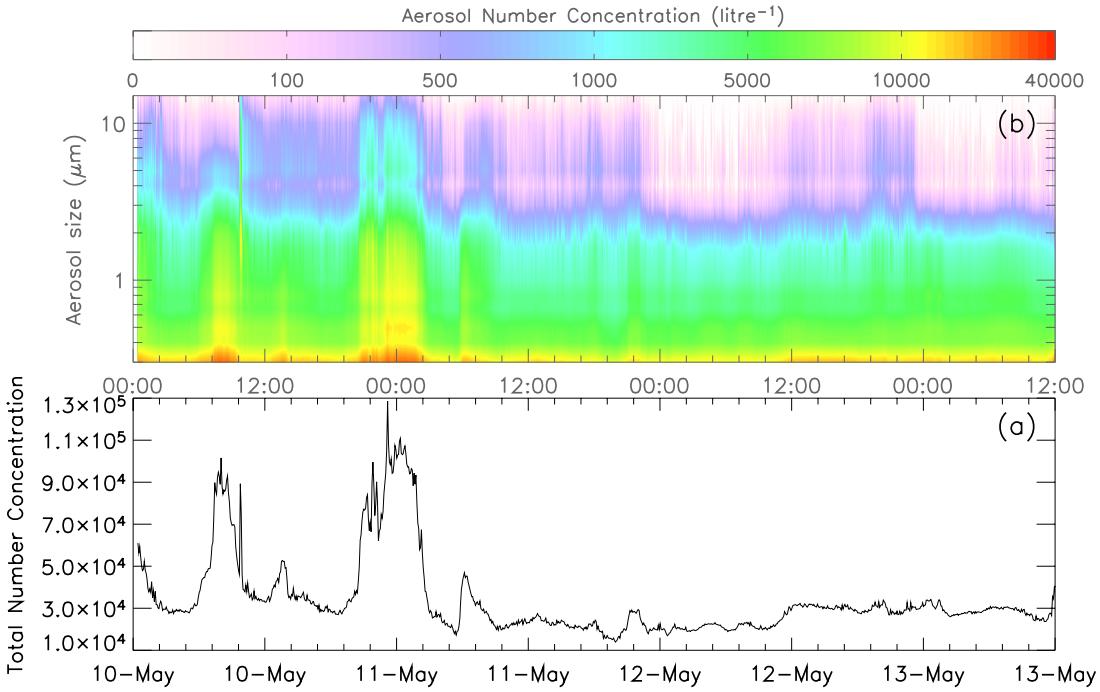

Figure 4.20: *(a)Time series of total particles concentrations (b) Time series of different sizes of aerosols over the hill top area during observation period using aerosol size spectrometer.*

of aerosols. The fine aerosols ($<0.5\mu$m) during the dust storm increased by a factor of four whereas the bigger coarse aerosols ($>0.5\mu$m) increased by an order of magnitude (as shown in the Fig. 4.20(b)). As defined by *Hess et al.* (1998) fine aerosols represents the transported mineral dust whereas the coarse aerosols are soil lifted coarse mineral dust. At the hill top region the wind carries lots of fine aerosols from the nearby desert region and enhances the fine dust by a factor of four whereas the coarse dust particles are enhanced in the atmosphere by strong winds lifting up local loose soil in the hill areas. Hence during the stormy periods the coarse aerosols are enhanced and rest of the times they go to background level. One of the important observation at the hill top area is that the coarse aerosols are increased only when the wind speed becomes greater than 10 m/s. This indicates that the coarse aerosols are lifted up into the atmosphere by strong winds.

During the stormy days (10 and 11^{th} May) aerosol index is relatively high than

normal days due to the dust storms observed in the western part of India. However, on normal days AI is greater than 1.0 (as shown in the Fig. 4.18) which indicates the large abundances of dust aerosols in this region. So the abundance of fine dust aerosols do not show any large variation during the steady wind speed (Fig. 4.20(b)) at Mt. Abu observatory.

During the normal days (like 12^{th} May) there is no variation in the fine as well as the coarse aerosols. The total aerosol number concentration reaches the background level. On 12^{th} May after 1200 noon an enhancement of background aerosol number concentration was observed, in all sizes of aerosols. The reason is the increase of local boundary layer height by the thermal convection, when the dust aerosols get more room to mix in the vertical direction. This effect is also observed in the time series variation of columnar AOD. AOD also increased as the day progressed because of the increasing boundary layer height. The boundary layer height enhancement effect is equally applicable to all sizes of background aerosols, hence the angstrom exponent has not changed as shown in the Fig. 4.19.

On 10 and 11^{th} May diurnal variation of total surface aerosol number concentration was very similar to the changes of columnar AOD. Dust storms enhance both the surface aerosol number concentration and columnar AOD. Also the midnight dust storm enhanced aerosol number concentration. So in the morning high columnar AOD was observed on 11^{th} May and as the day progressed the AOD decreased and angstrom exponent increased. The reason is the increase of wind speed at the hill top area. Midnight storm has enhanced the background fine dust which sustained up to morning hours whereas the bigger coarse dust aerosols settled very soon after the storm. So in the morning, AOD was relatively high than the normal days and α value was also very close to zero. But as the day progressed strong wind removed dust from the hill top areas and hence AOD reduced to 0.19 and α enhanced up to 0.3 which was equal to the normal day value.

4.3.4 Black Carbon Concentration and Aerosol Absorbtion Coefficient

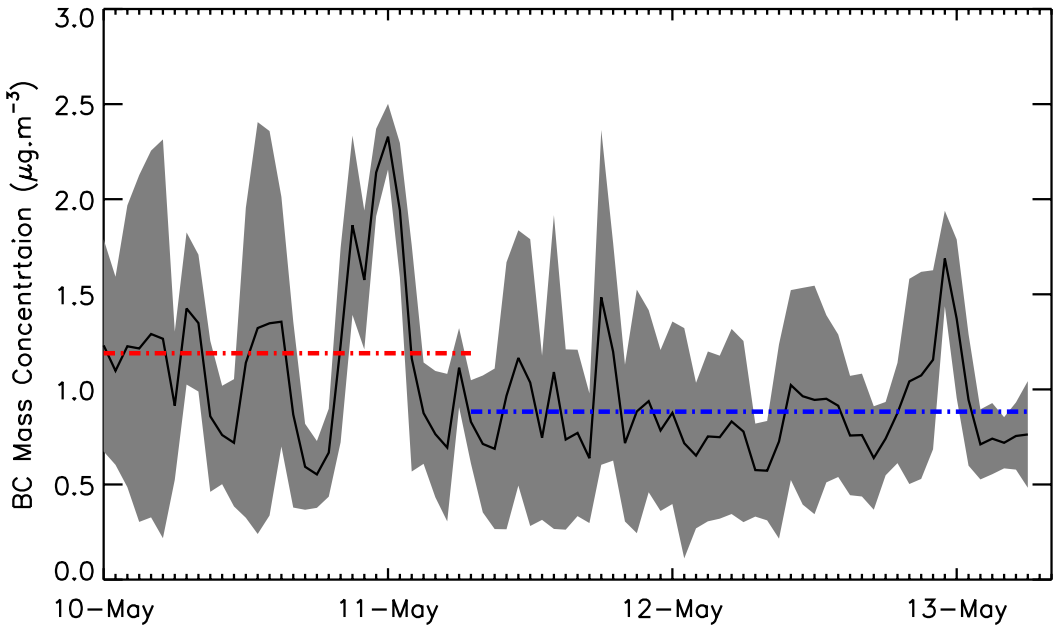

Figure 4.21: *Time series of BC mass concentration observed over Mt. Abu. The red and blue lines represent the background mean values of BC during stormy and normal days.*

One of the crucial anthropogenic radiative forcing agent is black carbon or soot (BC), released from incomplete combustion of carbon-based fuels (*Andreae and Gelencser*, 2006). Due to its absorbing properties BC contributes significantly to the global climate change and more importantly over the populous countries like China and India. *Jacobson* (2001) reported that BC is the potential positive radiative forcing agent which makes it the second most important atmospheric component for global warming after CO_2 in terms of direct radiative forcing estimation. India contributes nearly 8.5% of the total global BC emission (*Venkataraman et al.*, 2005) and therefore demands the regular monitoring of BC concentration in different parts of India not only on a regional scale but also on a global scale. Fig. 4.21 shows the time series variation of BC mass concentration at Mt. Abu during the study period. The shaded region shows the $\pm 1\sigma$ variation of the mean BC at the

hill top region. During the stormy period the BC varied from 0.2 to 2.3 μg.m^{-3}. At Mt. Abu the background BC concentration was observed to be 0.9 μg.m^{-3} during premonsoon season. During the normal days background BC concentration was observed to be 0.9 μg.m^{-3} over the hill top region. However, in dust storm periods during day time the background BC reached to 1.2 μg.m^{-3} whereas during the midnight background BC concentration has increased by factor of two and reached to 2.4 μg.m^{-3} (Fig. 4.21) because of the large transportation of BC from the urban regions as well as resuspension of BC particles from the soil surface during dust storm days.

Aerosol absorbtion coefficient is one of the important parameters of the radiative forcing and this parameter carries the information about the absorbing aerosol in the source region. In the present study, absorbtion coefficients are calculated at seven wavelengths, 0.380, 0.470, 0.520, 0.590, 0.660, 0.880 and 0.950 μm using the raw data obtained from Aethalometer. The detail procedure for the estimation of absorbtion coefficient calculation form Aethalometer raw data is described by several research workers (*Hansen et al.*, 1982; *Bodhaine*, 1995; *Weingartner et al.*, 2003; *Ganguly et al.*, 2005) and is not repeated here.

Measurement of the spectral absorbtion coefficient is useful to get the information about the absorbing particles in the atmosphere. In the atmosphere most important absorbing aerosols is the BC and it has a strong absorbance at 0.880 μm wavelength. The other stronger atmospheric absorbing aerosol is dust. However, at 0.880 μm the contribution of absorbance of dust aerosols is relatively small compared to BC due to smaller cross section whereas at shorter wavelength range it has higher absorbtion (*Bodhaine*, 1995). Wavelength dependence of absorption by aerosols has been investigated using a power law relationship of the form $\beta_{abs}(\lambda) = K.\lambda^{-\acute{\alpha}}$ where K and $\acute{\alpha}$ are the absorption Angstrom coefficients and $\acute{\alpha}$ is a measure of spectral dependence of aerosol absorption (*Kirchstetter et al.*, 2004).

Fig. 4.22 shows the spectral absorbtion coefficient during the stormy days (average of 10 and 11th May) and normal days (average of 12 and 13th May) and the vertical bar represent the $\pm\sigma$ variation of the mean. $\acute{\alpha}$ is highly variable and there is

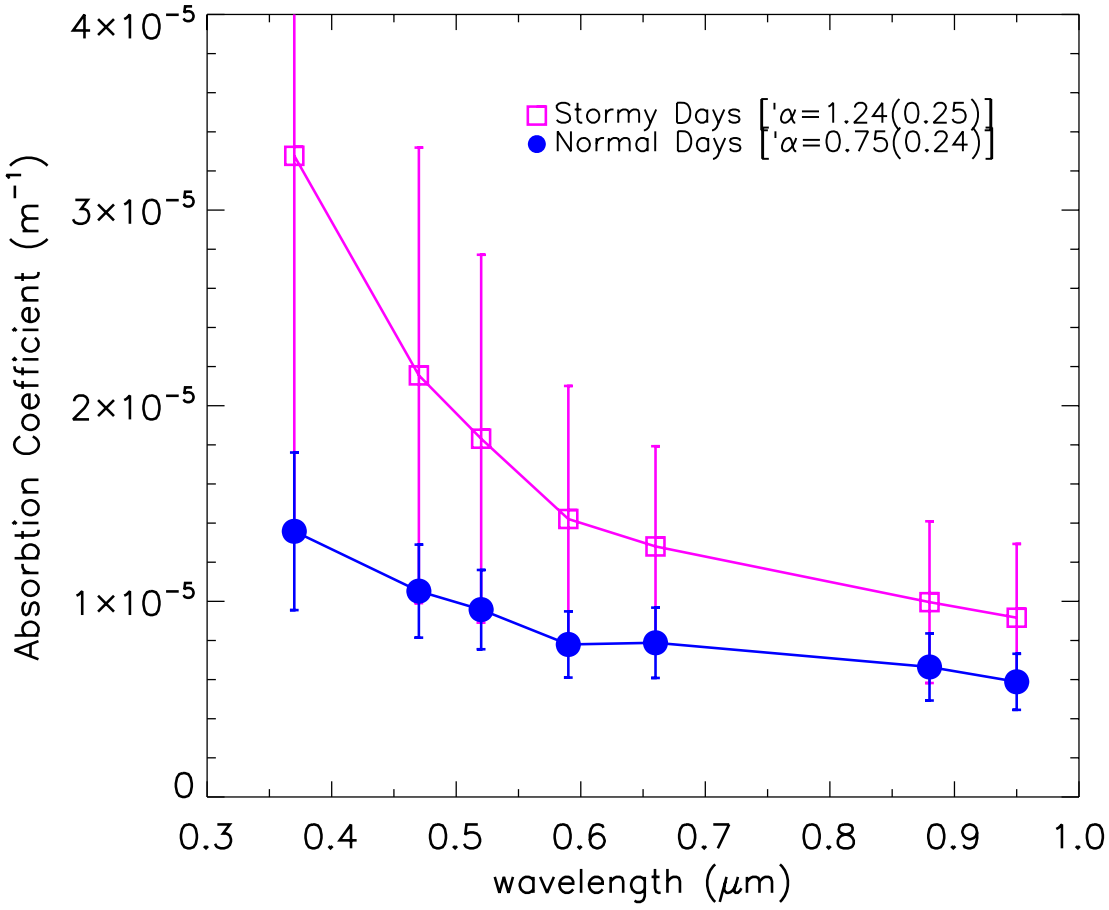

Figure 4.22: *Typical spectra of aerosol absorbing coefficient for stormy and normal days. Mean ά is obtained by best fitting of power law curves and the values within bracket represent the standard deviation of mean ά.*

large difference between stormy and normal days. During the stormy days ά was 1.24±0.25 whereas it represent the background value at 0.75±0.24 during normal days. During stormy days the strong spectral dependency is due to the enhancement of absorbance by a factor of about three at 0.380 μm wavelength whereas only a slight increase of absorbance is observed in 0.880 μm wavelength. This is because of the large abundance of fine dust particles during the stormy days in the hill top area. Not having any extra source of BC, the upwelling convection and long range transportation from urban region caused the enhancement of BC during the stormy days which resulted in a slight increase of absorbance at 0.880 μm.

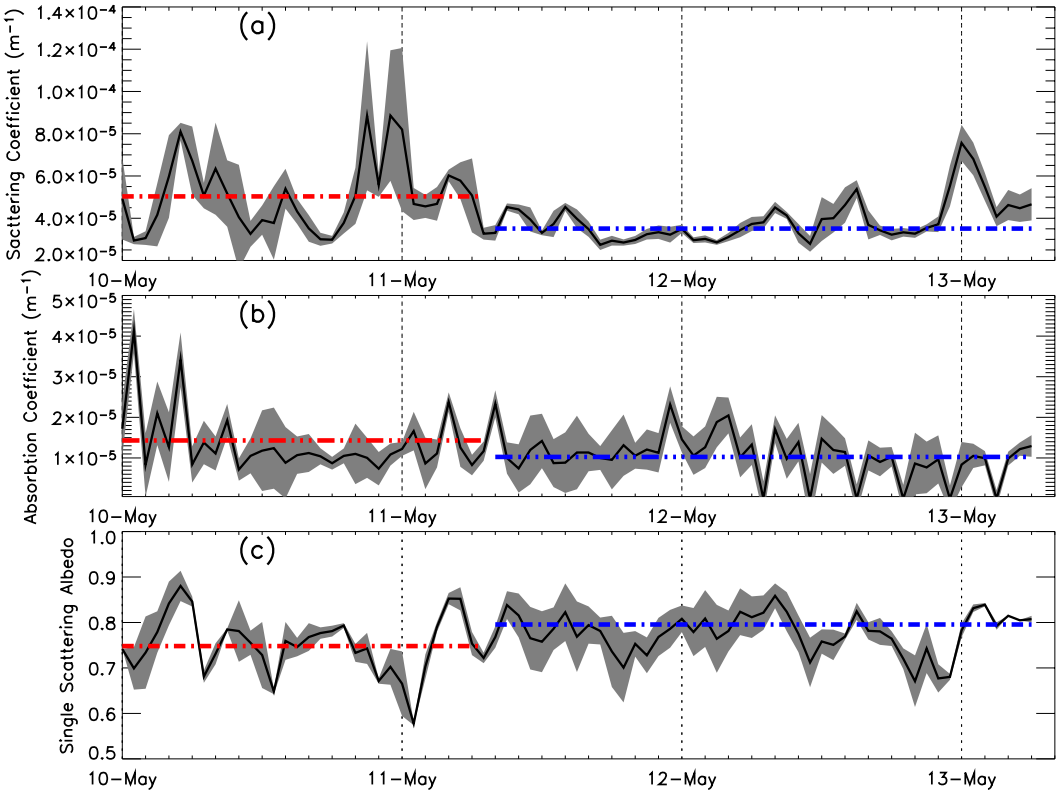

Figure 4.23: *Time series of (a) Aerosols scattering coefficient, (b) absorbtion coefficient and (c) Single Scattering Albedo at Mt. Abu during observation period. The line shows the background level of the aerosol parameter during stormy days (red color) and normal days (blue color).*

Fig. 4.23(b) shows the time series of absorbtion coefficient (at 0.520 μm) during the observation period. During the stormy days the background absorbtion coefficient is observed about $1.4\times10^{-5}\mathrm{m}^{-1}$ whereas during normal days the background absorbtion coefficient comes down to $1.0\times10^{-5}\mathrm{m}^{-1}$. The increase during the stormy periods is due to the large enhancement of absorbing particles which increase the background absorbtion coefficient.

4.3.5 Aerosol Scattering Coefficient and Single Scattering Albedo

The time series of aerosol scattering coefficient at 0.530 μm and single scattering albedo 0.525 μm are shown in Fig. 4.23 (a & c). The shaded region shows the $\pm1\sigma$ variation about the mean of the each parameter. The variation of single scattering

albedo (Fig. 4.23(a)) is very similar to the variation of AOD, surface aerosol number concentration and BC aerosols. In a semiarid atmosphere, dust contributes to a major part of the aerosol scattering coefficient and during the premonsoon season abundance of dust particles is high in the atmosphere. During the observation period the peaks of the scattering coefficient occurred in the dust storm periods and enhanced the background scattering coefficient to $5.0\times10^{-5}\mathrm{m}^{-1}$ whereas during the normal days it was to $3.5\times10^{-5}\mathrm{m}^{-1}$ which represents a proportional amount of fine scattering dust aerosols.

Single scattering albedo (SSA) has an crucial role in the aerosol radiative forcing because the atmospheric warming or cooling effect is mainly controlled by it. The knowledge of SSA is very crucial as any variation can cause the large uncertainty in the radiative forcing (*Takemura et al.*, 2002). SSA is the ratio of the scattering coefficient and the extinction coefficient and is calculated from the measured aerosol scattering coefficient obtained using Nephelometer and absorbtion coefficient using Aethalometer as described by *Ganguly et al.* (2006b). During the stormy days the background SSA was at 0.75 whereas during the normal days it increased to 0.80. During the stormy days background single scattering albedo was low. The reason is enhancement of dust which can absorb and scatter in the visible wavelength and hence during storm periods dust particles increased both the coefficients. The total extinction coefficient (scattering + absorbtion) has been enhanced and this enhancement reduces SSA. But during the normal days extinction coefficient reduces whereas the reduction in scattering coefficient was relatively small compared to the extinction coefficient because number concentration of background fine dust particles remains almost same and as a result the SSA increased to 0.80.

4.4 Study of Arid Aerosols

Arid aerosols are mainly concentrated over desert and its surroundings. Arid aerosols, which mainly consist of dust aerosols can perturb the climate of a pristine environment by transportation. In India, 'Thar' desert situated in the western part is a major source of dust aerosols. For the study of arid aerosols, their optical and physical properties are measured during April 2007 at three stations viz., Ahmedabad-an urban region, Mt. Abu-a pristine environment and Udaipur-a semi-arid region.

4.4.1 Observational sites and Meteorological Parameters

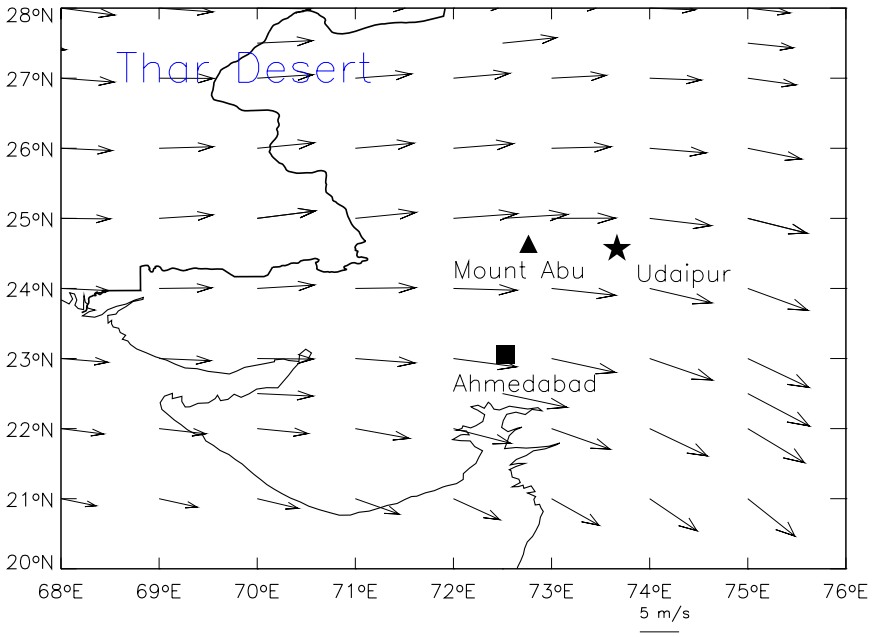

Figure 4.24: *Average wind pattern at 850 mb level during April 2007 over western part of India.*

Fig. 4.24 shows the location of the three stations and the wind pattern over these regions during April 2007. The first two stations, Ahmedabad and Mt. Abu, have been discussed in detail in Secs. 3.1 and 3.2, respectively. The third measurement site is Udaipur (24.58°N, 73.70°E, 500m asl), a city at the foothill of Aravalli range with 5.5 lakhs population. The city is nearer to the Thar desert and is at

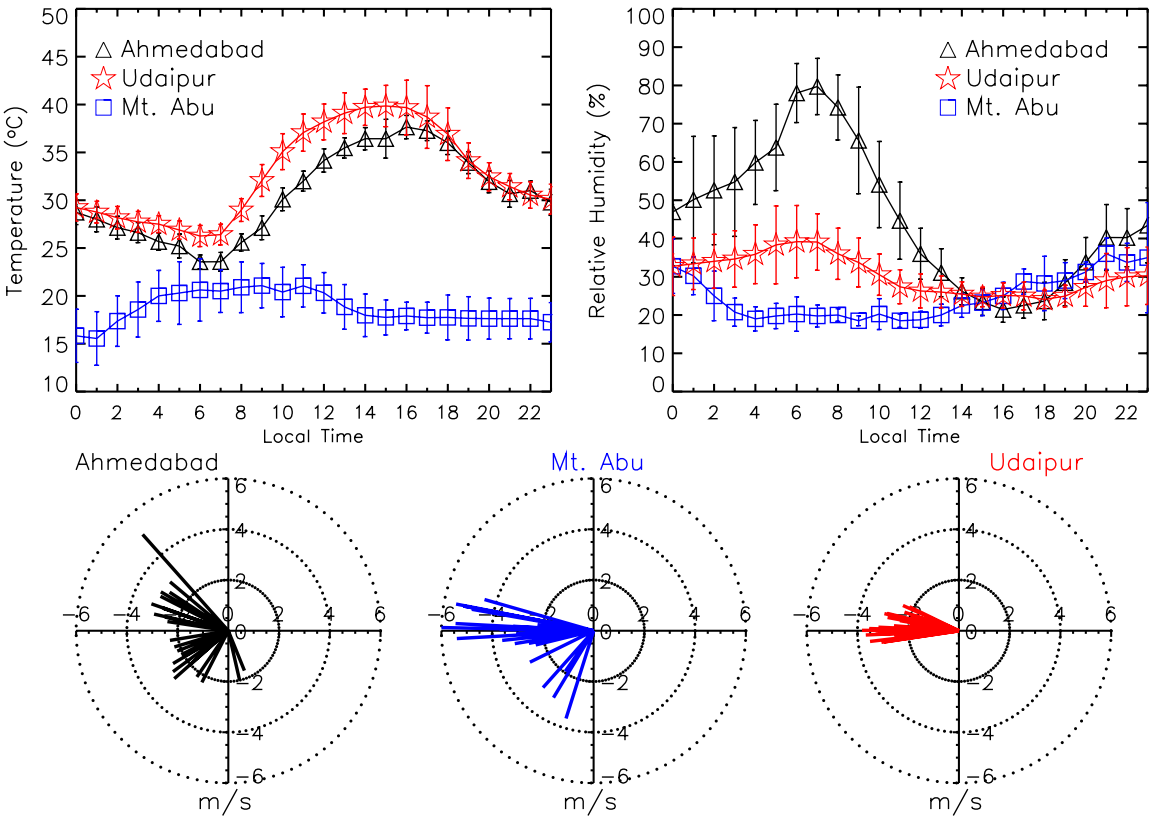

Figure 4.25: *Top panel shows the observed diurnal variation of temperature and RH at Ahmedabad, Mt. Abu and Udaipur during the study period. The bottom panels show the wind speed and direction for the same period at the three stations.*

a distance of ∼300 km. Compared to Ahmedabad, vehicular pollution is less at Udaipur due to less traffic, in spite of being a large tourist spot.

Fig. 4.24 shows the averaged wind pattern during April 2007 over western India. It shows that the wind was coming from west to the measurement sites during this period. The top panels of Fig. 4.25 show the diurnal variation of temperature and RH at Ahmedabad, Mt. Abu and Udaipur and the bottom panels show the wind speed and direction during the observation period at these stations. The daily averaged temperatures at these three stations are 30.6±4.5, 18.7±1.6 and 32.7±4.9°C, respectively. The daily variation of relative humidity is large at Ahmedabad with maximum RH of 80% at midnight and a minimum of 22% during 1000-1200 hours. At Mt. Abu and Udaipur, there is no significant diurnal variation in RH, however, the night time RH is higher than the daytime RH. The

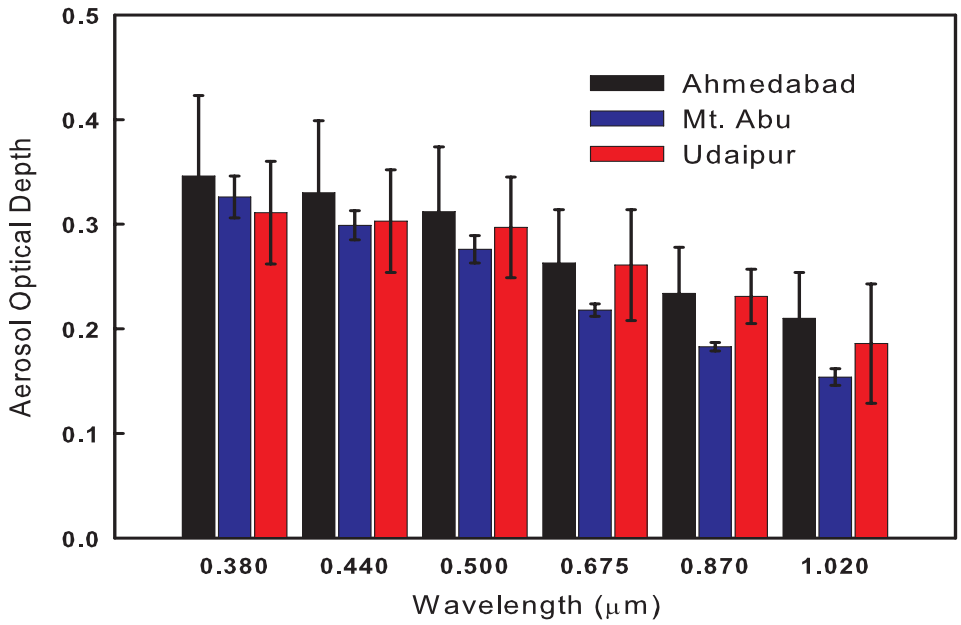

Figure 4.26: *The averaged AOD values are shown over Ahmedabad, Mt. Abu and Udaipur during April 2007.*

bottom panels of the figure show that the wind is westerly at all three stations with average speeds of 2.6±1.8, 3.6±1.6 and 2.7±0.6 m/s, respectively.

The same instruments have been used to take measurements at all the three stations to avoid any instrument bias. During first half of April 2007 the measurements have been carried out at Ahmedabad. The hill top measurements at Mt. Abu were conducted during 16^{th}-18^{th} April and during the last part of the month from 20^{th}-30^{th} April the measurements were carried out at Udaipur.

4.4.2 Aerosol Optical Depth

Columnar aerosol optical depth (AOD) spectra for the three different stations during April 2007 are shown in Fig. 4.26. The vertical bars are showing the $\pm 1\sigma$ variation of the mean AOD. Maximum AOD is observed over Ahmedabad during April. The lower wavelength AODs over Ahmedabad are consistently higher than that over Udaipur and Mount Abu. The lower wavelength AODs are largely

influenced by the submicron anthropogenic aerosols mainly coming into the atmosphere from the vehicular and industrial emissions and biomass burning. Over Ahmedabad AOD at 0.380 μm wavelength is 0.34$\pm$0.08. Over Udaipur and Mt. Abu, it is 0.31$\pm$0.05 and 0.32$\pm$0.02, respectively. The variation of mean AOD over Ahmedabad is very large due to uneven production of aerosols. The submicron particles production is high due to heavy anthropogenic activities in the morning, and in the afternoon hours it is low. However, as Udaipur and Mt. Abu are relatively less influenced by anthropogenic activities, the lower wavelength AODs are low and the variations about the mean are also small. Due to high wind speed and dry atmosphere large amount of soil born aerosols are lifted into the atmosphere and these aerosols mainly affect the larger wavelength AODs. Hence, over Ahmedabad and Udaipur, the higher wavelength AODs are comparable to each other within the variation. And Mt. Abu, being a hill top station, the AODs are minimum at both lower and higher wavelengths.

The Angstrom wavelength exponent (α), which gives basic information about the columnar particle size distribution, is different for different pair of wavelengths (*Reid et al.*, 1999). In the present study the α value calculated from the lower wavelength pairs (0.380-0.500 μm) gives information about the submicron particles and that calculated from higher wavelength pairs (0.500-1.020 μm) gives the information about micron size aerosols. Fig. 4.27 shows the α calculated for the wavelength regions, 0.380-0.500 μm, 0.500-1.020 μm and the entire wavelength (0.380-1.020 μm) for all the three stations. At the lower wavelengths $\alpha_{0.38/0.5}$ is maximum at Mt. Abu and minimum at Udaipur which implies that the smaller submicron particles are predominant at Mt. Abu while at Udaipur their abundance is low. For the soil particles α becomes near 0 (*Tanré et al.*, 1988; *Nakajima et al.*, 1989; *Tomasi et al.*, 1983). At Udaipur, $\alpha_{0.38/0.5}$ is very small, which implies that abundance of soil aerosols is high in the atmosphere. $\alpha_{0.5/1.02}$ at Ahmedabad and Udaipur are similar and the abundance of micron aerosols are comparable at these two stations. $\alpha_{0.38/1.02}$ also shows similar variation.

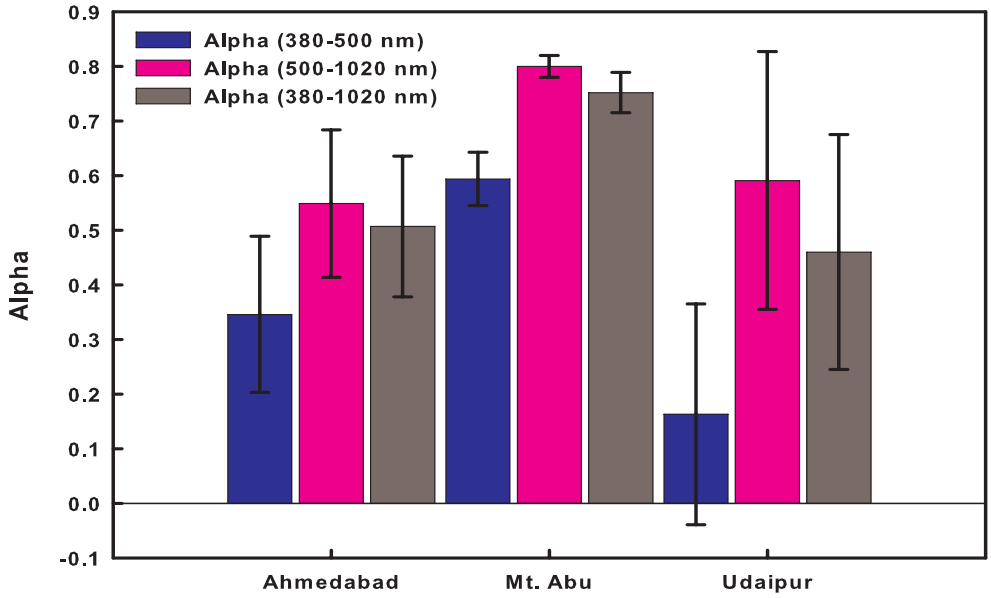

Figure 4.27: *Angstrom wavelength exponent for three wavelength pairs are shown for three stations.*

4.4.3 Surface Aerosol Mass Concentration

The average surface aerosol mass concentration (μg.m^{-3}) obtained at Ahmedabad, Mt. Abu and Udaipur using QCM are shown in Fig. 4.28. In general, uncertainty in the QCM measurements is caused due to variations in RH (*Jayaraman et al.*, 1998; *Ramachandran and Jayaraman*, 2002). In the present study, hourly measurements were taken from 0800-2400 local hours. The RH during the measurement period was mostly lower than 50% at all stations except during the midnight hours at Ahmedabad and its variations also was very less. Therefore, the effect of RH variability in aerosol mass especially the water soluble aerosol mass is very less. Mass concentration of 0.025 micron particles is maximum at Ahmedabad due to the large production of anthropogenic aerosols whereas the 12.5 micron particles' mass concentration is maximum at Udaipur due to the large abundance of soil particles. The average nucleation (size $\leq$0.1 μm) aerosol mass concentrations are 10.3, 2.5, 1.2 μg.m^{-3} at Ahmedabad, Udaipur and Mt. Abu, respectively. This anthropogenically produced submicron aerosol mass at Ahmedabad is 4 times larger than that

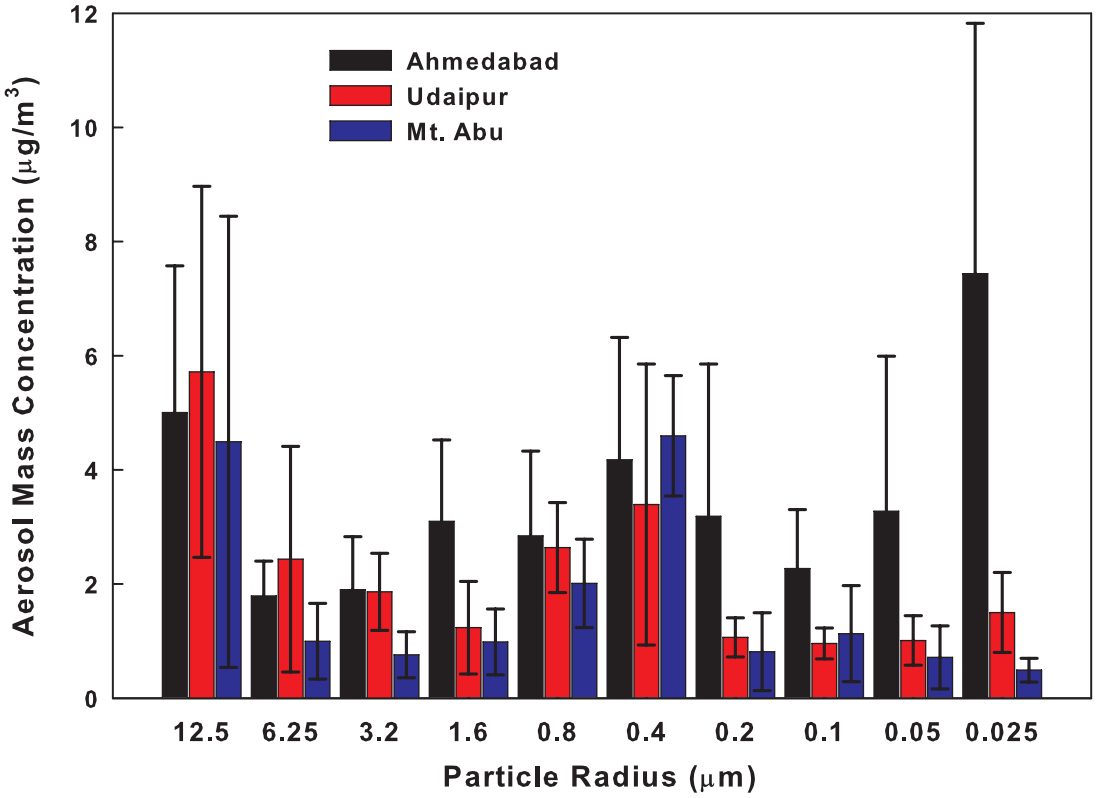

Figure 4.28: *Size resolved aerosol mass concentrations at Ahmedabad, Mt. Abu and Udaipur.*

at Udaipur and that of Udaipur is 2 times larger than that at Mt. Abu. The coarse mode ($\geq$1.0μm) aerosol mass concentrations are 11.2, 11.8 and 7.2 μg.m^{-3} for the three stations, respectively. These aerosols mostly consist of soil born dust particles. This shows that Udaipur has the maximum abundance of soil born aerosols which are mainly considered to be of natural origin. Ahmedabad also has high abundance of these aerosols whereas Mt. Abu has less abundance of soil aerosols.

4.4.4 Surface Aerosol Number Concentration

Aerosol number concentrations in different sizes are measured using aerosol particle spectrometer, Grimm. Aerosol number distribution at a particular location is mainly dependent on the particle formation and their removal mechanisms (*Jaenicke*, 1993). The presence of 'Thar' desert plays a major role in the aerosol particle size

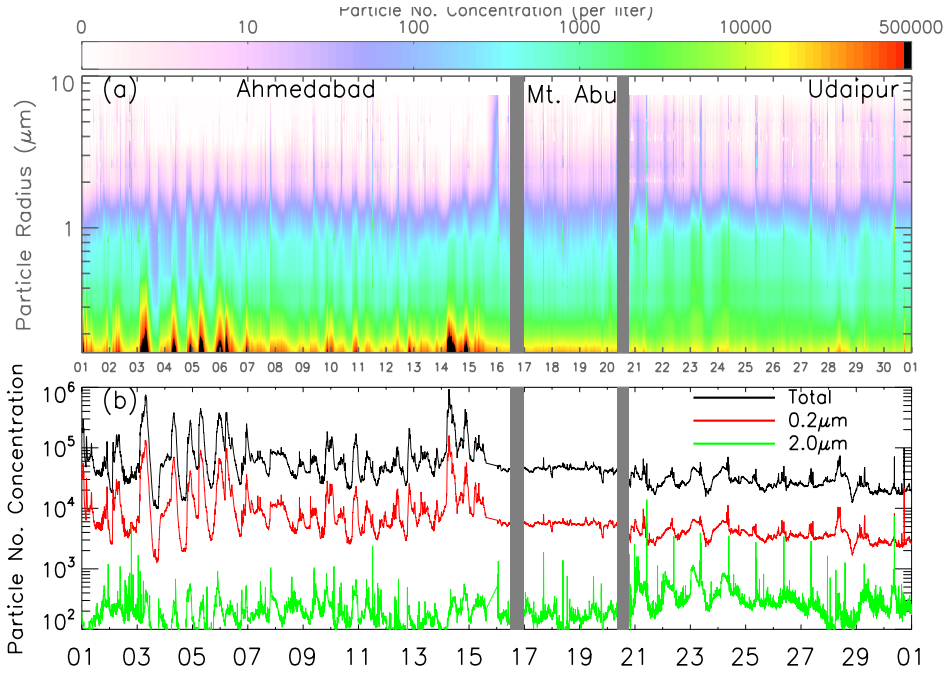

Figure 4.29: *(a) Variation of aerosol number concentration during the campaign period. The grey vertical bars show the transition period and differentiates the three stations. (b) Variation of total number concentration of all sizes particles, 0.2 micron and 2.0 micron radius particles.*

distributions at different locations in the western part of India. The time series of size resolved aerosol number concentration and the variation of number concentration of total, 0.2 and 2.0 micron radius particles are shown in Fig. 4.29(a). The number concentration observed at Ahmedabad is different from that observed at Mt. Abu and Udaipur. The variation of number concentration is maximum at Ahmedabad followed by Udaipur and minimum at Mt. Abu. The total number concentration is mainly dominated by the smaller particles. There is large variation in 0.2 micron aerosol number concentration with maximum during morning hours and minimum during afternoon hours at Ahmedabad (Fig. 4.29b). The major sources of smaller particles are vehicular and industrial emissions. At Ahmedabad due to large number of vehicles and industries smaller particles are dominating. During morning hours due to low wind speed and weak thermal convection smaller particles number concentration increase. As the day progresses temperature increases and local thermal convection also becomes strong. Thus, smaller

particles get more room to dilute and simultaneously large wind speed also helps to remove them from the measurement site during afternoon hours. In addition, strong wind helps to increase the bigger particles number concentration. At Mt. Abu 0.2 micron aerosol number concentration is almost same throughout the campaign period due to less variation of surface temperature. But 2.0 micron particles has a variation due to transportation of dust particles from desert region. At Udaipur 0.2 micron particles show less variation and small enhancement is observed during morning hours. 2.0 micron particles are dominating at Udaipur and have a strong diurnal variation. The coarse particles are highly abundant due to the large transportation of dust particles from adjacent desert regions.

4.4.5 Black Carbon Mass Concentration

The hourly averaged black carbon (BC) mass concentration at Ahmedabad, Mt. Abu and Udaipur are shown in Fig.4.30. At Ahmedabad, two peaks are observed in the diurnal variation of BC mass concentration during the observation period. The peaks are observed during 0700-0800 local hours in the morning and 2000-2100 hours in the evening at Ahmedabad. These peaks are mainly caused by the enhanced vehicular emission during the rush hours. The second minimum has occurred at 1500-1600 hours due to less vehicular activities, maximum boundary layer height and large wind speed. Less vehicular activities produce less BC and maximum boundary layer height gives more room for convection of the atmospheric BC and large wind speed advects out the BC concentration from the measurement site.

The hourly averaged BC concentration at Mt. Abu is also shown in Fig.4.30. No prominent peaks in the diurnal variation are observed at Mt. Abu. The averaged BC concentration here is 0.725 μg.m^{-3}. It is minimum during midnight with a concentration of 0.605 μg.m^{-3}. A maximum of 0.830 μg.m^{-3} is seen in the afternoon due to stronger convection which brings the BC from the foothill to the hill top and strong winds carry BC from surrounding polluted regions.

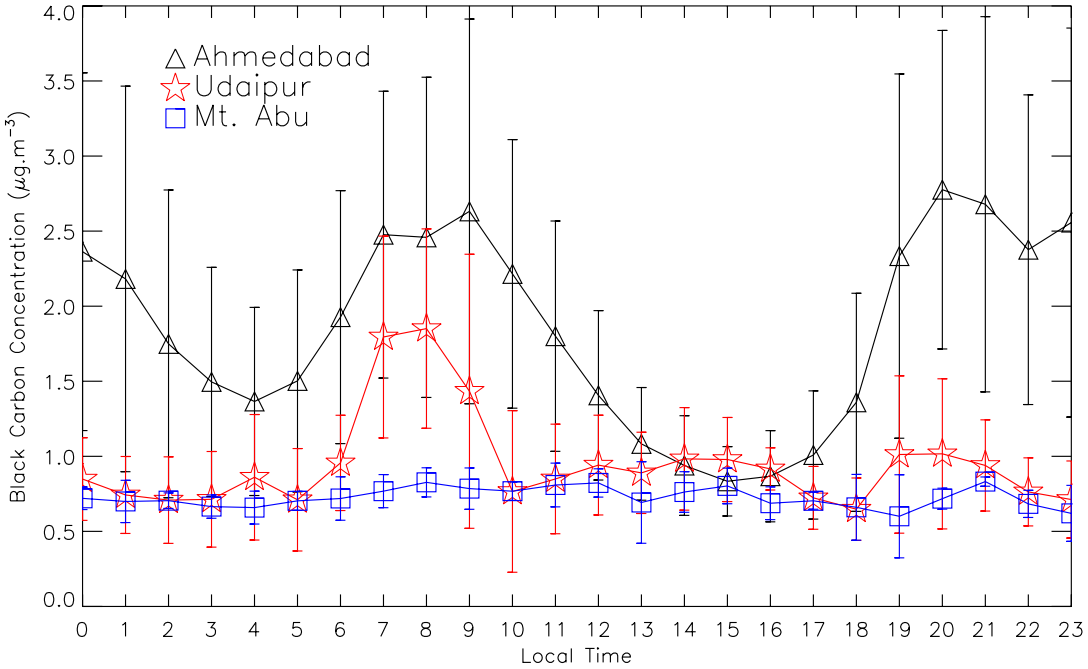

Figure 4.30: *Diurnal variation of BC mass concentration observed over Ahmedabad, Mt. Abu and Udaipur.*

In the diurnal variation of BC at Udaipur, in Fig. 4.30 a prominent morning peak is observed and the evening peak is not so strong as morning peak. The morning peak occurred due to the rush hour traffic where as during evening strong wind helps the removal of BC concentration from the measurement site. The wind is not so strong in the morning to reduce the morning peak intensity. During the late night hours the BC values go down to the background level which match quite well with the BC values of Mt. Abu. At 1500-1600 hours the BC concentrations are comparable to one another at all the three stations.

CHAPTER 5

Aerosol Radiative Forcing

The global climate system is balanced by interactions between its various subcomponents. The main processes that determine the overall equilibrium state of the climate system are heating by the incoming solar shortwave radiation and cooling by the outgoing longwave (infrared) terrestrial radiation. Any process that can disturb the energy balance can cause climate change. A process that alters the radiation balance of the climate system is known as radiative forcing (*Coakley et al.*, 1983; *Coakley and Cess*, 1985; *Ramanathan et al.*, 1989; *Charlson et al.*, 1991; *Bates*, 1999). Radiative forcing can be external or internal. External forcing operates from outside the Earth's climate system and includes orbital variations and changes in incident solar flux at the top of the atmosphere. Internal forcing is caused due to changes in atmospheric compositions and the best examples are the Greenhouse gases and aerosols in the atmosphere (*Haywood and Ramaswamy*, 1998; *Myhre et al.*, 1998; *Haywood et al.*, 2003). While Greenhouse gases are known to decrease the outgoing long wave radiation and contribute to global warming (positive forcing), aerosols can either increase or decrease the outgoing solar radiation by scattering

or absorption (direct effect) (*Jayaraman et al.*, 1998) or by changing the microphysical properties of the clouds (indirect effect) (*Lohmann and Feichter*, 2005).

The change in radiative fluxes due to aerosols is mainly by scattering and absorbtion of the incoming shortwave solar radiation and outgoing longwave terrestrial radiation. The interaction depends on the physical, optical and chemical properties of aerosols. Aerosols have different properties according to their natural and anthropogenic origin. Besides, the abundance of natural aerosols on the global scale is several times greater than that of the major anthropogenic aerosols. For example, sea-salt radiative forcing is in the range of -0.6 to -2 Wm^{-2} at low wind speeds and at higher wind speeds this can be as high as -1.5 to -4 Wm^{-2} (*Winter and Chylek*, 1997), whereas the change (between now and the early 20th century) in the reflected solar flux (the direct effect) due to anthropogenic sulfate averaged over the northern hemisphere is estimated as -1.1 Wm^{-2} (*Charlson et al.*, 1991). On the global scale, anthropogenic sources contribute a small fraction of 10-15% of aerosol to the total production from various sources (*Kiehl and Rodhe*, 1995; *Andreae*, 1995). But on a regional scale, it may be much greater than the global average due to large production rate and short residence time. Aerosols, with varying optical properties are non-uniformly distributed around the globe, and their radiative forcing also varies accordingly.

5.1 Models for Radiative Forcing Calculation

5.1.1 Optical Properties of Aerosols and Clouds

To compute the regional aerosol radiative forcing the spectra of Aerosol Optical Depth (AOD), Single Scattering Albedo (SSA) and asymmetry parameter are required for that particular location. The OPAC (Optical Properties of Aerosols and Clouds by *Hess et al.* (1998)) model is used to infer indirectly the chemical compositions of aerosols and derive these parameters, due to the unavailability of chemical data of the various aerosol components. OPAC mainly has 10 aerosol components

which are insolubles (mostly soil particles), water soluble aerosols (mainly sulfate and nitrate aerosols of anthropogenic origin), soot (of anthropogenic origin), sea salts (naturally produced on the oceanic surface by wind and also available in the atmosphere of coastal regions) in accumulation and coarse mode, mineral dust (generally coming into atmosphere from the arid surface by wind) in three modes, mineral-transported and sulfate droplets (mainly found at stratospheric altitude). This model is used to derive the AOD spectrum using a combination of these aerosol components and in the present study the sulfate droplets are not considered. OPAC model is useful to derive different microphysical and optical properties for suitable mixture of aerosol components at the measurement site to best fit the observed aerosol optical depth. Some of the aerosol components which are hygroscopic in nature, may change their optical properties, and hence OPAC outputs are available for eight different relative humidity (0%, 50%, 70%, 80%, 90%, 95%, 98% and 99%) conditions.

Optical properties for different aerosols are different. SSA, one of the important parameters for radiative forcing calculation, determines the sign of radiative forcing . Fig. 5.1 shows the computed SSA for different aerosol species using the data from OPAC. Water soluble (sulfate, nitrate, etc.) and seasalt do not absorb significantly in the visible range (SSA ≥ 0.9 at 0.5 μm) but they absorb significantly in the infrared region (SSA ≤ 0.4 at 10.0 μm). Major aerosol components are scattering type in the shortwave range (0.25-4.0 μm) whereas in the longwave range (4.0-40.0 μm) they can be totally absorbing such as soot. The SSA of soot in the shortwave is ~ 0.22 (at 0.5μm), whereas in the longwave range it is totally absorbing. Dust is mainly scattering in nature in the shortwave range and in the longwave range it exhibits significant absorbtion. On one hand in the longwave range absorbtion decreases the outgoing radiation while on the other hand the energy re-emitted consequent to this absorbtion increases the surface reaching infrared radiation. The net SSA over a particular location is weighted average of the SSA of all the aerosol components.

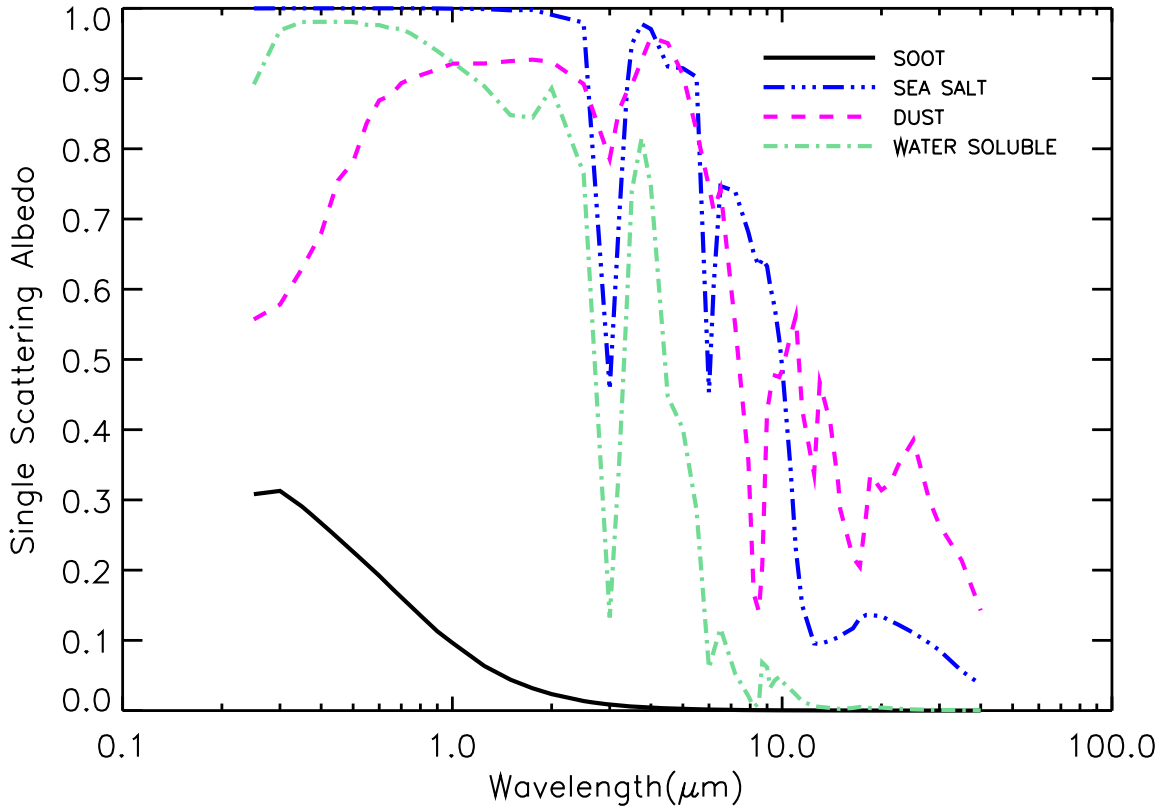

Figure 5.1: *Typical spectra of single scattering albedo for four major aerosol components obtained from OPAC. Dust and seasalt are natural aerosols and water soluble and soot are mainly anthropogenic aerosols.*

5.1.2 Santa Barbara Discrete Ordinate Radiative Transfer

Aerosol radiative forcing (ARF) is computed using Santa Barbara DISORT Atmospheric Radiative Transfer (SBDART) (*Ricchiazzi et al.*, 1998) code, a well established code for estimation of radiation flux in the shortwave (0.25-4.0 μm) as well as longwave (4.0-40.0 μm) range. SBDART is a radiative transfer code that computes plane-parallel radiative transfer in clear and cloudy conditions within the earth's atmosphere and at the surface. In the present study only clear sky conditions are considered. All the important processes that affect the ultraviolet, visible, and infrared radiation, are included in this code. For molecular absorption SBDART uses the low-resolution band models of LOWTRAN-7 atmospheric transmission code (*Pierluissi and Peng*, 1985). LOWTRAN-7 codes can take into account

the effects of all radiatively active molecular species found in the earth's atmosphere with wavelength resolution of about 5 nm in the visible and about 200 nm in the thermal infrared. In SBDART, the radiative transfer equations are numerically integrated with DISORT (Discreet Ordinate Radiative Transfer) code (*Stamnes et al.*, 1988). This discrete ordinate method provides a numerically stable algorithm to solve the equations of plane-parallel radiative transfer in a vertically inhomogeneous atmosphere. The intensity of both scattered and thermally emitted radiation can be computed at different heights and directions. Presently, SBDART is configured to allow up to 50 atmospheric layers and 20 radiation streams (20 zenith angles and 20 azimuthal modes).

The ground surface cover is an important determinant of the overall radiation environment because spectral albedo of the surface which defines the ratio of upwelling to downwelling spectral irradiance at the surface, determines upwelling irradiance from the surface. In SBDART there are five basic surface types, namely (1) ocean water (*Tanre et al.*, 1990), (2) lake water (*Kondratyev*, 1969), (3) vegetation (*Reeves et al.*, 1975), (4) snow (*Wiscombe and Warren*, 1980) and (5) sand (*Staetter and Schroeder*, 1978). The spectral albedo describing a given surface is often well approximated by combinations of these basic surface types. Input parameters in SBDART allow the user to specify a mixed surface consisting of weighted combinations of water, snow, vegetation and sand. SBDART can compute the radiative effects of several lower and upper atmosphere aerosol types. In the lower atmosphere, typical rural, urban, or maritime conditions can be simulated using the standard aerosol models of *Shettle and Fenn* (1975). SBDART gives the opportunity to calculate radiative effects up to five aerosol layers specified (i.e., at five different altitudes) that model fresh or aged volcanic, meteoric, and upper-tropospheric background aerosols. Fig. 5.2 shows the solar irradiance at top of atmosphere and at the surface.

The major inputs required to estimate the aerosol radiative forcing for DISORT module in SBDART include spectral values of solar radiation incident on the atmosphere, spectral values of columnar AOD, SSA and angular phase function of the

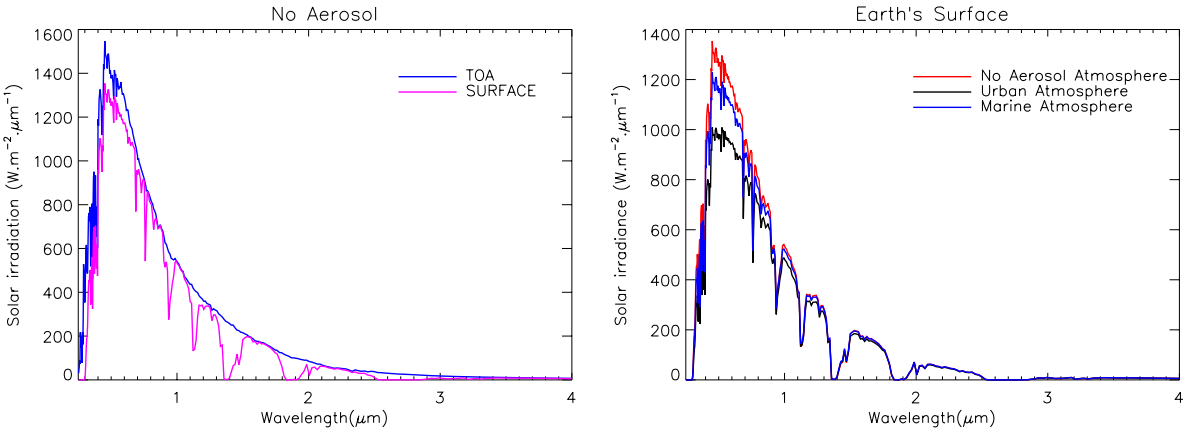

Figure 5.2: *Solar irradiance ($Wm^{-2}.\mu m^{-1}$) computed at 0° solar zenith angle at top of atmosphere (TOA) and Earth's surface for no aerosol condition (left) and at Earth's surface for different atmospheric conditions (right) obtained from SBDART code.*

scattered radiation or asymmetry factor (g). The asymmetry factor is used to generate a scattering phase function through the Henyey-Greenstein approximation. The Henyey-Greenstein parameterization provides good accuracy when applied to radiative flux calculations (*van de Hulst*, 1968; *Hansen*, 1969). Spectral values of AOD, SSA and asymmetry parameter are obtained from OPAC. OPAC model derived aerosol optical parameters are obtained by varying the number concentration of individual components in small steps until all the following criteria are satisfied. (1) Sum of root mean square difference between the model estimated and the observed AOD values at all the six wavelength channels is minimum (for the present study, we have constrained this sum to within 0.1 AOD). (2) Angstrom parameters for the observed and the model estimated AOD spectra are comparable. (3) Total mass concentration for the model estimated aerosol mixture are comparable with aerosol mass concentrations measured using QCM (Quartz Crystal Microbalance) cascade impactor from stage 2 to stage 10 (4) Black carbon (BC) mass used in the model is comparable to the measured value using Aethalometer. (5) Mass fraction of BC in the total aerosol mass are also constrained close to their actual values derived from simultaneous and co-located measurements using Aethalometer and QCM impactor. (6) Model derived values of SSA at 0.5 μm closely matches with the SSA at 0.525 μm estimated using simultaneous measurements of absorption

and scattering coefficient of aerosols.

5.2 Radiative Forcing for Different Environmental Conditions

5.2.1 Radiative Forcing in Urban Environment

In this study, aerosol radiative forcing is calculated over Ahmedabad, an urban region in the western part of India using Santa Barbara DISORT Atmospheric Radiative Transfer (SBDART) code (*Ricchiazzi et al.*, 1998) in the Short Wave (SW) region (0.25-4.0 μm). Radiative forcing calculations are performed only for clear sky days. The spectral values of SSA, assymetry parameter etc. required for the SBDART are obtained from OPAC by best fitting of model obtained AOD spectral values and measured AOD values at six wavelength channels (0.38, 0.44, 0.5, 0.675, 0.87 and 1.02 mm) using Microtops Sunphotometer, as discussed earlier. The measured values from Microtops are used for the columnar water vapor for individual days and ozone concentration data is obtained from TOMS (Total Ozone Mapping Spectrometer) satellite. One of the important parameters which can introduce large errors in radiative forcing calculation over land regions like Ahmedabad is the surface albedo of the location (*Wielicki et al.*, 2005). In the present study, MODIS (Moderate Resolution Imaging Spectroradiometer) derived surface reflectance data is used over Ahmedabad to estimate radiative forcing calculation. For this the surface reflectance data is obtained from Nadir BRDF-Adjusted Reflectance 16-Day L3 Global 0.5 km SIN Grid product which is derived at the mean solar zenith angle of Terra overpasses for every successive 16-day period, calculating surface reflectance as if every pixel in the grid are viewed from nadir direction. Surface reflectance data available in seven wavelength bands of MODIS centered around 0.47, 0.56, 0.65, 0.86, 1.24, 1.64 and 2.13 μm are used to reproduce the spectral dependence of surface albedo for the entire SW range using a combination of three

different surface types, namely, vegetation, sand and water. The monthly variation of surface reflectance data available at seven wavelength bands during 2007 is shown in Fig. 5.3. Vertical lines in this figure represents $\pm 1\ \sigma$ variation about the monthly mean value of surface reflectance measured. On an average surface reflectance values are found to be high during premonsoon (Apr-May) and low during postmonsoon (Sep-Nov) and winter (Dec-Feb). Another very important

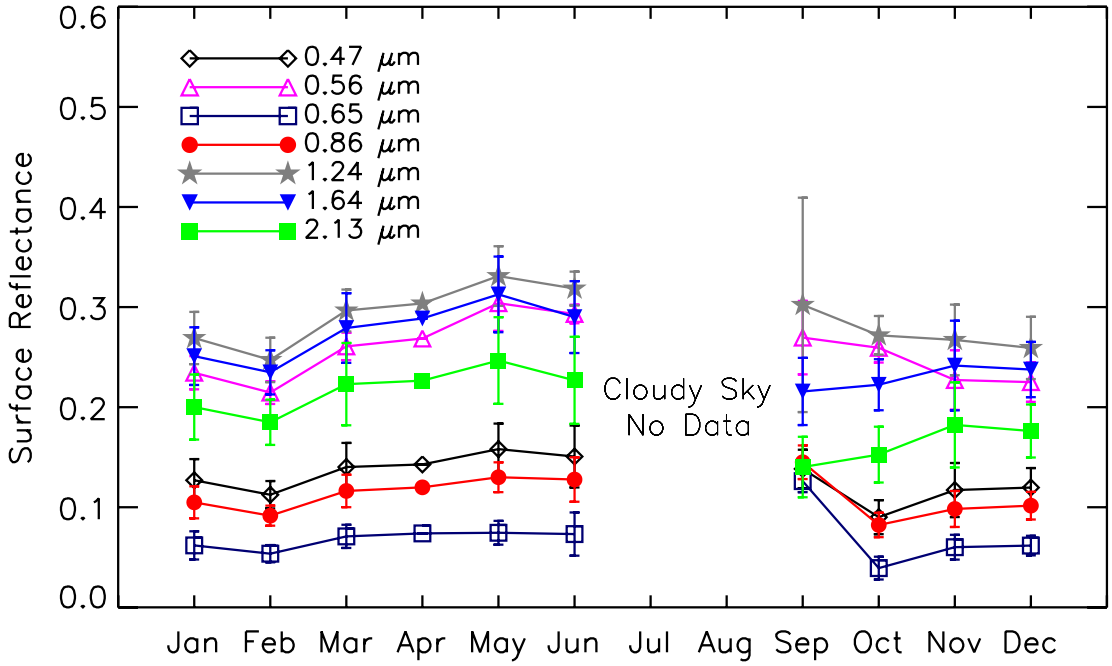

Figure 5.3: *Monthly variation of surface reflectance obtained from MODIS satellite at different wavelengths over Ahmedabad.*

aerosol parameter required for radiative transfer calculations, is the vertical profile of aerosols in the atmosphere. The major uncertainties introduced in the estimation of radiative forcing calculation are due to the uncertainty in the vertical distribution of aerosols and the single scattering albedo (*Haywood and Ramaswamy*, 1998; *Chung et al.*, 2005). Fig. 5.4 shows the seasonal variation of SSA at ahmedabad obtained from OPAC model. During monsoon SSA is maximum at 0.86 ± 0.04 whereas during postmonsoon SSA is minimum at 0.80 ± 0.09.

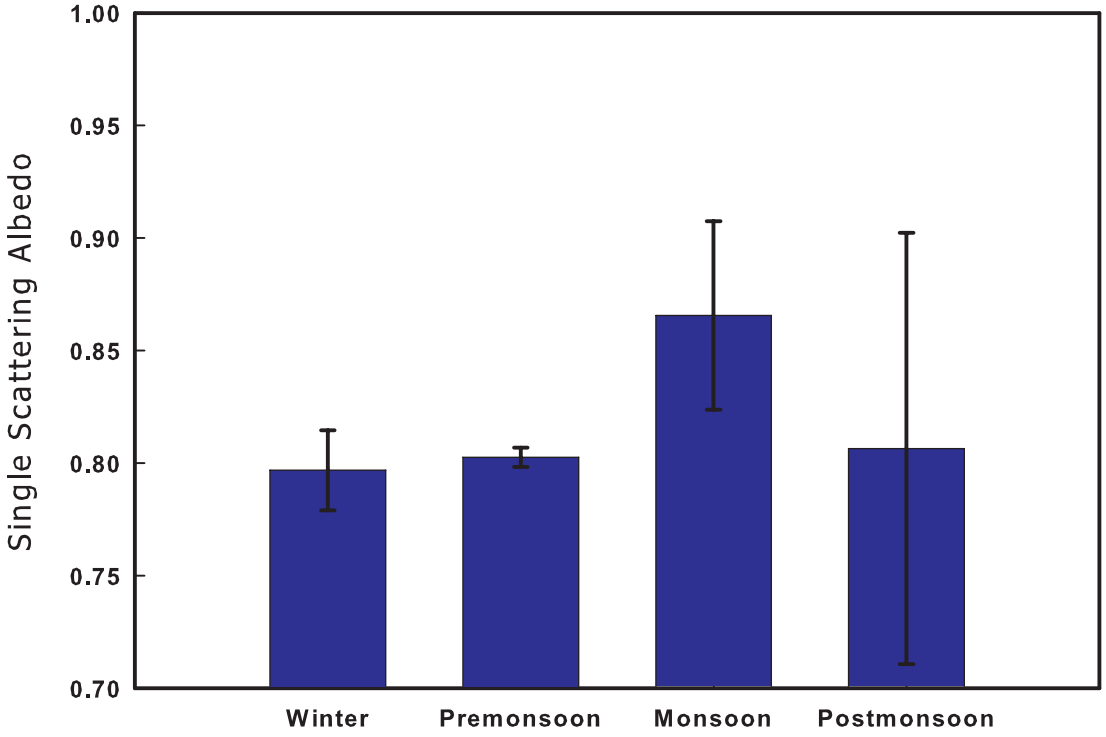

Figure 5.4: *Seasonal variation of Single Scattering Albedo at Ahmedabad obtained from OPAC model.*

The different kind of aerosols (scattering or absorbing) present at different altitude can cause cooling or heating in the atmospheric layer and influence the temperature profile. This can even further change the precipitation pattern in the tropical regions which is mainly caused by the convection processes in the atmosphere over those regions (*Chung and Zhang*, 2004). For the present radiative transfer calculations aerosol extinction profiles obtained from Micro Pulse Lidar measurements which are normalized for the AOD value at the MPL wavelength (0.523 μm) have been used. Fig. 5.5 shows the monthly variation of aerosol profile obtained from Micro Pulse Lidar over Ahmedabad during 2002-2004.

The aerosol radiative forcing estimation on clear sky days is obtained by running the radiative transfer model for the calculated radiant fluxes with and without

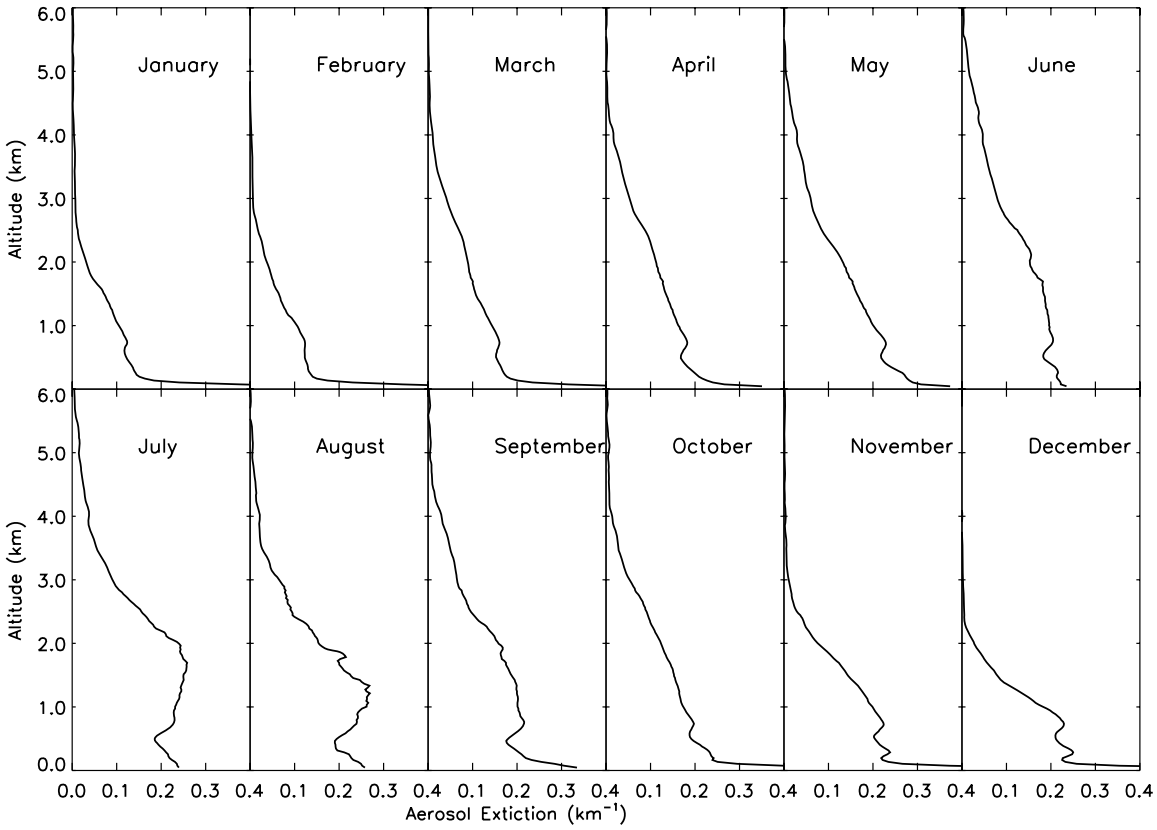

Figure 5.5: *Monthly variation of aerosol profile obtained from LIDAR observations over Ahmedabad. The data is taken from* ***Gadhavi (2005)*** *and Ganguly et al. (2006a).*

aerosol conditions in the atmosphere at every hour of the day over the entire SW region. Fig. 5.6 shows the seasonal variation of the averaged values of entire SW region of aerosol direct radiative forcing at TOA, surface and in the atmosphere over Ahmedabad for two years 2006 and 2007. Vertical lines on top of each bar represents $\pm 1\ \sigma$ variation about the mean value of radiative forcing for a particular season. The important results found from this study are as follows. During winter both the radiative forcing at surface and TOA are negative while during premonsoon surface forcing is negative and TOA forcing is positive. During monsoon and postmonsoon TOA forcing changes its sign from positive to negative. The radiative forcing values at surface level during premonsoon and postmonsoon are very similar and are -46.0$\pm$3.6 Wm^{-2} and -41.0$\pm$11.6 Wm^{-2}, respectively. During postmonsoon there is large variation about the mean. During monsoon surface

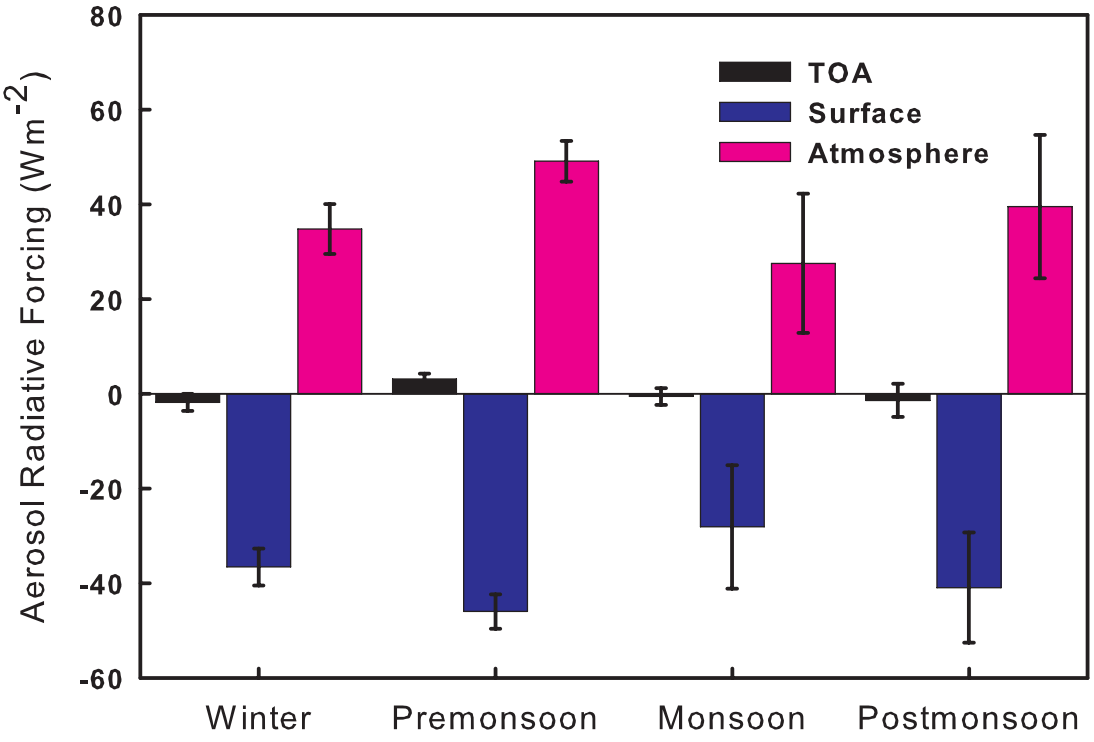

Figure 5.6: *Seasonal variation of aerosol radiative forcing over Ahmedabad at TOA, surface and in the atmosphere.*

radiative forcing is minimum at -28.1±13.3 Wm^{-2} and during winter the value is slightly higher at -36.6±3.9 Wm^{-2}. In case of TOA, aerosol radiative forcings are found at -1.8±1.8 Wm^{-2} during winter, 3.1±1.1 Wm^{-2} during premonsoon, -0.5±1.8 Wm^{-2} during monsoon and -1.4±3.5 Wm^{-2} during postmonsoon. The atmospheric aerosol radiative forcing is the difference between the TOA and surface radiative forcing. The atmospheric aerosol radiative forcing represents the amount of energy trapped in the atmosphere by aerosols and is a measure of the atmospheric heating (*Ramanathan et al.*, 2001a). This forcing generally increases as the TOA forcing becomes positive and decreases as TOA forcing becomes negative. During the study period, the atmospheric forcings are 33.8±5.3 Wm^{-2},

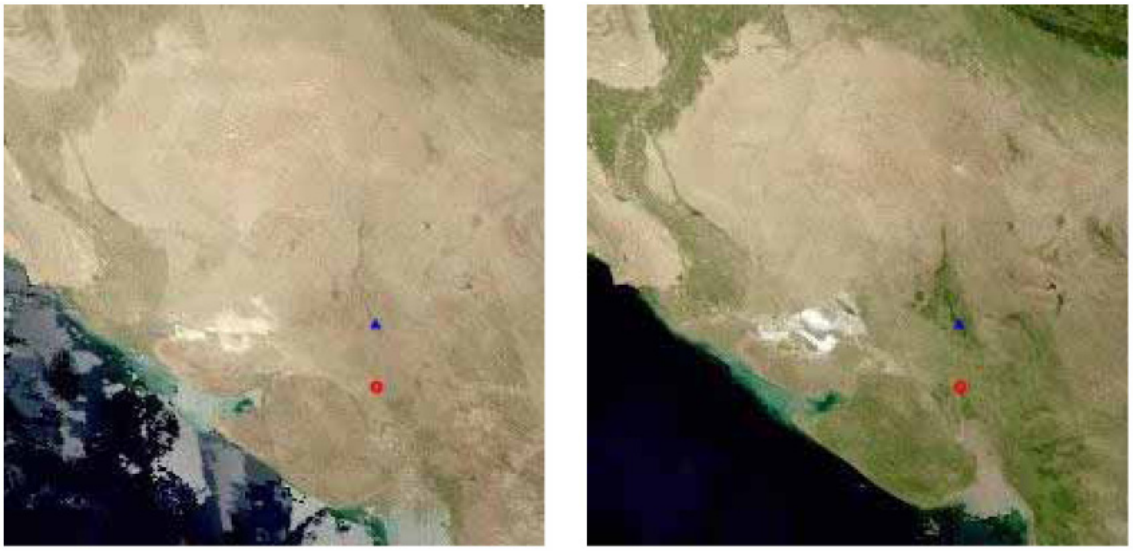

Figure 5.7: *surface reflectance of western part of India observed by the MODIS satellite during April and October. Red is marked over Ahmedabad and blue is marked over Mt. Abu.*

49.1±4.3 Wm^{-2}, 27.5±14.7 Wm^{-2} and 39.5±15.1 Wm^{-2} during winter, premonsoon, monsoon and postmonsoon, respectively. The aerosol radiative forcing over a location is highly influenced by several parameters like total aerosol load in the atmosphere, their vertical and size distribution, single scattering albedo, scattering phase function, reflectance of the Earth's surface, solar insolation, meteorological parameters mainly wind, temperature and relative humidity (*Haywood and Boucher*, 2000). The surface reflectance mainly changes by the area covered by vegetation. In Fig. 5.7 shows the surface reflectance of western part of India observed by the MODIS satellite during April and October, which has a large influence on the TOA radiative forcing. In this case, during premonsoon and monsoon forcings affect the regional dynamical systems such as wind, thermal convection and also the precipitation patterns (*Menon et al.*, 2002). Therefore, Earth-Atmospheric system can be perturbed on a large scale for this kind of regional cooling at the surface and warming of the lower troposphere. Normally the radiation flux reaching the surface is balanced by the evaporation (latent heat flux) and sensible heat flux from the surface. From the observations over the Indian Ocean region it is seen that there is greater probability of solar flux reduction at surface being balanced by

reduction in evaporation and therefore, this reduction of evaporation slows down the hydrological cycle (*Ramanathan et al.*, 2001b,a).

Large seasonal variation of the aerosol properties is observed in the present study and hence in the aerosol radiative forcings. Radiative forcing is useful for better understanding of how the various aerosol components in the atmosphere over a region can perturb the Earth-Atmospheric system. At Ahmedabad, during winter, the aerosols are mainly concentrated in the low level atmosphere and the BC mass concentration is significantly high at 3.3 μg.m^{-3}. So the surface solar reduction is high due to these absorbing BC aerosols. Similarly, radiative forcing is also negative at TOA. Therefore, energy is trapped significantly in the atmosphere. During premonsoon, aerosols are distributed in the higher altitudes also because the boundary layer height increases and BC mass concentration also reduced to 2.5 μg.m^{-3}. In addition, the abundance of dust aerosols is enhanced. This dust aerosols are mainly scattering particles and hence the forcing becomes positive at the TOA and large energy is trapped into the atmosphere. The atmospheric heating by absorbing aerosols can evaporate some of the low-level clouds, resulting in a decrease of cloud cover and planetary albedo (*Ackerman et al.*, 2000). This kind of cloud burnings can influence the cloud coverage and hence the precipitation amount over the Indian region where the maximum annual rainfall is received during monsoon season. In another work related to climate effects of BC aerosols over China and India *Menon et al.* (2002) have shown that large amounts of BC (soot) particles and other pollutants are responsible for causing the observed changes in precipitation patterns and temperature trends over China in particular. During 2006 and 2007 the rainfall during monsoon over Ahmedabad is relatively higher in comparison to previous years. During monsoon due to heavy rain aerosols are washed out and reduces the forcing value at surface. However, during the end of monsoon and the beginning of postmonsoon a stable aerosol layer is observed in the the vertical aerosol distribution (*Ganguly et al.*, 2006a) and therefore large amount of solar flux is reflected by this layer and the TOA atmosphere forcing becomes positive. In addition to that, during postmonsoon, BC mass concentration

is maximum at 5.7 μg.m^{-3} and these BC aerosols absorb large amount of solar radiation and further reduce the radiation at the surface. Therefore, a combination of all these effects results in large amount of energy being trapped in the atmosphere.

5.2.2 Radiative Forcing in Hilltop Environment

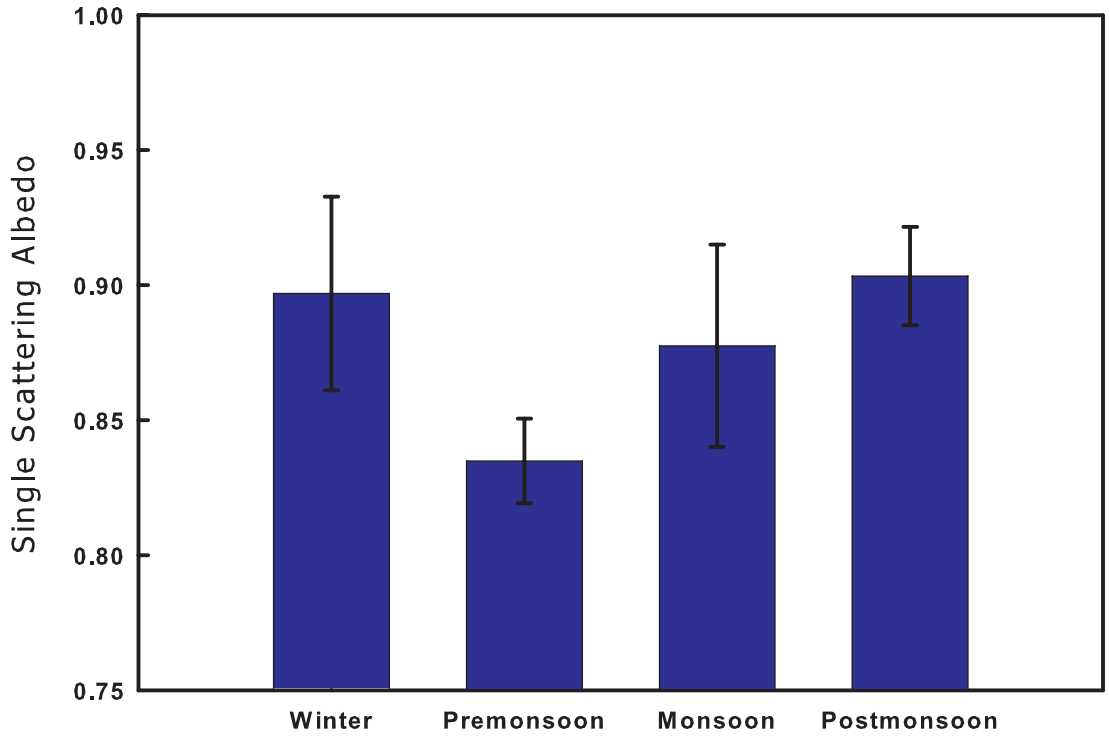

Figure 5.8: *Seasonal variation of Single Scattering Albedo at Mt. Abu computed using the OPAC model.*

Radiative forcing is calculated over Mt. Abu using the same procedure of that at Ahmedabad (Sec. 5.2.1). Fig. 5.8 shows the seasonal variation of SSA at Mt. Abu obtained from OPAC model. It shows a large value of 0.90$\pm$0.03 and 0.90$\pm$0.02 during winter and postmonsoon, respectively, due to less abundance of absorbing aerosols and a minimum of 0.83$\pm$0.01 during postmonsoon due to enhancement of anthropogenic activities.

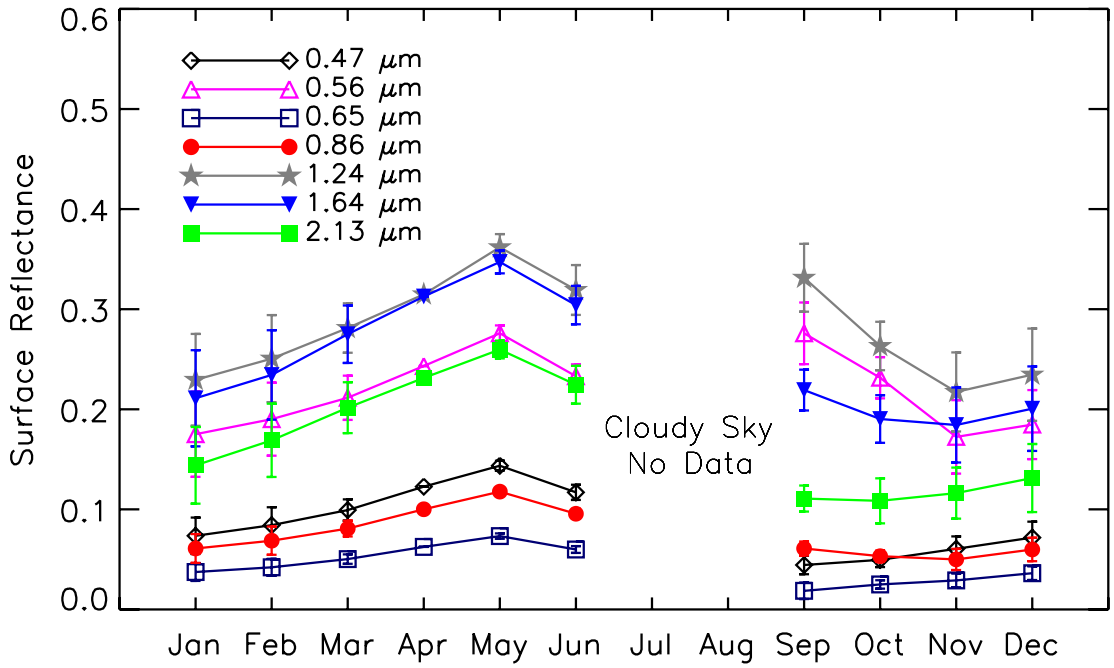

Figure 5.9: *Monthly variation of surface reflectance obtained from MODIS satellite at different wavelengths over Mt. Abu.*

Among the other inputs, ozone and water vapor values are used from the TOMS data and Microtops measurements, respectively. Another important parameter that can introduce large error in the TOA radiative forcing over land is surface reflectance. In the present study, 8-days MODIS derived Level 3 surface reflectance data with the grid of 0.5 km for seven wavelengths centered at 0.47, 0.56, 0.65, 0.86, 1.24, 1.64 and 2.13 μm have been used. Fig. 5.9 shows the monthly variation of surface reflectance values. The spectral surface reflectance values of Mt. Abu are considered as the combination of three different surfaces, *viz.*, water, sand and vegetation, and are used as input to the SBDART code for Mt. Abu radiative forcing calculation. In comparison with Ahmedabad, as shown in Fig. 5.10 Mt. Abu has higher surface reflectance values during premonsoon (Apr-May) while lower values during postmonsoon (Sep-Dec). This implies that during premonsoon, Mt. Abu has less vegetation and bare sandy surface enhances the surface reflectivity while during postmonsoon the surface is totally covered by vegetation which reduces surface reflectivity at 1.64 μm wavelength. In comparison to

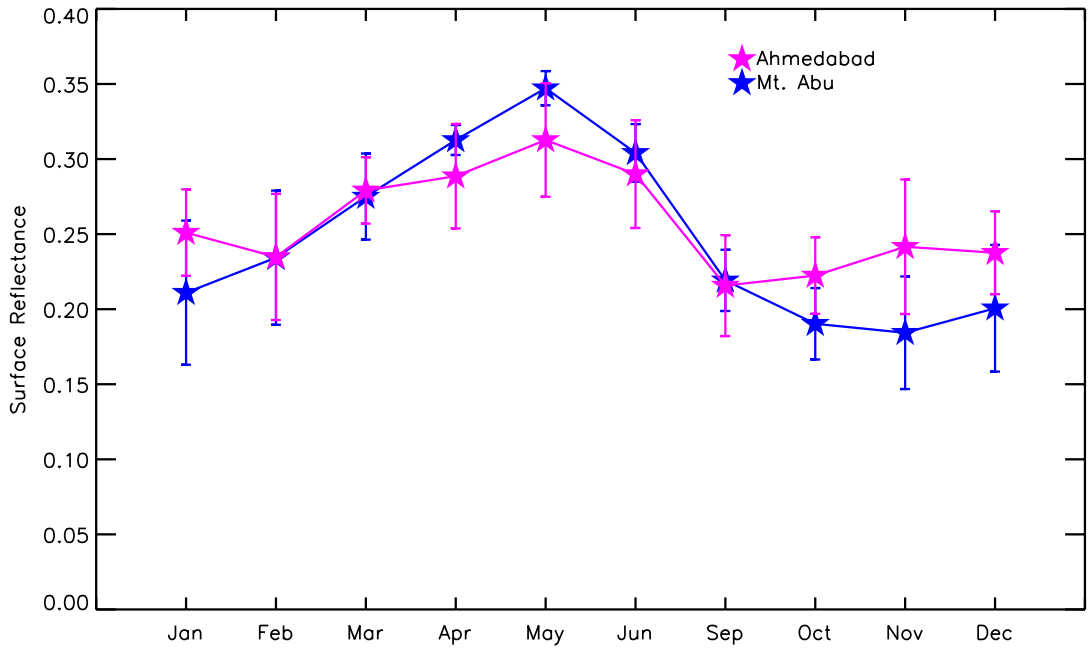

Figure 5.10: *The comparison of the monthly surface reflectance variation obtained from MODIS satellite at 1.64 µm over Mt. Abu and Ahmedabad.*

Ahmedabad the vegetation covered by the surface is more uniform and therefore, the reflectivity is higher at Mt. Abu.

Fig. 5.11 shows the seasonal variation of SW aerosol radiative forcing at the surface and TOA. The variation of surface forcing is very similar to variation of AOD. At the surface large variation of forcing has been found in the range -23.4 to -8.8 Wm^{-2} while at TOA forcing varied from -3.2 to +0.2 Wm^{-2}. During winter the estimated forcing is minimum at -8.8 Wm^{-2} at the surface and -2.7 Wm^{-2} at TOA. During premonsoon radiative forcing becomes maximum at -23.4 Wm^{-2} while at TOA forcing changes its sign and becomes +0.2 Wm^{-2}. After winter the forcing gradually decreases at surface and becomes negative at TOA. One of the main reason for the surface radiative forcing variation is due to the boundary layer height variation at hill top region. During winter the boundary layer height becomes less than the station's altitude and as a result the observatory region becomes clearer and therefore at the surface the solar radiation reduction has been reduced due

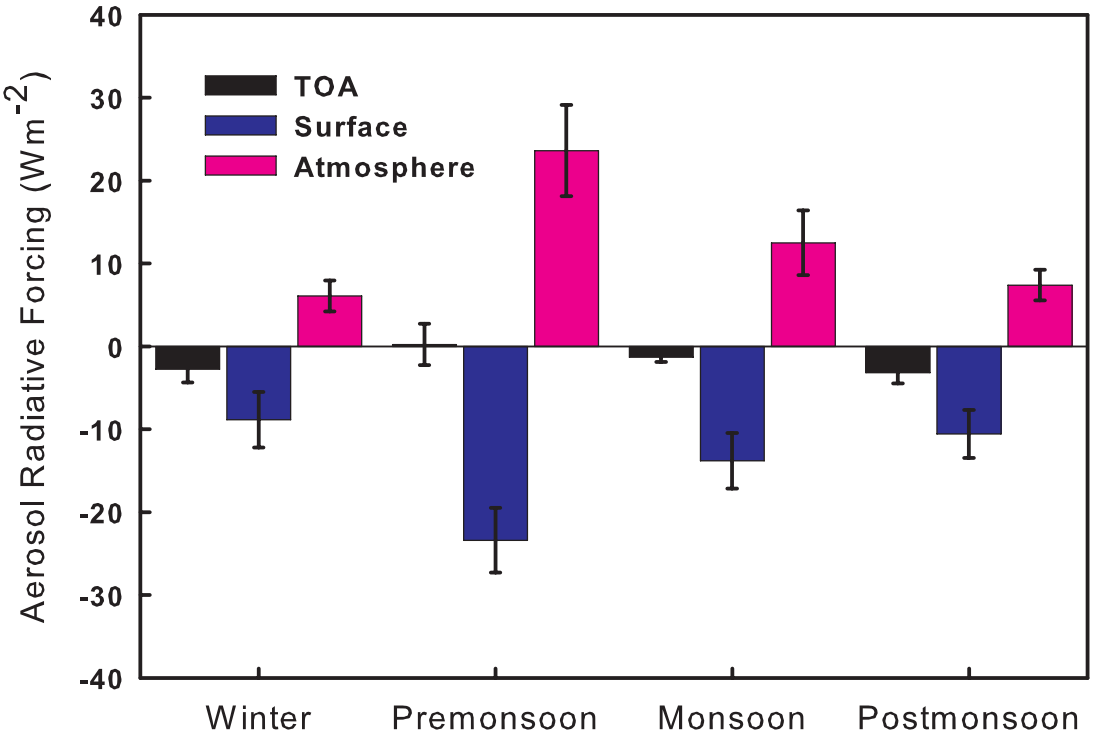

Figure 5.11: *Seasonal variation of aerosol radiative forcing over Mt. Abu at TOA, surface and in the atmosphere.*

to less aerosol present in the atmosphere. But surface forcing becomes more negative as the boundary layer height gradually increases and aerosols increases at the observation site. During April the surface forcing was enhanced by a factor of four not only due to the enhancement of boundary layer height but also due to an increase of anthropogenic activities by local tourists. The BC measurements also show an enhancement during April and these absorbing anthropogenic BC cause large reduction of solar radiation at the surface. During the rest of the season surface radiative forcing reduces. The absorbtion of BC reduces during that period due to transportation of the BC aerosols by strong wind. In addition enhancement of boundary layer height results in a larger room to dilute the BC concentration. Therefore, the reduction of solar radiation by the absorbing BC particles decreases

and hence surface forcing reduces. On the other hand, during premonsoon season dust storms occur frequently in the desert areas and due to these dust storms there is a large transportation of dust particles to the hill top region. This transported dust aerosol scatter more solar radiation and result in positive forcing at TOA. And during monsoon forcing reduces as heavy rainfall washes out the dust aerosols from the atmosphere. During monsoon there is also large transportation of seasalt aerosols from Arabian sea (*Rastogi and Sarin*, 2005a). These aerosols enhance the total aerosol burden in the atmosphere and forcing becomes -13.8$\pm$3.3 Wm^{-2} at surface. During postmonsoon the transportation of seasalt gradually decreases. Therefore, at TOA scattered solar radiation by aerosols reduces and TOA forcing becomes more negative at -3.2$\pm$1.2 Wm^{-2}. This also increases the surface reaching solar radiation and reduces the surfaces forcing at -10.6$\pm$2.9 Wm^{-2}. During winter the boundary layer height goes below the measurement site and the site is in free-tropospheric region. Therefore surface forcing reduces to minimum.

5.2.3 Fog Induced Aerosol Radiative Forcing

Estimation of aerosol components

To estimate chemical compositions of aerosol, OPAC (Optical Properties of Aerosols and Clouds) model is used to best fit the observed aerosol optical depth spectra. This will help in understanding the changes in aerosol physical and optical properties such as aerosol scattering, absorption and extinction coefficients and single scattering albedo (ω_0) during different RH conditions. When RH increases water soluble particles such as sea salt and sulfates will grow (*Hess et al.*, 1998) and when RH exceeds 80%, the aerosol components can be modified by both particle growth and transformation to an aqueous solution which in turn can affect the refractive index of the components (*Lubin et al.*, 2002). For all days, the AOD observed during the afternoon hours, when the RH value is less than 50% are compared with OPAC produced AOD (Fig. 5.12) and the relative abundances of aerosol components such as water soluble (WS), insoluble (IS), soot (SO) and mineral dust (MD)

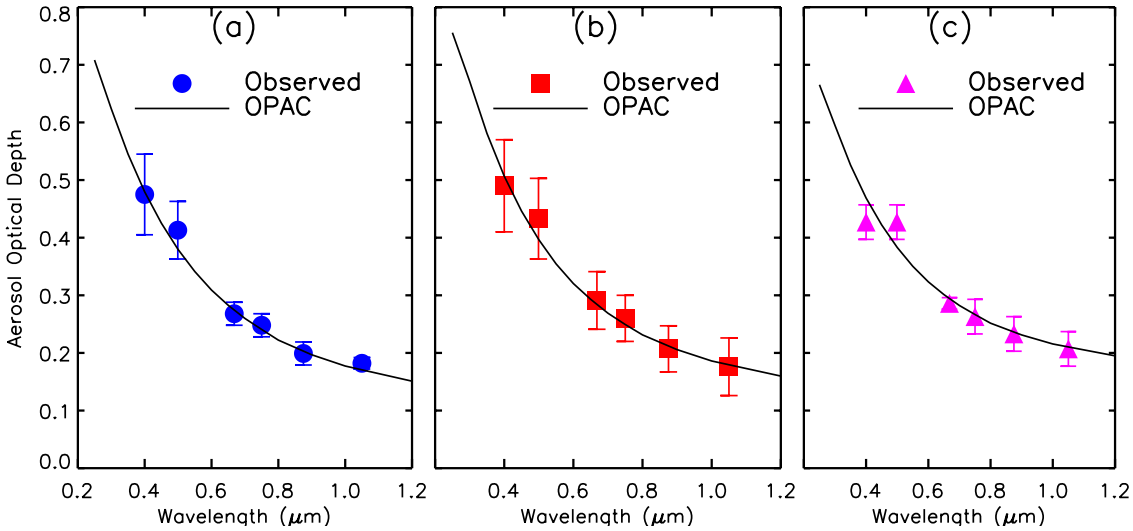

Figure 5.12: *Average aerosol optical depth spectra obtained on (a) 8 Dec 2004, (b) 13 Dec 2004 and (c) 27 Dec 2004 are fitted with OPAC model values.*

are estimated. The most dominating components are found to be WS and SO. The soot particle concentration is found between the continental average and the urban aerosol types as defined by Hess et al. (1998). In Table (5.1) aerosol components for three different days representing, prior to foggy days, during foggy days and after the foggy days are given and the corresponding angstrom parameter, are compared. During foggy days both soot and WS particle concentrations have increased and after foggy days though their number concentrations have decreased and they have not reached the values that were observed prior to the foggy days.

Table 5.1: *Aerosol components viz., Soot (SO), Water Soluble (WS), Water Insoluble (IS) and Mineral Dust (MD) are estimated from OPAC model fitting of the observed aerosol optical depth (AOD) spectra. The Angstrom Parameter (α) estimated for the observed as well as the fitted AOD spectra are compared*

Date	Aerosol Components				Angstrom Parameter (α)	
	SO (par/cc)	WS (par/cc)	IS (par/cc)	MD (par/cc)	Observed	OPAC
8 Dec 2004	24000	18000	2.0	2.0	1.14	1.1
13 Dec 2004	60000	27000	1.3	3.0	1.09	1.1
27 Dec 2004	55000	12000	1.5	8.5	0.80	0.83

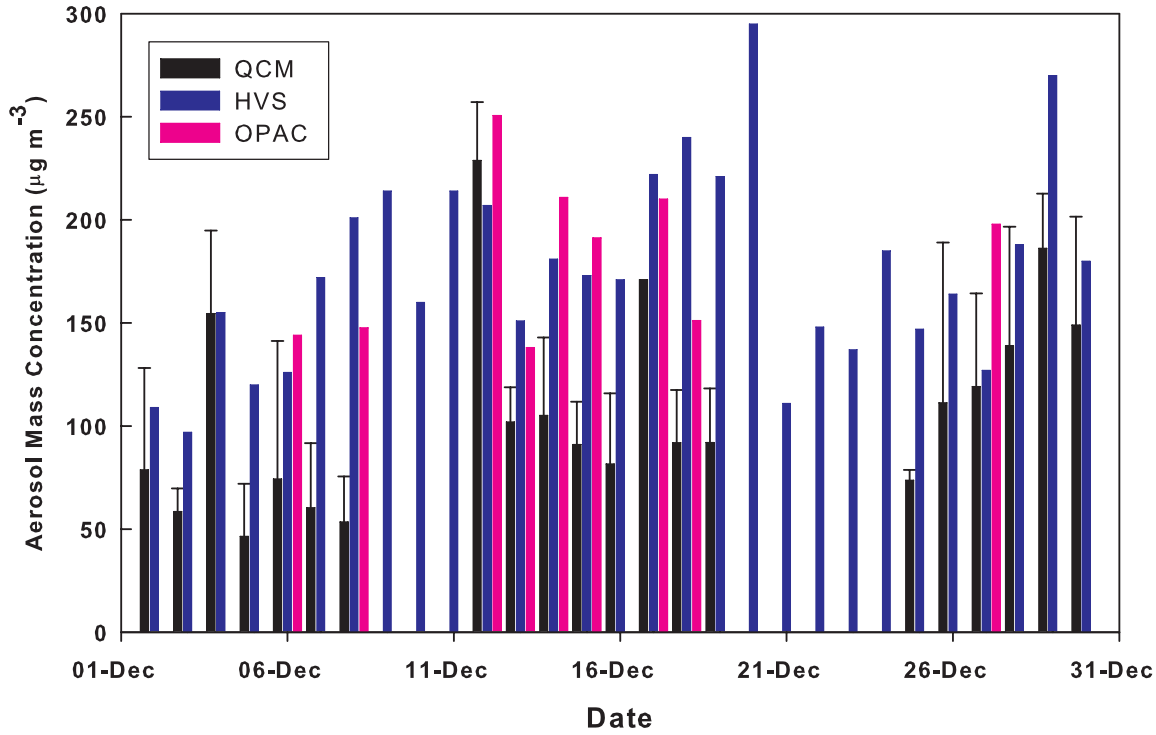

Figure 5.13: *QCM measured aerosol mass concentration at 50% RH condition compared with the estimated mass concentration using OPAC model, and High Volume Sampler (HVS) data.*

Aerosol mass concentrations measured by QCM and HVS are compared with the OPAC estimated aerosol mass concentration (Fig. 5.13). While HVS gives the total mass concentration of particles collected on quartz filter paper for a whole day (24 hours) and used further for chemical analysis (*Ramachandran et al.*, 2006) the QCM measurements were limited to only daytime and data corresponding to 50% RH or less are only considered. With increasing RH the WS component will undergo a major change in their size distribution. Also, the aerosol components can mix internally and externally with other components and hence the relative contribution of different components to the total aerosol loading can change after the foggy period. Therefore, on foggy days the AOD spectra obtained during the afternoon hours are only considered (after the fog has dissipated) and fitted with OPAC model. Prior to foggy days, the aerosol single scattering albedo (SSA) at 500

μm, determined by OPAC fitting the observed AOD spectra SSA was 0.83$\pm$0.03 at 50% RH while during foggy days (in the afternoon hours) the SSA value was 0.72$\pm$0.08 at RH 50% which however increases to 0.82 at 70%. The very low SSA value obtained after the foggy period was mainly due to the scavenging of scattering particles (which are also hygroscopic) such as sulfate and dust while the submicron soot particles, which are hygrophobic and contribute to the absorption, were less scavenged.

Aerosol radiative forcing

Aerosol radiative forcing (ARF) is calculated for the wavelength range 0.28-40 μm using the Santa Barbara DISORT Aerosol Radiative Transfer (SBDART) model (*Ricchiazzi et al.*, 1998) at the top of the atmosphere (TOA), within the atmosphere and at the surface. The ARF values are estimated by running the radiative transfer code for an assumed aerosol free tropical atmosphere and with the specified aerosol components derived by model fitting the observed AOD spectra. Fig. 5.14 shows the diurnally averaged ARF values for 50% RH computed for the campaign days when AOD values are available. Prior to the foggy days the ARF values are comparatively small with surface forcing in the range of -10 Wm^{-2}, and the TOA forcing in the range of 5 Wm^{-2} leading to an atmospheric forcing (difference between surface and the TOA forcings) of about 15 Wm^{-2}. However during the foggy days (12, 13, 14 Dec) there is a large increase in ARF values with surface forcing in the range of, -20 to -25 Wm^{-2}, TOA forcing in the range of 5 to 15 Wm^{-2} which give large atmospheric forcing in the range of 25 to 40 Wm^{-2}. The large forcing values are mainly due to the increase in the aerosol number concentration and size during the foggy days as well as due to the relative increase in the abundance of absorbing particles due to poor ventilation. After the foggy days there is a reduction in the ARF values (Fig. 5.13) though they remained higher than the values obtained prior to the foggy days. In order to study effect of fog on the radiative forcing, the ARF values are computed on hourly basis, taking into account the solar zenith angle

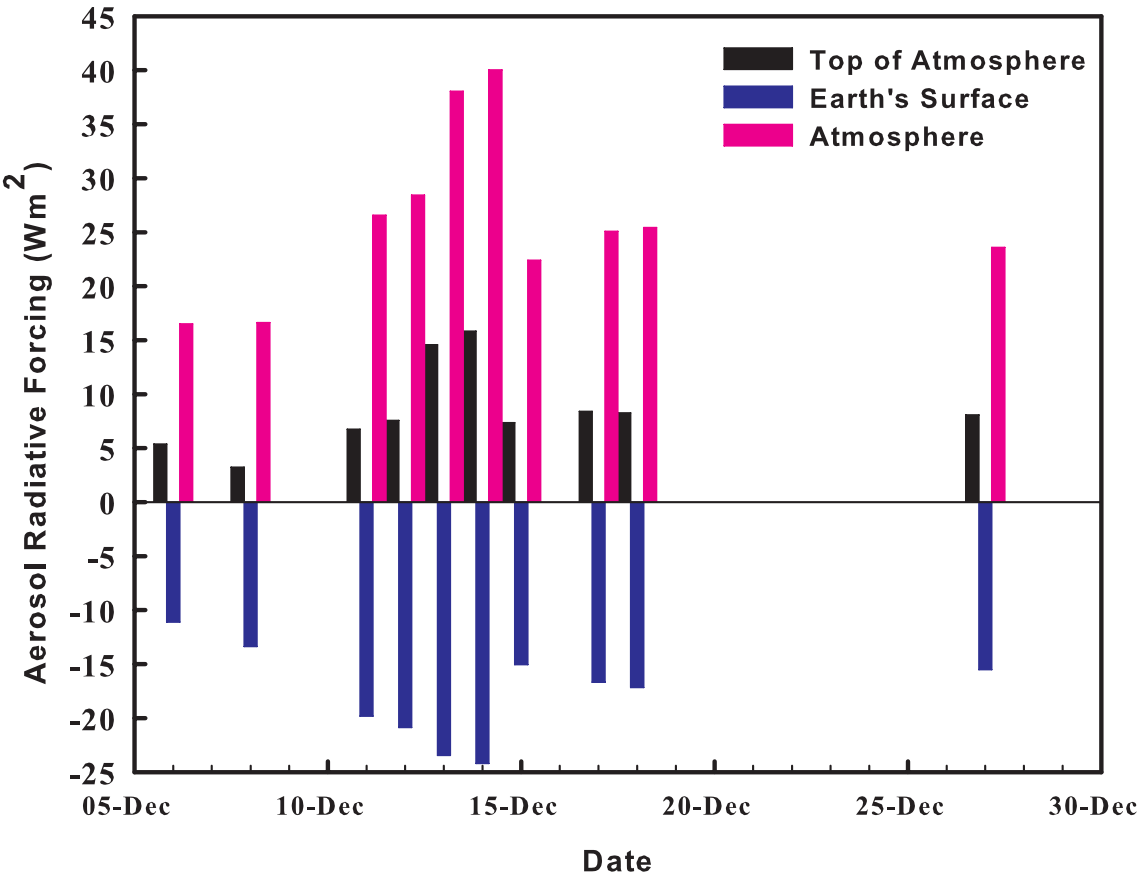

Figure 5.14: *Daily averaged aerosol radiative forcing over Hissar for those days when aerosol optical depth data are available.*

variation, independently for the aerosol components obtained for the 'before fog' days, foggy days and after the foggy days. The individual aerosol components estimated for the 50% RH values are allowed to undergo changes for the RH values of 80% and 99% according to the OPAC model, and the new optical properties are used further to estimate the diurnal variation in the ARF values. While for low RH values the dependence on aerosol optical properties on the change in RH values can be neglected (more true for shorter wavelengths) at higher RH values even small changes in RH can cause large variation in the aerosol optical properties.

It is known that radiative forcing depends on solar zenith angle. On foggy

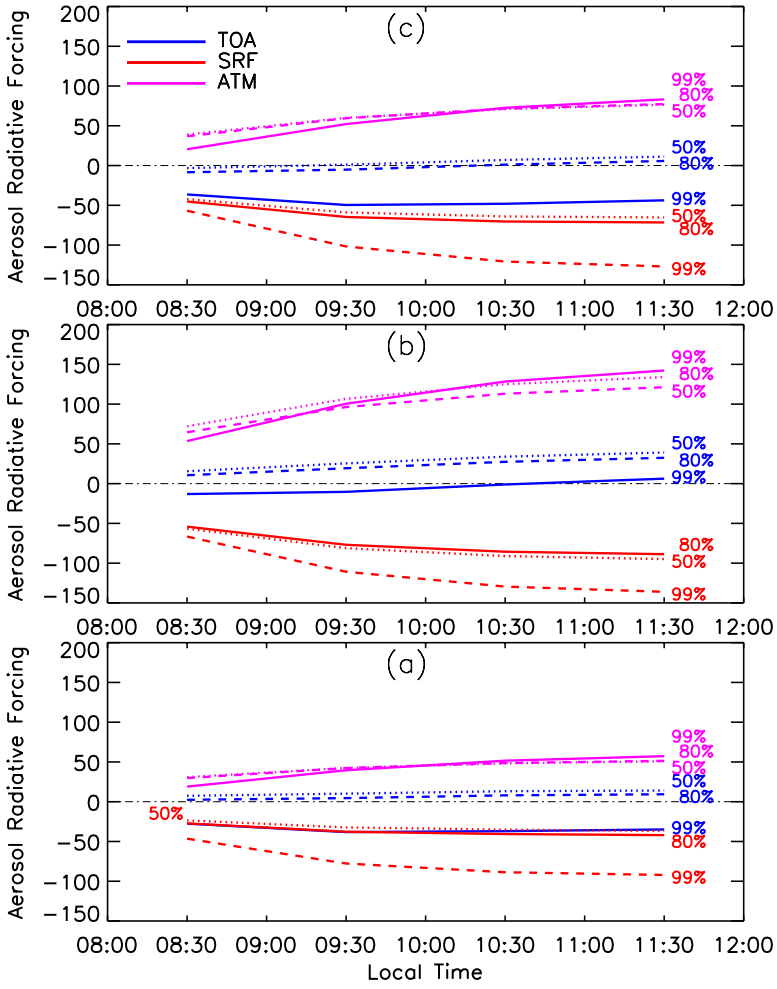

Figure 5.15: *Aerosol radiative forcing for 99%, 80% and 50% RH values, at the top of the atmosphere (TOA), at the surface (SRF) and within the atmosphere (ATM) for (a) 'before fog' day, 8 Dec 04 (b) foggy day, 13 Dec 04 and (c) after foggy day, 17 Dec 04.*

days however the RH value also undergo large diurnal variation from a morning high of more than 90% to an afternoon low of about 50% or less. Fig. 5.15a-c show the results of changes in the ARF values for both solar zenith angle and RH variations for the aerosol components estimated independently for the 'before fog' days, foggy days and after the foggy days. One of the main findings is that as the RH values become very high (shown for 99%) the TOA forcing becomes negative due to large backscattering of radiation to space as a consequence of changing SSA. Thus there is a corresponding decrease in the atmospheric forcing. Also the nature

of the diurnal variation depends on the relative abundances of different aerosol components, and in case of 'foggy days' the diurnal variation (Fig. 5.15b) is found larger as it is also evident from the low SSA values and high AOD values. Also, on foggy days, as the day progresses the decreasing RH value reduces the forcing value while the decreasing solar zenith angle increases the forcing values. Thus the effect of decreasing RH and the solar zenith angle have the opposite effect on the ARF, while the effect of latter is however found larger.

5.2.4 Aerosol Radiative Forcing during Land and Sea Breeze Conditions

Aerosol radiative forcing is calculated over Kalpakkam during different breeze conditions using the procedure described in Sec. 5.2.1. In the present study, the model derived AOD values are compared with the daily averages of the observed AOD values obtained from the Microtops during land breeze and sea breeze for the entire campaign. Using the observed AOD and BC mass concentration ω_0 is also obtained from OPAC (Optical Properties of Aerosols and Clouds by *Hess et al.* (1998)) model. Model derived ω_0 (0.5 μm) is 0.91 and the observed mean ω_0 is 0.91$\pm$0.05 (Table 5.2). The variation is because of the the change in BC concentration at the measurement site caused due to change in wind direction. During sea breeze model derived ω_0 is 0.93 which is same as observed. However, during 20-29 March when the wind is coming from the Indo-Gangetic basin (IGB) model derived ω_0 decreased to 0.89, whereas the observed ω_0 is 0.90. In Urban regions like Delhi and Kanpur in IGB ω_0 is even smaller. *Ganguly et al.* (2006b) reported that ω_0 is in between 0.60-0.80 with an average of 0.68 during December 2004 at Delhi. *Singh et al.* (2005) estimated SSA over Delhi to be 0.67 using the OPAC model. At Kanpur, another industrial region in IGB, ω_0 was estimated to be 0.76 (*Tripathi et al.*, 2005) and at Bangalore, another Urban region in southern India, ω_0 was estimated to be 0.73 (*Babu et al.*, 2002).

Fig. 5.16 shows the diurnal averaged SW ARF, calculated for individual days

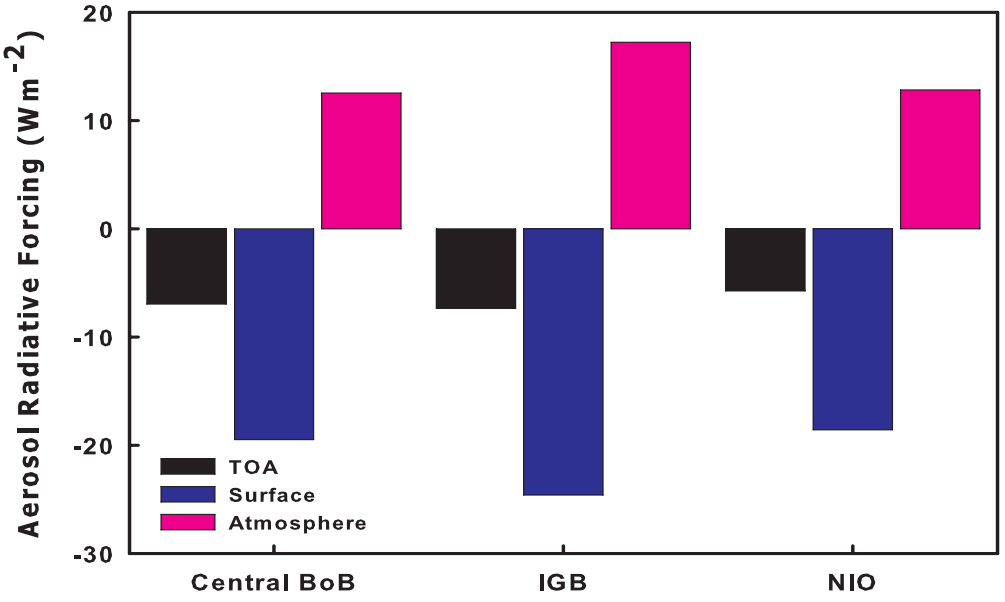

Figure 5.16: *Aerosol Radiative Forcing over Kalpakkam for three different wind regimes coming from Central BoB, Indo-Gangetic Basin via BoB (IGB) and Arabian sea via North Indian Ocean (NIO).*

and then grouped into three wind regimes coming from 1) Central BoB (16-19 March) 2) Indo-Gangetic Basin via BoB (IGB) (20-29 March) and 3) Arabian sea via North Indian Ocean (NIO) (30-31 March). During the study period a large negative forcing variation at the surface has been observed from -18.59 to -24.60 Wm^{-2} whereas at TOA it varies from -5.76 to -7.37 Wm^{-2}. The surface forcing is -19.48 Wm^{-2} for central BoB wind but the maximum forcing is estimated at -24.60 Wm^{-2} for winds from IGB and minimum at -18.59 Wm^{-2} for NIO. At TOA daily averaged forcing for central BoB is more negative (-6.95 Wm^{-2}) followed by IGB (-5.76 Wm^{-2}) and NIO (-7.37 Wm^{-2}). There is a small but significant difference in TOA forcing for IGB and NIO region. The maximum atmospheric forcing is estimated to be 17.23 Wm^{-2} for IGB. At surface the aerosol radiative forcing intricately depends on many aerosol parameters such as columnar AOD, ω_0 etc. During the NIO periods ω_0 was large and columnar AOD was minimum, so the surface ARF is minimum. But during 20-29 March surface ARF is showing maximum of -24.60

Table 5.2: *Aerosol parameters for Radiative forcing computation for three different wind regimes and OPAC derived modelled (Mod) parameters are compared with observed (obs), satellite (sat).*

Winds from	Period	AOD (0.5μm)			$\alpha_{0.38-1.02}$		BC		ω_0	
		Obs	Sat	Mod	Obs	Mod	Obs	Mod	Obs	Mod
Central BoB	16-19 Mar	0.27	0.25	0.29	1.2	1.1	1.73	1.75	0.90	0.91
IGB	20-29 Mar	0.32	0.33	0.34	1.2	1.0	2.38	2.40	0.89	0.89
NIO	30-31 Mar	0.20	0.23	0.24	1.1	1.0	1.69	1.65	0.93	0.91

Wm^{-2} due to large amount of BC that has been carried from IGB to the measurement site and hence at the surface more radiation is reduced due to enhancement of absorbing particles.

Satheesh et al. (2002) estimated the clear-sky short wave aerosol radiative forcing to be -38 Wm^{-2} at surface, -7 Wm^{-2} at TOA and 31 Wm^{-2} in the atmosphere over BoB from the cruise experiment during March 2001. *Ramachandran* (2005) reported the forcing to be -57, 9 and 62 Wm^{-2} respectively over Chennai during the same period. At the east coastal urban region the surface solar reduction is enhanced by a factor of 1.5 than the BoB and in the atmosphere the factor becomes 2. In the present study at Kalpakkam BC was mainly transported either from Chennai and its surrounding suburban region (during land breeze) or from Indo-Gangetic Basin via BoB and hence large variation in aerosol forcings is observed. Hence, depending upon wind direction at Kalpakkam the aerosol radiative forcing is different during different breeze conditions.

Sensitivity Test

Among all anthropogenic aerosols, BC plays a very major role in climate change by absorbtion of solar radiation, warming of the atmosphere and cooling of the surface (*Andreae et al.*, 2005; *Bond*, 2001). The aerosol radiative forcings are estimated over Kalpakkam during March 2006 for different measured BC concentration to investigate the sensitivity of forcing by changing the BC concentration. In the present study there is a large variation in the diurnal BC variation. During the land breeze BC concentration is maximum at 3.0 $\mu g.m^{-3}$ and during sea breeze it

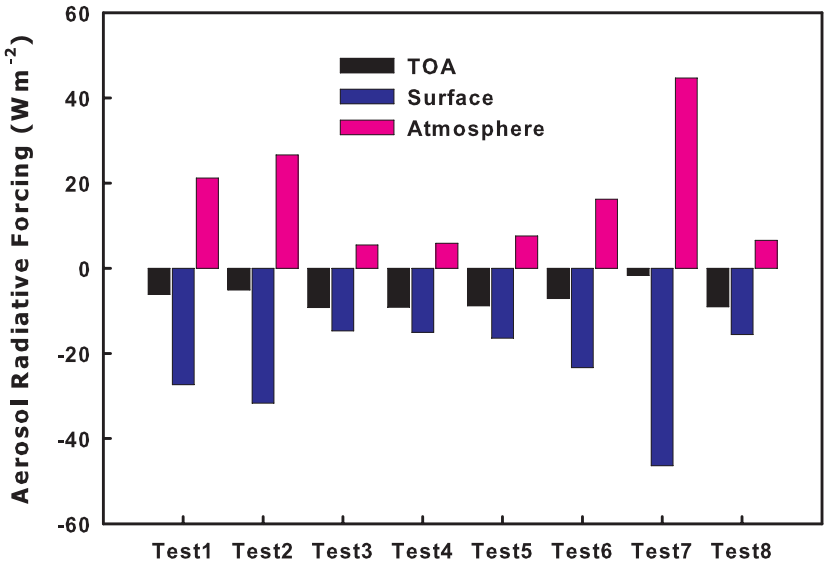

Figure 5.17: *Sensitivity tests for aerosol radiative forcing by varying the BC concentration when compared to the observed BC concentration under different conditions at Kalpakkam during March 2006. See text for more details. Top of atmosphere, surface and atmosphere aerosol radiative forcing are shown for BC equivalent to Continental Average (Test 5), Continental Polluted (Test 6), Urban (Test 7) and Marine Polluted (Test 8) for comparison.*

is 1.2 μg.m^{-3}. However, during 20-29 March when wind was mainly coming from IGB, BC concentration increased to 2.0 μg.m^{-3} during sea breeze and to 4.0 μg.m^{-3} during land breeze. So as an input to SBDART code BC concentration was varied according to breeze condition. For the different conditions sensitivity test has been performed to the mean BC during land breeze (test 1), mean BC during land breeze when wind was mainly coming from IGB (test 2), mean BC during sea breeze (test 3) and mean BC during sea breeze when wind was mainly coming from IGB (test 4). Top of atmosphere, surface and atmosphere aerosol radiative forcings are also being studied for BC equivalent to Continental Average (Test 5), Continental Polluted (Test 6), Urban (Test 7) and Marine Polluted (Test 8) for comparison. The results of these tests are shown in Fig. 5.17.

In Fig. 5.17 the forcings vary over a wide range from -1.71 to -5.6 Wm^{-2} at TOA. At the surface the forcing is always estimated to be negative and there is

Table 5.3: *Aerosol radiative forcing by varying the BC concentration as observed BC concentration under different wind conditions at Kalpakkam. Test 5 to 8 are for OPAC model values*

Test	BC	ω_0	Radiative Forcing			Condition
			TOA	Sur	Atm	
1	3.0	0.88	-6.2	-27.3	21.2	BC equivalent to Mean LB
2	4.0	0.85	-5.1	-31.7	26.6	BC equivalent to Mean LB during IGB
3	1.2	0.98	-9.2	-14.7	5.4	BC equivalent to Mean SB
4	2.0	0.97	-9.2	-15.1	5.9	BC equivalent to Mean SB during IGB
5	0.5	0.96	-8.8	-16.4	7.6	BC equivalent to Continental Averaged
6	2.0	0.91	-7.1	-23.3	16.2	BC equivalent to Continental Polluted
7	7.8	0.76	-1.7	-46.4	44.6	BC equivalent to Urban
8	3.1	0.97	-9.0	-15.6	6.5	BC equivalent to Marine Polluted

(LB: Land Breeze, SB: Sea Breeze, IGB: Wind from Indo-Gangetic Basin)

also a large variation depending on the BC concentration under different conditions because of large variation in ω_0. In test 1 and 2, TOA atmosphere forcings are negative and are -6.2 and -5.1 Wm^2 and the surface forcings are found to be -27.3 and -31.7 Wm^2, respectively. This implies that there is a reduction in surface solar radiation during land breeze due to enhancement of large amount of absorbing BC concentration. In test 2 wind carried large amount of BC from Indo-Gangetic Basin and surface aerosol radiative forcing became maximum during the campaign period. In test 3 and 4 also the TOA forcings estimated to be negative and are -9.2 and -9.2 Wm^{-2}, respectively. At surface they become -14.7 and -15.1 Wm^{-2}. During the sea breeze periods wind carried more scattering sea salt particles and less BC concentration, so at the surface there is less solar radiation reduction. During sea breeze conditions though background BC concentration was enhanced by a factor of 1.6 and ω_0 decreased very little from 0.97 to 0.98 the effect on radiative forcing at surface is significantly low. Therefore, the surface forcings are -14.7 and -15.1 Wm^{-2}, respectively, in tests 3 and 4. From the models comparison, surface forcings for test 5 (-16.4 Wm^{-2}) and test 8 (-15.6 Wm^{-2}) are similar to the sea breeze conditions (test 3 and 4). For test 6 surface forcing is -23.3 Wm^{-2} and at TOA forcing is -7.1 Wm^{-2}. For test 7 BC concentration is assumed to be maximum at 7.8 $\mu g/m^3$ equivalent to "urban" model. In this case SSA is a minimum of 0.76. At TOA forcing is found to be -1.7 Wm^{-2} and at surface forcing is -46.4 Wm^{-2}.

In test 7 forcing is found maximum. It is clearly understood that enhancement of BC at Kalpakkam has great effect on ω_0 and hence on the reduction of surface solar radiation and at TOA forcing becomes more positive as observed during land breeze.

5.2.5 Aerosol Radiative Forcing during Dust Storm at Mt. Abu

The impact of changes of background aerosol characteristics due to the dust storm at the hill top region has been quantified as their capability to perturb the radiation budget of the Earth's atmospheric system and is shown in Fig. 5.18 during (a) stormy days and (b) normal days. Aerosol radiative forcing has been calculated using the same procedure described in Sec. 5.2.1. The clear sky aerosol radiative forcing has been determined from difference of the solar radiation in no aerosol and with aerosol conditions in the short wave (0.25-3.9 μm), long wave (4.0-40.0 μm) and net (0.25-40.0 μm) regions. In the present study, 8-days MODIS derived Level 3 surface reflectance data during the observation period in May 2006 with the grid of 0.5 km for seven wavelengths centered at 0.47, 0.56, 0.65, 0.86, 1.24, 1.64 and 2.13 μm have been used for the estimation of radiative forcing over Mt. Abu. Spectral surface reflectance values are considered to be the combination of three different surfaces, *viz.,* water, sand and vegetation, and are used as input to the SBDART model (*Ganguly et al.*, 2006b).

Fig. 5.18 shows the short wave (SW), long wave (LW) and net radiation budgets at the background condition during (a) stormy days and (b) normal days. During the stormy days SW radiative forcing is 4.9 Wm^{-2} at top of atmosphere (TOA) and -28.8 Wm^{-2} at the Earth's surface. As a result the energy trapped in the atmosphere is 33.7 Wm^{-2}. The LW radiative forcing shows 4.2, 14.7 and -10.5 Wm^{-2} at TOA, surface and in the atmosphere respectively. As a result the net forcing is 9.1 Wm^{-2} at TOA, -14.1 Wm^{-2} at the surface and hence 23.2 Wm^{-2} in the atmosphere during the stormy days. During the normal days at TOA SW and LW forcing is 3.0 and 3.2 Wm^{-2}, respectively whereas at the surface they are -21.4, 12.2 Wm^{-2}

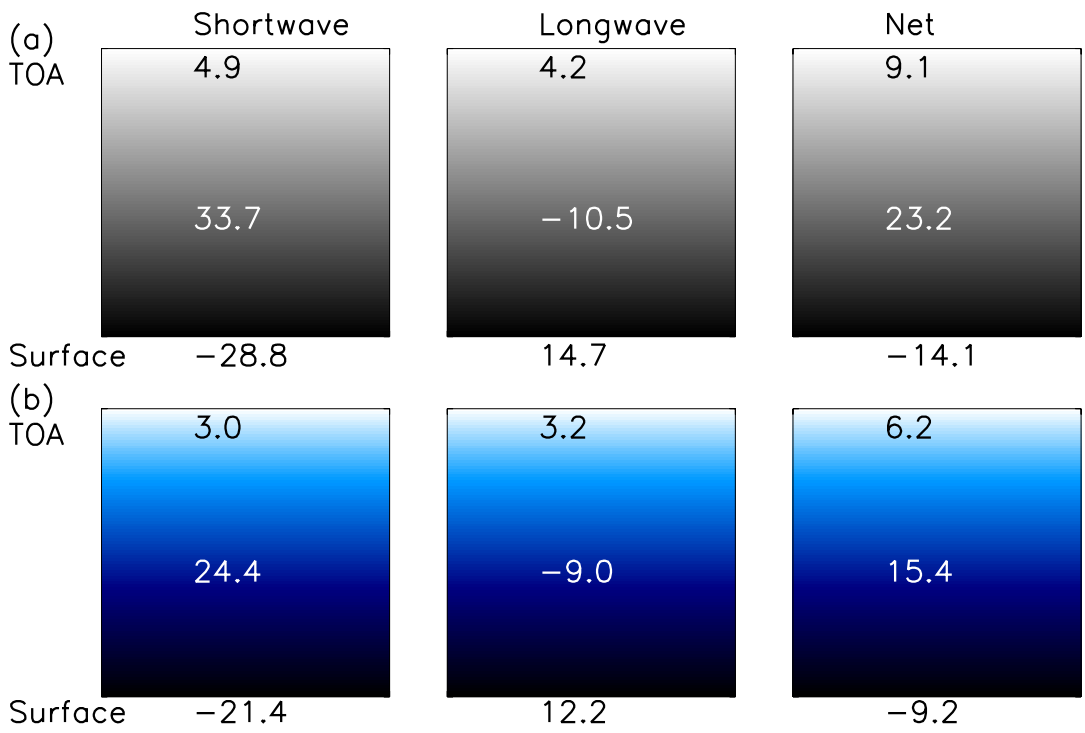

Figure 5.18: *Aerosol radiative forcing over Mt. Abu during (a) dust storm days and (b) normal days.*

respectively. So in the atmosphere SW and LW forcings are 24.4 and -9.0 Wm^{-2}, respectively. Therefore net forcings are 6.2 Wm^{-2} at TOA, -9.2 Wm^{-2} at surface and as a result in the net atmosphere forcing becomes 15.4 Wm^{-2}. *Pant et al.* (2006) has reported the surface radiative forcing to be -4.2 Wm^{-2} and background atmospheric forcing was 4.9 Wm^{-2} during winter at Nainital, a high altitude station in central Himalayas. However, in the Himalayan region at Nepal the surface radiative forcing efficiency has been reported to be -73 Wm^{-2} with single scattering albedo in the range 0.7 to 0.9 due to large abundance of BC particles (*Ramana et al.*, 2004). In case of western part of India during premonsoon the background surface radiative forcing is observed to be slightly higher than the earlier reported background forcing in Himalayan region. The reason is that the adjacent 'Thar desert' helps to enhance the background dust particles and urban regions of western part of India add BC particles in the background region. Due to more dust

and BC aerosols, more radiation is trapped in the atmosphere in SW region during the stormy days whereas the steady background fine dust aerosols trap almost the same LW terrestrial radiation in the atmosphere during the observation period. As a result the net forcing at TOA is slightly enhanced in comparison to normal days due to more reduction of radiation at the surface.

5.2.6 Aerosol Radiative Forcing over Arid Region

OPAC estimation of AOD and Aerosol Mass Comparison

Aerosol optical properties strongly depend on the chemical properties of aerosols. Hence it is necessary to have the knowledge of chemical properties of the various types of aerosols. However, in the absence of chemical composition information, AOD spectrum (0.25-40.0 μm) can be derived from the Optical Properties of Aerosols and Clouds (OPAC) (*Hess et al.*, 1998) using the known chemical compositions of aerosol over western part of India (*Ganguly et al.*, 2006a; *Rastogi and Sarin*, 2005a). The modelled AOD spectrum should match the observed AOD values. Detail procedure is discussed by the earlier researchers (*Ramachandran et al.*, 2006; *Ganguly and Jayaraman*, 2006) and hence not discussed here. The OPAC estimated AODs and observed AODs and the angstrom parameters match quite well with each other and are given in Table 5.4.

Table 5.4: *Aerosol parameters for Radiative forcing computation at the three different stations and OPAC modelled (Mod) parameters are compared with observed (obs), MODIS satellite (sat).*

Station	AOD			$\alpha_{0.38/1.02}$		Total Mass		BC		Model
	Obs	Sat	Mod	Obs	Mod	Obs	Mod	Obs	Mod	SSA
Ahmedabad	0.31	0.34	0.31	0.50	0.51	28.2	25.5	1.85	1.80	0.83
Udaipur	0.30	0.28	0.29	0.46	0.51	19.0	18.9	0.95	0.93	0.87
Mt. Abu	0.28	0.27	0.28	0.75	0.73	12.5	12.4	0.72	0.72	0.88

Single Scattering Albedo

Single scattering albedo (SSA) is an important parameter in the radiative forcing calculation. During April, dust storm is a common phenomena in the western part of India (*Deepshikha et al.*, 2006a). Due to the frequent dust storm occurrence the dust abundance in the atmosphere increases. Using chemical transport model, "Goddard Global Ozone Chemistry Aerosol Radiation and Transport" (GOCART) model (e.g., *Chin et al.*, 2003) and AERONET (e.g., *Holben et al.*, 1998) at 0.550μm, SSA was found to be 0.87-0.93 over western part of India during April (*Chung et al.*, 2005). But the SSA of dust strongly depends on the presence of BC concentration in the atmosphere . SSA of dust varies form 0.9-0.98 depending on the amount of BC present in the atmosphere and it decreases with increase in BC concentration (*Chung et al.*, 2005). Another satellite observation shows that infrared SSA over this region varies in the range 0.88-0.94 due to the moderate absorbing dust aerosols in the atmosphere (*Deepshikha et al.*, 2005, 2006a,b; *Moorthy et al.*, 2007).

In the present study SSA is estimated using OPAC model for Ahmedabad, Udaipur and Mt. Abu. During April, SSA is 0.83 over Ahemdabad and 0.87 over Udaipur, whereas over Mt. Abu SSA is 0.88. From simultaneous measurements of single scattering coefficient using Nephelometer and calculated absorbtion coefficient from Aethalometer observations, SSA has been calculated and reported to be 0.84$\pm$0.04 over Ahmedabad during premonsoon (*Ganguly et al.*, 2006a). Over Ahmedabad SSA becomes minimum compared to other stations due to large production of anthropogenic BC and the presence of dust particles. At the hilltop station Mt. Abu, SSA is high due to less concentration of BC. At Udaipur SSA is slightly less due to increase in dust particles concentrations.

Aerosol Radiative Forcing

The aerosol radiative forcing is computed using the same procedure as described in Sec. 5.2.1. A comparison of the observed and the model values are given in

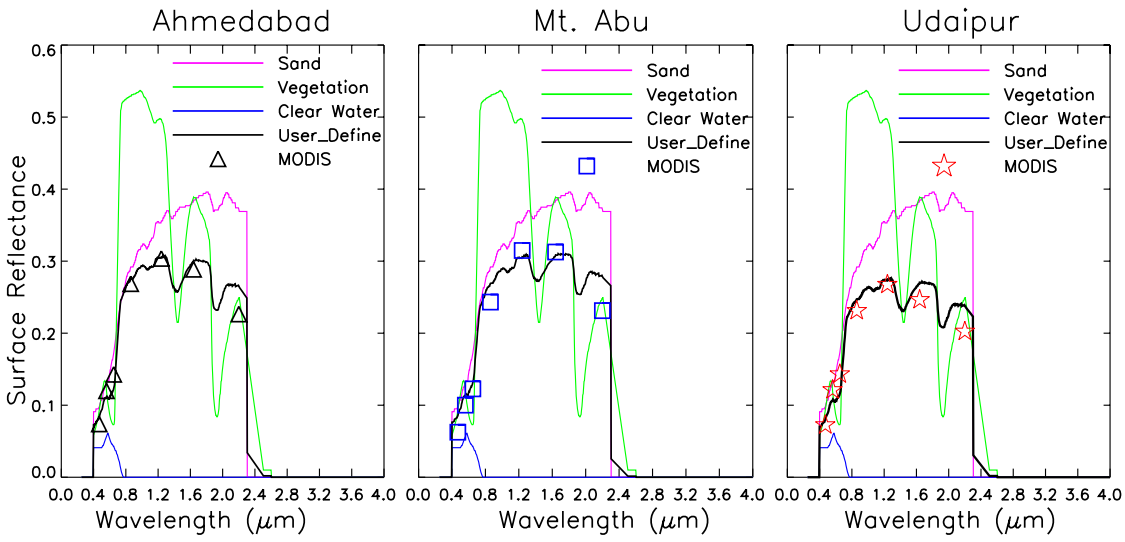

Figure 5.19: *Spectral Surface Reflectance over Ahmedabad, Mt. Abu and Udaipur during April 2007 that has been used in the present study to compute the aerosol radiative forcing.*

Table 5.4. The clear sky aerosol radiative forcing has been determined from difference of the solar radiation in no aerosol and with aerosol conditions in the short wave (0.25-3.9 μm), long wave (4.0-40.0 μm) and net wave (0.25-40.0 μm) regions. The spectral surface reflectance values are considered to be a combination of three different surfaces, *viz.*, water, sand and vegetation as shown in Fig. 5.19.

Fig. 5.20 shows the mean aerosol radiative forcing over Ahmedabad, Udaipur and Mt. Abu at the top of atmosphere (TOA), Earth's surface and in the atmosphere computed for individual days. During April the SW radiative forcing obtained at the surface over Ahmedabad is maximum at -44.3$\pm$5.2 Wm^{-2}. The forcing is also maximum at TOA over Ahmedabad and is 9.0$\pm$1.0 Wm^{-2}. The surface forcing is found to be governed by the magnitude of the AODs, presence of BC absorbing particles and hence SSA. But the TOA forcing is very intricately dependent on several other aerosol parameters, like scattering and absorbing particles concentration, surface albedo etc., in addition to AOD, SSA. The difference between

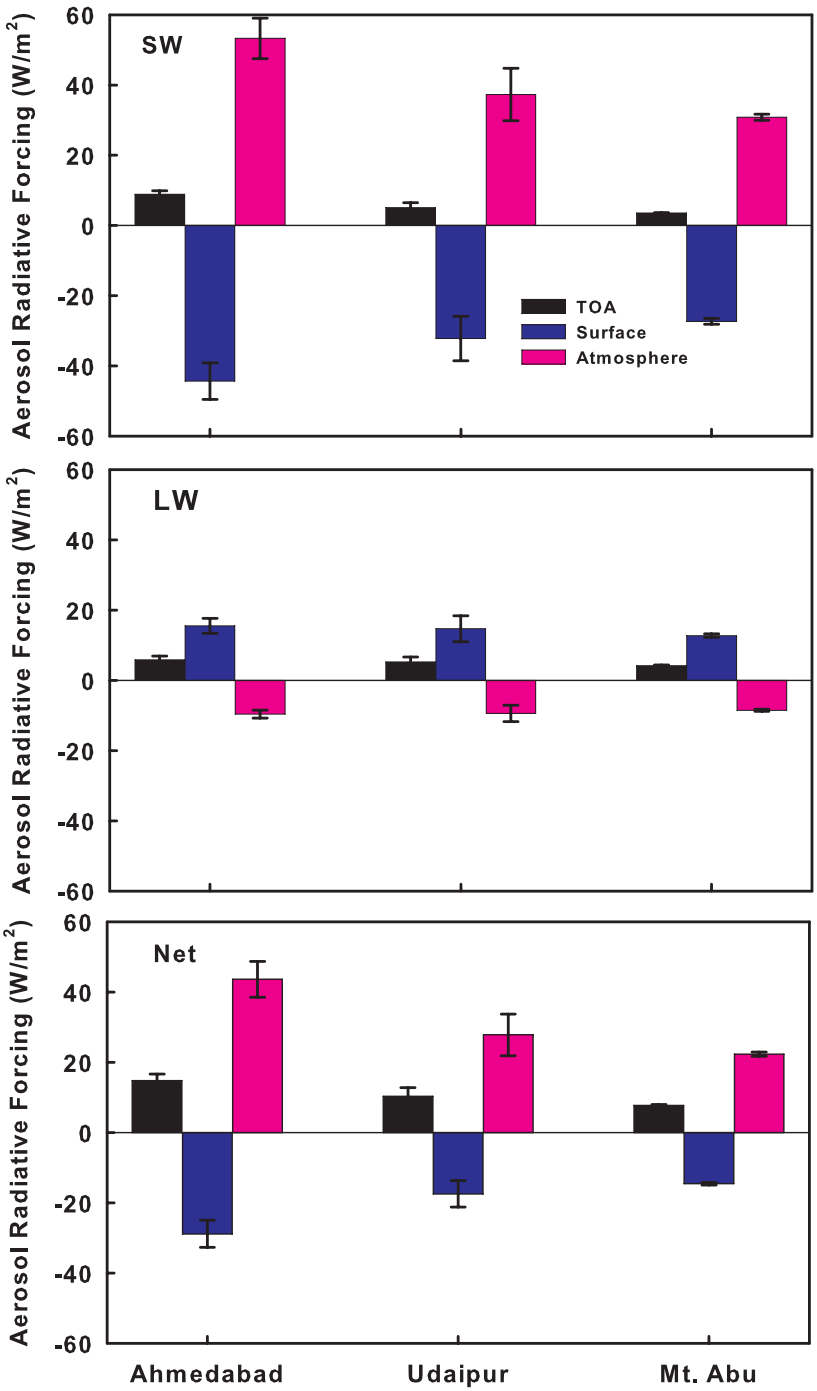

Figure 5.20: *Aerosol radiative forcing over Ahmedabad, Udaipur and Mt. Abu in the (a) shortwave (SW) and (b) longwave regions (LW) and (c) the Net forcing (SW+LW).*

the surface and TOA forcing gives the atmosphere forcing which indicates the energy trapped in the atmosphere. Earlier workers have shown that the TOA and surface forcings are 8.0±2.0, -41.4±5.0 Wm^{-2}, respectively, at Ahmedabad during premonsoon (*Ganguly et al.*, 2006a). The difference between surface and TOA forcing gives the atmospheric forcing which indicates the energy stored in the atmosphere. At Ahmedabad the SW atmospheric forcing is a maximum of 53.3±5.7 Wm^{-2} which represents the large SW radiative heating in the atmosphere. At Udaipur the forcings are 5.1 ±1.4 Wm^{-2}, -32.2±6.3 Wm^{-2} and 37.3±7.5 Wm^{-2} at TOA, surface and in the atmosphere, respectively. At Udaipur the SW radiative heating in the atmosphere is moderate as less amount of SW radiation is trapped. This is due to the presence of large abundance of scattering particles like dust. In the background environment at Mt. Abu, the forcings are 3.5±0.1 Wm^{-2} and -27.3±0.8 Wm^{-2} and 30.8±0.9 ± at TOA, surface and in the atmosphere, respectively, during April. The forcings are minimum due to the presence of less anthropogenic BC aerosols at this high altitude.

In the LW region soot is a perfect absorber and hence its single scattering albedo becomes zero whereas dust particles contributes to more scattering than the other aerosol components (*Hess et al.*, 1998; *Satheesh and Lubin*, 2003). Dust is an efficient scatterer in the 4.0-6.0μm range and beyond that starts exhibiting absorbing properties also. It has an absorbtion peak at $\sim$6μm and in the longer wavelength ($>$11.0μm) dust exhibits absorbing properties. This indicates that any variation in the amount of dust particles alone can affect the longwave terrestrial radiation and hence the LW aerosol radiative forcing. In addition to dust, the trace gases ozone and water vapor also have an impact on the LW radiative forcing. Ozone causes warming in the lower stratosphere whereas in upper stratosphere it helps to cool the atmosphere associated with water vapor and carbon dioxide in the LW radiation (*Ramaswamy*, 2002). LW radiative forcings are also shown in Fig. 5.20 for Ahmedabad, Udaipur and Mt. Abu. The forcings are comparable within $\pm 1\sigma$ at Ahmedabad and Udaipur due to similar water vapor and ozone concentrations and dust aerosols. The variation of LW forcing at Udaipur is large due to large

variation in dust aerosols. The forcings at Mt. Abu are slightly low due to the low abundance of water vapor and transported dust particles at this high altitude. The net (SW+LW) forcings are maximum at -28.8 and 43.6 Wm^{-2} at surface and in the atmosphere, respectively, at Ahmedabad followed by Udaipur at -17.5 and 27.8 Wm^{-2}, repectively. The minimum forcings are -14.6 and 22.3 Wm^{-2}, respectively, at Mt. Abu due to its background conditions. At Udaipur net forcing is moderate due to less anthropogenic SW forcing at the surface.

CHAPTER 6

Anthropogenic vs Natural Aerosol Radiative Forcing

The response of the Earth's climate to the perturbation in the radiative forcing is significantly increasing in the post industrial era due to continuous increase of anthropogenic aerosols in the atmosphere. In the recent years, this has become comparable to that of Greenhouse gases but with opposite sign. In view of the magnitude of these aerosol influences on climate change, it seems mandatory that these should be included now in efforts to obtain accurate estimates of anthropogenic perturbation to the Earth's radiation budget. The change in climate due to these aerosols is not uniform over the globe because of their short residence time in the atmosphere which results in the spatial and temporal nonuniformity of radiative forcing. Recent studies have shown that the industrial emissions, biomass burning and vehicular emissions are more responsible for the enhancement of regional anthropogenic aerosols like sulfate, Black Carbon (BC), etc., and have additive influence on the climate change associated with the natural background aerosols. Comparatively, the natural aerosols like sea salt and dust have more influence on climate than the anthropogenic aerosols due to their large abundance in the atmosphere. The study of natural aerosol radiative forcing is more important because it

gives a knowledge of the base level. As there is no control on the natural aerosols, many field campaigns and studies are mainly concentrated only on the anthropogenic aerosols. The seasonal variation of natural and anthropogenic aerosol radiative forcing over Ahmedabad, an urban environment and Mt. Abu, a pristine environment is discussed in the present study. The variation in diurnal radiative forcing due to BC variation in Western India and at the east coastal region of India is also discussed.

6.1 Seasonal Variation of Natural and Anthropogenic Radiative Forcing in Urban Environment

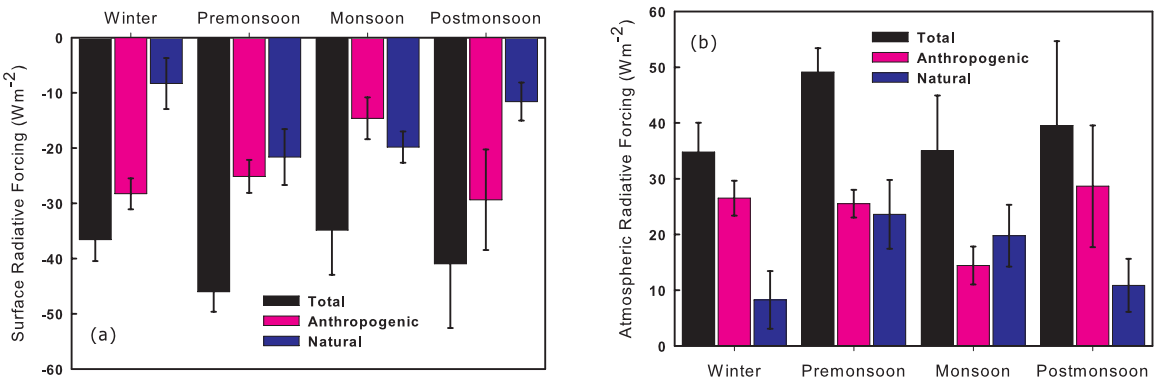

Figure 6.1: *Seasonal variation of natural, anthropogenic and total radiative forcing over Ahmedabad (a) at Surface and (b) in the Atmosphere.*

The seasonal aerosol radiative forcing is computed using SBADRT code and the major aerosol parameters which are necessary for SBDART code are obtained from OPAC model, as discussed in Chapter 5. The OPAC model gives the opportunity to distinguish the different aerosol components as natural and anthropogenic. The radiative forcing is calculated separately for the natural (dust and seasalt) and anthropogenic aerosols (Sulphate, Nitrate and BC) and their radiatively important parameters are obtained from OPAC model. Fig. 6.1(a) shows the seasonal

variation of both, natural and anthropogenic aerosol radiative forcing at the surface over Ahmedabad. The anthropogenic surface radiative forcing is minimum at -14.6 Wm^{-2} during monsoon and maximum at -29.3 Wm^{-2} during premonsoon, followed by winter (-28.3 Wm^{-2}) and premonsoon (-25.1 Wm^{-2}) whereas the natural surface radiative forcing is minimum at -8.3 Wm^{-2} during winter and maximum at -21.6 Wm^{-2} during premonsoon, followed by monsoon (-19 Wm^{-2}) and postmonsoon (-11.6 Wm^{-2}). The anthropogenic aerosol radiative forcing is dominating over the natural forcing at Ahmedabad during all the seasons except during monsoon where the natural forcing is dominating. During monsoon, the anthropogenic aerosols are washed out by the rain and the abundance of natural aerosols is enhanced due to large transportation of seasalt aerosols from Arabian sea. During premonsoon though natural dust aerosols are abundant, natural forcing is maximum but still less than the anthropogenic forcing.

In the atmosphere the trapped energy is scaled by the atmospheric radiative forcing. The atmospheric natural and anthropogenic radiative forcing also have similar seasonal variation, as shown in Fig. 6.1(b). The anthropogenic forcing is similar during all the seasons except monsoon, where it is less. The large abundance of anthropogenic BC during these seasons can absorb the solar radiation and trap large amount of solar radiation in the atmosphere. During premonsoon and monsoon the natural dust and seasalt are highly abundant, respectively, and these natural aerosols enhance the natural radiative forcing in the atmosphere. During monsoon, anthropogenic aerosols have reduced due to wash out by rain in the lower atmosphere and hence the anthropogenic forcing in the atmosphere is minimum. However, an aerosol layer has been seen in 0.5-2.0 km region in lidar observations (*Ganguly et al.*, 2006a). The chemical analysis of rain drop during this season shows that the rain drops contain 50% of dust, 25% of anthropogenic aerosols and rest is seasalt aerosols (*Rastogi and Sarin*, 2005b). This study indicates that during monsoon maximum amount of dust and anthropogenic aerosols in the atmosphere are washed out. Earlier studies reported that during monsoon there is large transportation of seasalt from Arabian sea to Ahmedabad and also to Mt.

Abu (for e.g., *Rastogi and Sarin*, 2005a). The observed high altitude aerosol layer over Ahmedabad, therefore, might contain large amount of seasalt aerosols. As a result, natural forcing is dominating at Ahmedabad during monsoon.

6.2 Seasonal Variation of Natural and Anthropogenic Forcing over Hilltop Environment

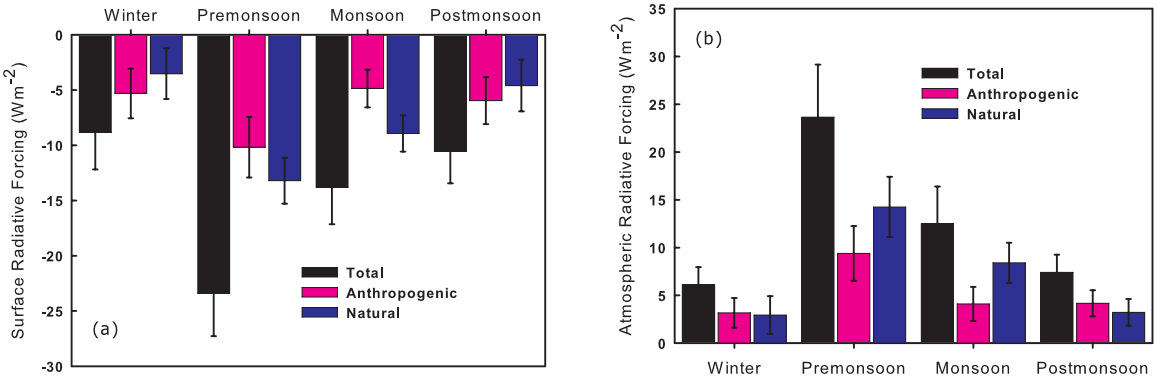

Figure 6.2: *Seasonal variation of anthropogenic radiative forcing over Mt. Abu*

Mt. Abu experiences large variation in aerosol properties and hence the radiation forcing. During premonsoon there is a large transportation of natural dust aerosols from surrounding arid region by the strong westerly wind whereas during monsoon large amount of seasalt is coming from Arabian sea carried by Southwesterly wind. The anthropogenic radiative forcing at Mt. Abu is four times less and the natural forcing is two times less than those at Ahmedabad. Fig. 6.2 shows the seasonal variation of natural, anthropogenic and total aerosol radiative forcing at the surface and in the atmosphere over Mt. Abu. The anthropogenic forcings are low and similar during all seasons except premonsoon. The atmospheric anthropogenic radiative forcing is minimum at 3.2 Wm^{-2} during winter and maximum at 9.4 Wm^{-2} during premonsoon followed by postmonsoon (4.2 Wm^{-2}) and monsoon (4.1 Wm^{-2}). The natural forcing shows a more pronounced seasonal variation and is minimum at 3.0 Wm^{-2} during winter and maximum at 14.2

Wm^{-2} during premonsoon followed by monsoon (8.4 Wm^{-2}) and postmonsoon (3.2 Wm^{-2}). Natural forcing is dominating at Mt. Abu during premonsoon and monsoon whereas the contributions of anthropogenic and natural forcing to the total forcing during winter and postmonsoon are almost equal.

Due to the proximity to the 'Thar' desert dust aerosols are transported to this hill-top region during premonsoon and hence natural forcing is maximum. Anthropogenic forcing is also maximum during this season due to increase in local anthropogenic activities by tourists, resulting in large abundance of anthropogenic aerosols. However, natural forcing is dominating at Mt. Abu during premonsoon, in contrast to Ahmedabad, where the anthropogenic forcing is dominating. During monsoon wind is mainly coming from Arabian sea and carries large amount of natural seasalt and at the same time lower troposphere anthropogenic aerosols are washed out by the heavy rain. The chemical analysis shows that during monsoon the anthropogenic compositions like non-seasalt potassium, ammonium and nitrate are relatively less and the natural compositions like seasalt are enhanced over Mt. Abu (*Rastogi and Sarin*, 2005a). Therefore, natural forcing is dominating and anthropogenic forcing reduces. During postmonsoon, there is no transportation of the seasalt aerosols to the measurement site due to low wind speed and hence the natural forcing has reduced. During winter, total aerosol mass concentration is minimum as observed by QCM measurement because the measurement site becomes a free tropospheric station. Therefore, during this season both natural and anthropogenic forcings are minimum.

6.3 Variation of Radiative Forcing at East Coast Region

The coastal region has an experience of land and sea breeze and therefore, there is large variation of aerosol properties and hence large changes are seen in the coastal radiation budget. Being a coastal region, Kalpakkam also has large variation of

aerosol properties due to changes in coastal breezes. These changes of aerosols properties are different when BC aerosols are transported from Indo-Gangetic Basin thereby enhancing the background BC concentration. In addition, cyclonic events enhance the seasalt aerosols in the coastal atmosphere. The effects of change in BC background level and the cyclonic events on radiative forcing are discussed in this section.

6.3.1 Influence of Breezes on ARF at Kalpakkam

At the east coastal region like Kalpakkam the main meteorological parameter which produces large changes in the aerosol properties is local wind. Due to the large variation in wind direction aerosol concentration, especially the anthropogenic BC particles, have a large diurnal variation. BC particles are the most efficient light absorbing particles in the visible range and responsible for the large reduction of solar radiation at the surface. In addition to this direct effect, aerosols can modify the cloud albedo by changing the droplet size and cause significant offset in the radiation budget. Fig. 6.3 (a and b) shows the diurnal variation of aerosol induced radiative forcing over Kalpakkam for a typical day (18 March) and a special day (28 March). There is a large transportation of BC aerosols form the Indo-Gangetic Basin via Bay of Bengal which enhanced the background BC aerosols by a factor of 1.6 during 20–29 March. A cyclonic event occurred over Bay of Bengal on 27–28 March which produced large amount of natural seasalt in the coastal atmosphere. These two things have made 28 March a special day to investigate the diurnal variation of costal radiative forcing. At Kalpakkam the wind had changed its direction from land to sea about 1100 local hours (Fig. 4.6). In the present study the aerosol radiative forcing is calculated for every 15-min interval during land and sea breeze periods for different BC concentrations and is shown in Fig. 6.3. The blue, black and the magenta colors represent the radiative forcing at TOA, surface and in the atmosphere, respectively. The shaded region during 1100–1300 local hours represents the transition period from land to sea breeze. The solid line to

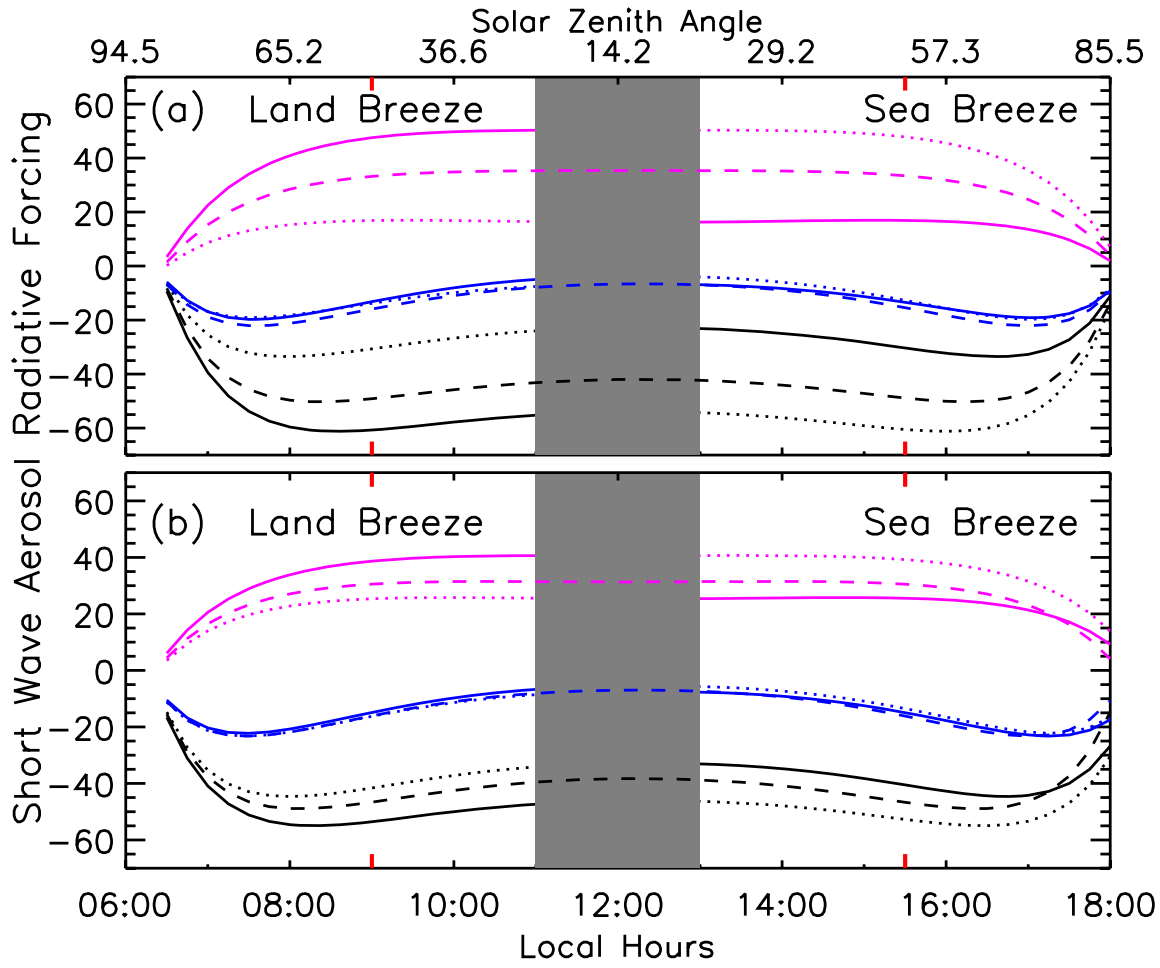

Figure 6.3: *Diurnal variation of aerosol radiative forcing over Kalpakkam during (a) 18 March and (b) 28 March for different breeze conditions. The shaded area represents the transition period from land breeze to sea breeze. See text for more details.*

the left (right) of the figure represents the land (sea) breeze radiative forcing calculated for the mean BC value during morning (evening) hours. The dotted line to the left (right) of the figure represents the possible aerosol radiative forcing if the sea (land) breeze continued for the other part of the day also. The dashed line represents the aerosol radiative forcing computed for the diurnally averaged BC concentration irrespective of the breeze condition.

On 18 March mean BC concentrations are 3.1±0.9 and 1.2±0.4 μg.m^{-3} during

land and sea breeze, respectively. Due to large decrease of absorbing BC component the columnar AOD (at 0.5μm) also decreased from 0.33 to 0.21 and the measured ω_0 showed a large enhancement from 0.79 to 0.90 (Fig 4.15). The radiative forcing during land and sea breeze conditions at 50° solar zenith angle (marked in red on the x-axes) are discussed such that the incoming solar radiation is similar and hence can be compared.

The surface radiative forcing becomes -60.7 Wm^{-2} during land breeze and -30.3 Wm^{-2} during sea breeze whereas mean forcing is -48.8 Wm^{-2} and as a result the forcing in the atmosphere becomes 47.8, 16.9 and 33.4 Wm^{-2}, respectively. This implies that surface reaching solar radiation is reduced more by aerosols during land breeze than during sea breeze. This enhancement of surface forcing is by a factor of 2 whereas atmospheric forcing is enhanced by a factor of 3. The main reason is that land breeze brings BC aerosols to the measurement site from Chennai and its surroundings. However, on 28 March BC concentration changes from 2.6$\pm$0.7 to 1.8$\pm$0.2 μgm^{-3} as breeze changes from land to sea. As a result, ω_0 has changed from 0.90 to 0.94. Therefore, at 50° solar zenith angle, the reduction of surface solar radiation has decreased from -53.5 to -41.6 Wm^{-2} and atmosphere forcing reduces from 38.6 to 25.3 Wm^{-2}. The background forcing is enhanced during sea breeze because of long range transportation of BC from Indo-Gangetic basin whereas the short range BC transportation from Chennai has not changed. In addition, the enhancement of scattering sea salt particles during the cyclonic event increased SSA during land breeze and hence the radiative forcing. Therefore, during land breeze anthropogenic forcing due to BC particles changes from -26.6 to -5.4 Wm^{-2} at surface and 27.7 to 6.1 Wm^{-2} in the atmosphere. It implies that the contribution of transported BC from Chennai and its surroundings on coastal radiative forcing reduces from 50% to 11% during land breeze.

The surface forcing is minimum during sea breeze and is considered as the background forcing. On 18 March it is -26.7 Wm^{-2} whereas on 28 March it becomes -36.8 Wm^{-2}. This is due to the increase of the average BC concentration by 1.6 times when compared to normal days. These absorbing BC aerosols cause 1.4 times

more reduction of solar radiation at surface. Therefore, the background surface forcing is enhanced by 40%.

6.4 Radiative Forcing due to Diurnal Variation of Black Carbon Concentration over Western India

Frequent dust storms in the desert areas of western part of India are large sources of dust aerosols which can be transported to long distances. Earlier studies have shown the influence of these dust aerosols on radiative forcing in regions as far as the Indo-gangetic basin (e.g., *Dey et al.*, 2004; *Deepshikha et al.*, 2006b; *Pant et al.*, 2006; *Panditharai et al.*, 2008). The radiative forcing is not only affected by dust but also by BC concentration. In the western part of India, anthropogenic BC is unevenly distributed, and hence, the radiative forcing also has an uneven distribution over this region. Over Ahmedabad, the aerosol radiative forcing is maximum due to the presence of maximum BC in the atmosphere followed by Udaipur and is minimum at Mt. Abu during premonsoon. At Ahmedabad and Udaipur there is also a large diurnal variation of BC particles whereas at Mt. Abu there is no such diurnal variation. In the morning (0600-1000 hours) BC is maximum at Ahmedabad and Udaipur but in the afternoon (1400-1600 hours) BC concentrations are equivalent in all the three stations. The present study investigates the influence of diurnal BC variation on short wave aerosol radiative forcing at Ahmedabad and Udaipur.

6.4.1 Influence of BC particles on Diurnal ARF

BC particles, the result of incomplete combustion, have a great impact on the climate change due to its large absorbtion of the visible solar radiation and produce a positive radiative forcing at the TOA. In the western part of India the BC spatial distribution is not uniform due to uneven production. Maximum BC is observed over Ahmedabad due to large vehicular and industrial emissions, followed

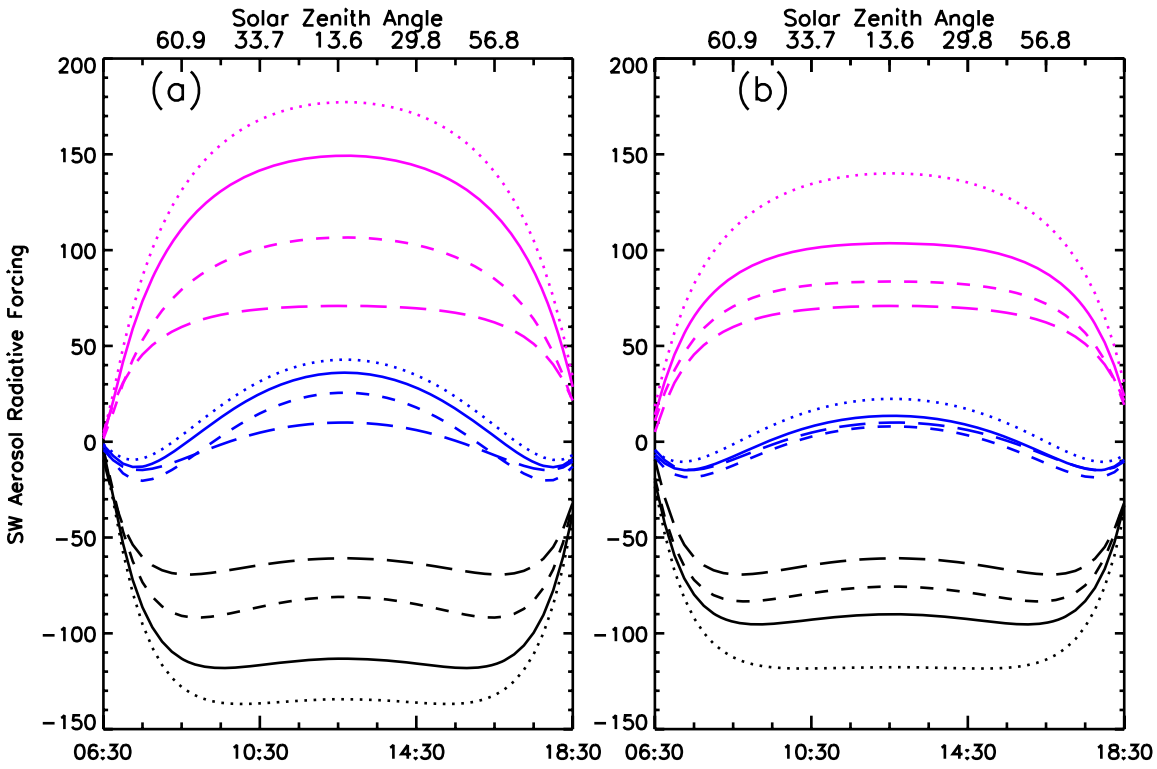

Figure 6.4: *Diurnal variation of aerosol radiative forcing over (a) Ahmedabad and (b) Udaipur. Blue, black and red lines represent ARF at TOA, surface and in the atmosphere, respectively. The dashed (small) lines represent the ARF corresponding to the minimum BC mass concentration during afternoon hours (1400-1600 hours) and dotted lines represent the ARF corresponding to maximum BC mass concentration during morning peak hours (0600-1000 hours). The continuous lines represent the ARF diurnal variation for mean BC mass concentration. The big dashed lines represent the diurnal background radiative forcing at Mt. Abu where BC mass concentration does not have any diurnal variation.*

by Udaipur and is minimum at Mt. Abu. However, during afternoon hours the BC concentrations over Ahmedabad and Udaipur are comparable to the background BC mass concentration at Mt. Abu (Fig. 4.30). There is large diurnal variation in BC concentration at Ahmedabad and Udaipur and therefore, for comparative study, ARF is calculated for maximum, minimum and average BC at these stations keeping all other aerosol components constant. Fig. 6.4 shows the diurnal variation of aerosol radiative forcings at (a) Ahmedabad and (b) Udaipur due to the large variation of BC mass concentration. Blue, black and red lines represent ARF at TOA, surface and in the atmosphere, respectively. The dashed (small) lines represent the ARF corresponding to the minimum BC mass concentration during afternoon

hours (1400-1600 hours) and dotted lines represent the ARF corresponding to maximum BC mass concentration during morning peak hours (0600-1000 hours). The continuous lines represent the ARF diurnal variation for mean BC mass concentration. The big dashed lines represent the diurnal background radiative forcing at Mt. Abu where BC mass concentration does not have any diurnal variation. During morning BC peak hours (about 1000 hours) and afternoon BC minimum hours (1500 hours) solar zenith angles are comparable and due to the large variation of BC mass concentration the ARF has a large difference as shown in the Fig. 6.4. During the morning hours at Ahmedabad the reduction of surface solar radiation is larger than that during afternoon hours by 48.2 Wm^{-2} as morning BC is a factor of 3 larger than the afternoon BC, whereas at Udaipur this reduction is 37.4 Wm^{-2} as BC reduces only by a factor of 2.

The average diurnal ARF (black line) derived from daily averaged aerosol components would move closer to the diurnal ARF derived for maximum BC concentration (red line) during morning hours and towards the one derived for minimum BC concentration (blue line) during afternoon hours (Fig. 6.4). At Ahmedabad diurnal averaged ARF forcing would have increased during morning hours by 3.0, -19.0 and 12.0 Wm^{-2} at TOA, surface and in the atmosphere, respectively, and at Udaipur by 5.7, -24.0 and 29.0 Wm^{-2}, respectively. During the afternoon hours the decrease would have been 10.0, -29.2 and 40.0 Wm^{-2} at TOA, surface and in the atmosphere, respectively, and at Udaipur by 5.2, -14.0 and 18.3 Wm^{-2}, respectively. Another important result of the present study is that at a semiarid region like Udaipur, the BC particles change ARF at TOA from negative to positive during periods of high BC concentration. The reason is that during background condition dust is dominating and scattering more solar radiation to the TOA and forcing is negative whereas when BC particles are enhanced in the atmosphere, the absorbtion of solar radiation is enhanced and hence the scattered solar radiation reduces at TOA and as a result forcing becomes positive.

The forcing during minimum BC concentration at each of the stations is considered as the background aerosol radiative forcing. The background atmospheric

ARF at Ahmedabad is 43.7 Wm^{-2}, followed by 36.7 Wm^{-2} at Udaipur and 31.4 Wm^{-2} at Mt. Abu. Although the minimum BC concentrations at all the three stations are equivalent the background ARF are not similar. Mt. Abu ARF represents the background forcing in the western part of India as it has a pristine environment. Other anthropogenic aerosols like sulfate, nitrate etc., that are present at Ahmedabad and Udaipur result in increased background ARF. The difference between the Ahmedabad background ARF and that of Mt. Abu ARF is more than a factor of two greater than the difference between those at Udaipur and Mt. Abu.

Another important result of the present study is that at Ahmedabad the background TOA forcing is much higher than the regional background TOA forcing of the region,i.e, at Mt. Abu, whereas at Udaipur the background TOA forcing is comparable to it. However, the background surface forcing at both the stations, Ahmedabad and Udaipur is higher than the regional background surface forcing due to the presence of other anthropogenic aerosols at both the stations. TOA forcing is more dependent on the fraction of radiation scattered into the upward hemisphere relative to the local horizon (*Pilinis et al.*, 1995). The upward scattered radiation mainly depends on the solar zenith angles and the aerosol scattering phase function. *Nemesure et al.* (1995) reported that at the zenith, upward scattered radiation by the bigger particles is low and at the horizon it is independent of particle size. This is due to the fact that at zenith, bigger particles scatter more radiation in the forward direction and hence the fraction of upward radiation reduces whereas at the horizon the upward radiation is also contributed by forward radiation and hence is independent of size of the particles. A diurnal variation is therefore seen in the radiative forcing at TOA but at the surface forcing is primarily governed by the AOD. Udaipur and Mt. Abu have similar amounts of coarser dust particles and as a result the TOA forcing remains same whereas the surface forcing is not similar due to the predominant presence of anthropogenic aerosols other than BC at Udaipur.

Summary and Scope for Future Work

Aerosols are an integral part of the atmosphere and play a vital role in maintaining the radiative balance. Naturally produced aerosols like seasalt and dust are more abundant whereas anthropogenically produced aerosols like Black Carbon (BC) and sulphate are less in concentration. However, the localized and inhomogeneous production of the anthropogenic aerosols perturbs the radiative balance on a regional scale and hence results in climate change. Motivated by this issue the present study is carried out to estimate the contribution of natural and anthropogenic aerosol radiative forcing in urban and pristine environments. To achieve this objective various aerosol properties like columnar AOD spectra, surface aerosol mass concentration, number concentration, BC concentration, absorbtion coefficient, scattering coefficient and single scattering albedo have been measured at Ahmedabad and Mt. Abu during the period starting from January 2006 to December 2007. Based on the meteorological conditions, the two year study period is classified into four main seasons viz, winter (December-March), pre-monsoon (April-May), monsoon (June-August) and post-monsoon (September-November).

Long range transportation of natural as well as anthropogenic aerosols also have been investigated in the present study. The proximity to Thar desert provided an opportunity to study transported dust aerosols during premonsoon at various

locations in western part of India and to estimate their effect on shortwave and longwave radiative forcings. Another study investigated the long range BC transportation from Indo-Gangetic Basin (IGB) to eastern coastal region of southern India during premonsoon. IGB is one of the largest source regions of anthropogenic aerosols over India. During winter these aerosols cause fog in the northern India and result in a large change in the regional radiative forcing. This fog induced radiative forcing is also investigated in the present study.

Important results obtained from these investigations are summarized as follows.

- A large seasonal variation is observed in the aerosol properties at Ahmedabad and Mt. Abu.

- At Ahmedabad columnar AOD (at 0.5μm) is found to be a minimum of 0.27$\pm$0.06 during monsoon and a maximum of 0.41$\pm$0.14 during postmonsoon. During winter and premonsoon AOD values were 0.35$\pm$0.02 and 0.30 $\pm$0.03, respectively. During monsoon rain washout of aerosols keeps the AOD low and during postmonsoon low wind speed increases the AOD by reducing the ventilation of aerosols.

- The surface aerosol mass concentration of different size modes showed a different seasonal variation with respect to AOD. The nucleation aerosol mass concentration showed a maximum during winter whereas the accumulation aerosols maximized during monsoon and coarser aerosols like dust were abundant during premonsoon. Similar variation was also observed in the surface number concentration.

- At Ahmedabad diurnal variation of BC mass concentration showed two sharp peaks during morning and evening hours due to increased traffic and boundary layer height variation.

- BC mass concentration showed a seasonal variation at Ahmedabad. During winter BC mass concentration was a maximum of 4.8$\pm$1.6 μg.m^{-3} and was

a minimum of 1.1±0.1 μg.m^{-3} during monsoon. There was an anomalous increase in BC concentration during November as it was a month of festivals like Diwali.

- The diurnal peak intensity of BC also showed a seasonal variation. A maximum was observed during winter due to large production and low boundary layer height and was minimum during monsoon due to washout by rain and higher boundary layer height.

- At Mt. Abu AOD (at 0.5μm) was a minimum of 0.09±0.03 during winter and a maximum of 0.18±0.05 during postmonsoon. During premonsoon and monsoon AOD was 0.16±0.08 and 0.10±0.02, respectively. In winter, the measurement site is above the boundary layer height and thus AOD was minimum whereas during monsoon, due to high amount of natural aerosols mainly seasalt aerosols and moisture AOD was found to be higher than in winter, in contrast to observations at Ahmedabad.

- At Mt. Abu the surface aerosol mass concentration also showed a different seasonal variation in comparison to Ahmedabad. Nucleation and accumulation aerosols mass was maximum during postmonsoon whereas coarse aerosol mass was maximum during premonsoon.

- There are no peaks in the diurnal variation of BC mass concentration in any of the seasons over Mt. Abu. However, BC mass concentration was enhanced during day time as the BC produced at the foothill area reaches the hilltop due to strong thermal convection.

- An enhancement in the coarse mode aerosols was observed at Ahmedabad and Udaipur during April 2007. This is a signature of increase in dust aerosols at these locations during the observation period.

- One prominent peak was observed in diurnal variation of BC concentration at Udaipur, whereas two peaks were observed at Ahmedabad and Mt. Abu did not show any prominent peaks.

- During dust prone season the angstrom exponent of the arid region, Udaipur, is close to zero and very low in urban and pristine regions due to high abundance of coarser dust particles in the atmosphere. Surface aerosol mass concentration also showed a large enhancement of coarser aerosols in all these three regions during this season.

- In the eastern coastal region at Kalpakkam, columnar AOD decreased as the day progressed in contrast to the diurnal variation of AOD at Ahmedabad and Mt. Abu. At the eastern coastal region this anomalous result has been observed because the coastal region has an experience of different breeze conditions, namely land and sea breeze.

- During premonsoon the results obtained from back-trajectory analyses show that wind is coming to the measurement site from 1) central Bay of Bengal (central BoB) 2) Indo-Gangetic Basin via Bay of Bengal (IGB) and 3) Arabian Sea via North Indian Ocean.

- Wind carried large amount of BC form Indo-Gangetic Basin to eastern coast of India via Bay of Bengal (BoB) and hence background BC increased by a factor of 1.6 and columnar AOD increased from 0.27 to 0.32.

- During winter the visible aerosol optical depth was relatively low at 0.3 prior to foggy days, which however increased up to 0.86 during foggy days at Hissar in the Indo-Gangetic basin.

- The fog event is also found to alter the aerosol size distribution by enhancing the hygroscopic accumulation mode aerosols at Hissar.

- Over Hissar top of the atmosphere forcing is found to increase during foggy days due to large backscattering of radiation back to space.

- During foggy days RH value decreases as the day progresses. This reduces the aerosol radiative forcing while the increasing solar elevation increases the forcing value. Thus the fog event which prolongs longer into the daytime

has a stronger effect on the diurnally averaged aerosol radiative forcing than those events which are confined to early morning hours only.

- OPAC model derived single scattering albedo (SSA) shows large variation at Ahmedabad and Mt. Abu. During monsoon SSA is maximum at 0.86$\pm$0.04 whereas during postmonsoon SSA is minimum at 0.80$\pm$0.09. At Mt. Abu SSA is observed to be larger than that at Ahmedabad. At Mt. Abu model shows a large value of 0.90$\pm$0.03 and 0.90$\pm$0.02 during winter and postmonsoon, respectively, due to less abundance of aerosols and a minimum of 0.83$\pm$0.01 during postmonsoon due to enhancement of anthropogenic activities.

- The aerosol radiative forcing for different seasons are computed using SBDART code. The top of atmosphere (TOA) aerosol forcing shows a large variation. One of the reasons is the large seasonal variation of surface reflectivity at Ahmedabad and Mt. Abu. During premonsoon the surface reflectivity is more at Mt. Abu than that at Ahmedabad as most of the area at hilltop is bare whereas the reflectivity during postmonsoon is less due to larger area of greenery.

- Over Ahmedabad there is a large variation of aerosols loaded into the atmosphere due to both natural and anthropogenic sources and hence there is a large variation of radiative forcing. During monsoon the atmospheric forcing is a minimum of 27 Wm^{-2} due to wash out of aerosols from the atmosphere by rain and a maximum of 49 Wm^{-2} during premonsoon due to the large transportation of dust particles from 'Thar Desert'.

- Over Ahmedabad the atmospheric anthropogenic forcing is almost same and dominating the natural forcing during all seasons except monsoon. During

monsoon anthropogenic forcing is minimum and natural forcing is dominating. The atmospheric natural forcing shows a large seasonal variation. During premonsoon and monsoon the natural forcing is large due to the transportation of dust and seasalt aerosols, respectively.

- Over Mt. Abu both the natural and anthropogenic atmospheric forcings show large seasonal variation. During winter both the forcings are minimum as the measurement site is above the boundary layer. During premonsoon both the forcings show large values. Due to the enhancement of local tourist activity the anthropogenic forcing is enhanced and large transportation of dust aerosols increases the natural forcing.

- At Mt. Abu mainly natural forcing is dominating during premonsoon and monsoon whereas anthropogenic and natural forcing have equivalent contribution to the total forcing during winter and postmonsoon.

- Mt. Abu has a factor of four times less atmospheric radiative forcing and a factor of two times less natural forcing than that of Ahmedabad.

- Ahmedabad has a maximum diurnal variation of radiative forcing due to BC, followed by Udaipur and minimum at Mt Abu during premonsoon.

- The background aerosol radiative forcing is higher at Ahmedabad than that at Udaipur due to the presence of more anthropogenic aerosols over Ahmedabad.

- In the eastern coastal region diurnal BC variation due to land and sea breezes causes a large diurnal radiative forcing change. During land breeze the surface aerosol forcing is enhanced by factor of two whereas the atmospheric forcing is enhanced by a factor of three.

- The long range transportation of BC from Indo-Gangetic Basin enhances the coastal background radiative forcing by 40% during sea breeze.

The present study in the western part of India shows that during premonsoon and monsoon natural dust and seasalt aerosols are dominating, respectively, whereas during postmonsoon anthropogenic aerosols are dominating. However, these anthropogenic aerosols are not uniformly distributed over this region and recent times have seen the increase of these aerosols due to increased anthropogenic activities. Therefore, the inhomogeneous seasonal and spatial distribution of anthropogenic aerosols produce a large variation of surface and atmospheric radiative forcing. In addition, there is also a large seasonal and spatial variation of surface reflectivity which has a large impact on the TOA radiative forcing. These changes in the radiative forcing affect the regional scale atmospheric dynamics and consequently thermal convection, temperature structure, etc. In addition, aerosols have a major role in the cloud formation and precipitation. Aerosol modified cloud can have a large impact on the radiation budget and most importantly unforeseen changes in the rainfall have a direct effect on the economy of a country like India. It is therefore very important to understand the atmospheric aerosol forcing over different parts of India. Continued ground- and satellite-based observations coupled with modelling studies are necessary to fully understand the consequences of aerosol radiative forcing on the regional scale climate change over the Indian continent.

References

Acharya, Y. B., and A. Jayaraman (1995), Sun-photometry using photodiode open circuit voltage measurements, *Review Sci. Instruments*, *66*, 4087 – 4090.

Ackerman, A. S., O. B. Toon, D. E. Stevens, A. J. Heymsfield, V. Ramanathan, and E. J. Welton (2000), Reduction of tropical cloudiness by soot, *Science*, *288*, 1042–1047.

Anderson, L. T., et al. (1996), Performace Characteristics of a High-Sensitivity, Three-wavelength, Total Scaterring/Backscatter Nephelometer, *Journal of Atmospheric and Oceanic Technology*, *13*, 967–986.

Andreae, M. O. (1995), Climate effect of changing atmospheric aerosol levels in: Henderson-Sellers and A. (Ed.) and World Survey of Climatology, *Future Climates of the World and Elsevier and New York*, *16*, 341–392.

Andreae, M. O., and A. Gelencser (2006), Black carbon or brown carbon? The nature of light-absorbing carbonaceous aerosols, *Atmospheric Chemistry and Physics*, *6*, 31313148.

Andreae, M. O., C. D. Jones, and P. M. Cox (2005), Strong present-day aerosol cooling implies a hot future, *Nature*, *435*, 1187–1190, doi:10.1038/nature03671.

Arimoto, R. (2001), Eolian dust and climate: relationships to sources, tropospheric chemistry, transport and deposition, *Earth-Science Reviews*, *54 (1-3)*, 29–42.

Babu, S. S., S. K. Satheesh, and K. K. Moorthy (2002), Aerosol radiative forcing due to enhanced black carbon at an urban site in india, *Geophysical Research Letters*, *29(18)*, 1880, doi:10.1029/2002GL015826.

Bates, T., V. Kapustin, P. Quinn, D. Covert, D. Coffman, C. Mari, P. Durkee, W. D. Bruyn, and E. Saltzman (1998), Processes controlling the distribution of aerosol particles in the lower marine boundary layer during the First Aerosol Characterization Experiment (ACE 1), *J. Geophy. Res.*, *103(D13)*, 16,369–16,383.

Bates, T. S. (1999), Preface to special section: First Aerosol Characterization Experiment (ACE-1), Part 2, *J. Geophy. Res.*, *104*, 21,645.

Bates, T. S., D. J. Coffman, D. J., D. S. Covert., and P. K. Quinn (2002), Regional marine boundary layer aerosol distributions in the India, Atlantic, and Pacific Oceans: A comparison of INDOEX measurements with ACE-1, ACE-2, and Aerosols99, *J. Geophy. Res.*, *107(D19)*, 8026, doi:10.1029/2001JD001174.

Bergstrom, R. W., P. B. Russell, and P. Hignett (2002), Wavelength Dependence of the Absorption of Black Carbon Particles: Predictions and Results from the TARFOX Experiment and Implications for the Aerosol Single Scattering Albedo, *American Meteorological Society*, *59*, 567–577.

Birmili, W., and A. Wiedensohler (2000), New particle formation in the continental boundary layer: Meteorological and gas phase parameter influence, *Geophysical Research Letters*, *27*, 3325–3328.

Blanchard, D. C., and A. H. Wookcock (1980), The production, concentration and vertical distribution of the sea-salt aerosols., *Annals of the NewYork Academy of Sciences*, *338*, 330–347.

Bodhaine, B. A. (1995), Aerosol absorption measurements at Barrow and Mauna Loa and the South Pole, *J. Geophy. Res.*, *100*, 8967– 8975.

Bond, T. C. (2001), Spectral dependence of visible light absorption by carbonaceous particles emitted from coal combustion, *Geophysical Research Letters*, *28*, 4075–4078.

Bond, T. C., and R. W. Bergstrom (2006), Light Absorption by Carbonaceous Particles: An Investigative Review, *Aerosol Science and Technology*, *40*, 27–67, doi:10.1080/02786820500421521.

Boucher, O., M. Pham, and R. Sadourny (1998), General circulation model simulations of the indian summer monsoon with increasing levels of sulfate aerosols, *Ann. Geophys.*, *16*, 346–352.

Cachorro, V. E., R. Vergaz, and A. M. de Frutos (2001), A quantitative comparison of α-Angstrom turbidity parameter retrieved in different spectral ranges based on spectroradiometer solar radiation measurements, *Atmos. Environ.*, *35*, 5117–5124.

Charlson, R. J., N. C. Ahlquist, and H. Horvath (1968), On the generality of correlation of atmospheric aerosol mass concentration and light scatter, *Atmospheric Envirnment*, *2*, 455–464.

Charlson, R. J., J. Langner, H. Rodhe, C. B. Leovy, and S. G. Warren (1991), Perturbation of the northern hemisphere radiative balance by backscattering from anthropogenic sulphate aerosols, *Tellus*, *43AB*, 152–163.

Charlson, R. J., S. E. Schwartz, J. M. Hales, R. D. Cess, J. A. Coakley, J. E. Hansen, and D. J. Hoffmann (1992), Climate forcing by anthropogenic aerosols, *Science*, *255*, 423–430.

Chiapello, I., P. Goloub, D. Tanre, M. Marchand, J. Hermann, and O. Torres (2000), Aerosol detection by TOMS and POLDER over oceanic region, *J. Geophy. Res.*, *105*, 7133–7142.

Chin, M., et al. (2003), A global aerosol model forecast for the ACE-Asia field experiment, *J. Geophy. Res.*, *108(D23)*, 8654, doi:10.1029/2003JD003642.

Christopher, S. A., and J. Wang (2004), Intercomparison between MISR and Sunphotometer AOT in Dust Source Regions over China: Implication for satellite retrievals and radiative forcing calculations, *Tellus Ser. B*, *56(5)*, 451–456, doi: 10.1111/j.1600-0889.2004.00120.x.

Christopher, S. A., X. Li, R. M. Welch, J. S. Reid, P. V. Hobbs, T. F. Eck, and B. Holben (2000), Estimation of Surface and Top-of-Atmosphere Shortwave Irradiance in Biomass-Burning Regions during SCAR-B, *J. Appl. Meteo.*, *39*, 1742–1753.

Christopher, S. A., J. Wang, Q. Ji, and S.-C. Tsay (2003), Estimation of diurnal shortwave dust aerosol radiative forcing during PRIDE, *J. Geophy. Res.*, *108 (D19)*, 8596, doi:10.1029/2002JD002787.

Chung, C. E., and G. J. Zhang (2004), Impact of absorbing aerosol on precipitation: Dynamic aspects in association with convective available potential energy and convective parametrization closure and dependence on aerosol heating profile, *J. Geophys. Res.*, *109*, D22,103, doi:10.1029/2004JD004726.

Chung, C. E., V. Ramanathan, D. Kim, and I. A. Podgorny (2005), Global anthropogenic aerosol direct forcing derived from satellite and ground-based observations, *J. Geophy. Res.*, *110*, D24,207, doi:10.1029/2005JD006356.

Chýlek, P., V. Ramaswamy, and V. Srivastava (1984), Graphitic carbon content of aerosols, clouds and snow and its climatic implications, *The Science of the Total Environment*, *36*, 117–120.

Clarke, A., V. Kapustin, S. Howell, K. Moore, B. Lienert, S. Masonis, T. Anderson, and D. Covert (2003), Sea-salt size distributions from breaking waves: Implications for marine aerosol production and optical extinction measurements during SEAS, *J. Atmos. Oceanic Technol*, *20*, 1362–1374.

Clarke, A. D., J. N. Porter, F. P. J. Valero, and P. Pilewskie (1996), Vertical profiles, aerosol microphysics, and optical closure during the Atlantic Stratocumulus Transition Experiment: measured and modelled column optical properties, *J. Geophy. Res.*, *101*, 4443–4453.

Coakley, J. A., and R. D. Cess (1985), Response of the NCAR Community Climate Model to the radiative forcing by the naturally-occurring tropospheric aerosol, *J. Atmos. Sci.*, *42*, 1677–1692.

Coakley, J. J. A., R. D. Cess, and F. B. Yurevich (1983), The effect of tropospheric aerosols on the earths radiation budget: a parameterisation for climate models, *J. Atmos. Sci.*, *40*, 116–138.

d'Almeida, G. A., P. Koepke, and E. P. Shettle (1991), *Atmospheric Aerosols: Global Climatology and Radiative Characteristics*, 559 pp., A. Deepak, Hampton, Va.

Deepshikha, S., S. K. Satheesh, and J. Srinivasan (2005), Regional distribution of absorbing efficiency of dust aerosols over India and adjacent continents inferred using satellite remote sensing, *J. Geophy. Res.*, *32*, L03,811, doi:10.1029/2004GL022091.

Deepshikha, S., S. K. Satheesh, and J. Srinivasan (2006a), Dust aerosols over india and adjacent continents retrieved using METEOSAT infrared radiance Part I: sources and regional distribution, *Ann. Geophys.*, *24*, 37–61.

Deepshikha, S., S. K. Satheesh, and J. Srinivasan (2006b), Dust aerosols over india and adjacent continents retrieved using METEOSAT infrared radiance Part ii: quantification of wind dependence and estimation of radiative forcing, *Ann. Geophys.*, *24*, 6379.

Dey, S., S. N. Tripathi, R. P. Singh, and B. N. Holben (2004), Influence of dust storms on the aerosol optical properties over the Indo-Gangetic basin, *J. Geophy. Res.*, *109*, D20,211.

Dickerson, R. R., S. Kondragunta, G. Stenchikov, K. L. Civerolo, B. G. Doddridge, and B. N. Holben (1997), The impact of aerosols on solar ultraviolet radiation and photochemical smog, *Science*, *278*, 827–830.

Draxler, R. R., and G. D. Hess (1998), An overview of the Hysplit_4 Modeling System for Trajectories, Dispersion, and Deposition, *Aust. Met. Mag.*, *47*, 295–308.

Eck, T. F., B. N. Holben, J. S. Reid, O. Dubovik, A. Smirnov, N. T. O'Neill, I. Slutsker, and S. Kinne (1999), Wavelength dependence of the optical depth of biomass burning, urban, and desert dust aerosols, *J. Geophy. Res.*, *104(D24)*, 31,333–31,349.

Gadhavi, H. (2005), Experimental investigation of aerosol properties and modelling of its impact on radiation budget, Ph.D. thesis, Gujarat University.

Ganguly, D., and A. Jayaraman (2006), Physical and optical properties of aerosols over an urban location in western India: Implications for shortwave radiative forcing, *J. Geophy. Res.*, *111*, D24,207, doi:10.1029/2006JD007393.

Ganguly, D., A. Jayaraman, H. Gadhavi, and T. A. Rajesh (2005), Features in wavelength dependence of aerosol absorption observed over central India, *Geophysical Research Letters*, *32*, L13,821, doi:10.1029/2005GL023023.

Ganguly, D., A. Jayaraman, and H. Gadhavi (2006a), Physical and optical properties of aerosols over an urban location in western India: Seasonal variabilities, *J. Geophy. Res.*, *111*, D24,206, doi:10.1029/2006JD007392.

Ganguly, D., A. Jayaraman, T. A. Rajesh, and H. Gadhavi (2006b), Wintertime aerosol properties during foggy and non foggy days over urban center Delhi and their implications for shortwave radiative forcing, *J. Geophys. Res.*, *111*, D15,217 and doi:10.1029/2005JD007,029.

Ginoux, P., J. M. Prospero, O. Torres, and M. Chin (2004), Long-term simulation of dust distribution with the GOCART model: correlation with the North Atlantic oscillation, *Environmental Modeling and Software*, *19*, 113–128.

Graf, H. F. (2004), The complex interaction of aerosols and clouds, *Science*, *303*, 1309–1311.

Griffiths, F. B., T. Bates, P. Quinn, L. Clementson, and J. Parslow (1999), Oceanographic context of the First Aerosol Characterization Experiment (ACE 1): A physical, chemical, and biological overview, *J. Geophy. Res.*, *104(D17)*, 21,649 21,671.

Gupta, P., S. A. Christophera, J. Wangb, R. Gehrigc, Y. Leed, and N. Kumar (2006), Satellite remote sensing of particulate matter and air quality assessment over global cities, *Atmos. Environ.*, *40*, 5880–5892.

Hainsworth, A. H. W., A. L. Dick, and J. L. Gras (1998), Climatic context of the First Aerosol Characterization Experiment (ACE 1): A meteorological and chemical overview, *J. Geophy. Res.*, *103(D13)*, 16,319 16,340.

Hansen, A. D. A., H. Rosen, and T. Novakov (1982), Real-time measurement of the absorption coefficient of aerosol particles, *Appl. Opt.*, *21*, 3060–3062.

Hansen, A. D. A., H. Rosen, and T. Novakov (1984), The aethalometer - an instrument for the real-time measurement of optical absorption by aerosol particles, *Sci. Total Environ.*, *36*, 191–196.

Hansen, J. E. (1969), Exact and approximate solutions for multiple scattering by cloudy and hazy planetary atmospheres, *J. Atmos. Sci.*, *26*, 478–487.

Haywood, J., and O. Boucher (2000), Estimates of the direct and indirect radiative forcing due to troposheric aerosos: A Review, *Reviews of Geophysics*, *38*, 513–543.

Haywood, J., et al. (2003), Radiative properties and direct radiative effect of Saharan dust measured by the C-130 aircraft during SHADE. 1.Solar spectrum, *J. Geophy. Res.*, *108 (D18)*, 8577.

Haywood, J. M., and V. Ramaswamy (1998), Global sensitivity studies of the direct radiative forcing due to anthropogenic sulfate and black carbon aerosols, *J. Geophy. Res.*, *103 (D3)*, 6043–6058.

Haywood, J. M., and K. P. Shine (1995), The eect of anthropogenic sulfate and soot aerosol on the clear sky planetary radiation budget, *Geophysical Research Letters*, *22*, 603–606.

Hegg, D. A., J. Livingston, P. Hobbs, T. Novakov, and P. Russell (1997), Chemical apportionment and aerosol column optical depths off the mid-atlantic coast of the united states, *J. Geophy. Res.*, *102*, 25,293–25,303.

Herman, J. R., P. K. Bhartia, O. Torres, N. C. Hsu, C. J. Seftor, and E. Celarier (1997), Global distribution of uv-absorbing aerosols from Nimbus-7/TOMS data, *J. Geophy. Res.*, *102*, 16,91116,922.

Hess, M., P. Keopke, and I. Schult (1998), Optical properties of aerosols and clouds: The software package OPAC, *Bull. Am. Meteorol. Soc.*, *79*, 831–844.

Holben, B. N., et al. (1998), AERONET-A federated instrument network and data archive for aerosol characterization, *Remote Sens. Environ.*, *66*, 1–16.

Houghton, J. T., L. G. M. Filho, J. P. Bruce, H. Lee, B. A. Callander, and E. F. Haites (1995), Climate change 1994: Radiative Forcing of Climate Change and an Evaluation of the IPCC, *Cambridge University Press*, p. 347.

Houghton, J. T., L. G. Filho, B. A. Callander, N. Harrish, A. Kattenburg, and K. Maskell (1996), *Climate Change 1995. The Science of Climate Change*, Cambridge Univ. Press., New York.

Hsu, N. C., J. R. Herman, O. Torres, B. N. Holben, D. Tanre, T. F. Eck, A. Smirnov, B. Chatenet, and F. Lavenu (1999), Comparisons of the TOMS aerosol index with Sun photometer aerosol optical thickness: Results and applications, *J. Geophy. Res.*, *104*, 62696279.

Hsu, N. C., J. R. Herman, and C. Weaver (2000), Determination of radiative forcing of Saharan dust using combined TOMS and ERBE data, *J. Geophy. Res.*, *105*, 20,649 20,661.

Huebert, B. J., T. Bates, P. B. Russell, G. Shi, Y. J. Kim, K. Kawamura, G. Carmichael, and T. Nakajima (2003), An overview of ace-asia: Strategies for quantifying the relationships between asian aerosols and their climatic impacts, *J. Geophy. Res.*, *108(D23)*, 8633, doi:10.1029/2003JD003550.

Ichoku, C., et al. (2002), Analysis of the performance characteristics of the five-channel Microtops ii sun photometer for measuring aerosol optical thickness and precipitable water vapor, *J. Geophy. Res.*, *107 (D13)*, doi:10.1029/2001JD001302.

IPCC (2007), Intergovernmental Panel on Climate Change. 2007.Climate Change 2007: The Physical Science Basis. Contribution of Working Group I to the Fourth Assessment Report of the Intergovernmental Panel on Climate Change., New York: Cambridge University Press.

Jacobson, M. J. (2000), A physical-based treatment of elemental carbon optics: Implications for global direct forcing of aerosols, *Geophysical Research Letters*, *27*, 217–220.

Jacobson, M. Z. (2001), Strong radiative heating due to the mixing state of black carbon in atmospheric aerosols, *Nature*, *409*, 695–697.

Jaenicke, R. (1993), *Tropospheric aerosols, in Aerosol-Cloud-Climate Interactions*, 1 31 pp., Elsevier, New York.

Jayaraman, A., and B. H. Subbaraya (1993), In situ measurements of aerosol extinction profiles and their spectral dependencies at tropospheric levels, *Tellus B*, *45*, 473–478.

Jayaraman, A., S. Ramachandran, Y. B. Acharya, and H. B. Subbaraya (1995), Pinatubo volcanic aerosol layer decay observed at Ahmedabad (23°N), India, using neodymium:yttrium/aluminium/garnet backscatter lidar, *J. Geophy. Res.*, *100(D11)*, 23,209–23,214.

Jayaraman, A., D. Lubin, S. Ramachandran, V. Ramanathan, E. Woodbridge, W. D. Collins, and K. S. Zalpuri (1998), Direct observation of aerosol radiative forcing over the tropical Indian Ocean during the January-February 1996 pre-INDOEX cruise., *J. Geophy. Res.*, *103 (D12)*, 13,827–13,836.

Jayaraman, A., H. Gadhavi, D. Ganguly, A. Misra, S. Ramachandran, and T. A. Rajesh (2006), Spatial variations in aerosol characteristics and regional radiative forcing over India: Measurements and modeling of 2004 road campaign experiment, *Atmospheric Environment*, *40*, 6504–6515.

Jethva, H., S. K. Satheesh, and J. Srinivasan (2005), Seasonal variability of aerosols over the indo-gangetic basin, *J. Geophy. Res.*, *110*, D21,204, doi:10.1029/2005JD005938.

Jones, A., and A. Slingo (1996), Predicting cloud-droplet effective radius and indirect sulphate aerosol forcing using a general circulation model, *Quart. J. R. Met. Soc.*, *122*, 1573–1595.

Kiehl, J. T., and H. Rodhe (1995), *Modeling geographical and seasonal forcing due to aerosols in Aerosol Forcing of Climate*, 281-296 pp., Wiley, New York.

Kiehl, T. J., and B. P. Briegleb (1993), The radiative roles of sulphate aerosols and greenhouse gases in climate forcing, *Science*, *260*, 311–314.

Kirchstetter, T. W., T. Novakov, and P. V. Hobbs (2004), Evidence that the spectral dependence of light absorption by aerosols is affected by organic carbon, *J. Geophy. Res.*, *109*, D21,208, doi:10.1029/2004JD004999.

Koepke, P., M. Hess, I. Schult, and E. P. Shettle (1997), Global aerosol data set. mpi meteorologie hamburg report no. 243, p. 44.

Kondratyev, K. Y. (1969), *Radiation in the Atmosphere*, 912 pp pp., Academic Press.

Koponen, I. K., A. Virkkula, R. Hillamo, V. M. Kerminen, and M. Kulumala (2003), Number size distributions and concentrations of continental summer aerosols

in Queen Maud Land, Antarctica, *J. Geophy. Res.*, *108(D18)*, 4587, doi:10.1029/2003JD003614.

Krishnan, P., and P. K. Kunhikrishnan (2004), Temporal variations of ventilation coefficient at a tropical indian station using uhf wind profiler, *Current Science*, *86(3)*, 477–451.

Krishnan, R., and V. Ramanathan (2002), Evidence of surface cooling from absorbing aerosols, *Geophysical Research Letters*, *29*(9 and 1340), doi:10.1029/2002GL014687.

Lavanchy, V. M. H., H. W. Gäggeler, S. Nyeki, and U. Baltensperger (1999), Elemental carbon (EC) and black carbon (BC) measurements with a thermal method and an aethalometer at the high-alpine research station Jungfraujoch, *Atmos. Environ.*, *33(17)*, 2759–2769.

Lelieveld, J., et al. (2001), The Indian Ocean Experiment: Widespread Air Pollution from South and Southeast Asia, *Science*, *291*, 1031–1036.

Liepert, G. G., J. Feichter, U. Lohmann, and E. Roeckner (2004), Can aerosols spin down the water cycle in a warmer and moister world?, *Geophys. Res. Lett.*, *31*, L06,207, doi:10.1029/2003GL019060.

Lindberg, J. D. (1993), Carbon and the optical properties of atmospheric dust, *Appl. Opt.*, *32*, 60776081.

Liousse, C., H. Cachier, and S. G. Jennings (1993), Optical and thermal measurements of black carbon aerosol content in different environments: Variation of the specific attenuation cross-section, sigma (s), *Atmos. Environ.*, *27A*, 1203–1211.

Liu, M., and D. L. Westphal (2001), A study of the sensitivity of simulated mineral dust production to model resolution, *J. Geophy. Res.*, *106,D16*, 18,099 18,112.

Lohmann, U., and J. Feichter (2005), Global indirect aerosol effects: a review, *Atmos. Chem. and Phys.*, *5*, 715–737.

Lohmann, U., and G. Lesins (2002), Stronger constraints on the anthropogenic indirect aerosol effect, *Science*, *298*, 1012–1015.

Lubin, D., S. K. Satheesh, and G. M. A. J. Heymsfeild (2002), Longwave radiative forcing of Indian Ocean tropospheric aerosol, *J. Geophy. Res.*, *107(D19)*, doi:10.1029/2001JD001183.

McMurry, P. H., X. Zhang, and C. Lee (1996), Issues in aerosol measurement for optics assessments, *J. Geophy. Res.*, *101*, 19,189–19,197.

Menon, S., J. Hansen, L. Nazarenko, and Y. Luo (2002), Climate effects of black carbon aerosols in China and India, *Science*, *297*, 2250–2253.

Moorthy, K. K., S. S. Babu, S. K. Satheesh, J. Srinivasan, and C. B. S. Dutt (2007), Dust absorption over the Great Indian Desert inferred using ground-based and satellite remote sensing, *J. Geophy. Res.*, *112*, D09,206, doi:10.1029/2006JD007690.

Morys, M., F. M. M. III, S. Hagerup, S. E. Anderson, A. Baker, J. Kia, and T. Walkup (2001), Design and calibration and and performance of MICROTOPS II handheld ozone monitor and Sun photometer, *J. Geophy. Res.*, *106 (D3)*, 14,573–14,582.

Myhre, G., E. Highwood, K. Shine, and F. Stordal (1998), Newestimates of radiative forcing due to well mixed greenhouse gases, *Geophysical Research Letters*, *25(14)*, 2715–2718.

Nair, V. S., et al. (2007), Wintertime aerosol characteristics over the Indo-Gangetic Plain (IGP): Impacts of local boundary layer processes and long-range transport, *J. Geophy. Res.*, *112*, D13,205, doi:10.1029/2006JD008099.

Nakajima, T., M. Tanaka, M. Yamano, M. Shiobara, K. Arao, and Y. Nakanishi (1989), Aerosol optical characteristics in the yellow sand events observed in May, 1982 at Nagasaki, part 2, Models, *J. Meteorol. Soc. Jpn*, *67*, 279–291.

Nemesure, S., R. Wagner, and S. E. Schwartz (1995), Direct shortwave forcing of climate by the anthropogenic sulfate aerosol: Sensitivity to particle size, composition, and relative humidity, *J. Geophy. Res.*, *100(D2)*, 26,105– 26,116.

Nicolet, M. (1984), On the molecular scattering in the terrestrial atmosphere: An emperical formula for its calculation in the homosphere, *Planet. Space Sci.*, *32*, 1467 – 1468,.

Nobre, C. A., L. F. Mottes, C. P. Dereczynski, T. A. Tarasova, and I. V. Trosnikov (1998), Overview of atmospheric conditions during Smokes, Clouds and Radiation-Brazil (SCAR-B) field experiment, *J. Geophy. Res.*, *103*, 31,809–31,820.

Novakov, T., M. O. Andreae, R. Gabriel, T. W. Kirchstetter, O. L. Mayol-Bracero, and V. Ramanathan (2000), Origin of carbonaceous aerosols over the tropical Indian Ocean: Biomass burning or fossil fue, *Geophysical Research Letters*, *27(4)*, 4061–4064.

Pandis, S. N., and J. H. Seinfield (1990), The smog-fog-smog cycle and acid deposition, *J. Geophy. Res.*, *95*, 18,489–18,500.

Pandithurai, G., S. Dipu, K. K. Dani, S. Tiwari, D. S. Bisht, P. C. S. Devara, and R. T. Pinker (2008), Aerosol radiative forcing during dust events over New Delhi, India, *J. Geophy. Res.*, *113*, D13,209, doi:10.1029/2008JD009804.

Pant, P., P. Hegde, U. C. Dumka, R. Sagar, S. K. Satheesh, K. K. Moorthy, A. Saha, and M. K. Srivastava (2006), Aerosol characteristics at a high-altitude location in central Himalayas: Optical properties and radiative forcing, *J. Geophy. Res.*, *111*, D17,206, doi:111,D17206,doi:10.1029/2005JD006768,2006.

Parungo, F., C. Nagamoto, M. Y. Zhou, A. D. A. Hansen, and J. Harris (1994), Aeolian transport of aerosol black carbon from China to the ocean, *Atmos. Environ.*, *28*, 3251 3260.

Penner, J. E., et al. (1994), Quantifying and minimizing uncertainty of climate forcing by anthropogenic aerosols, *Bull. Am. Meteorol. Soc.*, *75*, 375400.

Petzold, A., and R. Niessner (1995), Method comparison study on soot-selective techniques, *Mikrochimica Acta*, *117*, 215–237.

Petzold, A., C. Kopp, and R. Niessner (1997), The dependence of the specific attenuation cross-section on black carbon mass fraction and particle size, *Atmos. Environ.*, *31(5)*, 661–672.

Pierluissi, J. H., and G. S. Peng (1985), New molecular transmission band models for LOWTRAN, *Opt. Eng.*, *24(3)*, 541–547.

Pilinis, C., S. N. Pandis, and J. H. Seinfeld (1995), Sensitivity of direct climate forcing by atmospheric aerosols to aerosol size and composition, *J. Geophy. Res.*, *100(D9)*, 18,739–18,754.

Podgorny, I. A., and V. Ramanathan (2001), A modeling study of the direct effect of aerosols over the tropical Indian Ocean, *J. Geophy. Res.*, *106(D20)*, 24,09724,105.

Porter, J. N., and A. D. Clarke (1997), Aerosol size distribution models based on in situ measurements, *J. Geophy. Res.*, *102*, 6035–6045.

Prospero, J. M., R. A. Glaccum, and R. T. Nees (1981), Atmospheric transport of soil dust from Africa to South America, *Nature*, *289*, 570–572.

Prospero, J. M., P. Ginoux, O. Torres, S. E. Nicholson, and T. E. Gill (2002), Environmental characterization of global sou7rces of atmospheric soil dust identified with the nimbus 7 total ozone mapping spectrometer (TOMS) absorbing aerosol product, *Rev. Geophys.*, *40(1)*, 1002, doi:10.1029/2000RG000095.

Quinn, P. K., and D. Coffman (1998), Local closure during the First Aerosol Characterization Experiment (ACE 1): Aerosol mass concentration and scattering and backscattering coefficients, *J. Geophy. Res.*, *103*, 15,575–15,596.

Raes, F., T. Bates, F. McGovern, and M. van Liedekerke (2000), The second Aerosol Characterization Experiment: General overview and main results, *Tellus*, *52*, 111–125.

Ramachandran, S. (2005), Aerosol radiative forcing over Bay of Bengal and Chennai: Comparison with maritime, continental, and urban aerosol models, *J. Geophy. Res.*, *110*, D21,206, doi:10.1029/2005JD005861.

Ramachandran, S., and A. Jayaraman (2002), Premonsoon aerosol mass loadings and size distributions over the Arabian Sea and the tropical Indian Ocean, *J. Geophy. Res.*, *107(D24)*, 4738, doi:10.1029/2002JD002386.

Ramachandran, S., and A. Jayaraman (2003), Spectral aerosol optical depths over Bay of Bengal and Chennai: Imeasurements, *Atmospheric Environment*, *37*, 1941–1949.

Ramachandran, S., and T. A. Rajesh (2007), Black carbon aerosol mass concentrations over Ahmedabad, an urban location in western India: Comparison with urban sites in Asia, Europe, Canada, and the United States, *J. Geophy. Res.*, *112, D06211*, doi:10.1029/2006JD007488.

Ramachandran, S., R. Rengarajan, A. Jayaraman, M. M. Sarin, and S. K. Das (2006), Aerosol radiative forcing during clear, hazy, and foggy conditions over a continental polluted location in north India, *J. Geophy. Res.*, *111*, D20,214, doi: 10.1029/2006JD007142.

Ramana, M. V., V. Ramanathan, I. A. Podgorny, B. B. Pradhan, and B. Shrestha (2004), The direct observations of large aerosol radiative forcing in the Himalayan region, *J. Geophy. Res.*, *31*, L05,111, doi:10.1029/2003GL018824.

Ramanathan, V., R. D. Cess, E. F. Harison, P. Minnis, B. R. Barkstrom, E. Ahmed, and D. Hartmann (1989), Cloud-Radiative Forcing and Climate: Results from the Earth Radiation Budget Experiment, *Science*, *243*, 57–63.

Ramanathan, V., P. J. Crutzen, J. T. Kiehl, and D. Rosenfeld (2001a), Aerosols, climate and the hydrological cycle, *Science*, *294*, 2119–2124.

Ramanathan, V., et al. (2001b), Indian ocean experiment: An integrated analysis of the climate forcing and effects of the great Indo-Asian haze, *J. Geophy. Res.*, *106*, 28,371–28,398.

Ramaswamy, V. (2002), *Infrared radiation, in Encyclopedia of Global Environmental Change*, vol. vol. I, 470-475 pp., John Wiley.

Rastogi, N., and M. M. Sarin (2005a), Long-term characterization of ionic species in aerosols from urban and high-altitude sites in western India: Role of mineral dust and anthropogenic sources, *Atmospheric Environment*, *39*, 55415554.

Rastogi, N., and M. M. Sarin (2005b), Chemical characteristics of individual rain events from a semi-arid region in India: Three-year study, *Atmos. Environ.*, *39*, 3313–3323.

Reeves, R. G., A. Anson, and D. L. Eds (1975), *Manual of Remote Sensing*, 2144 pp pp., Amer. Soc. Photogrammetry.

Reid, J. S., T. F. Eck, S. A. Christopher, P. V. Hobbs, and B. N. Holben (1999), Use of the angstrom exponent to estimate the variability of optical and physical properties of aging smoke particles in brazil and, *J. Geophy. Res.*, *104*, 473–489.

Ricchiazzi, P., S. Yang, C. Gautier, and D. Sowle (1998), SBDART, A research and teaching tool for plane-parallel radiative transfer in the Earths atmosphere, *Bull. Am. Meteorol. Soc.*, *79*, 2101–2114.

Russel, P. B., P. V. Hobbs, and L. L. Stowe (1999), Aerosol properties and radiative effect in the United States east coast haze plume: An overview of the Tropospheric Aerosol Radiative Forcing Observational Experiments (TARFOX), *jgr*, *104*, 2213–2222.

Russell, P. B., and J. Heintzenberg (2000), An overview of the ACE-2 clear sky column closure experiment (CLEARCOLUMN), *Tellus Ser. B*, *52(2)*, 463483.

Sabbah, I., C. Ichoku, Y. J. Kaufman, and L. Remer (2001), Full year cycle of desert dust spectral opticla thickness and precipitable water vapor over Alexandria, Egypt, *J. Geophy. Res.*, *106*, 18,305–18,316.

Satheesh, S. K., and D. Lubin (2003), Short wave versus long wave radiative forcing by Indian Ocean aerosols: Role of sea-surface winds, *Geophysical Research Letters*, *30(13)*, 1695, doi:10.1029/2003GL017499.

Satheesh, S. K., and V. Ramanathan (2000), Large differences in tropical aerosol forcing at the top of the atmosphere and Earth's surface, *Nature*, *405*, 60–63.

Satheesh, S. K., and J. Srinivasan (2002), Enhanced aerosol loading over Arabian Sea during the pre-monsoon season: Natural or anthropogenic?, *Geophysical Research Letters*, *29(18)*, 1874, doi:10.1029/2002GL015687.

Satheesh, S. K., V. Ramanathan, B. N. Holben, K. K. Moorthy, N. G. Loeb, H. Marine, J. M. Prospero, and D. Savoie (2002), Chemical, microphysical, and radiative effects of Indian Ocean aerosols, *J. Geophy. Res.*, *107(D23)*, 4725, doi: 10.1029/2002JD002463.

Satyanarayana, A. N. V., U. C. Mohanty, and N. C. Sam (1999), A study on the characteristics of the marine boundary layer over Indian Ocean with ORV Sagar Kanya cruise 120 during1997, *Current Science*, *76*, 890–897.

Schmid, O., P. Artaxo, W. P. Arnott, D. Chand, L. V. Gatti, G. P. Frank, A. Hoffer, M. Schnaiter, and M. O. Andreae (2006), Spectral light absorption by ambient aerosols influenced by biomass burning in the Amazon Basin. I: Comparison and field calibration of absorption measurement techniques, *Atmos. Chem. Phys*, *6*, 3443–3462.

See, S. W., R. Balasubramanian, and W. Wang (2006), A study of the physical and chemical and and optical properties of ambient aerosol particles in Southeast asia during hazy and nonhazy days, *Journal of Geophysical Research*, *111*(D10S08), doi:10.1029/2005JD006180.

Seinfeld, J. H., and S. N. Pandis (1998), *Atmospheric Chemistry and Physics: From Air Pollution to Climate Change*, 11326 pp., John Wiley & Sons.

Seinfeld, J. H., et al. (2004), Regional climatic and atmospheric chemical effects of Asian dust and pollution, *Bull. Am. Meteorol. Soc.*, *85 (3)*, 367 , 380.

Shettle, E. P., and R. W. Fenn (1975), Models of the atmospheric aerosols and their

optical properties., *AGARD Conf. Proc., Optical Propagation in the Atmosphere, Lyngby, Denmark, NATO Advisory Group for Aerospace Research*, pp. 2.1–2.16.

Singh, S., S. Nath, R. Kohli, and R. Singh (2005), Aerosols over Delhi during premonsoon months: Characteristics and effects on surface radiation forcing, *Geophysical Research Letters*, *32*, L13,808, doi:10.1029/2005GL023062.

Staetter, R., and M. Schroeder (1978), Spectral characteristics of natural surfaces, *Proc. Int. Conf. on Earth Observation from Space and Management of Planetary Resources, Toulouse, France, Council of Europe, Commission of the European Communities, and European Association of Remote Sensing Laboratories*,, p. 661.

Stamnes, K., S. Tsay, W. Wiscombe, and K. Jayaweera (1988), Numerically stable algorithm for discrete-ordinate-method radiative transfer in multiple scattering and emitting layered media, *Appl. Opt.*, *27*, 2502–2509.

Subbaraya, B. H., A. Jayaraman, K. Krishnamoorthy, and M. Mohan (2000), Atmospheric aerosol studies under isros geosphere biosphere programs, *J. Ind. Geophys. Union*, *4*, 77–90.

Sun, J., M. Zhang, and T. Liu (2001), Spatial and temporal characteristics of dust storms in China and its surrounding regions, 1960-1999: Relations to source area and climate, *J. Geophy. Res.*, *106(D10)*, 10,325–10,333.

Takemura, T., T. Nakajima, O. Dubovik, B. N. Holben, and S. Kinne (2002), Single scattering albedo and radiative forcing of various aerosol species with a global three dimensional model, *J. Clim.*, *15(4)*, 333 352.

Takemura, T., T. Nozawa, S. Emori, T. Y. Nakajima, and T. Nakajima (2005), Simulation of climate response to aerosol direct and indirect effects with aerosol transport-radiation model, *J. Geophy. Res.*, *110*, D02,202, doi:10.1029/2004JD005029.

Tanré, D., P. Deschamps, and C. D. M. Herman (1988), Estimation of saharan

aerosol optical thickness from blurring effects in thematic mapper data, *J. Geophy. Res.*, *93(D12)*, 15,955–15,964.

Tanre, D., C. Deroo, P. Duhaut, M. Herman, J. J. Morcrette, J. Perbos, and P. Y. Deschamps (1990), Description of a computer code to simulate the satellite signal in the solar spectrum: The 5S code, *Int. J. Remote Sens.*, *11(4)*, 659–668.

Tegen, I. (2003), Modeling the mineral dust aerosol cycle in the climate system, *Quat. Sci.*, *22*, 18211834.

Tegen, I., and I. Fung (1994), Modelling of mineral dust in the atmosphere: sources, transport, and optical thickness, *J. Geophy. Res.*, *99*, 22,897–22,914.

Tomasi, C., E. Caroli, and V. Titale (1983), Study of the relationship between ångstroms wavelength exponent and junge particle size distribution exponent, *J. Clim. Appl. Meteorol.*, *22*, 1707–1716.

Torres, O., P. K. Bhartia, J. R. Herman, Z. Ahmad, and J. Gleason (1998), Derivation of aerosol properties from satellite measurements of backscattered ultraviolet radiation, Theoretical basis, *J. Geophy. Res.*, *103*, 17,099 17,110.

Tripathi, S. N., S. Dey, V. Tare, and S. K. Satheesh (2005), Aerosol black carbon radiative forcing at an industrial city in northern India, *Geophys. Res. Lett.*, *32, L08802*, doi:10.1029/2005GL022515.

van de Hulst, H. C. (1968), Asymptotic fitting, a method for solving anisotropic transfer problems in thick layers, *J. Comput. Phys.*, *3*, 291–306.

Venkataraman, C., G. Habib, A. Eiguren-Fernandez, A. H. Miguel, and S. K. Friedlander (2005), Residential biofuels in South Asia:carbonaceous aerosol emissions and climate impacts, *Science*, *307*, 1454–1456.

Vinoj, V., S. S. Babu, S. K. Satheesh, K. K. Moorthy, and Y. J. Kaufman (2004), Radiative forcing by aerosols over the Bay of Bengal region derived from shipborne,

island-based, and satellite (Moderate-Resolution Imaging Spectroradiometer) observations, *J. Geophy. Res.*, *109*, D05,203, doi:10.1029/2003JD004329.

Wang, C. (2004), A modeling study on the climate impacts of black carbon aerosols, *J. Geophy. Res.*, *109*, D03,106, doi:10.1029/2003JD004084.

Weingartner, E., H. Saathoff, M. Schnaiter, N. Streit, B. Bitnar, and U. Baltensperger (2003), Absorption of light by soot particles: Determination of the absorption coefficient by means of aethalometers, *J. Aerosol Sci.*, *34*, 1445–1463.

Wenny, B. N., J. S. Schafer, J. J. DeLuisi, V. Saxena, W. Barnard, I. Petropavlovskikh, and A. Vergamini (1998), A study of regional aerosol radiative properties and effects on ultraviolet-B radiation, *J. Geophy. Res.*, *103*, 17,083–17,097.

Wielicki, B. A., T. Wong, N. Loeb, P. Minnis, K. Priestley, and R. Kandel (2005), Changes in earths albedo measured by satellite, *Science*, *308*, 825.

Winter, B., and P. Chylek (1997), Contribution of sea salt aerosol to the planetary clear-sky albedo, *Tellus-B*, *49(1)*, 72–79.

Wiscombe, W. J., and S. G. Warren (1980), A model for the spectral albedo of snow. Part I: Pure snow, *J. Atmos. Sci.*, *37*, 2712–2733.

Young, T. A. (1994), Air mass and refraction, *App. Opt.*, *33*, 1108–10.

Zender, C. S., H. Bian, and D. Newman (2003), Mineral Dust Entrainment and Deposition (DEAD) model: description and 1990s dust climatology, *J. Geophy. Res.*, *108 (D14)*, 4416.

List of Publications

PUBLICATIONS IN REFERRED JOURNALS

1. **Sanat Kumar Das**, A. Jayaraman and A. Misra, "Fog induced variations in aerosol optical and physical properties over the Indo-Gangetic Basin and impact to aerosol radiative forcing", Ann. Geophys., 26, 13451354, 2008

2. S. Ramachandran, R. Rengarajan, A. Jayaraman, M.M. Sarin, **Sanat Kumar Das**, "Aerosol radiative forcing during clear, hazy and foggy conditions over a continental polluted location in north India", J. Geophys. Res., 111. D20214, doi:10.1029/2006JD007142, 2006.

3. **Sanat Kumar Das**, A. Jayaraman and H. Gadhavi, "Study of changes of aerosol apportionment in different breeze conditions at eastern coastal region of India", (In preparation)

4. **Sanat Kumar Das** and A. Jayaraman, "Dust Influenced Aerosol Radiative Forcing in Western India during Premonsoon", (In preparation)

5. **Sanat Kumar Das** and A. Jayaraman, "Impact of dust storm on aerosol properties at Mount Abu", (In preparation)

PAPERS PRESENTED IN CONFERENCES/SYMPOSIA

1. **Sanat Kumar Das** and A. Jayaraman, "Seasonal variation of black carbon at a high altitude station, Mount Abu", submitted at XV National Space Science Symposium (NSSS 2008), at Radio Astronomy Centre, NCRA-TIFR, Ooty, 26-29th February, 2008.

2. **Sanat Kumar Das** and A. Jayaraman, "Aerosol Characteristics over Urban and Pristine Regions: A comparative Study", at Aerosol-Chemistry-Climate Interactions (ACCLINT-2007) at Physical Research Laboratory, Ahmedabad, 20-22nd December 2007.

3. **Sanat Kumar Das** and A. Jayaraman, "Changes in Aerosol characteristic due to changes in land-sea breeze observed over Kalpakkam", at Indian Aerosol Science And Technology Association (IASTA 2007), at National Physical Laboratory, Delhi, 14-16th November 2007.

4. **Sanat Kumar Das** and A. Jayaraman, "Aerosol size distribution variation in winter time aerosols over north India and its impact on aerosol radiative forcing", XIV National Space Science Symposium (NSSS 2006), at Andhra University, Visakhapatanam, 09-12th February 2006

5. Amit Misra, **Sanat Kumar Das**, A. Jayaraman, "Study of aerosol properties during fog events from satellite and ground based observations", 4th Asian Aerosol Conference (AAC-2005), BARC, Mumbai, 13-16th December 2005

Memoirs

In the end I want to share a few unforgettable moments of my Ph.D. life. (a) Taking sunphotometer observations at Mt. Abu, (2) During the ICARB campaign at Kalpakkam, (3) With Dr. R. Bhaskaran and others at Kalpakkam, (4) During the campaign at Udaipur, (5) With our Mt. Abu staff at Gurushikhar, (6) With the poster at NSSS2006, (7) With my thesis supervisor, Prof. A. Jayaraman, (8) During Dr. APJ Abdul Kalam's visit to PRL, (9) Some of our volleyball teammates, (10) With Maa, Baba and Sisters just before joining PRL, (11) With Maa and Baba at Gandhi Ashram, Ahmedabad, (12) Our football team, (13) With my wife, Uma, (14) Our Marriage, (15) Adi, Uma and Myself.

Figure .2: